University of Southampton

Faculty of Natural and Environmental Science

Centre for Biological Sciences

Development of a sensitive cell culture system to assess prion infectivity and the efficacy of prion decontamination technologies

by

Thomas James Secker *BSc*

Thesis for the degree of Doctor of Philosophy

November 2012

UNIVERSITY OF SOUTHAMPTON

ABSTRACT

FACULTY OF NATURAL AND ENVIRONMENTAL SCIENCES

CENTRE FOR BIOLOGICAL SCIENCES

Doctor of Philosophy

DEVELOPMENT OF A SENSITIVE CELL CULTURE SYSTEM TO ASSESS PRION INFECTIVITY AND THE EFFICACY OF PRION DECONTAMINATION TECHNOLOGIES

by Thomas James Secker

Creutzfeldt-Jakob disease (CJD) can be iatrogenically transmitted during transplants, grafts and transfusions from CJD infected donors and also contaminated surgical instruments. A variety of methods to amplify and detect the presence of infectious prions as disease markers are available. However, these techniques do not measure the infectivity potentially associated with these markers. Currently, animal-bioassays are used to detect infectivity; however, they have limitations in detectable prion strains, cost, ethical considerations and assay length. Novel cell-based infectivity assays offer the potential to overcome these limitations, lower the requirements for animal use and the application of different cell lines could detect a wider range of prion strains. This project utilised murine neuroblastoma, N2a #58 cells infected with 22L-murine scrapie to develop a highly sensitive assay for the *in situ* detection of amyloid-rich prion (PrP^{Sc}) accumulation as an indication of prion infectivity. The autofluorescence quenching properties of Sudan black (SB) were incorporated into a novel Thioflavin T (ThT) based protocol for amyloid staining with improved specificity and sensitivity. Cell passages were incorporated into the assay to increase incubation time, improve cell viability and subsequently improve assay sensitivity; thus, demonstrating the detection of infectivity from a final 10^{-10} dilution of 22L-infected brain homogenate. Introduction of 22L-inoculated, surgical grade stainless steel wires to the N2a #58 cells demonstrated the SB/ThT detection of prion infectivity pre and post decontamination, which was comparable to animal bioassay data. Furthermore, preliminary work on the incorporation of the SB/ThT detection of prion infectivity within neural stem cells (NSC's), for prion propagation within a cell line that did not require genetic manipulation for increased prion susceptibility, highlighted problems with unspecific fluorescence of dead cells during NSC differentiation. Improvements in culture conditions of the NSC's regarding atmospheric conditions and trophic support were addressed in preparation for their use in future prion infectivity assays.

Contents

List of Figures

List of Tables

Authors Declaration

I, Thomas James Secker, declare that the thesis entitled "Development of a sensitive cell culture system to assess prion infectivity and the efficacy of prion decontamination technologies" and the work presented in the thesis are both my own, and have been generated by me as the result of my own original research. I confirm that:

- this work was done wholly or mainly while in candidature for a research degree at this University;
- where any part of this thesis has previously been submitted for a degree or any other qualification at this University or any other institution, this has been clearly stated;
- where I have consulted the published work of others, this is always clearly attributed;
- where I have quoted from the work of others, the source is always given. With the exception of such quotations, this thesis is entirely my own work;
- I have acknowledged all main sources of help;
- where the thesis is based on work done by myself jointly with others, I have made clear exactly what was done by others and what I have contributed myself;
- none of this work has been published before submission

Signed: ……..

Date: …….

Acknowledgements

Firstly, I would like to greatly thank my primary and secondary supervisors; Professor Bill Keevil and Dr Neil Smyth for all of their help, knowledge and guidance throughout this PhD project. I would also like to give thanks and appreciation to Dr Gerry McDonnell and Dr Vincent Thomas from my industrial sponsors Steris© for their interest, commercial ideas and knowledge throughout this project.

Secondly, I would like to thank all members, both past and present, of the EHU and the Microbiology group at the University of Southampton who have all had input with this project and also for the fun times and laughter both within and outside of work. I would like to give special thanks to Dr Rodolphe Hervé for his initial input on setting up the cell culture work and his presence and knowledge within meetings, Dr Sandra Wilks for her lab management and her eagerness to help and Dr Robert Howlin for his support in both lab and written work, especially during thesis preparation, who's help has made this whole process a lot easier. I would also like to thank Dr Emmanuel Comoy from the CEA in Paris for his help and support during Steris© meetings; especially regarding the decontamination infectivity work. Thanks also go to Professor Sylvain Lehmann for supplying the N2a #58 cells and the NSC's and also to Dr Ayodeji Asuni for supplying the 22L infected brain homogenates.

Finally many thanks and appreciation goes to all of my friends both within Southampton and the rest of the world. Extended thanks goes to my family, especially my Mum, Dad and two brothers who have loved and supported me through both the difficult personal times and hard work of the PhD.

Last but definitely not least I would like to thank and dedicate this work to my beautiful son, Joshua James Secker, who has put a smile on my face every day during my PhD and his good behaviour has made this time a lot easier than could have been imagined. Thank you all. This work was funded by a BBSRC Industrial CASE studentship BB/F018215/1 with Steris©.

Publications

Publications currently in preparation arising from the research carried out throughout this PhD project.

Secker, T.J., Herve, R., Keevil, C.W. Sensitive, *in situ,* SB/ThT staining for the analysis of prion infectivity and subsequent decontamination efficacy of stainless steel wires within a Neuroblastoma cell system. (In preparation for PNAS)

Secker, T.J., Keevil, C.W. Mild hypoxic conditions and improved supplements enhance neural stem cell culture and aid *in vitro* differentiation. (In preparation for Nature methods or PLOS Biology)

Abbreviations

Aβ	-	β-Amyloid plaques
AB	-	Animal bioassay
ACDP	-	Advisory Committee on Dangerous Pathogens
AD	-	Alzheimer's disease
ANOVA	-	Analysis of variance
APP	-	Amyloid precursor protein
ASA	-	Amyloid seeding assay
bFGF	-	Basic Fibroblast growth factor
BSE	-	Bovine spongiform encephalopathy
CDI	-	Conformation-dependant immunoassay
CJD	-	Creutzfeldt-Jakob disease
CNS	-	Central nervous system
CWD	-	Chronic wasting disease
DH	-	English Department of Health
DIC	-	Differential interference contrast
DLC	-	Diamond-like carbon
DMEM	-	Dulbecco's modified eagle medium
DMSO	-	Dimethyl sulfoxide
DY	-	Drowsy (TME strain)
EDIC	-	Episcopic differential interference contrast
EF	-	Epi-fluorescence

ELISA	-	Enzyme linked immunosorbent assay
FBS	-	Fetal bovine serum
fCJD	-	Familial Creutzfeldt-Jakob disease
FCS	-	Fetal calf serum
FFI	-	Fatal Familial insomnia
FT-IR	-	Fourier transform infrared spectroscopy
FSE	-	Feline spongiform encephalopathy
$GABA_A$	-	γ-aminobutyric acid type A
GFAP	-	Glial fibrillary acidic protein
GPI	-	Glycophosphatidylinositol
GSS	-	Gerstmann-Straussler-Scheinker syndrome
HBSS	-	Hanks buffered salt solution
HC	-	Hydrophobic core
HEPES	-	4-(2-hydroxyethyl)-1-peperazineethanesulfonic acid
HPA	-	Health protection agency
Htn	-	Huntington's disease
HTT	-	Huntingtin gene
HY	-	Hyper (TME strain)
iCJD	-	Iatrogenic transmission of variant Creutzfeldt-Jakob disease
IHC	-	Immunohistochemistry
kDa	-	Kilo-Dalton
MA	-	Membrane attachment region
MBM	-	Meat-and-bone meal
MM	-	Methionine/methionine homozygous

MS	-	Mass spectrometry
MV	-	Methionine/valine heterozygous
N2a	-	Murine neuroblastoma cells
NB	-	Neurobasal media
NBH	-	Normal brain homogenate
NCJDRSU	-	National Creutzfeldt-Jacob Disease Research and Surveillance Unit
NMR	-	Nuclear magnetic resonance spectroscopy
NR	-	Nile red
NR/ThT	-	Nile red/Thioflavin T assay
NSC	-	Neural stem cells
OR	-	Octapeptide repeat region
PBS	-	Phosphate buffered saline
PBS-T	-	Phosphate buffered saline and tween
PCR	-	Polymerase chain reaction
PD	-	Parkinson's disease
PFA	-	Paraformaldehyde
PI	-	Propidium iodide
PI-PLC	-	Phosphoinositide phospholipase C
PK	-	Proteinase K
PMCA	-	Protein misfolding cyclic amplification
PMCAb	-	Protein misfolding cyclic amplification with PrP capture beads
PRNP	-	Prion protein gene
$PrP^{0/0}$	-	PrP^{c} knockout mice

PrP	-	Prion protein (generic term)
PrP*	-	Prion protein (intermediate fraction)
PrP^{27-30}	-	Prion protein (insoluble fragment (27-30 kDa))
PrP^{c}	-	Prion protein (cellular isoform)
PrP^{cyto}	-	Cytotoxic associated prion protein
PrP^{res}	-	Prion protein (fragment resistant to PK digestion)
PrP^{Sc}	-	Prion protein (Scrapie disease associated isoform)
QUIC	-	Quaking induced conversion assay
RML	-	Rocky mountain laboratory strain (a.k.a. 139A or chandler)
RNA	-	Ribose nucleic acid
ROS	-	Reactive oxygen species
RT- QUIC	-	Real time quaking induced conversion assay
SB	-	Sudan black
SB/ThT	-	Sudan black/Thioflavin T analysis
SCEPA	-	Scrapie cell endpoint assay
sCJD	-	Sporadic Creutzfeldt-Jakob disease
scN2a	-	Scrapie infected neuroblastoma cells
SEAC	-	Spongiform Encephalopathy Advisory Committee
SEM	-	Standard error of the mean
SOD	-	Superoxide dismutase
SOD-1	-	Superoxide dismutase-1
SOD-2	-	Superoxide dismutase-2
sPMCA	-	Serial protein misfolding cyclic amplification
$sPrP^{Sc}$	-	Disease associated prion protein (sensitive to PK digestion)

SR	-	SYPRO Ruby blot stain
SR/ThT	-	SYPRO Ruby/Thioflavin T analysis
SS	-	Stainless steel
SSBA	-	Stainless steel binding assay
SSBP/1	-	Sheep scrapie brain pool 1
SSCA	-	Standard scrapie cell assay
SSD	-	Sterile service departments
TCIA	-	Tissue culture infectivity units
ThS	-	Thioflavin S
ThT	-	Thioflavin T
TME	-	Transmissible mink encephalopathy
TSE	-	Transmissible spongiform encephalopathy
UK	-	United Kingdom
UV	-	Ultra-violet
vCJD	-	Variant Creutzfeldt-Jakob disease
VV	-	Valine/Valine homozygous
WB	-	Western blot

Chapter 1

General introduction

1.1 Introduction

Transmissible spongiform encephalopathies (TSEs) such as Creutzfeldt-Jakob disease (CJD) in humans are a group of neurodegenerative diseases characterised by the accumulation of the infectious, misfolded prion protein (Prusiner 1998). The prion associated "protein only" hypothesis describes the basis of protein aggregation in TSE's as an autocatalytic conversion of the α-helical, host encoded cellular prion protein (PrP^{c}) to form the infectious, β-pleated sheet isoform (designated PrP^{sc} or PrP^{res}) (Prusiner 1998, Weissmann et al. 2002). The main cause of neurodegeneration in TSE's is thought to be the aggregation of PrP^{Sc} which accumulates as PrP^{Sc} rich amyloid fibrillar plaques thus altering the normal morphology of the brain tissue leading to degeneration of neuronal pathways, causing the associated symptoms of dementia. Post-mortem microscopic evaluation of the brains of infected patients typically demonstrates several common diagnostic traits associated with protein aggregation in TSE's including spongiform degeneration, caused by cell death leading to degeneration of the normal tissue morphology, the accumulation of PrP^{Sc} and astrocytic gliosis (Prusiner 1997).

The accumulation of the mis-folded prion protein is implicated in a broad range of TSE's across a number of mammalian species. The range of TSE's associated with PrP^{Sc} deposition and potentially caused by accumulation of the infectious prion protein include; Creutzfeldt-Jakob disease (CJD), Kuru and Gerstmann-Straussler-Scheinker syndrome (GSS) affecting humans, Bovine spongiform encephalopathy (BSE) affecting cattle, scrapie affecting sheep and chronic wasting disease (CWD) effecting elk and deer, alongside a number of less common TSE diseases. All of these TSE's have varying routes of transmission which are summarised in Table 1.

TSE	Species	Mechanism of Transmission
Kuru	Human	Transmission of infectious prions from cannibalistic rituals, thought to be the earliest link to CJD.
Sporadic CJD (sCJD)	Human	The spontaneous formation of infectious PrP^{Sc} caused by a mutation in the prion protein gene (PRNP gene).
Familial CJD (fCJD)	Human	A genetic variation of CJD caused by a mutation in the PRNP gene that can potentially be passed to offspring.
Variant CJD (vCJD)	Human	Horizontal transmission of infectious prions from BSE infected matter to humans.
Iatrogenic CJD (iCJD)	Human	Transmission of infectious material via medical accidents including neurosurgery and infected tissue transplants.
Gerstmann-Straussler-Scheinker disease (GSS)	Human	A genetic mutation in the PRNP gene, thought to be an atypical CJD.
Fatal Familial insomnia (FFI)	Human	A genetic mutation in the PRNP gene.
Bovine spongiform encephalopathy (BSE)	Cattle	Infection via transmission of contaminated feed, milk or land.
Scrapie	Sheep	Transmission of PrP^{Sc} from infected sheep and contaminated soil.
Chronic wasting disorder (CWD)	Cervids	Infection via transmission of PrP^{Sc} from contaminated feed and soil.
Feline spongiform encephalopathy (FSI)	Cats	Infection via transmission of PrP^{Sc} from contaminated food.
Transmissible mink encephalopathy	Mink	Horizontal transmission of prions from BSE and Scrapie infected animals.

Table 1 – Transmissible spongiform encephalopathies

Comparison of Transmissible spongiform encephalopathies (TSE) and their varying mechanisms of transmission (Adapted from Collinge 2001, Prusiner 1997).

1.2 Creutzfeldt-Jakob disease

The transmission of PrP^{Sc} was first discovered from the spread of Kuru, a TSE that affected the Fore tribe in Papua New Guinea in the early 1950's which was established to spread via the tribe's cannibalistic rituals, reaching total reported deaths of ~2500 people (Gajdusek et al. 1957, Lumley 2008). Kuru showed similarities in dementia based symptoms as scrapie and subsequently CJD, which lead to the conclusion that the causes of these diseases evolved from a common infectious unit. Furthermore, it was shown that Kuru could be transmitted to chimpanzee models, and comparable tests with CJD and GSS followed suggesting the transmission of a related or identical infectious unit (Collinge 2001, Gajdusek et al. 1966, Gibbs et al. 1968, Masters et al. 1981).

Creutzfeldt-Jakob disease can be divided into three subcategories based on the mode of acquisition: inherited, sporadic and acquired. Sporadic CJD was first discovered in a 22 year old woman in the 1920s and is the most common type of CJD, affecting around 1 - 2 people per million each year, accounting for around 85% of all CJD cases (Belay 1999, Lumley 2008, Wadsworth et al. 2007). It is associated with the spontaneous conversion of PrP^{c} to PrP^{Sc} which is hypothesised to be a consequence of either; a somatic mutation in the gene that encodes the prion protein (PRNP) that is associated with increased age, or by a spontaneous conversion of PrP^{c} to PrP^{Sc}, caused by an error during PRNP gene expression (Belay 1999, Collinge 2001). Familial or inherited CJD accounts for around 10 – 15% of all CJD cases and is characterised by a dominant autosomal genetic defect of the PRNP gene of which there are around 20 distinct mutations discovered (Collinge 1997). The conformation of PrP^{Sc} from inherited and sporadic CJD cases is thought to be different from that of acquired diseases as the potential of transmission of the sporadic/inherited agent is a lot lower than the variant form (Collinge 1997).

The two acquired types of CJD are variant CJD (vCJD) and iatrogenic CJD (iCJD). Variant CJD is caused by the horizontal transmission of infectious prions from

BSE infected cattle to humans. The spread and outbreak of BSE was later attributed to the cross species transmission of sheep scrapie from the feed produced from rendered carcasses (Wilesmith et al. 1991). A further hypothesis was the spread of prions from unknown sporadic BSE cases as rendered cattle carcasses had also been used for cattle feed (Collinge 2001). The BSE epidemic hit its peak in the UK in 1992 and began to decline towards the end of the 1990's to the mid 2000's (Figure 1) as a nation-wide culling of infected livestock was introduced and the use of meat-and-bone meal (MBM) feed was halted (Wilesmith et al. 1992). Over 180,000 cases of BSE were discovered in the UK and an estimate of around a million total infected cattle (Anderson et al. 1996). Following the UK epidemic, an increase in BSE in non-UK countries was observed, most likely caused by the transmission of PrP^{Sc} from imported contaminated meat or MBM feed from the UK (Bradley et al. 2012). The first case of vCJD was recognised in 1995 and the link between BSE and vCJD established due to the fact that the isolated prion protein from both diseases had the same biochemical properties and there was a clear correlation regarding timing with the BSE epidemic and vCJD outbreak (Figure 1) (Will et al. 1996). Variant CJD is clear evidence of the ability of the infectious prion to cross the "species barrier".

Importantly, there is clearly an established link between disease susceptibility and genetic variation of codon 129 of the prion protein gene. There are three genetic variations of the PrP^{Sc} mutation located at codon 129 (typically encoding for methionine and valine) of the PRNP gene. These three genetic variations are known as methionine/valine (MV) heterozygous, methionine homozygous (MM) and valine homozygous (VV). These account for 50%, 40% and 10% of the Caucasian population, respectively (Lumley 2008, Owen et al. 1990, Wadsworth and Collinge 2007). Individuals that are homozygous (both VV and MM) for this polymorphism are more susceptible to sCJD, with 95.5% or cases in one study being homozygous for either methionine or valine (Belay 1999, Palmer et al. 1991). Furthermore over half of the healthy controls were heterozygous (MV) for this polymorphism (Palmer et al. 1991). This was also determined to be the case with the susceptibility of acquiring vCJD from the BSE outbreak with all cases to date being MM homozygous at codon 129 (Asante et al. 2006, Ironside et al. 2006). However, the susceptibility of transmission to VV and MV humanised mice has been demonstrated; with an increased asymptomatic state and an increased incubation period which in some cases outlasted the rodent lifespan

(Bishop et al. 2006). More recently a case of transmission of vCJD from blood transfusion was observed in an MV heterozygous subject, suggesting that the MV polymorphism can be associated with disease transmission (Ironside et al. 2006). This also highlights that there is the potential of a second wave of CJD in individuals that are VV or MV at codon 129 that are presently asymptomatic carriers of disease with a far increased incubation period; this would also increase the unknown risk of iatrogenic transmission between/from these unknown cases. In addition, homozygotes, particularly with the MM mutation were more susceptible to acquiring iatrogenic CJD from pituitary hormone inoculation (Collinge et al. 1991, Collinge 1997, Palmer et al. 1991). It has also been demonstrated that 12 cases of disease transmission from dura matter grafts were all associated with individuals carrying the MM homozygous polymorphism (Collinge et al. 1991). Furthermore, it has been shown that a similar genetic susceptibility is observed in sCJD and iCJD cases (Deslys et al. 1994). These findings suggest that the heterozygosity of MV at codon 129 has a protective effect on the individual which is also found in inherited TSE's including GSS and FFI (Baker et al. 1991, Collinge 2001, Hsiao et al. 1992).

Variant CJD is to this day the most common acquired TSE in humans in the UK; however the incidence is relatively low with 176 deaths recorded from the start of surveillance in 1990 up to the end of August 2012 (Data from the National Creutzfeldt-Jacob Disease Research and Surveillance Unit (NCJDRSU)). Although the mortality rate of vCJD is relatively low, possible future outbreaks of BSE potentially due to the discovery of atypical strains alongside our still limited understanding of this unique infectious agent could lead to a second outbreak of vCJD or an atypical vCJD. Furthermore, there is still a risk of the iatrogenic transmission of CJD from asymptomatic carriers which is discussed in depth later in this report.

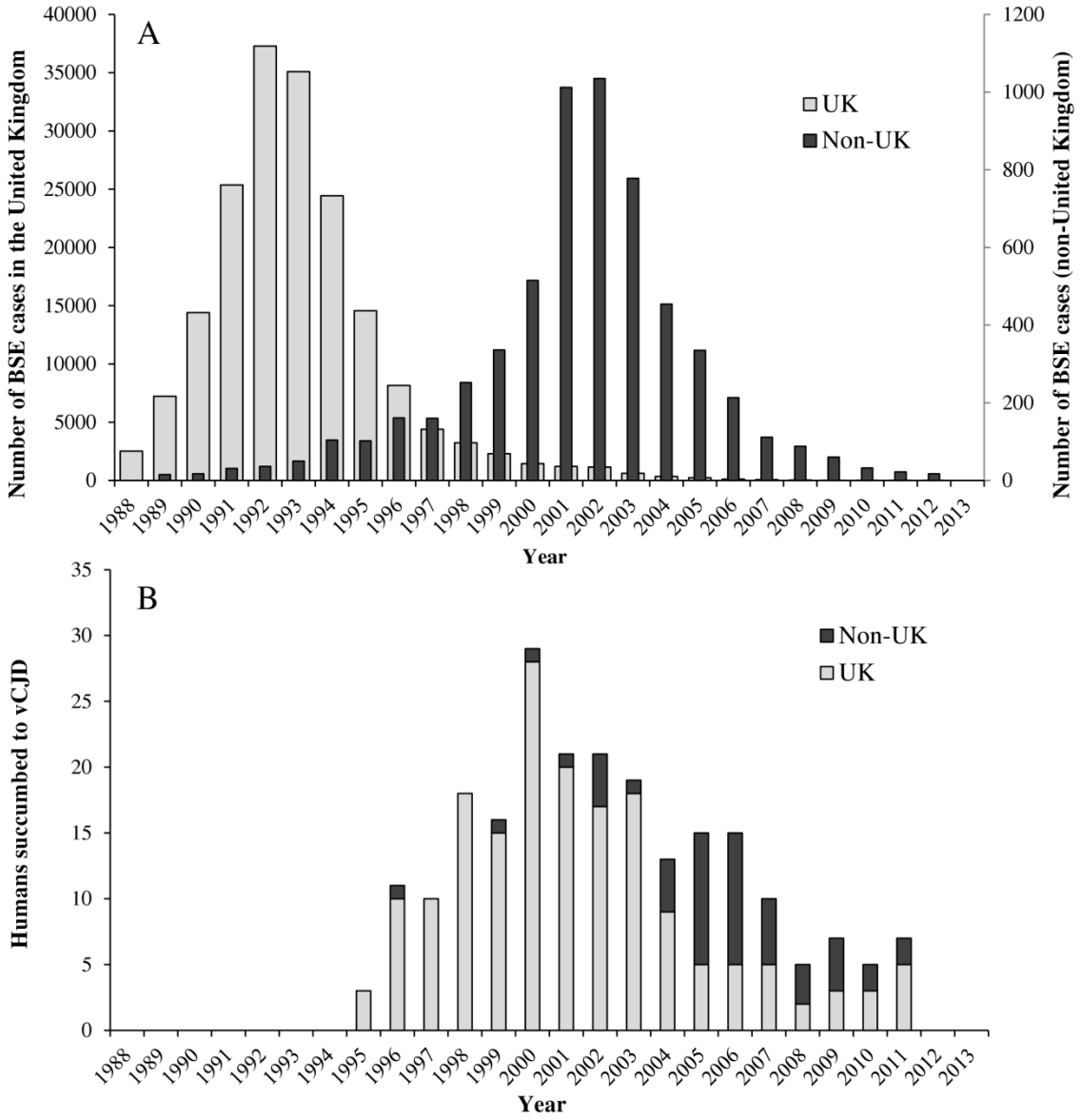

Figure 1 – Incidences of BSE and vCJD

The incidences of A) BSE and B) vCJD in both the UK (light grey) and Non-UK countries (dark grey), highlighting the correlation between the epidemic of BSE and the onset of vCJD especially within the UK (Data obtained from the National CJD Surveillance Unit (NCJDSU, Edinburgh).

1.3 The prion protein

Neurodegeneration caused by the accumulation of protein aggregates which precedes the breakdown of normal tissue morphology seems to be a common occurrence in many diagnosed neurodegenerative diseases. However, different proteins or precursor proteins/molecules seem to be the disease-associated agents (Caughey et al. 2003). For example, Alzheimer's disease (AD) is caused by the formation of β-amyloidal (Aβ, amyloid β) plaques produced from aggregation of the amyloid precursor protein (APP). More recently it has been observed that an increase in intracellular tau and phosphorylated tau leading to the breakdown of microtubules could also be a disease mechanism associated with AD. Parkinson's disease (PD) is associated with the formation of lewy bodies produced by α-synuclein. Finally, Huntington's (Htn) disease is caused by a mutation in the huntingtin gene (HTT) which leads to the production of fibrillar Htn plaques (Caughey and Lansbury 2003). The main difference of TSE's compared to other neurodegenerative diseases is that PrP^{Sc} can transmit between hosts, whereas none of the other mentioned protein precursors have currently demonstrated any host to host transmission (Caughey and Lansbury 2003). However, within the last 12 years it has been shown that AD can be induced in APP transgenic mice (Kane et al. 2000, Meyer-Luehmann et al. 2006) and APP transgenic rats (Rosen et al. 2012) after the introduction of AD infected human brain homogenate. More recently the *de novo* formation of Aβ deposits has been demonstrated in mice expressing wild-type human APP (Morales et al. 2011). Although there is currently no evidence that AD is transmissible, these recent studies have shown that the disease can be induced under certain conditions.

The mechanisms in which these infectious protein precursors lead to the formation of protein aggregates in many of these diseases is unknown, especially in TSE's where various potential mechanisms have been thoroughly studied and will be discussed further in this report (Collinge 2001, Moore et al. 2009, Prusiner et al. 1981, Prusiner 1997, Redecke et al. 2009). The protein that causes TSE's is characterised by a stoichiometric transformation of the host cellular glycoprotein precursor PrP^{c} to form the partial Proteinase K (PK) resistant, infective isoform known as PrP^{Sc} (Aguzzi et al. 2008).

The human cellular prion protein is encoded by a single copy gene, denoted the PRNP gene, located on the short arm of chromosome 20 (Oesch et al. 1985, Robakis et al. 1986). PrP^c is a monomeric glycoprotein attached to cell membrane surfaces by commonly occurring glycophosphatidylinositol (GPI) anchors, and is thought to be transported out of the cell by an endocytic pathway (Caughey et al. 2006). PrP^c is around 231 amino acids in length, with a molecular mass of 35-36 kDa (Figure 2). Structurally it is largely α-helical and found ubiquitously in the body, but more predominantly on cells of the CNS (Moore et al. 2009). PrP^c is characterised by N-linked glycosylation at two sites of the protein and is modified post-transcriptionally with a GPI anchor in the endoplasmic reticulum (Figure 2). Followed by attachment to the cell surface by binding of the C-terminal end with the cell surface phosphatidylinositol group anchor associated with the GPI proteins. The cellular prion protein contains two highly conserved regions at the N-terminal side; one region comprising the 5 octapeptide repeats, consisting of 5 repeats of an octameric amino acid structure with the sequence; Proline, Histidine, Glycine, Glycine, Glycine, Tryptophan, Glycine and Glutamine (PHGGGWGQ) and a charged cluster also known as the hydrophilic region sitting next to the hydrophobic core. The C-terminal end of the protein primarily consists of the Proteinase K (PK) resistant core which is associated with the infectious misfolded isoform. In addition, it contains the two N-linked glycosylation regions situated at asparagines 181 and 197, a single disulphide bridge between cysteines 179 and 214 and the GPI anchor region at the far C-terminal end. The number of glycosylation sites present on each PrP molecule can be determined by the number of glycosylation bands present during Western blot analysis. The position of PK cleavage is speculated to be around the hydrophobic core of the N-terminal region (Figure 2) (Aguzzi et al. 2008, Caughey and Lansbury 2003, Charvériat et al. 2009).

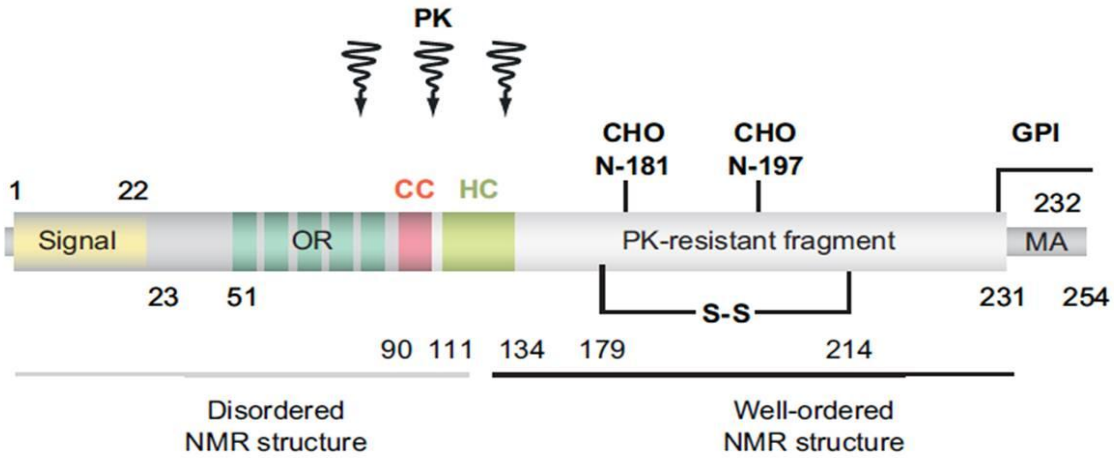

Figure 2 – The primary structure of PrP^c

A diagrammatic representation of PrP^c structure highlighting the octapeptide-repeat region (OR), hydrophobic core (HC), two N-Linked glycosylation sites (N-181 and N-197), the GPI anchor at the C-terminal end and the membrane attachment region (MA), the PK-resistant core fragment which is associated with PrP^{Sc} and the area of PK cleavage (Aguzzi et al. 2008, Harrison et al. 1997).

The use of nuclear magnetic resonance spectroscopy (NMR) to determine the secondary structure of natural PrP^c has not been possible due to difficulty in producing an adequate amount of purified PrP^c (Riesner 2003). Consequently, the structure has been determined using recombinant mouse PrP^c (Riek et al. 1997). The cellular isoform of the prion protein has been demonstrated to be predominantly α-helical, comprising three α-helixes; one spanning residues 144-154, one at residues 175-193 and the third spanning residues 200-219. Two small β-strands forming an anti-parallel β-sheet are found between residues 128-131 and 161-164. The remaining N-terminal region from residues 23-121, containing the octapeptide repeats has been observed to be considerably unstructured and flexible (Figure 3) (Riesner 2003).

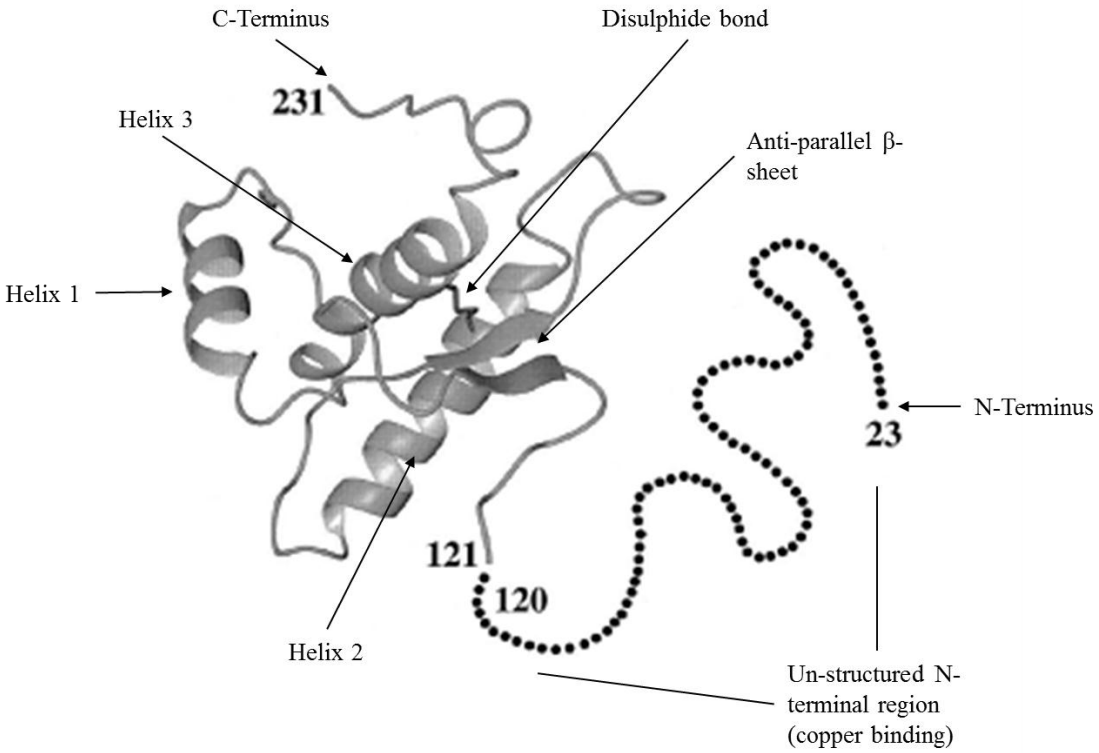

Figure 3 – Secondary structure of PrP^c

A diagrammatic representation of the proposed secondary structure of PrP^c, highlighting the α-helix and β-sheet positions and the unstructured N-terminal region. (adapted from Riek et al. 1997).

1.3.1 The suggested functions of PrP^c

The role of PrP^c is not fully understood, due in part to the fact that PrP^c knockout mice ($PrP^{0/0}$), which have been genetically modified to inhibit PRNP gene expression, do not display any overt clinical symptoms. Initial studies using knockout mice showed normal development and behaviour (Bueler et al. 1992), with no obvious change in physiology other than a resistance to infection from scrapie (Büeler et al. 1993). However, more recently studies have shown that PrP^c is believed to be involved in a number of cellular pathways. Research has demonstrated certain subtle changes in the normal neurological processes observed in the knockout mice, including pathways within the central nervous system controlling synaptic function and neuronal neurite

outgrowth. It has been demonstrated that PrP^c can act as a ligand for laminin binding, instigating an increase in neurite growth and outreach in primary neurons of rodents (Graner et al. 2000). PrP null mice confirm that the cellular prion protein is not essential to maintain the important synaptic functions required for normal life. In mice devoid of PrP^c it has been observed that there is no change in a number of synaptic functions apart from a partial increase in locomotor activity when in a novel environment (Roesler et al. 1999). However, in stark contrast, other studies have shown that the loss of PrP^c can instigate neurological changes. The loss of PrP^c has shown to effect circadian activity rhythm, resulting in an altered sleep pattern in PrP null mice (Tobler et al. 1996). Mice devoid of PrP^c also have weakened $GABA_A$ (γ-aminobutyric acid type A) receptor mediated fast inhibition and impaired long term potentiation, demonstrating reduced long term learning and memory (Collinge et al. 1994).

PrP^c has also demonstrated involvement in functional activities and acts as a ligand for various molecules in a diverse number of cells, including neurons, T-cells, leukocytes, neural stem cells and haematopoietic stem cells (Caughey and Baron 2006, Isaacs et al. 2006). The binding of copper and zinc to the OR region of PrP^c could be a clue to its potential role in redox control (Aguzzi et al. 2008, Caughey and Baron 2006). Cu^{2+} ions bind to 5 or 6 binding sites situated in the 4 to 5 octapeptide repeats found within the N-terminal side of PrP^c. The relationship between PrP^c and copper was confirmed when it was established that PrP null mice contained 50% lower levels of synaptosomal copper than wild-type mice suggesting a role of PrP^c in synaptic copper homeostasis (Herms et al. 1999). The decreased activity of copper-dependant enzyme superoxide dismutase-1 (SOD-1) in PrP null mice suggest that PrP^c may act as a chaperone for the delivery of Cu^{2+} to SOD-1 (Brown et al. 1998). It is unknown if PrP^c is the principle Cu^{2+} binding molecule in the brain, however the use of PI-PLC (an enzyme that digests GPI anchors) causes a release of Cu^{2+} ions from cerebellar cells suggesting that the principle molecule contains a GPI anchor, as is found in PrP^c (Brown et al. 1997). It has also been suggested that PrP^c itself has SOD like activity. Increased levels of PrP^c located at the synapse of neurons suggests PrP^c mimics SOD and controls the levels of Cu^{2+} ions at this location as SOD has been shown to cause detrimental neurological effects in the presence of synapses (Brown et al. 1999). However, further research has suggested this is not the case as no PrP^c dependant SOD-1 or SOD-2 activity has been observed *in vivo* in the heart, spleen or brain (Hutter et al.

2003). This also excludes the possibility that PrP^{c} may act as a chaperone to deliver excess Cu^{2+} to SOD-1. A more likely hypothesis is that the high levels of PrP^{c} situated on the pre-synaptic membrane and the high affinity binding of Cu^{2+} ions to PrP^{c} could be involved in buffering the increased levels of copper released during synaptic vesicle fusion and the fact that nerve endings release copper during depolarization (Vassallo et al. 2003). The affinity of PrP^{c} for copper binding correlates with the Cu^{2+} concentrations observed at the synapse, thus further supporting this hypothesis (Millhauser 2007). This would also relate to findings discussed earlier regarding the impaired synaptic ability in PrP null mice that could be caused by the toxicity of excess copper and the lack of the previously hypothesised neuroprotective capabilities of PrP^{c} (Collinge et al. 1994). This is supported by the fact that wild-type neurons and glial cells are much more resistant to oxidative stress caused by the increased build-up of copper associated reactive oxygen species (ROS), than the neurons and glial cells associated with PrP null cultures (Brown et al. 1998). Therefore, neurodegeneration observed in TSE's may not only be caused by the formation of protein aggregates and altered brain tissue morphology but may also be exacerbated by the loss of normal functions of PrP^{c} once converted to PrP^{Sc}.

1.3.2 The pathological prion (PrP^{Sc})

Preliminary misperceptions occurred in determining whether the causative agent in TSE's was a microbe or virus due to its infectious and variable properties. The lack of nucleic acids present in the causative agent was suggested after the infectious unit was determined to be resistant to UV and ionizing radiation which would usually destroy nucleic acids (Alper et al. 1967). Soon after, Griffith, 1967, determined that a protein with the ability to replicate in its host was the likely cause of prion diseases (Griffith 1967). Furthermore, Nobel Prize winner Stanley Prusiner confirmed the protein nature of the causative agent when he was the first person to isolate the prion protein (Aguzzi et al. 2009, Prusiner et al. 1981, Prusiner 1998). Subsequently, Prusiner described in 1981, that the infectious agent is a modification of a host encoded protein and designated this as the "proteinaceous infectious unit" or prion (Lumley 2008, Prusiner et al. 1981, Prusiner 1998). The main structural alteration that occurs between PrP^{c} and PrP^{Sc} is the misfolding of the monomeric PrP^{c} bulk α-helix structure to the multimeric β-sheet rich protein isoform PrP^{Sc} (Figure 4) (Aguzzi et al. 2008, Caughey

and Baron 2006). Difficulties in determining the proportion of α-helix and β-sheet content of PrP^{Sc} arose due to the insolubility of the infectious unit. However estimates showed that PrP^{c} comprises of roughly 42% α-helix and 3% β-sheet compared to 30% α-helix and 43% β-sheet in PrP^{Sc}. The insoluble fragment post PK digestion, denoted PrP^{27-30}, contains 21% α-helix and 54% β-sheet (Table 2) (Pan et al. 1993). This confirmed that the insolubility of the undigested, infectious prion sub-unit was most likely due to its highly β-sheet nature.

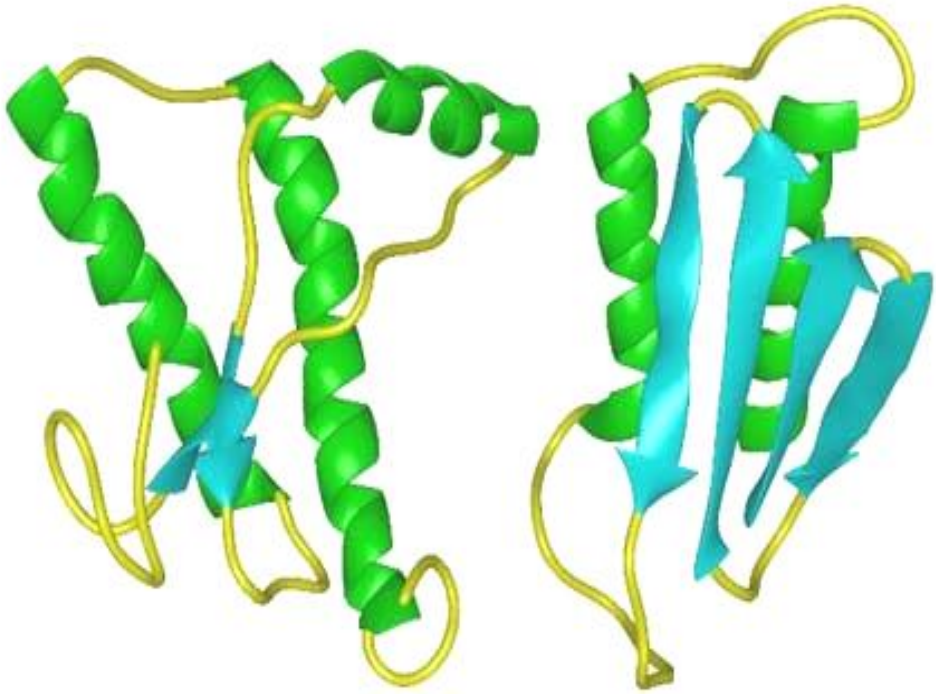

Figure 4 – The PrP structural differences

A representation of the differences in structure of PrP^{c} (left) and PrP^{Sc} (right), highlighting the differences in α-helix (green) and β-sheet (blue) content.

Isoform	α-helix content (%)	β-sheet content (%)
PrP^{c}	42	3
PrP^{sc}	30	43
$PrP^{27\text{-}30}$	21	54

Table 2 – Composition of prion secondary structures

Comparison of the composition of the different prion protein isoform secondary structures

1.3.2.1 Conversion of PrP^{c} to PrP^{Sc}

The processes or mechanisms involved in the transformation of PrP^{c} to PrP^{Sc} have been extensively researched but are still not fully understood. The majority of research has suggested that there are two proposed mechanisms, involving a "protein only" reaction with or without a part folded protein intermediate named "Protein X" or a number of intermediates that are involved in the conversion of PrP^{c} to PrP^{Sc}, classed as the template assisted models and finally the presence of non-protein intermediates has also been considered.

The "protein only" hypothesis, also known as the nucleation-polymerisation model states that the conversion of PrP^{c} to PrP^{Sc} is an autocatalytic reaction that occurs in the presence of already misfolded PrP^{Sc} which binds to form a nucleated structure which then polymerises (Figure 5 and Figure 6) (Laurent 1996, Soto et al. 2001). This process involves the self-replication of PrP^{Sc} once bound to PrP^{c} to form a hetero-dimer. PrP^{c} is then converted to form a PrP^{Sc} monomer which joins to the original PrP^{Sc} to form a PrP^{Sc} – PrP^{Sc} dimer. Additional PrP^{c} leads to further conversion to PrP^{Sc} which attaches to the dimer to form a PrP^{Sc} oligomer. In time more PrP^{c} undergoes conversion and ultimately a PrP^{Sc} protofibril is formed (Figure 5). During this conversion monomers of PrP^{Sc} can break off and themselves initiate the conversion of more PrP^{c}

monomers (Aguzzi et al. 2008). Subsequently the stocks of PrP^{c} are replenished by cellular synthesis, occurring in the endoplasmic reticulum, due to the reduction in PrP^{c} levels, further fuelling the self-replication of PrP^{Sc} (Figure 6) (Stohr et al. 2008).

$PrP^{0/0}$ knockout mice are one of the supporting experiments for the "protein only" hypothesis, in which they show no signs of infection when inoculated with PrP^{Sc}, confirming the need of the cellular prion protein, not just the PrP^{Sc} isoform, for the replication of the infectious agent (Büeler et al. 1993, Weissmann et al. 2002). More recently, PMCA (protein misfolding cyclic amplification) and cell free assay experiments are further proof of the "protein only hypothesis", discussed in depth later. Briefly, PMCA involves the artificial amplification of PrP^{Sc} in the presence of PrP^{c} (Deleault et al. 2007, Saborio et al. 2001, Soto et al. 2005). Furthermore, experiments using yeast prion models, the [PSI^{+}] prion form of the protein Sup35 and [URE3] prion form of the protein Ure2 show similar properties to misfolded β-sheet proteins that demonstrate an increased formation in the presence of the normal protein and form protease resistant protein aggregates, thus again supporting the "protein only hypothesis" (Soto et al. 2004).

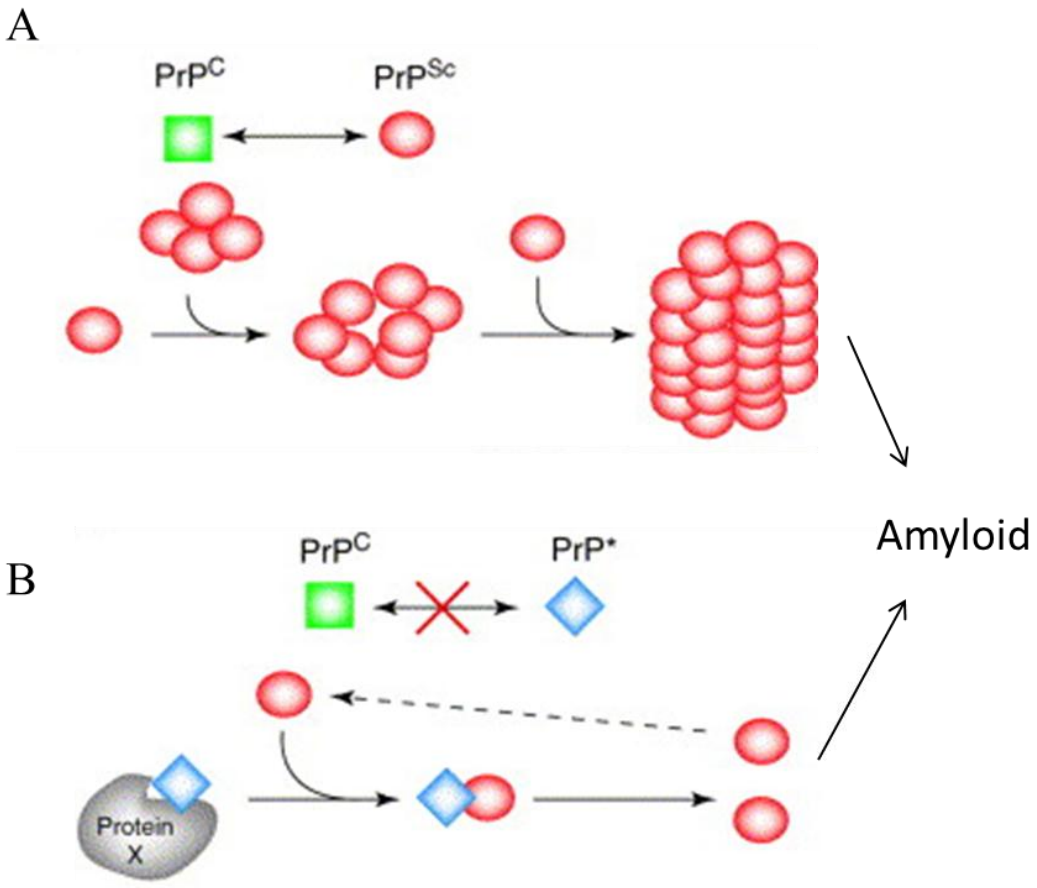

Figure 5 – Proposed mechanisms of PrP conversion

Schematic diagram of the two predominant proposed mechanisms of prion conversion. (A) The "protein only" or nucleation-polymerisation model where the conversion or PrP^{c} is initiated by the seeding of PrP^{Sc}. (B) The template-assisted model where the conversion of PrP^{c} to PrP^{Sc} is instigated by the formation of a PrP intermediate (PrP^{*}) which binds to a chaperone ("protein x") that initiates the conversion. (adapted from Soto and Saborío 2001)

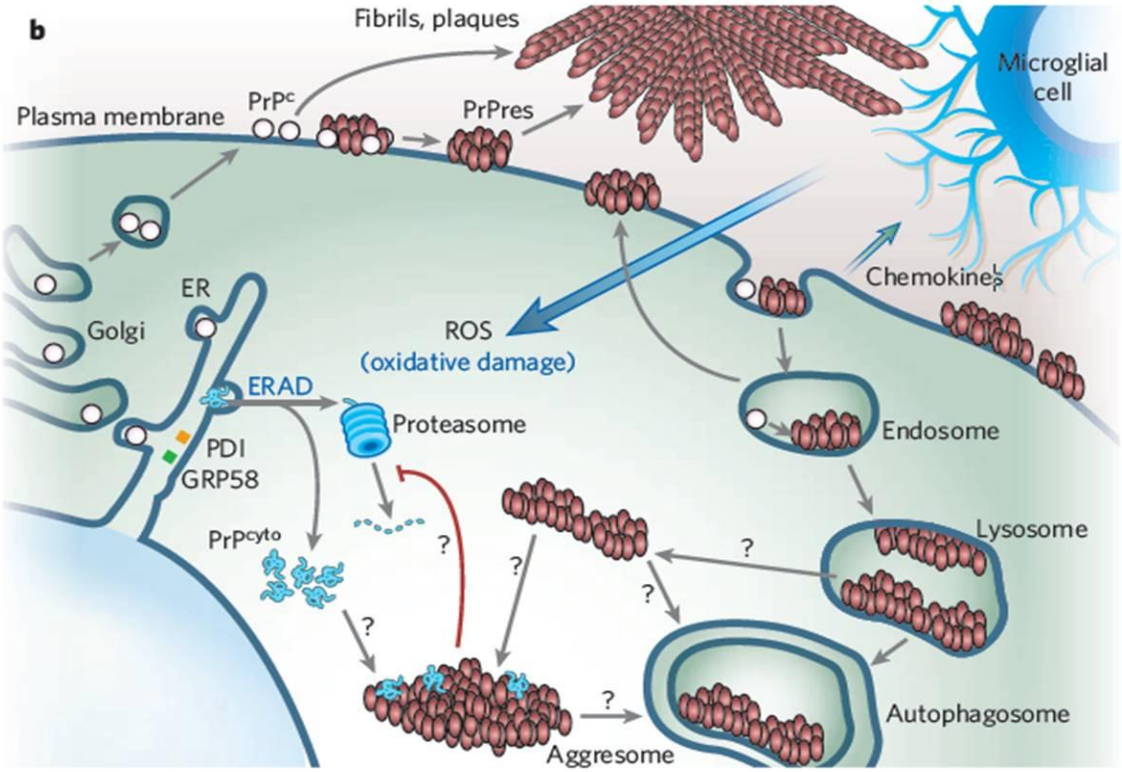

Figure 6 – Proposed locations of PrP conversion and toxicity

Taken from Caughey and Baron (2006) showing the PrP^{c} processing and proposed locations of the transformation of PrP^{c} (white) to the infectious PrP^{res} (red) preceding amyloid formation. Potential mechanisms of toxicity caused by the presence of PrP^{res} or PrP^{cyto} within the cell are highlighted by the red PrP^{res} molecules and question marks.

The template assisted model which involves the occurrence of a protein intermediate involved in the conversion of PrP^{c} to PrP^{Sc} is a dominant area of prion research, due to the potential of a therapeutic target to inhibit the PrP^{c} conversion. The "protein X" was described by Prusiner as "a factor defined by molecular genetic studies that binds to PrP^{c} and facilitates PrP^{Sc} formation" (Figure 5) (Prusiner 1998). The most recent evidence for a protein intermediate is again from using PMCA. Firstly, the use of homogenised normal brain containing PrP^{c} and an un-purified PrP^{Sc} seed could mean that a number of other factors within these samples are contributing to the prion conversion (Caughey 2003). Secondly, using PMCA researchers have managed to produce *de novo* infectious prions from purified PrP^{c} and poly(A) RNA without using a PrP^{Sc} seed (Benetti et al. 2009, Deleault et al. 2007). Additionally, the purified PrP^{c}

used in these experiments still contains some natural lipids which could also be involved in PrP conversion. As such, the production of *de novo* prions could suggest that polyanions or lipids could be intermediate factors involved in prion conversion. However, it has been observed that once these *de novo* formed infectious prions are introduced into wild-type hamsters they produced disease with a new phenotype, whether this is a factor of the technique or the production of a new prion strain is unknown (Barria et al. 2009). It has recently been demonstrated using serial PMCA (sPMCA) to amplify different prions strains with or without different cofactors, that the cofactors determine the different strain properties (Deleault et al. 2012). Therefore, cofactors affect the infectious nature of different strains and must be involved in either PrP^{Sc} conversion or disease progression. A study into the capability of PrP^{Sc} to transmit across the "species barrier" further postulates the proof of the protein intermediate theory. Mice that expressed both human and mouse PrP^{c} were not infected by human PrP^{Sc}. Conversely, mice that only expressed the human PrP^{c} were infected with human PrP^{Sc} suggesting the presence of a species dependant cofactor in the mouse PrP^{c} that was inhibiting the human PrP^{Sc} transmission and is therefore required for mouse PrP^{Sc} conversion (Prusiner 1998). Work by Simoneau et al, 2007 also studied the possibility of a protein intermediate between the production of PrP^{Sc} and PrP^{c} which is involved in the structural conversion, but may also represent the infectious unit in TSE diseases. They discovered the presence of β-PrP oligomers that may represent the so called "Protein X" and these oligomers also showed major neurotoxicity, thus suggesting these β-PrP oligomers could be potential therapeutic targets in the future (Simoneau et al. 2007). The one thing that is known is that there is an interaction between PrP^{c} and PrP^{Sc} for there to be propagation of further PrP^{Sc} and ultimately disease, whether there is an intermediate or not is still an interesting, on-going area of research.

1.3.2.2 Prion strains and the "species barrier"

The existence of a number of different natural prion strains and the production of laboratory adapted strains complicates prion research. Variations in the properties of the various prion strains can be misleading in comparing different studies, especially regarding infectivity, decontamination and the time to disease onset. Different strains can be distinguished by their varying susceptibility to decontamination and banding

pattern on Western blot analysis due to their different glycosylation patterns. Clinically, strain variability can also be observed by the location of PrP^{Sc} deposition within the CNS (Bruce et al. 1989), degree of spongiosis (Fraser et al. 1968, Pattison et al. 1961), incubation period in different mammals (Dickinson et al. 1968) and the ability to infect different species (Figure 7) (Béringue et al. 2008b).

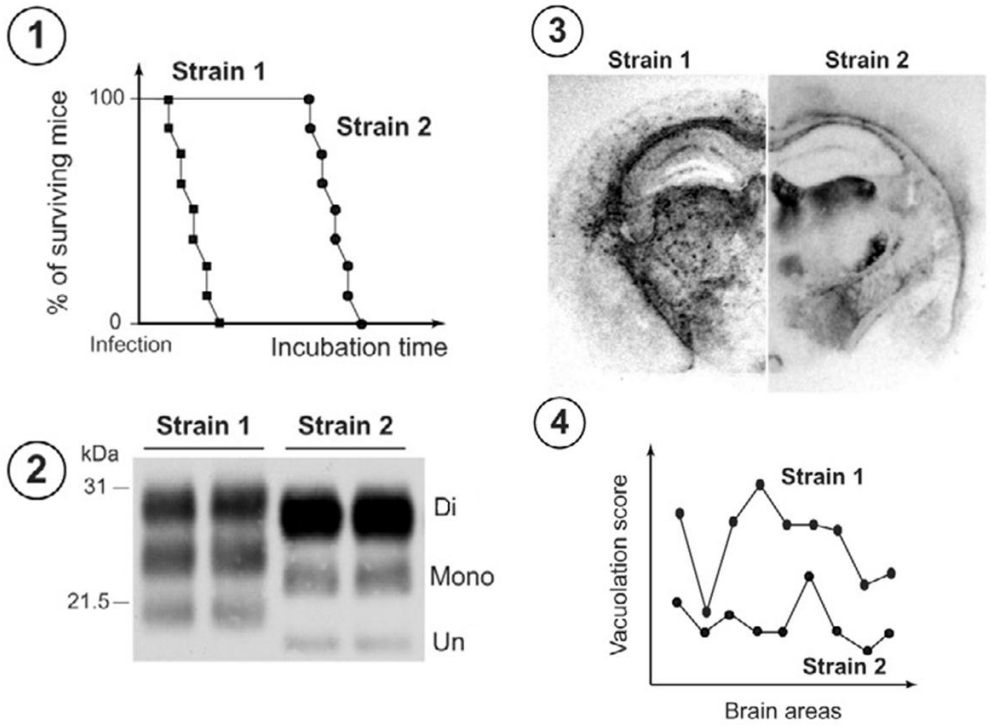

Figure 7 – Analysis of strain variation

The variation in phenotypes of two different prion strains inoculated in the same susceptible animal shown via different biochemical techniques. 1) The variations in incubation period and attack rate. 2) The difference in the banding pattern observed on Western blot analysis, showing variations in Di, Mono and Un-glycosylated glycoforms. 3) Variations in regional PrP^{Sc} deposition in immunochemically labelled histoblot brain sections. 4) The legion profiles demonstrating the differences in the distribution and intensity of vacuolation/spongiosis in standardised brain regions (adapted from Béringue et al. 2008b).

The phenomenon known as the "species barrier" describes the ability of the infectious agent to transmit disease from one species to another. Prion strain variation is observed when one prion strain is introduced into a host containing a different PrP^{c} molecule, for example the introduction of BSE prions into humans which led to the generation of infectious prions that caused variant Creutzfeldt Jacob disease (vCJD). The cross-species transmission of prions can lead to disease with prolonged incubation periods and lower attack rate over the early passages, thought to be caused by the "species barrier", and ultimately result in different disease phenotypes (Collinge et al. 2007). However, these differences in phenotype can be reversed after several sub-passages within the new host, highlighting the adaptability of prions to different hosts (Béringue et al. 2008b).

It is thought that the structural conformation, genotype, glycosylation pattern and compatibility of donor PrP^{Sc} with host PrP^{c} are the primary aspects that affect prion strain phenotypic discrimination and transmission (Bruce 1993, Carlson et al. 1989, Collinge et al. 1996, Telling et al. 1996). For example PrP^{Sc} from classical CJD does not infect wild-type mice whereas it does infect humanised transgenic mice that contain human PrP^{c}. However, vCJD that has already been passaged through a bovine host infects wild-type mice more efficiently than the classical CJD prions (Hill et al. 1997). The emergence of experimentally produced strains highlights the adaptable conformation of PrP in developing new phenotypes. The transmission of a pool of scrapie infected sheep brains (SSBP/1) into goats produced two different clinical phenotypes that were conserved after several passages and were denoted as either "drowsy" or "scratching" relating to the goats consequent behaviour pattern (Pattison and Millson 1961). This suggests that within the SSBP/1 there are at least two conformations of PrP^{Sc} that led to the production of the two phenotypes observed upon transmission to goats. This has also been witnessed in similar experiments in hamsters, where the transmission of the transmissible mink encephalopathy (TME – Stetsonville isolate) to hamsters produced, again, two phenotypes denoted "drowsy" (DY) and "hyper" (HY) (Bessen et al. 1992b). Both strains displayed differences in incubation period and PrP^{Sc} deposition. Moreover, DY remained infectious in mink following four passages in hamsters, suggesting it was the more dominant isolate within the mink population (Bessen et al. 1992a).

Small changes in the PrP gene can also lead to variations in prion strain when transmitted to a different host. Lines of inbred mice that expressed either the a or b alleles (*Prn-p*^{a} or *Prn-p*^{b}), originally known as the *Sinc*^{S7} and *Sinc*^{P7} alleles (*Sinc* standing for scrapie incubation gene), which encode two PrP proteins that have different amino acids at position 108 and 189, yield varied strains once inoculated with an infectious experimental strain (Bruce 1993, Dickinson et al. 1968). For example, a strain originally cloned in *Prn-p*^{a} mice, denoted 22C, produces a different strain denoted 22H when passaged in *Prn-p*^{b} mice. Similarly the 22A strain originally cloned in *Prn-p*^{b} mice produces 22F when passaged in *Prn-p*^{a} mice, with all strains showing slightly different phenotypes (Béringue et al. 2008b). The study of eight different prion isolates which can be propagated in Syrian hamsters demonstrated that it is possible for similarities in certain phenotypes, including denaturation and incubation time, to occur. This suggests that some of these prion isolates are similar or possess the same PrP^{Sc} confirmation, although it should be noted that differences in PrP deposition and clinical signs have been observed between these strains (Peretz et al. 2001, Safar et al. 1998). Therefore, the number of different prion conformations and real differences between some strain phenotypes is questionable. As mentioned earlier, the use of sPMCA with or without various cofactors demonstrates that prion strain conformation is altered by the cofactors present in different species (Deleault et al. 2012). The prions strains exhibited different biochemical characteristics without the presence of a cofactor however when a single cofactor was introduced all of the prion strains demonstrated the same properties suggesting it is the cofactors that are present that determine strain characteristics (Deleault et al. 2012). The different experimentally produced prion strains are summarised in Table 3.

Name	Origin	Host
ME7	Sheep scrapie[a]	Mouse (*Prn-p*^{a})
87A	Sheep scrapie[a]	Mouse (*Prn-p*^{a})
221C	Sheep scrapie[a]	Mouse (*Prn-p*^{a})
87V	Sheep scrapie[a] SSBP/1[b]	Mouse (*Prn-p*^{b})
79A	SSBP/1[b]	Mouse (*Prn-p*^{a})
79V	SSBP/1[b]	Mouse (*Prn-p*^{b})
139A[c]	SSBP/1[b]	Mouse (*Prn-p*^{a})
22C	SSBP/1[b]	Mouse (*Prn-p*^{a})
22H	Uncloned 22C	Mouse (*Prn-p*^{b})
22L	SSBP/1[b]	Mouse (*Prn-p*^{a})
22A	SSBP/1[b]	Mouse (*Prn-p*^{b})
22F	Cloned 22A	Mouse (*Prn-p*^{a})
301C[d]	BSE	Mouse (*Prn-p*^{a})
301V	BSE	Mouse (*Prn-p*^{b})
139H	Cloned 139A	Syrian Hamster
263K[e]	SSBP/1[b]	Syrian Hamster
ME7-H	Cloned ME7	Syrian Hamster
HY	TME	Syrian Hamster
DY	TME	Syrian Hamster

Table 3 – Summary of experimental prion strains

The experimental strains produced in rodents, highlighting their origin and host that the strain is cloned in. [a] Scrapie field isolate, [b] SSBP/1 sheep scrapie brain pool 1, [c] Also known as Rocky Mountain Laboratory (RML) or chandler, [d] It is possible that 301C succumbs to 301V in *Prn-p*^{b} mice, [e] Sc237 is also a subclone of 263K. (Béringue et al. 2008b)

More worryingly from a human perspective is the discovery of two variations of the BSE strain in cattle. These two atypical BSE strains have been named the H-type (due to higher PrP^{Sc} band when analysed on Western blot) originally found in eight French BSE cases, (Biacabe et al. 2004) and L-type BSE (due to lower PrP^{Sc} bands when analysed on Western blot) originally observed in two Italian BSE cases (Casalone et al. 2004). Although no transmission of these BSE strains to humans has been confirmed, unlike classical BSE, transmission of L-type BSE has been demonstrated in two different humanised transgenic mice lines; firstly *tg40* mice (overexpressing human PrP M/M at codon 129 of the Prnp gene) (Kong et al. 2008) and in *tg650* mice (Béringue et al. 2008a). These findings suggest that there is an interaction between the atypical bovine and human prions which highlights the possibility of transmission of atypical BSE to humans causing a new vCJD-like disease with a potentially different phenotype. Moreover, the ability of the infectious agent associated with chronic wasting disease (CWD) in cervids to transmit to humans is unclear. As the epidemic of CWD in North America and two Canadian provinces is still on-going this could pose a potential risk to humans in regards to the ingestion of contaminated meat as was observed with the BSE outbreak (reviewed in Sigurdson 2008).

1.3.2.3 PrP^{Sc} infectivity

The formation of PrP^{Sc} rich proteinaceous aggregates and amyloid plaques are associated with TSE pathology and thought to be involved in the fundamental neurodegeneration, however the mechanisms are still unknown. Aggregates of PrP^{Sc} are primarily found in tissues of the central nervous system. However, studies have identified PrP^{Sc} in the spleen, (Bruce et al. 2001, Doi et al. 1988) lymph nodes (Doi et al. 1988) and tonsil (Bruce et al. 2001). A number of questions have risen regarding whether it is the smaller subfibrillar oligomer deposits, the intermediate amyloid fibrils or the larger amyloid plaques that are the dominant infectious units associated with TSE's. Amyloid plaques are ordered structures formed from the non-covalent polymerisation of single protein monomers aligned in the cross-β configuration. These evolve through a number of states including dimers, trimers leading up to protofibrils and ultimately insoluble plaques (Malchiodi-Albedi et al. 2011, Shewmaker et al. 2011).

Although the outcome of the aggregating proteins in prion diseases is the development of amyloid plaques, it is not thought that the plaques are the cause of neurodegeneration. However, neurotoxicity associated with mature amyloid fibrils produced from recombinant PrP has been demonstrated (Legname et al. 2004, Novitskaya et al. 2007). Due to the loss of disease manifestation in $PrP^{0/0}$ mice it is suggested that the prion protein is involved in the infectivity of prion diseases. However, the presence of disease with no detectable PrP^{res} can question whether the PK resistant prion is the sole infectious agent (Gambetti et al. 2008, Thackray et al. 2007). It is hypothesised that smaller aggregates or small sequences of the prion protein are the neurotoxic species that, once converted from PrP^{c}, aggregate in abundance around neurons inhibiting there function causing the neurodegeneration observed (Bucciantini et al. 2002, Malchiodi-Albedi et al. 2011).

Work by Silveira et al, 2005 concluded that the most infectious protein aggregates per mass of PrP were around 17-20 nm in size and around a mass of 300-600 kDa, which are on the smaller size of protein aggregates, thus contradicting the hypothesis that the larger aggregates demonstrated increased infectivity. They also determined that if these protein aggregates were made up mainly of PrP of an average size of 21.5 kDa each, then that would be an oligomer of around 14-28 PrP molecules which is the same as the smaller infectious units that have been observed previously (Silveira et al. 2005). This potentially suggests that novel decontamination techniques need to be able to denature or break up the PrP^{Sc} aggregates to single monomers rather than breaking up the larger aggregates into intermediate more infections oligomers of 14 – 28 molecules, subsequently resulting in residual infectivity and potentially an increase in the transmission of PrP^{Sc}.

Although it is still unknown if PrP^{Sc} is the sole infectious agent in prion disease it is really the only available marker that correlates with disease infectivity. PrP^{Sc}, when compared to PrP^{c}, has altered biochemical as well as structural properties, including a partial resistance to Proteinase K, strong adhesion to many surfaces predominantly stainless steel and plastics, insolubility in most detergents and resistance to numerous chemical and physical decontamination methods including formaldehyde treatment and autoclaving at $121^{o}C$ (Jackson et al. 2005). It is these biochemical properties that

contribute to the observed difficulty in the inactivation and decontamination of PrP^{Sc}. This difficulty is the main contributing factor regarding the prevalence of acquired diseases caused by this infectious agent or infectious oligomers as suggested previously. In relation to decontamination protocols it is important that the PrP^{Sc} oligomers are broken down to either single molecules or that the proteins are denatured entirely to remove the most infectious units (Gale 2007). Proteinase K used for diagnostic tools, cleaves the infectious PrP^{Sc} at around the 90^{th} residue, leaving the C-terminal end, denoted PrP^{27-30} (corresponding to the kDa mass of the infectious subunit post PK digestion) which is the region of the PrP^{Sc} that is deemed the main disease associated sub-unit (Figure 2) (Caughey et al. 1991, Stohr et al. 2008).

1.4 Iatrogenic transmission

The iatrogenic transmission of vCJD is the primary concern of this study although a low prevalence is documented. Nevertheless, the long incubation period associated with CJD and the currently unclear effect of genetic background on disease progression and prognosis could imply there are an unknown number of carriers within the population, representing potential transmission sources. The incubation period of vCJD is to a certain degree unknown, due to variations in genetic susceptibility, but is currently estimated to be around 12 years; however, if compared to Kuru, with the potential of up to 50 years in a minority of cases, then the incubation period could be relatively longer than initially thought (Collinge et al. 2006). Furthermore, the initial interim data from the analysis of PrP^{Sc} prevalence in appendix specimens suggests that there could be potentially 18,000 carriers of the infectious prion within the UK population (Hilton et al. 2004, HPA 9 September 2011). However, more recent results from a second appendix study suggests there could be as many as double (1/2000 compared to 1/4000) the number of carriers in the UK as was initially proposed (Data from the Advisory Committee on Dangerous Pathogens (ACDP)). Therefore, the number of estimated carriers and the potential for long incubation periods suggests there is still an increased risk of iCJD transmission.

The first documented case of iatrogenic CJD involved a corneal transplant from an undiagnosed CJD patient in 1974 (Duffy et al. 1974). The most common iatrogenic transmission routes since this study are cadaveric dura mater grafts (136 cases worldwide) and the inoculation of prion contaminated human growth hormone (162 cases) extracted from the pituitary gland of CJD infected patients (Furtner et al. 2008, Will 2003). Other reported modes of transmission include infected blood transfusions, (Hewitt et al. 2006, Llewelyn et al. 2004, Wroe et al. 2006) infected tissue transplants (Aguzzi et al. 2008, Lemmer et al. 2008) and an increased risk from contaminated instruments during surgery on the spinal cord (Bosque et al. 2002). Infectious prions have also been found in urine (Andrievskaia et al. 2008, Gonzalez-Romero et al. 2008, Van Dorsselaer et al. 2011) and faeces (Maluquer de Motes et al. 2008) of infected animals. Levels of prion are around 10 fold less in urine than infected blood samples, although this could still pose a risk of disease transmission in both animals and humans.

At present there is still concern over the risk of transmission of PrP^{Sc} from inadequately decontaminated surgical instruments after potential use in asymptomatic CJD patients (Lipscomb et al. 2006e, Murdoch et al. 2006). The resistance of PrP^{Sc} to sterilisation was highlighted by the study of surgical electrodes that became infected from an unknown CJD patient. These were decontaminated following standard hospital sterile service department (SSD) protocols and used in two further patients, who both developed CJD. These electrodes were experimentally reprocessed following SSD standards and implanted in the brain of a test chimpanzee, which also subsequently developed CJD (Gibbs et al. 1994). This work demonstrated that despite numerous decontamination cycles PrP^{Sc} still remained intact and infectious. Iatrogenic vCJD is rare but as more modes of transmission have been reported it has become a greater health issue. Especially as recent reports of the transmission of PrP^{Sc} from blood and blood products, suggesting that any surgery where an instrument comes in contact with human tissue potentially infected with PrP^{Sc} could transmit the disease (Hewitt et al. 2006, Wroe et al. 2006). Furthermore, the transmission of PrP^{Sc} from surgical stainless steel has been clearly demonstrated in both animal infectivity bioassays and more recently in cell culture assays (Edgeworth et al. 2009, Fichet et al. 2007b, Flechsig et al. 2001, Yan et al. 2004).

Protease-resistant prions bind to many surfaces, including stainless steel, and display a marked resistance to conventional methods of decontamination used in SSDs (Lemmer et al. 2004). Conventional methods will breakdown and remove most of the blood, protein and biofilm contamination, but are less effective at the removal of proteinaceous and potentially prion based contamination (Murdoch et al. 2006). Poor decontamination methods and standard controls used in hospital sterile service departments have been demonstrated to be potential risk factors influencing iCJD transmission (Howlin et al. 2010, Lipscomb et al. 2006d, Lipscomb et al. 2006e, Ungurs et al. 2010). Moreover, some decontamination chemistries, when combined with autoclaving at 121^{o}C for 30 minutes, were demonstrated to be less effective than autoclaving alone, suggesting a chemistry-dependent protective effect on the infectious agent (Jackson et al. 2005). Standard tissue fixation methods based on formalin or aldehydes were found to preserve PrP^{Sc} infectivity on surfaces due to its proteinaceous nature (Stephenson 2007). Furthermore, it is hypothesised that formaldehyde treatment cross links the proteins, thus holding together the PrP monomers, potentially forming oligomers containing 14-28 PrP molecules which have previously demonstrated increased infectivity when compared to other disease associated aggregate sizes (Gale 2007, Silveira et al. 2005). Treatment with 1-2 M NaOH or 2% NaOCl for 24 hours has been demonstrated to inactivate PrP^{Sc}. However, from a practical standpoint in terms of SSD management, using such concentrated alkaline solutions has a detrimental effect on instrument integrity and is particularly incompatible with box joints, carbide jaws, gold-coated handles and is completely incompatible with electronic equipment and endoscopes (Brown et al. 2005, Fichet et al. 2007b, Lemmer et al. 2004, McDonnell et al. 2003).

1.5 Prion decontamination

Although heavily researched there is no current cure for this fatal disease and the minimum infectious dose required for CJD transmission is unknown (McDonnell and Burke 2003). Therefore, it is crucial that a precautionary principle is adhered to regarding the risk that instruments may not be decontaminated to a high enough standard to prevent infection (Secker et al. 2012a). Furthermore, prion protein

aggregates have been visualised by direct instrument staining to accumulate in the imperfections within stainless steel surfaces providing greater concerns regarding contamination and potential infectivity in older, damaged equipment (Herve et al. 2010, Jackson et al. 2005). The easiest way to reduce the risk of iCJD is to improve hospital policy's and to make sure that all instruments used on suspected CJD patients are quarantined and destroyed or to implement single use instruments in high risk surgeries (McDonnell and Burke 2003). However it is neither practical nor cost effective for all instruments to be single use, especially due to the intricate nature of many instruments used in neurosurgery. As such it is important to address current SSD decontamination policies. Certain steps have already been taken by the English Department of Health (DH) and the Spongiform Encephalopathy Advisory Committee (SEAC) to decrease iatrogenic transmission. These include the destroying and/or quarantining of all surgical equipment that has been in contact with known or suspected CJD patients and the upgrading of SSD's across the UK, in regards to decontamination protocols and the introduction of novel, specialised prion sterilisation techniques (Stephenson 2007).

Currently many instruments are processed at centralised SSDs and decontaminated through washer-disinfector cycles. There are a number of areas of concern during the decontamination process of surgical instruments. Recent publications have highlighted a significant reduction in the efficacy of the decontamination process if a soiling is allowed to dry onto a surface (Howlin et al. 2010, Lipscomb et al. 2007b, Ungurs et al. 2010). Studies have demonstrated that a drying time of 15 minutes or longer significantly increases both residual protein and prion-associated amyloid biofouling following decontamination, relative to a surface which was cleaned immediately (Secker et al. 2011). Furthermore, to address long processing times often associated with the use of a centralised SSD system, it was demonstrated that storing instruments in a moist environment post contamination for up to 24 hours greatly reduced both protein and prion-associated amyloid bio-burden when compared to storage in atmospheric conditions (Secker et al. 2011). This highlighted how simple, cost effective changes in current hospital practice could improve decontamination and therefore reduce the risk of iCJD transmission.

Washer-disinfector cycles involve 3 main steps; a pre clean or pre-soak, usually in an enzymatic cleaner or pre-soak gel, followed by a water rinse and main wash in either an alkaline or enzymatic cleaner and a final disinfection step in deionised water at 90^{o}C. After the washer-disinfector phase, instruments are sterilised through an autoclave cycle before visual checks to confirm the instrument is clean for use. Instruments are processed within their surgical sets in large trays with no brushing or mechanical removal step and therefore there is no guarantee that all of the instruments surfaces will be cleaned evenly or efficiently during this process. The cleaning chemistries used within these cycles have been tested within both small laboratory washer-disinfectors and simulated cycles within the lab. Both of these studies relied on different detection methods for remaining contamination but agreed that the lowest levels of protein and prion-associated amyloid contamination was observed when an alkaline cleaner was used in the main wash (Howlin et al. 2010, Ungurs et al. 2010). Both studies also confirmed that prevention measures (either a pre-soak gel or pre-clean step) to ensure that surface soiling was not permitted to dry increased the efficacy of further decontamination steps and greatly reduced residual contamination thus correlating with the results of the wet vs. dry study (Secker et al. 2011).

Murdoch et al, 2006 concluded that SSD washer disinfectors showed better decontamination results compared to hand washing of the surgical instruments, however the inadequate SSD decontamination highlighted in this study was likely caused by the poor cleaning chemistries or poor knowledge of optimal conditions for protein decontamination or poor maintenance of the washer/disinfectors. Another practice that has potential adverse effects on instrument contamination that has been documented is the handling of instruments, post decontamination, by SSD staff who do not, in standard practises, wear gloves. Whilst not an issue with regards to microbial contamination of the instrument surfaces by normal skin flora due to the fact that instruments go through a sterilisation process after handling, it has been described that touching the instruments with bare hands increases the proteinaceous bio-burden which, during the subsequent sterilisation process, will get hardened onto the instrument and potentially decrease the efficacy of further decontamination procedures during repeat use (Howlin et al. 2009). These proteinaceous deposits could in time harbour infectious prions increasing iCJD risk.

A number of enzymatic cleaning chemistries have also been tested for the removal of prion infected brain homogenate from stainless steel surfaces. Data demonstrated that there were significant discrepancies between the contamination remaining following the different enzymatic cleaners, suggesting that better knowledge of each commercially available cleaner is key to improving decontamination (Herve et al. 2010). Importantly however, this study only tested residual contamination and not the infectivity of the remaining biofouling which is key due to the uncertainty over the nature of the infection agent. Two different infectivity assays have previously been utilised to assess the levels of infectivity remaining after decontamination in commercially available cleaning chemistries. Studies using the 263K hamster infectivity assay have determined that although enzymatic cleaners have the capacity to remove significant concentrations of soiling, they did not reduce the levels of infectivity. This is in contrast to an alkaline cleaner which was demonstrated to greatly reduce residual soiling in addition to infectivity (Fichet et al. 2007b, Yan et al. 2004). Importantly, contradictory results have been obtained using another infectivity assay using the same alkaline chemistry. In this study, the standard steel-binding assay (SSBA) using N2a-PK1 cells and RML infected brain homogenate demonstrated that the contamination remaining after the same alkaline cleaner treatment used by Fichet et al. 2007 had a significantly higher level of residual infectivity compared to other products and 2 M NaOH treatment (Edgeworth et al. 2011b). Thus, both of these assays relying on two different detection methods and two different prion strains showed contradicting results highlighting the importance of experimental design in the interpretation of infectivity data and decontamination efficacy.

There are a number of scientific groups researching novel prion decontamination techniques which could either be incorporated into current protocols or could be employed as specialised techniques for prion decontamination. Work by Fichet et al, 2007 experimented with liquid and gaseous hydrogen peroxide treatments. Fichet et al, 2007 discovered that using gaseous hydrogen peroxidise treatment on 263K hamster scrapie prion and mouse 6PB1-adapted BSE strain inoculated on stainless steel wire models in hamsters completely attenuated disease transmission, reducing infectivity by >5.5 log lethal doses compared to no gaseous hydrogen peroxide treatment. Vaporised

hydrogen peroxide decontamination demonstrated a reduced 263K infectivity of 4.5 log lethal doses without damaging electronic components (Fichet et al. 2004). Other examples include studies by Jackson et al, 2005 and Weissmann et al, 2002, which tested seven different proteolytic enzymes for the decontamination and degradation of PrP^{Sc}. The most promising results from these studies indicate that a combination of PK and Pronase (a combination of proteases taken from the extracellular fluid of *Streptomyces griseu*) in conjunction with SDS removed PrP^{Sc} to below the limit of Western blot detection and significantly reduced infectivity in Tg20 PrP^{c} overexpressing mice (1/18 mice developed disease) with a complete attenuation of disease transmission in the CD-1 mouse model (Jackson et al. 2005). Jackson et al, 2005 also showed that autoclaving at 134^{o}C with a weak alkali, such as NaOH reduces the infectivity of 263K hamster-adapted scrapie prion on wires with only 1 out of 10 hamsters showing signs of disease post intracranial implantation. Fichet et al, 2004 showed autoclaving at 134^{o}C in only water demonstrated an infectivity reduction of 5.6 log lethal doses of 263K and without water an infectivity reduction of 4.4 log lethal doses. Other novel decontamination methods include photocatalytic degradation using photo-fenton reagents which breaks down the prion by photo induced oxidative intermediates, which has demonstrated reduced prion contamination below immunoblotting detection range (Paspaltsis et al. 2009). The use of proteases has also been tested for prion decontamination. The protease MC3, a genetically modified protease engineered from *Bacillus lentus subtilisin,* has been shown by Western blot to reduce contamination levels of BSE strain 301V at alkaline pH (Dickinson et al. 2009). A further study has claimed that a secreted protease from *Aeropyrum pernix* (a hyperthermophilic marine archeon) has the ability to digest PrP^{Sc} from mouse, bovine and human prion strains and may show promise as a novel decontamination agent (Alper et al. 1967).

In addition to the improvement or introduction of novel decontamination protocols, advances have also been made in modifications to instrument surface chemistry. Alternative anti-burden coatings consisting of diamond-like carbon (DLC) that can be incorporated onto surgical instruments have demonstrated a reduction in the initial attachment of protein and prion and, as a consequence, an improvement in subsequent decontamination efficacy (Secker et al. 2012b). The diamond-like carbon (DLC) coating study investigated several DLC coated stainless steel tokens doped with

various chemical elements and their effect on contamination and decontamination efficacy of prion biofouling. DLC coatings alone have a number of useful properties within a surgical environment including improved biocompatibility, low friction, hard wearing, high chemical inertness, low corrosion and increased smoothness (Roy et al. 2007). Of particular benefit is that DLC has an amorphous structure which allows the doping of a number of different elements at different concentrations, enabling modification to the surface energies and hydrophobicity of the DLC surface. The doping of DLC with elements has been shown theoretically to produce the right surface conditions for reducing protein adhesion (Borisenko et al. 2008). The integration of silicon and nitrogen to DLC surfaces has also shown a reduction in the attachment of bacterial biofilms, especially with nitrogen doping, compared to un-doped DLC (Liu et al. 2008). Furthermore the incorporation of silicon in DLC improves the friction wear and shows lower corrosion compared to DLC alone (Kim et al. 2008). This study demonstrated that doped DLC coated tokens reduced ME7-scrapie prion attachment and improved decontamination; however different doped tokens showed varying results depending on the cleaning chemistry used (Secker et al. 2012b). This highlights the potential of a new generation of surgical instruments that could reduce the risk of iCJD without the need of changing current decontamination protocols.

1.6 Prion detection technologies

To properly utilise the research and development of new decontamination protocols there needs to be a standard comparable method of detection for accurate comparison. Current prion detection technologies are split into two categories: those that detect PrP^{Sc} or prion-associated amyloid, or those assays which evaluate infectivity, primarily studied using animal infectivity bioassays (Fichet et al. 2007b, Lawson 2008). However, more recently technologies have moved towards the use of cell-based assays. The original methods used for prion detection on surgical instruments assessed total protein presence, including the ninhydrin chromogenic and biuret assays, in conjunction with visual assessment of surgical instrument contamination which have been reported to be grossly insensitive at detecting the protein contamination accurately (Lipscomb et al. 2006b). There is currently no set standard for prion detection and there is room for

improvement of current techniques and the production of novel methods. The following section highlights the key techniques used in the field.

1.6.1 Detection of prion proteins

A number of techniques, both standard and novel have been produced to detect the presence of the prion protein or other markers of prion disease including amyloid plaques. These include Western Blot, Enzyme-linked immunosorbent assay (ELISA), Immunohistochemistry (IHC), Conformation-dependant immunoassay (CDI), Fourier transform infrared spectroscopy (FT-IR) (Reviewed in Sakudo et al. 2007) and mass spectrometry (MS) to name a few (Silva et al. 2011). However, this section is going to concentrate on Western Blot detection of PrP^{Sc}, as it is the most widely used method for prion detection and the SYPRO Ruby/Thioflavin T (SR/ThT) dual stain as it is the most relevant technique to this study.

1.6.1.1 Western blot

Western blot detection of PrP^{Sc} has been the most widely used method for prion detection. This involves the forceful removal of contamination from a surface or instrument being assessed, or from the detection of PrP^{Sc} within infected brain homogenates, cell lysates and formalin fixed or fresh tissue (Nicholson et al. 2007). Samples are firstly digested with proteinase K (PK) to breakdown the PK sensitive PrP^{c} and leave the PK resistant region of PrP^{Sc} (PrP^{res} or $PrP^{27\text{-}30}$) for immuno-detection. Briefly, the digested proteins are separated on a SDS/polyacrylamide gel, blotted overnight and immunochemically stained using one of many commercially available prion specific antibodies. The PK digestion is required because currently there are no commercially available antibodies which distinguish between PrP^{c} and PrP^{Sc}. Some groups have claimed to have produced PrP^{Sc} specific antibodies, for example 15B3 from Prionics, but further studies have highlighted problems in their design (Korth et al. 1997). 15B3 and three other motif-grafted monoclonal antibodies were shown to react to both infectious and non-infectious residues of the prion protein, suggesting a lack of

specificity to the resistant core of PrP^{Sc} alone (Biasini et al. 2008). Different prion strains demonstrate different intensities of the three glycoforms of PrP^{Sc} (di-glycosylated, mono-glycosylated and un-glycosylated) which can be mapped using Western blot (Grassi et al. 2008). As a result, Western blotting can also be used to characterise different prions strains by utilising a range of antibodies which bind to different regions of the prion protein. Although Western blotting is widely utilised it has a limited sensitivity of detection of around 100ng of PK digested prion using chemiluminescence detection (Herve et al. 2009, Lipscomb et al. 2007a). Furthermore, the need to forcefully remove prion contamination from a test surface before PK digestion can give inaccurate results due to the inherent variability in the removal process and the methods used. Western blot detection is also an *in vitro* detection method. Whilst this is useful for the study of prion removal, results have been shown to correlate poorly with *in vivo* animal infectivity bioassays (Fichet et al. 2007b, Howlin et al. 2010).

1.6.1.2 SR/ThT dual stain

A novel technique involving the use of Episcopic differential interference contrast microscopy (EDIC) coupled with epi-fluorescence (EF) to detect both stained protein and prion-associated amyloid contamination on instruments or experimental metal token surfaces has been studied at the University of Southampton (Keevil 2003, Lipscomb et al. 2006c). Differential interference microscopy (DIC) is used to produce rapid, pseudo 3-dimensional images of specimens without the need of taking optical slices. Briefly, plane-polarised light is produced by passing the light beams through a polarizer situated beneath the stage condenser. This light then travels through a Nomarski-prism which splits that light beam into two perpendicularly vibrating rays. These rays travel in parallel until they come into contact with the specimen at which point the wave path of the rays of light are altered by the surface properties and refractive index of the sample. The beams of light pass through the objective lens where the beams are focused and passed through a second prism which unites the two separate beams. These beams then travel through another polarizer to create interference that brings the beams into the same focal plane and axis which can then be viewed through the eyepiece as the highly contrasted 3-dimensional image. DIC relies on transmitted

light that requires transparent samples and oil immersion that poses difficulties when analysing contamination on solid, opaque surfaces. EDIC microscopy relies on the rearrangement of the DIC concept where one DIC polarizer is positioned in one of the filter bloc cubes above the stage and an adjustable analyser is fitted between the DIC block and the eyepiece (Keevil 2003). The adjustable analyser can be removed and the DIC filter block replaced for the use of the microscope for EF analysis that can be coupled with the EDIC images (Keevil 2003). Furthermore, the EDIC microscopes are fitted with long distance working lenses that negate the need for coverslips and oil immersion (Keevil 2003). The use of episcopic light and the long distance lenses allows the EDIC analysis of opaque, curved solid samples such as surgical instruments, surgical surfaces and leaves. Furthermore, the EF analysis of protein, amyloid or microbes can be coupled with the EDIC analysis of the surface for the correlation of surface topography with contamination (Herve et al. 2009, Herve et al. 2010, Lipscomb et al. 2006c, Lipscomb et al. 2006d, Secker et al. 2011, Secker et al. 2012b, Warner et al. 2008).

Using EDIC/EF, the use of SYPRO ruby (SR – A protein blot stain usually used for staining total protein on Western blot membranes) as a rapid method for the detection of protein contamination on stainless steel instrument surfaces was reported (Lipscomb et al. 2006c). Subsequently Lipscomb et al 2007 went on to develop a staining protocol to detect prion-associated amyloid contamination on surgical surfaces. This method involves the use of either of two thiazole derivatives, Thioflavin T (ThT) and Thioflavin S (ThS) (Lipscomb et al. 2007a). Thiazole derivatives and Congo red are known stains that readily bind to amyloid fibrils (Kroes-Nijboer et al. 2009, Maezawa et al. 2008). One significant benefit of ThT in fluorescent microscopy is that it possesses a large Stoke's shift when bound to amyloid, compared to ThS, which improves its contrast against background autofluorescence (Colby et al. 2007). Amyloid fibrils are formed from the polymerisation of β-sheets that run in both parallel and anti-parallel directions forming rows and subsequently neat channels that have been proposed as the binding sites for ThT which is thought to bind in parallel to these channels (Wilesmith et al. 1992). Due to the size of ThT and the channels, it is only possible for the ThT molecules to fit in one direction and it is this conformation of the ThT within these channels that yields the highest levels of fluorescent emission (Wilesmith et al. 1992). Interestingly, ThT has also been demonstrated to form micelles at higher concentrations

in aqueous solutions (Bradley and Brown 2012). It has been observed using atomic force microscopy (AFM) that these ThT micelles bind in the channels of the amyloid fibrils and therefore show increased fluorescent properties (Bradley and Brown 2012). Therefore, Thioflavin T is used in this protocol as it will bind to prion rich amyloid thus, detecting the presence of prion contamination; however, ThT is not specific to prion-associated amyloid but it will also bind to amyloid aggregates formed in AD and other neurodegenerative diseases. Lipscomb et al, 2007a concluded that ThT staining visualised using EDIC/EF was at least 2 logs more sensitive than Western blot for the detection of prion contamination. Recently these two stains were brought together to produce a SR/ThT dual stain which was able to detect protein and prion-associated amyloid contamination down to less than 1ng *in situ* on surgical instruments maintaining the increased sensitivity previously reported by Lipscomb et al. 2007a over the Western blot technique (Herve et al. 2009).

1.6.2 PrP^{Sc} amplification methods

One of the biggest breakthroughs in the research of prion detection methods has been the development of methods to artificially amplify small, undetectable levels of PrP^{Sc} to levels that can be detected via standard techniques such as Western Blot or ThT fluorescence. However these techniques, although very useful do have their limitations which are discussed within the next sections.

1.6.2.1 Protein misfolding cyclic amplification (PMCA)

To address the problem of low sensitivity in current detection methods an innovative technique has been developed that amplifies the low levels of PrP^{Sc} in dilute samples prior to detection using Western blot. Protein misfolding cyclic amplification (PMCA) relies on a similar logical process as the polymerase chain reaction (PCR), where the template-assisted model of prion propagation is utilised to amplify levels of PrP^{Sc} (Grassi et al. 2008, Saborio et al. 2001). Samples potentially containing PrP^{Sc} are incubated with large quantities of PrP^{c} from the same species. This initiates the

formation of PrP^{Sc} - PrP^{C} protein aggregates which are then broken down to smaller PrP^{Sc} aggregates/single proteins by sonication thereby seeding further conversion reactions (Saborio et al. 2001, Soto et al. 2005). These steps are repeated until a detectable level of PrP^{Sc} is reached via the detection of PrP^{res} utilising WB analysis. The theory of these reactions suggests there should only be PrP^{Sc} amplification if there is infectious prion present in the sample in the first place.

PMCA has been demonstrated to amplify various prions strains including 263K, BSE, sCJD, vCJD, RML (Rocky Mountain laboratory derived mouse scrapie) and goat scrapie (Saborio et al. 2001, Soto et al. 2005). Following this, Soto's group studied the infectivity of various amplified prion strains following 20 cycles of PMCA. It was concluded that the artificially amplified prions displayed the same infectious properties as their parental PrP^{Sc} samples, suggesting that PMCA does not alter the biochemical properties or conformation of PrP^{Sc} (Castilla et al. 2008). PMCA has also been used to amplify PrP^{Sc} after dry heating and autoclave inactivation to determine if these methods removed and/or denatured the prion. This work was confirmed by analysis of the samples utilising infectivity bioassays which correlated with the WB PrP^{Sc} detection after PMCA (Murayama et al. 2006).

Adaptations to the original PMCA protocol have been made to improve the sensitivity and speed of the reactions. Serial PMCA (sPMCA) involves the same underlying protocol as standard PMCA with the exception that after every 10 rounds the reaction mixture is diluted with normal hamster brain homogenate to restock the depleted PrP^{c} levels to instigate more PrP^{Sc} conversion and therefore improve sensitivity of this assay (Weber et al. 2007). The sPMCA assay produced infectious prions with the same characteristics as the original prion seed and no loss of PrP^{Sc} infectivity in animal infectivity models (Weber et al. 2007). Another adaption of PMCA, denoted PMCAb, involves the incorporation of small beads of differing materials into the assay. This has two beneficial effects. Firstly, PrP^{Sc} will favourably bind to some of the bead surfaces, thus, concentrating the PrP^{Sc} molecules within a sample. Secondly, during the sonication stages the nano-beads will further aid the breakup of PrP^{c} and PrP^{Sc} aggregates producing a favourable environment for further propagation (Gonzalez-Montalban et al. 2011). Different beads instigate varying rates of amplification of

different prion strains, therefore it is crucial to understand which beads are required for the optimal amplification of the prion strain that is being assessed (Gonzalez-Montalban et al. 2011).

Although PMCA is a useful tool it does present some limitations. It is difficult to obtain large amounts of PrP^{c} from specific species samples (Grassi et al. 2008). Whilst recombinant PrP can be used, it is not fully understood whether this may alter the structure of PrP^{Sc} in unknown ways or introduce false amplification within the assay. The other limitation is that the infectivity of amplified PrP^{Sc} appears to drop with increasing PMCA cycles up to and over three. This could suggest that PMCA is not just amplifying PrP^{Sc} but it is also altering its properties or conformation (Murayama et al. 2006). Critically however, a study by Deleault et al, 2007 managed to use PMCA to form *de novo* infectious prion in a prion free environment with no PrP^{Sc} seed. They used the PMCA reaction with only PrP^{c} and co-purified lipid molecules and managed to form infectious PrP^{Sc} within 16 rounds of PMCA. This potentially highlights a severe drawback in the PMCA technique demonstrating that PMCA can produce artificial infectious molecules after excessive amplification rounds under the right conditions, therefore questioning the reliability of PMCA based assays (Deleault et al. 2007).

1.6.2.2 Real-time quaking induced conversion assay (RT-QUIC)

The Real-time quaking induced conversion assay (RT-QUIC) is an amalgamation of two different assays; the quaking induced conversion assay (QUIC) (Atarashi et al. 2008) and the amyloid seeding assay (ASA) (Atarashi et al. 2011a, Colby et al. 2007, Wilham et al. 2010) to produce an assay that amplifies prions with a highly sensitive method of detection. The QUIC method involves the amplification of PrP^{Sc} by incubation with recombinant PrP^{c} in order to solve the issue of poor availability of large quantities of natural PrP^{c}. The amplification is induced by the periodic shaking or quaking of the sample to break-up formed aggregates and therefore induce further PrP^{Sc} conversion (Atarashi et al. 2008). Instead of Western blot detection, the ASA technique is used to increase detection sensitivity. This method involves the detection of amyloid production as a pathological marker of prion propagation using ThT

fluorescence detected via spectroscopy (Colby et al. 2007). The RT-QUIC assay has demonstrated improved sensitivity and has no observed issues when compared to PMCA regarding the observation of the spontaneous production of *de novo* prions. However, one concern that has arisen pertains to the question of how much of the amplification of PrP^{Sc} using a recombinant PrP^{c} source and subsequent amyloid detection relates to prion infectivity (Wilham et al. 2010). Nevertheless, RT-QUIC has demonstrated a sensitivity matching animal bioassay models with an additional benefit of the ability of RT-QUIC to obtain results in several days compared to the hundreds of days required for standard animal bioassays. In addition, RT-QUIC has demonstrated 100% specificity and 80% sensitivity of PrP^{Sc} detection in cerebral spinal fluid (CSF) samples from sCJD patients (Atarashi et al. 2011b, McGuire et al. 2012). The RT-QUIC assay has also established the detection of prion amplification from 263K, nasal lavage from HY TME samples, CSF from 263K infected hamsters, scrapie and CWD samples (Wilham et al. 2010). Furthermore, RT-QUIC has been adapted to involve an immuno-precipitation step utilising the prion-specific monoclonal antibody 15B3, for the sensitive detection of vCJD prions in blood plasma (Orrú et al. 2011).

1.6.3 Detection of PrP^{Sc} in blood

Since the heightened concern over the risk of vCJD transmission from infected blood transfusions, there has been an increase of research into methods capable of detecting PrP^{Sc} in blood. The use of substrates to capture PrP^{Sc} within blood samples prior to detection seems to be the crucial step for these assays. The immuno-precipitation of prions within the blood samples uses antibody labelled beads to capture PrP^{Sc}, which can then be detected using an improved ELISA sandwich method allowing for the sensitive detection of PrP^{Sc} in vCJD spiked whole blood without the use of PK digestion (Tattum et al. 2010). This is of particular relevance as the detection of disease with PrP^{Sc} sensitive to PK digestion has been noted (D'Castro et al. 2010, Kuczius et al. 1999, Pastrana et al. 2006, Thackray et al. 2007). The use of a magnetic bead system, called Magnabind beads or magnetite nanoparticles, has been utilised to capture and remove PrP^{Sc} from biological samples that can then be detected using PMCA and WB

detection (Miller et al. 2011). However, whilst this technique has the potential for the detection of prions in vCJD bloods, it has not yet been validated.

There are two promising techniques for the detection of vCJD infected blood regarding increased sensitivity and specificity above other techniques. Enhanced RT-QUIC, that has involved the specific detection of vCJD in plasma (but not whole blood) has demonstrated a detection limit of 10^{-14} fold dilutions of vCJD in plasma (Orrú et al. 2011). The second technique is the use of a solid state matrix, containing stainless steel particles used to capture the PrP^{Sc} from vCJD infected blood, allowing the sensitive detection of PrP^{Sc} using super signal ELISA (Edgeworth et al. 2011a). This technique has demonstrated the ability to detect both vCJD and sCJD infected whole blood samples from a cohort of 190 masked bloods with 100% specificity showing its potential as a blood screening technique (Edgeworth et al. 2011a). However this technique is ~10,000 fold less sensitive than the enhanced RT-QUIC assay (Edgeworth et al. 2011a, Orrú et al. 2011). Whilst these techniques are valuable tools for the detection of the potential for blood transmission of vCJD, they cannot demonstrate the infectivity of the prions within the blood samples and therefore the real risk of vCJD transmission.

1.6.4 Detection of PrP^{Sc} infectivity

1.6.4.1 Infectivity Bioassays

The methods described previously are the foremost methods used for detecting the presence of PrP^{Sc} within a sample or on a surgical instrument, but they do not detect the infectivity of the remaining contamination. The only current methods used to detect prion infectivity are animal infectivity bioassay models (Fichet et al. 2007b, Grassi et al. 2008, Lawson 2008, Lemmer et al. 2008). Bioassays involve the controlled infection of small rodents, usually mice or hamster. The samples are introduced to the animal by an injection of an infected sample or brain homogenate via the intracranial route, or by

inserting pre-infected wires, as instrument models into the prefrontal sub-cortical region of the rodent's brain (Figure 8) (Fichet et al. 2007b, Grassi et al. 2008). The animals are then left, typically for 365 days or until they succumb to disease. At this point, common detection methods, such as Western blot and immunohistochemistry, are used to determine the presence of PrP^{Sc} and TSE disease symptoms. Fichet et al, 2007b used infectivity bioassays to study the effects of heat and chemical decontamination on prion infectivity and also the difference between 263K and 6PB1 prion homogenates tested *in vivo*. Their conclusions showed that there were no discrepancies in the resistance of 263K and 6PB1 to various decontamination methods. This has been contradicted by the work of others including Giles et al, 2008 where they have shown differences in the resistance of the same prion strains to different decontamination methods, highlighting the importance of understanding the efficacy of different decontamination protocols on different prion strains.

A significant limitation of the animal bioassay model is that it relies on Western blot detection which has previously reported low sensitivity. Additionally, the use of wires implanted into the brain could pose problems because the prion contamination could be partially removed during implantation. Moreover, implantation wires have been proven to be easier to decontaminate relative to bigger, flat stainless steel surfaces and so represent a poor model to replicate the complexities of surgical instruments (Lipscomb et al. 2006a). Furthermore, the problem with current animal infectivity bioassays is there suitability to only analyse the infectivity of animal prion strains, which previously seemed like a good model for vCJD. However, recent studies have demonstrated variations in the resistance of different prion strains to different decontamination strategies (Giles et al. 2008, Peretz et al. 2006). This questions whether animal prion strains are valid models for vCJD decontamination and inactivation and opens the scope for novel infectivity assays that have the ability to assess the infectivity and decontamination of vCJD.

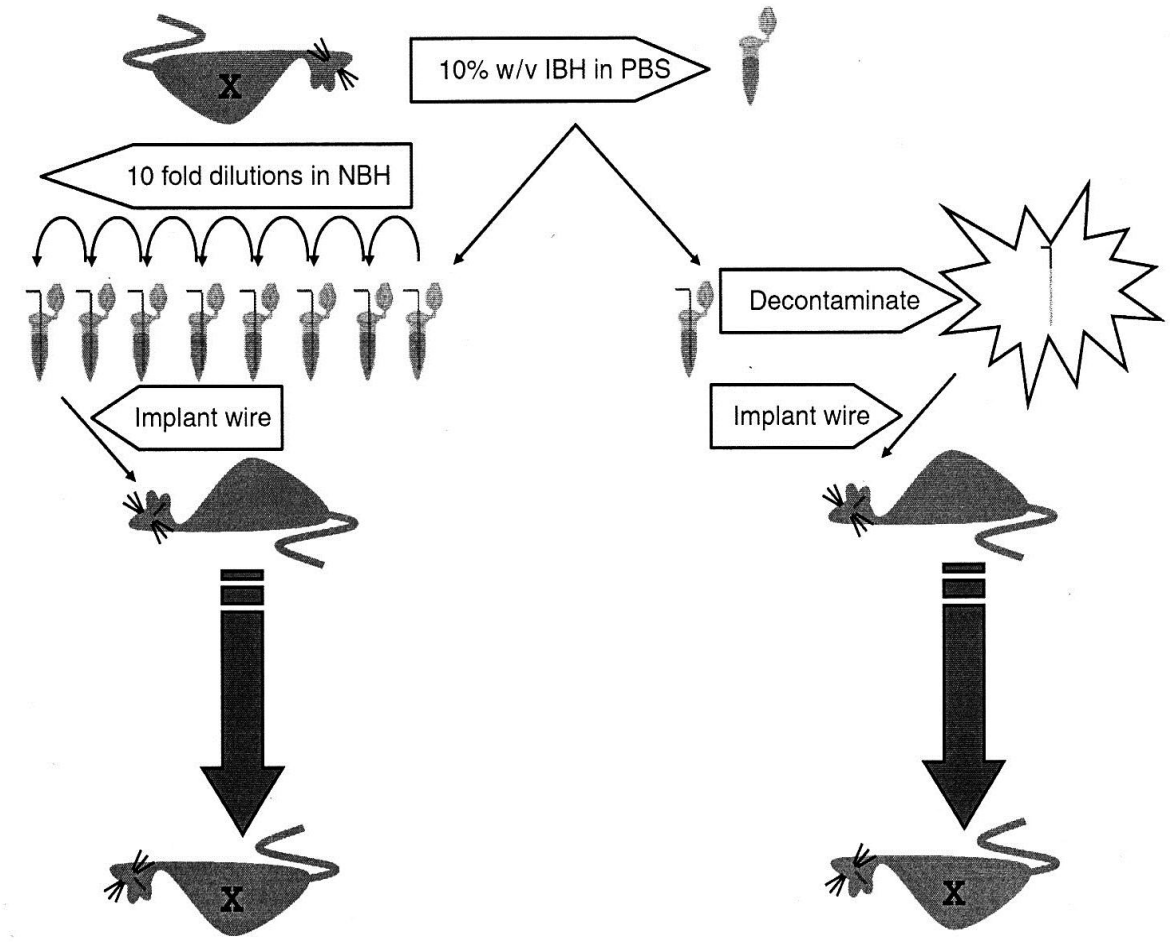

Figure 8 – Schematic of animal infectivity bioassays

A schematic diagram of model PrP^{Sc} animal infectivity assays for the determination of PrP^{Sc} infectivity and decontamination. The infectivity of infected brain homogenate (IBH) is either tested by serial dilution in normal brain homogenate (NBH) or from IBH inoculated wires. (adapted from Lawson 2008)

1.6.4.2 Cell culture assays

There are currently a large variety of prion detection methods, but all have limitations. Some lack sensitivity, whilst others are not specific enough. Moreover, no method is currently capable of assessing both infectivity and prion presence *in situ.*

New cell-based assays have the potential to detect the infectivity after decontamination of both animal and human prions without the need to remove contamination from instruments prior to analysis (Reviewed in Solassol et al. 2003, Vilette 2008). Another advantage of utilising cell culture systems for the detection of prion infectivity is that different cell lines are susceptible to infection from different prion strains. A sensitive detection method can then be utilised to detect the prion propagation or accumulation within the cell as a marker of infectivity. Table 4 highlights a number of neuronal cell lines and the prion strains that have been transmitted to these cells. However, a single cell line has not yet been demonstrated to be capable of being infected by more than a few prion strains and so far only one cell line has demonstrated the ability to detect infectivity from CJD samples. Therefore the method of detection has to be transferable between different cell lines to improve the dynamic range of prion strains that can be analysed.

			Prion strains or isolates																
Cell type	**Species**	**Tissue or cell of origin**	**Chandler**	**Compton**	**RML**	**139A**	**22L**	**22F**	**ME7**	**C506**	**301C**	**Rodent-BSE**	**Fukuoka-1**	**SY**	**CJD**	**Scrapie**	**263K**	**CWD**
N1E-115	Mouse	Neuroblastoma	■							■								
C-1300	Mouse	Neuroblastoma	■															
N2a	Mouse	Neuroblastoma	■		■								■					
N2a #58	Mouse	Subclone of N2a	■			■	■						■					
N2a-PK1	Mouse	Subclone of N2a			■		■											
N2a-R33	Mouse	Subclone of N2a					■											
SHSY-5Y	Human	Neuroblastoma													■			
PC12	Rat	Phenochromocytoma				■			■									
GTI-1	Mouse	Hypothalamic neuronal cells subclone 1	■		■								■					
GTI-7	Mouse	Hypothalamic neuronal cells subclone 2	■			■	■						■	■				
SN56	Mouse	Hybrid septal neuron/neuroblastoma	■				■		■									
CAD-2A2D5	Mouse	CNS catecholaminergic cell line			■		■		■		■							
HpL3-7	Mouse	Hippocampal cells					■											
CGN^{ov}	Mouse	Cerebellar granule neurons														■		
NSC	Mouse	Neural stem cells			■		■											

Table 4 – Cell lines and reported prion strain susceptibility

Neuronal cell lines from various hosts susceptible to infection from different prion strains. (adapted from Nuvolone et al. 2009).

The most commonly used cell lines for prion research are neuroblastoma cells. Neuroblastoma cells are a cancer cell line that show one of the highest rates of tumour regression (Schwartz et al. 2013). Neuroblastoma cells characteristically demonstrate a small, round, tear shaped morphology. In addition, mature cells tend to grow neurite processes and a portion of cells group to form a large number of tumour spheroids within confluent cells (Figure 9) (Schwartz and Boles 2013).

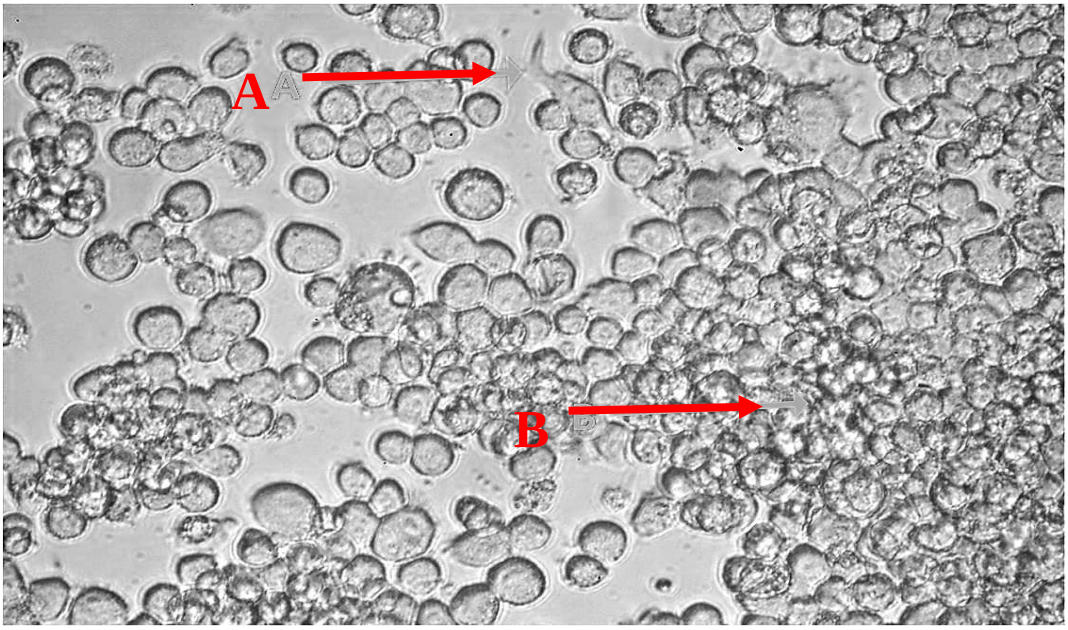

Figure 9 – Micrograph of N2a #58 cells

A micrograph of N2a cells captured using inverted phase contrast microscopy. A) The beginning of neurite process formation. B) Early accumulation of cells associated with spheroid growth.

Mouse neuroblastoma or "N2a" cells have been utilised for prion research, particularly infectivity based studies because of their ease of culture and their ability to be transfected easily, thus adapting their susceptibility to infection of different prion strains. The prion transmission within these cell lines has been studied from the late 1980's. Butler et al, 1988 studied neuroblastoma cell lines relative to other cell lines for their ability to propagate scrapie prions (Butler et al. 1988). This work demonstrated that other cell lines, for example mouse L cell lines and N1E 115 (a murine neuroblastoma cell line) lost detectable prion infectivity after several passages. Also

PC12, a rat cell line showed "species-barrier" compatibility problems after infection with murine prions (Butler et al. 1988).

Different clones of N2a cells have demonstrated susceptibility to infection from various prion strains (Table 4). An assay using a clone of scrapie N2a cells, denoted scN2a, which overexpresses the wild type mouse cellular prion protein, managed to be infected by three different mouse adapted prion scrapie strains; 139a, Chandler and 22L. However these cells were not infected by similar murine scrapie strains; 87V and 22A (Nishida et al. 2000). Klohn et al, 2003 first published work on a new cell assay they called the standard scrapie cell assay (SSCA). Using this assay they demonstrated the Rocky mountain laboratory (RML) prion infection of two sub-clones of N2a cells, denoted N2aPK1 and N2a PD88, and concluded that the SSCA is about as sensitive as the mouse bioassay, 10 times faster, less expensive and suitable for production within an automated system (Klohn et al. 2003). This assay also demonstrated the transmission of prion infectivity from a 10^{-8} dilution of RML infected brain homogenate (Klohn et al. 2003). The SSCA has been further utilised to assess four different N2a sub-clones; PK1, R33, CAD5 and LD9 and the transmissibility of four different prion strains; RML, 22L, 301C and ME7 was compared in these four cell lines (Mahal et al. 2007). The infectivity of the four prion strains varied in each of the N2a sub-clones with different prions strains showing infectivity in different sub-clones. Mouse 22L showed the greatest infectivity in all of the cell lines whereas 301C only showed infectivity in the CAD5 cell line (Mahal et al. 2007).

More recently the SSCA was adapted to form the scrapie cell endpoint assay (SCEPA) which involved the analysis of cells exposed to serial dilutions of prion strains to analyse the sensitivity of this assay (Edgeworth et al. 2009, Klohn et al. 2003, Mahal et al. 2007). The SCEPA was then further adapted to evaluate prion contamination absorbed onto model stainless steel wires (Edgeworth et al. 2009). This assay managed to detect prion down to a 10^{-10} dilution of RML prion infection on inoculated wires (Edgeworth et al. 2009). However this assay involved a large number of cell passage steps, post infection, which could pose a problem when adapting this assay for the use of different, less hardy cell lines. In addition, the infected cells are analysed by each well of a 96 well plate being filtered off, PK digested and the detected via antibody

labelling. Therefore, it is unknown whether PK digestion is digesting the cells captured on the filter membrane and whether the results are a true representation of the natural propagation. Furthermore, the same group demonstrated the propagation of infectious prions from wires that had only been inoculated with uninfected normal mouse brain homogenate using the SCEPA assay (Edgeworth et al. 2010). The spontaneously formed prions observed in this assay are likely a consequence of either *de novo* formation, as in the PMCA assay, or a consequence of minute, undetectable infectious prions in normal, uninfected brain homogenate; furthermore it could also be a limitation or the production of an artefact with in this assay. However, the SCEPA assay utilised to detect infectivity of prions absorbed on stainless steel wires, also known as the stainless steel-binding assay (SSBA), was later utilised to assess the efficacy of various cleaning chemistries in relation to remaining infectivity post treatment (Edgeworth et al. 2011b).

N2a cell lines have also been used in a number of other aspects of prion research ranging from the search for anti-prion agents to detecting the mechanisms behind PrP^{Sc} infectivity. A common factor in these studies seems to be the addition or subtraction of certain molecular factors to understand the effects these have on prion infectivity or to try and further our understanding of the infectious agent. Further studies of the PK digestion of PrP^{Sc} confirmed the resistance of PrP^{Sc} to PK digestion and demonstrated remaining infectivity (Neary et al. 1991). Zhang et al, 2003 studied the effects of cathepsin activity on the conversion of PrP^{c} to PrP^{Sc} and determined there may be a second autocatalytic route in the production of PrP^{Sc} (Zhang et al. 2003). Various reports have used N2a cell infectivity to look at the use of anti-prion agents in preventing prion transmission and propagation. Agents that have been proven to stop prion infection using these cell assays include β-cyclodextrins and methyl β-cyclodextrins, (Prior et al. 2007) various monoclonal antibodies including; 7H6, 7A12 (Pankiewicz et al. 2006) and 6H4 (Enari et al. 2001) and finally phosphatidylinositol-specific phospholipase C for the digestion of the GPI anchors associated with PrP^{c} (PIPLC) (Enari et al. 2001). N2a cells have recently been used to visualise the immunolocalisation of PrP^{Sc} using novel light and electron microscopy techniques to understand more of the prion cellular pathways and the routes of transmission of PrP^{Sc} involved in prion infection (Veith et al. 2009). All of these techniques highlight N2a cells as good models for prion infectivity, albeit only utilising animal derived prion

strains. Subsequently cell lines need to be determined and selected for each prion strain; currently none are versatile for a range of prion strains or, most importantly, CJD infected material.

PrP^{c} is predominantly found on cells of the CNS, especially neuronal cells and are the main cell type associated with the neurodegenerative symptoms associated with PrP^{Sc} infection in TSE's. Neural stem cells (NSC) are multi-potent primary cells that self-proliferate into various progenitor cells which have the ability to differentiate to three important cell types of the CNS; neurons, astrocytes and oligodendrocytes. It is possible to culture NSC's and induce differentiation of these cells by the removal of the mitotic factor at which point different supplements can be introduced to control differentiation to favour one of the three cell types. In the case demonstrated in Figure 10, B27 supplement was used to initiate differentiation of a neuronal rich culture, instead of oligodendrocytes and astrocytes. This highlights the potential to produce a neuron rich culture with the possibility of utilising them for a cell based prion infectivity assays without the need to genetically manipulate the cells and therefore the development of an assay that utilises natural PrP^{c}.

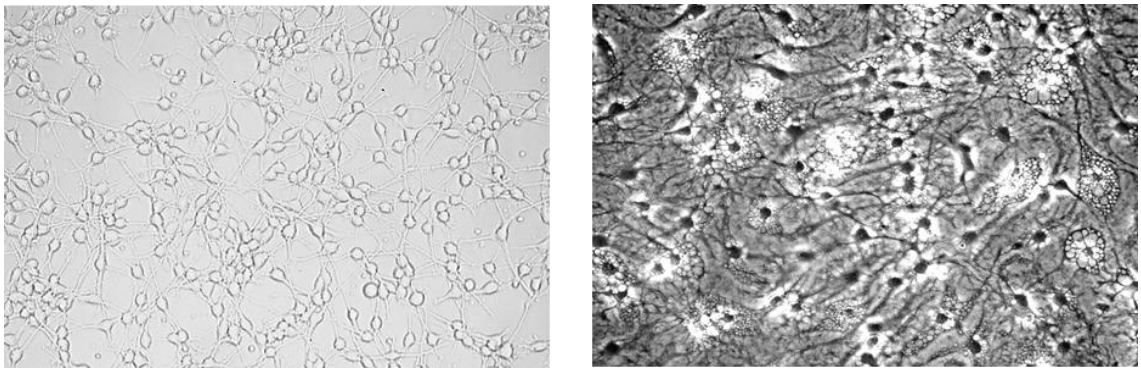

Figure 10 – Example micrographs of NSC's

Example micrographs of neural stem cells both undifferentiated (left) and differentiated (right) captured using phase contrast microscopy.

The use of NSC's for prion infectivity studies is a relatively new concept and very little information has been reported on this subject. Kellermann et al, 2002 have

studied an F9 teratocarcinoma cell line, denoted 1C11, which has similar differentiation properties to NSC's. The 1C11 line has been infected with three prion strains; Chandler, 22L and Fukuoka-1. However this cell line is not capable of evaluating CJD prions (Kellermann et al. 2002). RML prion infection into mouse neurospheres, which contain stem cells of the CNS has also been demonstrated, but again this is a mouse based model and is unlikely to be susceptible to CJD infection (Giri et al. 2006). Sylvain Lehmann's group from Montpellier have produced a NSC based model for the detection of prion infectivity. For this study they used mouse foetal NSC's in which they studied the use of various growth factors at the point of differentiation to aid prion transmission post differentiation. This confirmed that growth factors play an important role in the sustainability of prion infection within NSC cultures and also demonstrated that fetal calf serum (FCS) induced the highest propagation of prion infectivity within this culture system (Milhavet et al. 2006). This assay demonstrated the ability to infect mouse NSC's with 22L mouse adapted scrapie prion (Milhavet et al. 2006). However, whether mouse NSC's have the ability to propagate CJD prions is unknown. It is possible that a mouse NSC or human NSC cell line has the ability to propagate infection from human CJD samples, which would give rise to a cell-based assay to detect prion infectivity before and after decontamination of suspected CJD contaminated surgical instruments.

1.7 Aims and objectives

The current risk of iCJD appears to be in decline; however, with the increased number of PrP^{Sc} carriers discovered during the recent appendices study, the potentially long incubation periods of CJD and the unknown effects of genetic predisposition on disease outcome, the risk of iCJD could be very much larger than anticipated. Cell-based bioassays for the detection of prion infectivity offer the potential for a new generation of infectivity assays that can be easily adapted to detect multiple disease markers alongside being flexible for the detection of different prion strains. Furthermore, they have fewer limitations, when compared to the currently used animal-bioassays, which have been previously highlighted within this report. Current cell-based assays utilise *ex situ* analysis of PrP^{res} accumulation by immuno labelling post digestion

of PrP^{c} with PK. However it has been documented that up to 80% of disease associated material is also digested by PK, thus, questioning the viability of these assays as standalone techniques in relation to relevant risk of disease. Therefore, this project has three main aims:

- To produce a sensitive, *in situ*, amyloid-based detection method for the analysis of prion infectivity in neuroblastoma cells.

- To adapt this sensitive cell-based assay for the detection of prion infectivity in relation to prion decontamination efficacy, alongside comparison with animal-bioassay data.

- To study the use of neural stem cells (NSC) for the detection of prion infectivity with a cell line that does not require genetic manipulation to enhance propagation susceptibility.

    - To also study adaptations in NSC culture conditions to improve assay reliability and to produce optimal conditions for enhanced prion propagation.

Murine neuroblastoma subclone, N2a #58, that express ~4-fold higher levels of PrP^{c} compared to wild-type neuroblastoma cells were utilised to propagate 22L-infected brain homogenate and to develop a sensitive prion infectivity detection protocol. Chapter 3 of this report summarises the optimisation of a ThT-based, amyloid specific staining protocol for the analysis of 22L infectivity in the N2a #58 cells over a fortnight-based time course assay and directly compares the sensitivity of this staining protocol to Western blot detection of PrP^{res} within the cell lysates.

Animal-bioassays rely on the natural turnover of PrP^{c} within the experimental host to aid the propagation of PrP^{Sc} to reach detectable levels and to instigate disease pathology. Consequently, published cell-based bioassays utilise cell passages to increase cell turnover and subsequently increase the PrP^{c} that the infectious material comes into contact with, thus increasing the sensitivity of these assays. Therefore,

Chapter 4 of this report describes the adaptation of the N2a/22L SB/ThT time-course assay described in Chapter 3 to include cell passage steps to further improve the sensitivity and reliability, regarding levels of cell death, of this assay. Furthermore, the sensitivity of WB analysis of PrP^{res} content in the infected cell lysates will be directly compared to the ThT-based amyloid detection.

To test the infectivity of surface-bound prion biofouling pre and post-decontamination animal bioassays utilise small lengths of surgical grade stainless steel wire that is inoculated in the prion strain in question, decontaminated and then incorporated into the rodent brain. Cell based-bioassays also incorporate prion inoculated wires as a means to analyse prion decontamination technologies in regards to residual prion infectivity. Therefore, Chapter 5 of this report aims to adapt the N2a/22L SB/ThT assay, optimised in the previous two chapters, for the analysis of wire bound infectivity. Furthermore, this assay for the detection of wire bound infectivity will be utilised for the analysis of commercially available cleaning chemistries and the infectivity data will be compared to previously published animal-bioassays investigating the same cleaning chemistries.

The N2a #58 cells, utilised in the first three results chapters of this report, are genetically modified to express increased levels of PrP^{c} to artificially improve their susceptibility to prion infection. Furthermore, they are limited to prion infection from only four murine prion strains. Different cell lines can offer varying properties that could aid the production of novel assays that can propagate different prion strains but also present a closer representation of wild-type disease propagation. Therefore, Chapter 6 of this report aims to utilise murine neural stem cells (NSC's) for the propagation of murine 22L scrapie as a neuronal rich culture naturally contains high levels of PrP^{c} without genetic manipulation. Furthermore, the number of prions strains infectable in NSC's is currently unknown. However, natural cell loss at the point of induced differentiation hindered the SB/ThT staining utilised within the infectivity assay. Therefore, adaptations in the culture protocol regarding atmospheric conditions and improved trophic support at the point of differentiation will be addressed to improve quality of the NSC culture for future prion infectivity assays.

Chapter 2

General Methods

2.1 Cells and Brain homogenates

2.1.1 Neuroblastoma cells

Neuroblastoma cell sub-clone (N2a #58), previously transfected with wild-type mouse PRNP α-cDNA to increase the levels of PrP^{c} production within the cells and therefore increase the cells susceptibility to PrP^{Sc} infection, was kindly supplied by Sylvain Lehmann's group (Institut de Génétique Humaine, Montpellier, France) (Mange et al. 2002, Nishida et al. 2000). N2a #58 cells were received in 1ml DMEM media in cryo frozen aliquots ready for seeding.

2.1.2 Neural Stem cells (NSC)

Neural stem cells (NSC) were dissociated, isolated and again supplied by Sylvain Lehmann's group (Institut de Génétique Humaine, Montpellier, France). Briefly, multipotent progenitor cells were isolated from the cortices of pregnant female CD1 mice E13.5 embryos and collected in hanks buffered salt solution (HBSS; excluding magnesium and calcium) and frozen in NSC proliferation media in liquid nitrogen cryo-vials for long term storage (Milhavet et al. 2006).

2.1.3 Brain homogenates

Murine-scrapie 22L-infected brain homogenate, supplied by Ayodeji Asuni (Neuroscience department, University of Southampton), was prepared from the brains of C57BL mice infected via bilateral intra-hippocampal injections of 22L-infected homogenate (sourced from the TSE resource centre, The Roslin Institute, University of Edinburgh), animals were culled between 19-21 weeks and infected brains were dissected and homogenised to 10% (w/v) in phosphate buffered saline (PBS) (Šišková et al. 2013).

Murine-scrapie ME7-infected brain homogenate (supplied by the TSE resource centre, The Roslin Institute, University of Edinburgh) was prepared from C57BL mice infected via bilateral intra-hippocampal injections of ME7 infected homogenate, animals were then culled at 171 days post infection and infected brains were dissected and homogenised to 10% (w/v) in PBS.

Hamster 263K-infected brain homogenate (supplied from the TSE resource centre, The Roslin Institute, University of Edinburgh) was prepared from LVG golden Syrian hamsters infected via bilateral intra-hippocampal injections of 263K infected brain homogenate, animals were culled at 73 days post infection and infected brains were dissected and homogenised to 10% (w/v) in PBS.

Murine normal brain homogenate (NBH – supplied by The Roslin Institute, University of Edinburgh) was prepared from brains dissected from adult C57BL mice homogenised to 10% (w/v) in PBS. Brain homogenates were stored at -80^{o}C for long term and -20^{o}C for short term storage prior to use.

2.2 General cell culture

2.2.1. Neuroblastoma cell culture

N2a cells were cultured in sterile, pre-warmed Dulbecco's Modified Eagle Medium (DMEM – Gibco, Invitrogen) supplemented with 10% (v/v) fetal bovine serum (FBS – Gibco, Invitrogen or Biosera), 1% (v/v) 100x Penicillin/Streptomycin (pen/strep – Gibco, Invitrogen) and 1% (v/v) 100x GlutiMAX (Gibco, Invitrogen). Media was prepared in 500 ml batches, sterile filtered in a 0.22 µm filter unit (Nalgene) and refrigerated until required.

N2a cell stock aliquots (1 ml) were removed from the -196^{o}C liquid nitrogen stores and allowed to defrost slowly at room temperature. Each aliquot was seeded into 14 ml of media in 75 mm tissue culture flasks (Nunc) for stock production or in 9 ml of media in 90 mm tissue culture dishes (Greiner bio-one) for experimental preparation. N2a cultures were incubated in a humidified environment at 37^{o}C and 5% (v/v) CO_2 (in a Galaxy® 170S incubator, New Brunswick) and media was replaced 24 h post seeding, then every 2-3 days after depending on the confluency of the cultures. Once 90 – 100% confluency (~8.8 x 10^6 cells) was reached the cells were passaged into either 1ml aliquots (DMEM diluted with 10% (v/v) Dimethyl sulphoxide (DMSO)) for frozen stocks or split at a ratio of 1:50 into small, 35 mm dishes for infection studies. N2a cells were passaged by dislodging the cells from the surface of the tissue culture dishes using a sterile cell scraper, re-suspended in fresh media and split between the required dishes.

2.2.2 Neural Stem cell culture

Prior to NSC culture all tissue culture dishes were coated with 15 µg/ml Poly-L-Ornithine (PLO - Sigma) overnight and 1 µg/ml bovine fibronectin (Sigma) for at least 4 hours. NSC aliquots (1 ml) were defrosted rapidly at room temperature and then seeded into 10 ml of N2 max media, for NSC proliferation, in a pre-coated 90 mm tissue culture dish. N2 max media comprised of DMEM/F12 medium (Gibco, Invitrogen), 1% (v/v) 100x GlutiMAX (Gibco, Invitrogen), 1% (v/v) 100x penicillin/streptomycin (Gibco), 25 µg/ml Insulin (Sigma), 20 nM Progesterone (Sigma), 100 nM Putrescine (Sigma), 30 nM Sodium Selenite (Sigma) and 100µg/ml Human apo-transferin (Sigma). Media was prepared in 500 ml batches, sterile filtered in a 0.22 µm filter unit (Nalgene) and refrigerated until required. The NSC's were cultured at 37^{o}C and 5% (v/v) CO_2 for normoxia experiments and 37^{o}C, 5% (v/v) CO_2 and 8% (unless stated otherwise) (v/v) O_2 (in a specialised Galaxy® 170R incubator with sensitive oxygen control) for the hypoxia experiments. Media was replaced 24 hours after seeding and then every 48 hours thereafter, cultures were supplemented with 10% (v/v) basic fibroblast growth factor (bFGF - R&D systems) every 24 hours to inhibit spontaneous differentiation. Once 80% confluency was reached, either differentiation was induced or NSC's were sub-cultured by covering the cells in Hanks buffered salt solution (HBSS, Gibco) supplemented with $NaHCO_3$ (Sigma), 4-(2-hydroxyethyl)-1-

peperazineethanesulfonic acid, (HEPES, Sigma) and 1% (v/v) 100x pen/strep. This modified HBSS solution alters the pH causing the cells to detach from the coated surface, the cells are then gently dislodged, re-suspended in fresh N2 max media and split between the required dishes.

Differentiation was induced by the removal of the bFGF (mitotic factor) supplement and replacement of the N2max media with Neurobasal media to aid neuronal growth. Neurobasal (NB) media (Gibco) was supplemented with 1% (v/v) 100x Penicillin/Streptomycin (pen/strep – Gibco), 1% (v/v) 100x GlutiMAX (Gibco) and 2% (v/v) B27 supplement (Invitrogen). Media was prepared in 500 ml batches, sterile filtered in a 0.22 µm filter unit (Nalgene) and refrigerated until required. The differentiated NSC's were cultured as described previously with media changes every 24-48 hours.

2.3 Neuroblastoma prion infections

2.3.1 Preparation of infectious material

Infectious material was prepared from previously 22L-infected N2a cell lysates or from 22L-infected brain homogenate. Infected cell lysates were tested for the presence of PrP^{Sc} by Western blot prior to preparation for cell infection studies. Firstly, lysates were centrifuged at 10,000 g for 5 min and the supernatant was discarded. The pellet was re-suspended in 20 µl lysis buffer (0.5% (w/v) sodium deoxycholate, 150 mM NaCl, 0.5% (v/v) Triton X-100 and 50 mM Tris-HCl) for 15 min on ice, followed by centrifugation at 10,000 g for 5 min. The supernatant was transferred to a fresh Eppendorf, made up to 1 ml with DMEM medium and the pellet was discarded. The 22L-infected solution was filtered through a 0.22 µm filter and further diluted to the required dilutions, taking into account the volume of media in the 35 mm cell culture dishes.

Prior to cell infection the 22L-infected homogenate was partially purified to prevent brain material sticking to the cells and hindering microscopic detection using a previously described method (Milhavet et al. 2006). Briefly, homogenate was lysed in small volumes of lysis buffer (0.5% (w/v) sodium deoxycholate, 150 mM NaCl, 0.5% (v/v) Triton X-100 and 50 mM Tris-HCl) for 20 min on ice, followed by 10 min centrifugation at 10,000 g. The supernatant was then re-suspended in DMEM media and sterile filtered through a 0.22 µm filter and further diluted to the required concentration, taking into account the volume of media in the 35mm cell culture dishes.

2.3.2 Neuroblastoma time-course infection

To determine the sensitivity of prion detection methods (Western blot, ThT staining and SB/ThT staining) and the susceptibility of N2a #58 cells to prion infection N2a cells were infected with varying dilutions of either 22L-infected lysate or 22L-infected brain homogenate. N2a cells were infected just after passage with final dilutions of 22L in DMEM media ranging between 10^{-2} and 10^{-9} of the original 22L infected solution. Cells were infected in 14x 35 mm dishes for each experiment and 2 dishes of un-infected cells were kept for the 14 days as controls and analysed in the same way. After 24 hours post infection the DMEM media was replaced to remove any excess un-established infectious material. Subsequently the DMEM media was replaced every 48 hours and the cells were incubated at 37^{o}C humid conditions and 5% CO_2 for the whole duration of the study. Two dishes were analysed for prion infection by fluorescent staining or lysed to detect PrP^{Sc} content by Western blot analysis every two days throughout the 14 day time course.

2.3.3 Neuroblastoma passage infections

To improve the sensitivity and viability of the N2a cell infections, PrP^{Sc} was propagated within the cells for longer by analysing the increase in 22L infection of the N2a cells over several passages as opposed to 14 days.

Firstly, the optimal time point post infection for passaging the infected cells was determined by infecting the N2a cell cultures with a final 10^{-4} dilution of 22L homogenate at the point of passage. The media was then replaced after the first 24 hours and every 48 hours thereafter. Infected cells and control (un-infected) cells were then analysed for prion infection by Sudan black/Thioflavin T (SB/ThT – section 2.4.2) staining and lysed for detection of PrP^{Sc} content by Western blot after 8, 10 and 12 days post infection. The final dish of both infected and un-infected cells (~1.2 x 10^6 cells) were split at a ratio of 1:20 and left to propagate for a further 8, 10 or 12 days at which point the levels of prion infection were again analysed as above (Figure 11). The cells were passaged and analysed as described previously until an endpoint was reached when the loss of cell viability was observed.

Secondly, the N2a cells were subjected to a titre of 22L brain homogenate with final dilutions ranging from 10^{-2} – 10^{-10} to determine if propagating the prion infection over several passages in the N2a cells increases the sensitivity of this assay. The N2a cells were infected at the point of passage and the media was replaced after 24 hours and every 48 hours thereafter. Then the level of prion propagation in both the infected and uninfected cell cultures was detected by SB/ThT staining (section 2.4.2) and Western blot (section 2.4.6) analysis of the cell lysates after 10 days post infection. At this point both the infected and uninfected cells (~ 1.2 x 10^6 cells) were split at a ratio of 1:20 and the levels of prion propagation were again analysed after 10 days. The cells were passaged and analysed by the described method (Figure 11) until an endpoint was reached when the loss of cell viability was observed.

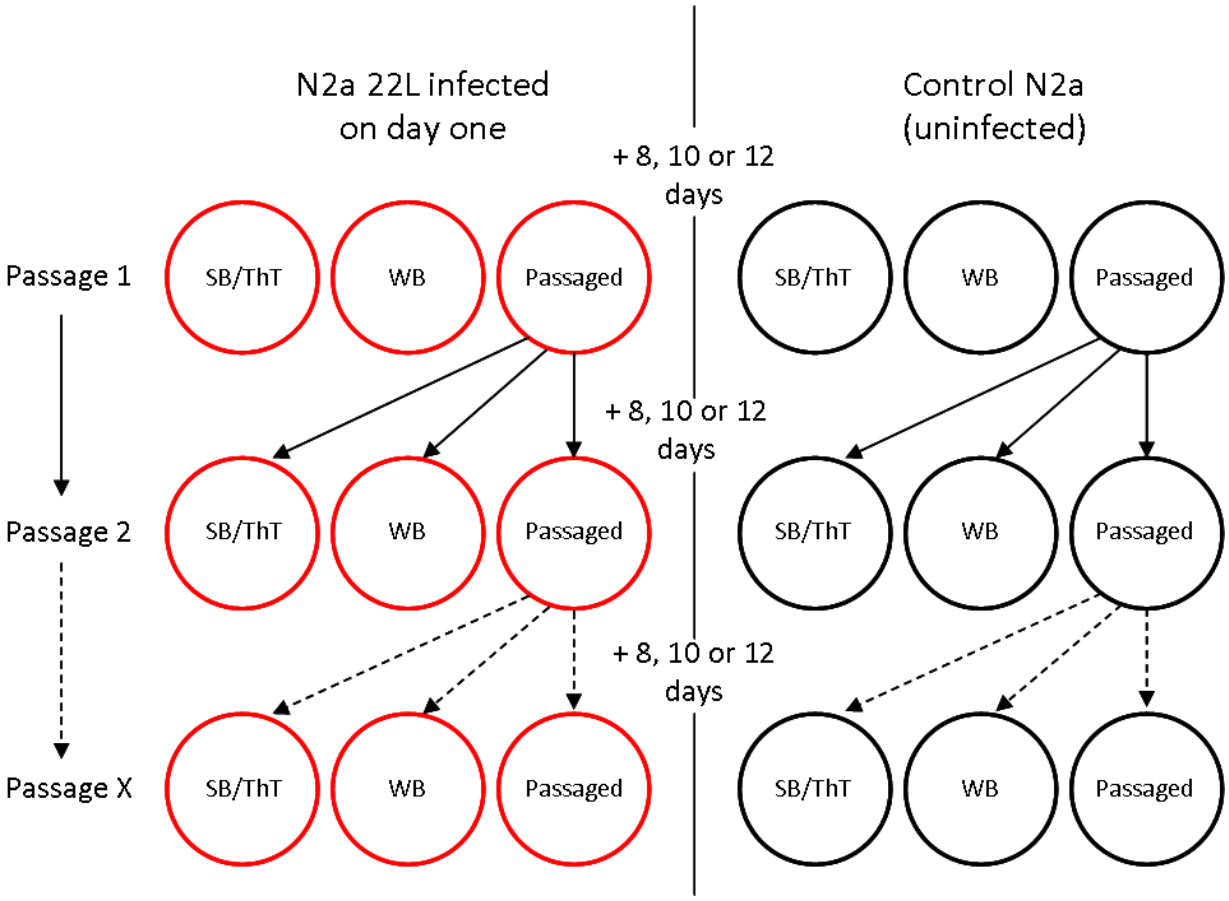

Figure 11 – Schematic diagram defining the passage study experiments

Three 35 mm dishes were infected with serial dilutions of 22L-infected homogenate (red) and three were left uninfected (controls, black). After 8, 10 or 12 days one dish from each parameter was stained with Sudan black/Thioflavin T (SB/ThT) and the other dish was lysed for Western blot detection (WB). The third dish was passaged into a further 3 dishes and cultured for the same number of days to produce the passage 2 samples. These steps were repeated until an end point passage was obtained and cell viability was lost (passage x).

2.3.4 Neuroblastoma wire infectivity assays

To adapt the N2a 22L infectivity assay, described previously to assess decontamination efficacy at reducing prion infectivity, the introduction of 22L-inoculated wires to transmit PrP^{Sc} infection pre and post decontamination to the cells was studied. Firstly, the number of inoculated wires required to induce optimal prion infection per 35 mm dish of cells was analysed. All wires were prepared, decontaminated and deemed clean prior to each assay using the following method.

Surgical grade 316 stainless steel wires (0.16 mm diameter, Ormiston wire - UK) were cut to 5 mm lengths, soaked in acetone to remove any organic material, and then autoclaved in distilled water for 20 min at 121^{o}C. The wires were removed from the autoclave and dried on filter-paper covered Petri dishes overnight at room temperature. To determine the number of wires required per well for optimal propagation 5, 10, and 20 wire batches were inoculated in 10^{-4} and 10^{-6} dilutions of 10% (w/v) 22L-infected brain homogenate in DMEM media, for infected samples or 10% (w/v) NBH in DMEM media for uninfected controls. Wires were inoculated in the diluted brain homogenates for 2 hours at room temperature and then removed and dried in separate filter-paper covered Petri dishes for 2 hours at 37^{o}C. Inoculated wires were placed in separate 35 mm cell culture dishes and covered with 2 ml of fresh pre-warmed DMEM media and N2a cells split at a ratio of 1:50 from cells grown to confluency (~8.8 x 10^{6} cells) in 90 mm culture dishes (prepared as described earlier). Cells were grown over the wires to confluency (around 7 day's culture) with media changes every 48 - 72 hours. Once a confluent culture was established, the cell covered inoculated wires were removed and placed in 2 ml of fresh pre-warmed DMEM media in new 35 mm dishes. The cells remaining in the original dishes were analysed by SB/ThT (section 2.4.2) staining to determine initial 22L propagation from the wires. In the new dishes the cells were grown from the wires to confluency (around 7 day's culture) with media changes every 48 – 72 hours (Figure 12). At the time of confluency the wires were removed and discarded, the cells were then passaged into fresh 35 mm dishes and treated like the passage infection studies (described in section 2.3.3); with passages and SB/ThT analysis every 7 days until cell viability was lost (Figure 11).

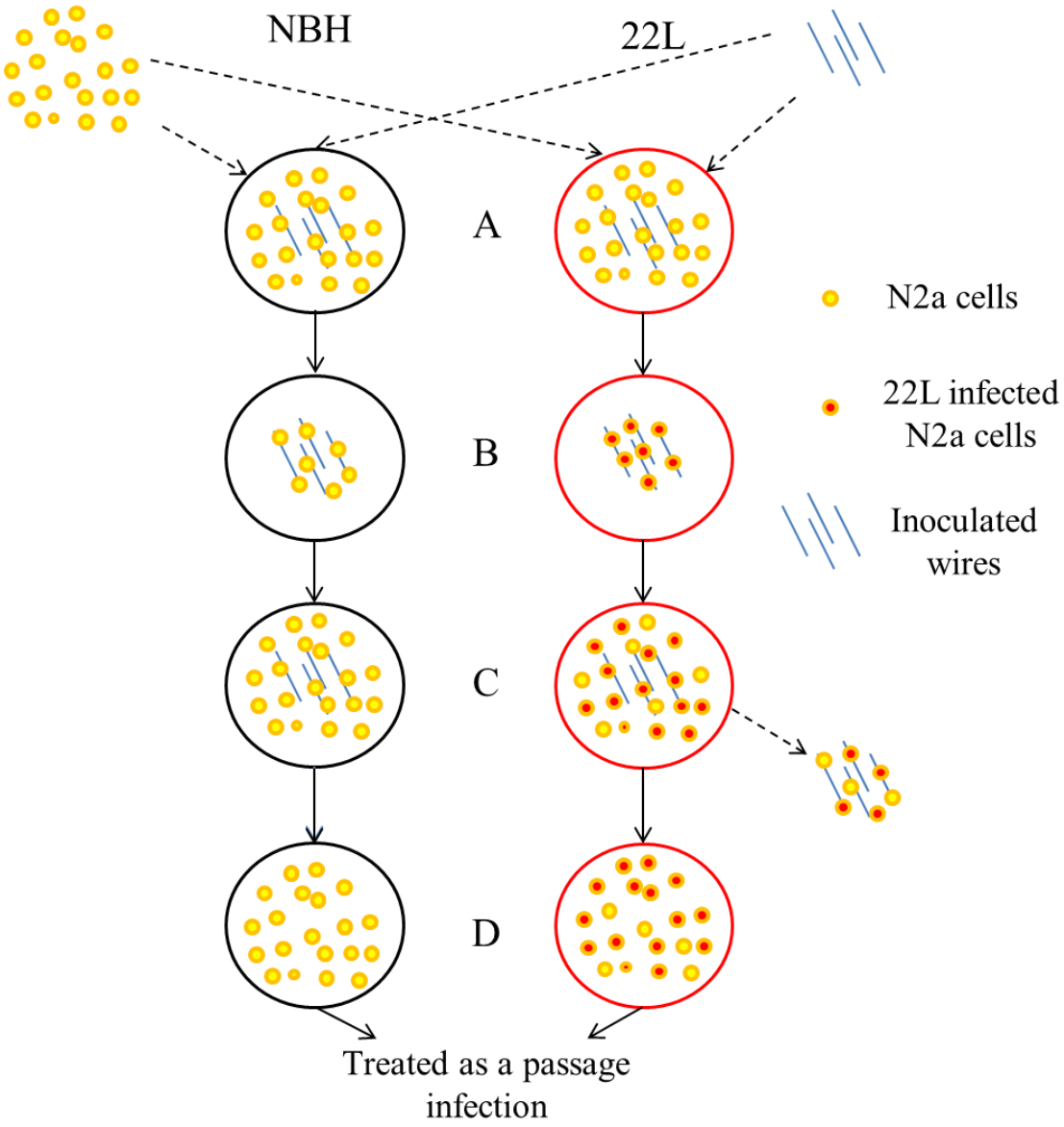

Figure 12 – Schematic of N2a wire infectivity assay

A schematic diagram to demonstrate the steps involved in the N2a wire infectivity assay. A) NBH or 22L Inoculated wires and N2a #58 cells introduced to 35 mm tissue culture dishes and cultured to confluency. B) Wires coated in N2a cells transferred to fresh 35mm tissue culture dishes and again cultured to confluency. The cells remaining in the dishes from step A were analysed with SB/ThT staining. C) The wires were removed and discarded and the remaining cells were passaged and grown to confluency. D) The confluent cells were treated as an N2a Passage study shown in Figure 11 cells were split and SB/ThT analysis every 7 days until cell viability was lost.

Once the number of wires required for optimal 22L propagation within the N2a cells was confirmed, the sensitivity of the wire infectivity assay was determined. The number of wires required for optimal propagation was determined to be 20 wires per 35 mm dish. Therefore, 20, 5 mm wires per dish were inoculated with titre dilutions of 22L, for infected samples, or NBH for un-infected controls, ranging from 10^{-4} to 10^{-10} dilutions of original brain homogenate. The wires were then introduced to the N2a cells and 22L propagation was analysed as described in the previous section (2.3.4, Figure 12).

2.3.5 Neuroblastoma wire decontamination infectivity assays

The sensitive 22L N2a wire infectivity assay with SB/ThT detection, described in the previous section was utilised for the analysis of decontamination efficacy. Firstly efficacy of 3 cleaning chemistries for the removal of protein, lipid and prion-associated amyloid from the wire surfaces was determined. Wires (5 mm length) were prepared as described earlier and inoculated in 10% 22L or 10% 263K-brain homogenate (for comparison of two prion strains originating from different hosts) for 2 hours at room temperature. Wires were dried for 2 hours on filter covered Petri dishes at 37^{o}C. Once dried, the wires were treated using one of three commercially available cleaners; Enzol (20 ml/l, Room temperature, 10 min, Johnson and Johnson); Klenzyme (8 ml/l, 43^{o}C, 5 min, Steris©) and HAMO 100 (8 ml/l, 43^{o}C, 7 min, Steris©). Furthermore, the working pH for each cleaning chemistry was determined. All wires were processed in separate soda glass vials, per condition, throughout the cleaning and staining process. Cleaning was carried out in an Electrothermal STEM RS900 reaction station with gentle agitation from a stirring rod throughout. Control, untreated wires were left at room temperature for analysis in parallel with decontaminated wires. Once wires were subjected to the decontamination protocols they were rinsed in deionised water and dried at room temperature for 1 hour before analysis of remaining contamination. Both control and decontaminated wires were stained, in separate soda glass vials, with either SYPRO Ruby/Thioflavin T (SR/ThT – section 2.4.3) staining for the detection of protein and prion-associated amyloid or Nile red/Thioflavin T (NR/ThT – section 2.4.4) staining for the detection of lipid and prion-associated amyloid. Fluorescent signal was visualised

using EF microscopy and analysed using Image J software (Version 1.44p, National institute for health, USA) both described later in section 2.4.5.

To determine infectivity of residual contamination post decontamination within one of the three cleaners presented previously, wires decontaminated as described were analysed using the 22L wire N2a infectivity assay and SB/ThT detection described earlier. Briefly, 20 wires per sample inoculated in 10% 22L-infected brain homogenate were decontaminated in one of the three cleaners described earlier or left un-cleaned as positive controls. The wires were then analysed using the wire infectivity N2a assay described in the previous section (section 2.3.4) for remaining infectivity post decontamination (Figure 12).

2.4 Prion detection

2.4.1 Sudan black (SB) for reduced autofluorescence

The autofluorescent quenching properties of Sudan black staining with relevance to the autofluorescence associated with the wavelengths required for the detection of ThT (excitation 405 – 445 nm and emission ≥475 nm) fluorescence was analysed. It was hypothesised that the autofluorescence was caused by lipids within the tissue. Therefore the autofluorescence was compared to the lipid content of ME7 infected brain homogenate using Nile red staining (9-diethylamino-5H-benzo[α]phenoxazine-5-one, NR, Sigma). Nile red is a lipid soluble fluorescent dye that when prepared within a solvent based solution it emits a deep red colour once bound to lipids. Sudan black (SB), a histological stain that stains lipids black and does not fluoresce itself was tested for its ability to quench lipid based autofluorescence. Spots of 1 µl of 1 mg/ml ME7 infected brain homogenate (diluted in PBS and 1% (v/v) tween 20) were pipetted onto a 316 surgical stainless steel token and left to dry at 37^{o}C for 1 hour. One spot was stained with NR (25 mM diluted in DMSO, Sigma Aldrich), one spot was left unstained to show the autofluorescence and the third spot was stained with SB (0.3% (w/v) SB

made up in 70% ethanol) and analysed for remaining autofluorescence using the ThT microscope filter block.

2.4.2 Prion amyloid staining within cells

Prion-associated amyloid levels were detected in the cell culture samples using the amyloid specific fluorescent fluorophore Thioflavin T (ThT). The cell cultures were stained every two days during the time-course experiments or at every passage point for the passage infection studies with either ThT alone or SB/ThT to try and produce an optimal staining protocol for the detection of prion-associated amyloid as a pathological marker of prion infection. The staining protocol was adapted for amyloid staining in cells from previously described ThT staining protocols used on tissue sections and surface contamination (Herve et al. 2009, Herve et al. 2010, Lipscomb et al. 2007a).

All staining was completed at room temperature and in a dark environment to prevent loss of fluorescence signal from photo-bleaching. Culture medium was removed and the cells were washed thoroughly in phosphate buffered saline (PBS, Gibco) to remove excess media, then fixed for 6 min in 4% (v/v) paraformaldehyde in PBS (PFA, VWR). Cells were permeablised in 0.1% (v/v) Triton X-100 in PBS for 10 min, followed by three PBS washes. The cells being stained with ThT alone were left in dH_2O while other cells were stained with 0.3% (w/v) SB made up in 70 % ethanol for 10 min. After SB staining cells were washed in PBS and all cells were stained with 0.02% (time-course and passage day optimisation) or 0.004% (passage and wire studies) (w/v) ThT made up in 0.01 M hydrochloric acid for 15 min. After ThT staining the cells were washed in 0.1% (v/v) acetic acid for 2 min to remove any non-specifically bound ThT, followed by washes in PBS and dH_2O. Cells were left in the final wash of dH_2O until microscopic analysis.

2.4.3 SR/ThT dual staining

The dual staining procedure for prion-associated amyloid and total protein contamination, as well as detection and analysis methods, have been described previously (Herve et al. 2009). Briefly, prion amyloid contamination was identified using Thioflavin T (ThT; 0.2% (w/v) in 0.01 M HCl; Sigma Aldrich), and total protein was visualised using SYPRO Ruby protein blot stain (SR; Invitrogen UK, Renfrew, UK). Fluorescent signal was visualised by EF microscopy (Keevil 2003) and analysed using Image J software.

2.4.4 NR/ThT dual staining

NR/ThT staining involved an adaptation of the SR/ThT staining described in the previous section. The main differences to the SR/ThT protocol were that the SR was replaced with NR (25 mM diluted in DMSO, Sigma Aldrich) to analyse total lipid as opposed to total protein. In addition, the NR staining preceded the ThT staining as the DMSO would quench the ThT signal. The remaining protocol was left unchanged regarding the ThT staining and steps described previously (Herve et al. 2009).

2.4.5 Epifluorescence (EF) microscopy and image analysis

Stained cells were analysed using epifluorescence (EF – Best scientific) with long distance working lenses (Nikon) to analyse the fluorescent signal directly on the sample without the need for cover slips or oil immersion. This allows for the rapid analysis of staining without the hindrance of using coverslips in a large well of cells. This also allows the potential for *in situ* analysis of inoculated wires within the cultures in future work. Cells were analysed by capturing images using the 100x magnification objective from 10 random areas spanning the whole visual area of each sample, using the ThT filter block (excitation 405 – 445 nm, emission barrier 475 nm, Nikon). Images

were captured using a CCD colour camera (Roper Industries, UK) with identical camera detection settings for each individual experiment, optimised to detect low levels of background in the control samples and subsequently positive fluorescence in infected samples. Images were analysed using Image J software to count pixel intensities of positive ThT signal observed in all of the images. The threshold of the image analysis was set to pick up pixel intensities of ThT staining above the background levels observed in the controls for each experiment.

EF microscopy with long distance working lenses (Nikon) was also utilised for the analysis of the SR/ThT and NR/ThT staining of the inoculated wires pre and post decontamination. Scans of the contaminated areas were acquired at x10 objective magnification showing the SYPRO Ruby or NR signal (excitation: 470 nm; emission: 618 nm) and ThT signal (excitation: 450 nm; emission: 480 nm) signal. Captured images were analysed using Image J software and positive signal was standardised to the surface areas of the wires and reported in pg/mm^2 as described previously (Lipscomb et al. 2006c). Briefly, 1 µl spots of 22L-infected brain homogenate (normalised to 1 mg/ml as determined using the D_c protein assay kit (Bio-rad) with BSA standards, therefore a 1 µl spot would correspond to 1 µg of protein) were dried onto 316 grade stainless steel tokens for 4 hours at 37^{o}C. The homogenate spots were then stained with SR and scans were taken of the whole spots as previously described. Image analysis was carried out to determine the number of pixels per 1 µg of protein which was then used as a standard to convert the number of pixels remaining post decontamination to pg/mm^2.

2.4.6 Western blot analysis

Western blot (WB) analysis was carried out alongside the ThT and SB/ThT staining as a comparison of the sensitivity of these novel assays against a current and routinely used methodology for prion detection. Cells were washed thoroughly in PBS to remove excess cell media, re-suspended in cold PBS, centrifuged at 13,000 rpm and the pellet was treated in lysis buffer for 15 min. Once lysed the samples were stored at -20^{o}C until the end of each experiment once all of the samples were collected. Protein

content was determined using the D_c (Detergent compatible Bradford assay) protein assay kit (BioRad), the protein volume in each sample was standardised for each Western blot. The samples were digested in proteinase K (PK, Sigma) to a final concentration of 10 ng/µg of total protein for 30 min at 37^{o}C which was followed by the addition of Pefabloc (Sigma-Aldrich) to halt the digestion. After digestion samples were boiled for 5 min in loading buffer (2% (w/v) SDS, 10% (v/v) glycerol, 2% (v/v) β-mercaptoethanol, 0.01% (v/v) bromophenol blue, in 50 mM Tris–HCl, pH 6.8). Samples were loaded into a pre-cast, 12% (v/v) polyacrylamide gel (BioRad) and run in SDS, Tris – glycine buffer (BioRad) at 90 V for 1.5-2 hours. Once separated the proteins were transferred in Tris-glycine-methanol buffer and captured on a nitrocellulose membrane (BioRad) overnight at 30 V. Following transfer the unspecific binding sites were blocked by submerging the membrane in 5% (w/v) skimmed milk powder (Marvel) in PBS-T (PBS containing 0.1% (v/v) Tween 20, Sigma) for 1 hour at room temperature. After 3 washes in PBS-T, PrP detection was carried out using the anti-prion mouse monoclonal antibodies SAF 60 (Commissariat à l'Énergie 198 Atomique, Saclay, France; 1/5000 – 1/10,000 in PBS-T) or 6H4 (Prionics, 1/5000 in PBS-T) for 1 hour at room temperature. Following another 3 washes in PBS-T, the membrane was incubated in horseradish peroxidase-conjugated anti-mouse IgG secondary antibody (GE Healthcare, UK; 1/10000 in PBS-T) for 1 hour at room temperature. The immunoreactive bands were visualised using the enhanced chemiluminescence substrate (Amersham, ECL plus, GE Healthcare, UK) and developed on X-ray film (Amersham, GE Healthcare, UK or Fuji Film, UK).

2.5 Improving NSC culture conditions

Improvements in culture conditions for the neural stem cells (NSC) were required to improve the viability of the cells and therefore improve the quality of the NSC prion infectivity assays without the hindrance of compromised cells during prion detection. Firstly the confluency of the undifferentiated neural stem cells prior to differentiation was varied to see if the density of the cells affected the level of cell death. Then the cells were incubated in varying levels of oxygen (hypoxic environment) to closer mimic the physiological environment of the cells cerebral cortex origin.

Following this, the effect of introducing different supplements at the point of differentiation were tested in both normoxia and hypoxia environments.

2.5.1. Hypoxia

Neural stem cells were grown, according to the protocol described in section 2.2.2, in varying levels of oxygen to mimic the physiological environment that the cells were dissociated from. The cells were incubated in the Galaxy 170R incubator (New Brunswick) with sensitive oxygen control capabilities. The level of cell proliferation was observed in increasing oxygen levels starting at 1% O_2 until an environment was found that the level of cell proliferation and viability was optimal. At this point further experiments were carried out to compare cells grown in the lower O_2 atmosphere with cells grown at normoxia (~20% O_2), including the addition of supplements at the point of differentiation and the ratio of live and dead cells.

2.5.2. Improved supplements post differentiation

When differentiation of the NSC's is induced the media is changed to Neurobasal media and the growth supplements (bFGF) are removed. So another hypothesis for cell death could be the lack of nourishment and growth factors for the cells at the point of differentiation. To study this affect NSC's were differentiated in the presence of further doses of bFGF or with the addition of FBS or no supplement at all in both normoxia and hypoxia environments. At the point of differentiation dishes of cells were subjected to either daily doses of 0.1% (v/v) bFGF, to continue the supplements from the proliferation stage or 0.1% (v/v) daily doses of FBS. Some cells were given no supplements post-differentiation and were treated as the controls for this study. The supplements were administered to the cells for two days post-differentiation to reduce the initial cells shock of nutrient removal when differentiated. After two days the Neurobasal media was replaced and the cells were cultured for a further 7 days until analysis of the cell type and viability was performed.

2.6 NSC microscopy analysis

The changes in NSC growth were analysed using phase contrast microscopy and fluorescent microscopy utilised to determine the number of neuronal and glial cells post differentiation as well as the ratio of live and dead cells to compare cell viability between conditions.

2.6.1 Phase contrast microscopy

Phase contrast microscopy was used to acquire live images of the cells before and during the differentiation process to document the changes in cell morphology between the different culture conditions. Phase contrast microscopy was introduced by Frits Zernike in 1934 as a technique that improves the contrast of transparent specimens, such as living cells, by detecting minute changes in the refractive index between cell components and the surrounding media, without the need to pre-stain the sample (Zernike 1942). Briefly, phase contrast microscopy involves the incorporation of a phase condenser annulus situated near the condenser, and a phase ring plate usually situated within specialised objective lenses to a standard bright field microscope. Light passes through the phase condenser annulus and is split into two light beams which either pass straight through the specimen and are classed as un-deviated or diffracted by the changes in phase by structures within the specimen. The light travels through the phase plate within the objective lens which segregates the un-deviated light from the diffracted light with shifted phase which forms the highly contrasted image observed in the eyepiece. Images (x20 and x40 objective magnification) were captured every other day from the time of differentiation and used to document the variations in culture quality and confluency of the cells post-differentiation between the different conditions.

2.6.2 NSC Cell type analysis

2.6.2.1 Nestin

Nestin is an intermediate filament protein that is expressed on proliferating neuronal cells and is widely used as a marker for undifferentiated neural stem cells. The level of nestin expression was determined before and after differentiation to show the confluency of undifferentiated NSC cultured in hypoxia and normoxia and to show the efficiency of differentiation by showing the number of remaining undifferentiated cells seven days after initial induced differentiation in the various pre mentioned conditions.

Culture medium was removed from the cells followed by three washes in PBS. The cells were fixed in 4% (v/v) paraformaldehyde (PFA) for 10 min before three further washes in PBS. Unspecific binding was blocked with 5% (v/v) FBS in PBS for 1 hour followed by three washes in PBS. The anti-nestin primary antibody (Millipore, 1:100 dilutions (v/v) in PBS) was incubated on the cells for 1 hour and then removed with three further washes in PBS. Visualisation was carried out using an Alexa Fluor® 488 conjugated goat anti-mouse IgG secondary antibody (Invitrogen, 1:500 dilution (v/v) in PBS) for 1 hour then removed with three washes in PBS. The nuclei were counter stained with SYTO 59 nucleic acid stain (Invitrogen, 1:1000 dilutions (v/v) in PBS) and then visualised immediately. Random field of view (50x magnification) images were captured using EF microscopy with the excitation 470-495 nm, emission 510-550 nm filter for the Alexa Fluor® 488 dye and excitation 510-550 nm, emission 590 nm for the SYTO 59 (Best scientific, UK). Images were analysed using Image J image analysis software by counting pixels of nestin staining compared to the number of cells (SYTO 59 staining) and cell counts of nestin positive cells was performed to determine the ratio of nestin positive and negative cells between samples.

2.6.2.2 GFAP staining

Glial fibrillary acidic protein (GFAP) is a type III intermediate filament protein that is largely expressed on astrocytic cells of the central nervous system. The number of astrocytes was determined by staining the differentiated neural stem cells with an anti-GFAP antibody to study the effect on the different supplements and growth conditions on the number of astrocytes.

Culture medium was removed from the cells followed by three washes in PBS and the cells were fixed in 4% (v/v) paraformaldehyde for 10 min before three further washes in PBS. Unspecific binding was blocked with 5% (v/v) FBS in PBS for 1 hour followed by three washes in PBS. The anti-GFAP primary antibody (Millipore, 1:200 dilutions (v/v) in PBS) was incubated on the cells for 1 hour and then removed with three further washes in PBS. Visualisation was carried out using an Alexa Fluor® 488 conjugated goat anti-mouse IgG secondary antibody (Invitrogen, 1:500 dilution (v/v) in PBS) for 1 hour and washed off with three washes in PBS. The nuclei were counter stained with SYTO 59 nucleic acid stain (Invitrogen, 1:1000 dilutions (v/v) in PBS) and then visualised immediately. Random field of view (50x magnification) images were captured with the epi-fluorescence microscope using excitation 470-495 nm, emission 510-550 nm filter for the Alexa Fluor® 488 dye and excitation 510-550 nm, emission 590 nm for the SYTO 59 (Best scientific, UK). Images were analysed using Image J image analysis software by counting pixels of GFAP staining compared to the number of cells (SYTO 59 staining) and cell counts of GFAP positive cells was performed to determine the ratio of GFAP positive and negative cells between samples.

2.6.2.3 β-III-Tubulin staining

Class 3 β-Tubulin is a globular protein expressed exclusively on the microtubules of neuronal cells and is widely used as a marker for neurons. Therefore, the level of neurons post-differentiation was visualised using an anti-β-Tubulin antibody on cells grown in the different conditions with altered supplements.

Culture medium was removed from the cells followed by three washes in PBS and then the cells were fixed in 4% (v/v) paraformaldehyde for 10 min before three further washes in PBS. Unspecific binding was blocked with 5% (v/v) Goat serum in PBS-tween (PBS and 1% (v/v) tween 20) for 1 hour followed by three washes in PBS. The anti-β-Tubulin primary antibody (E7, The Developmental Studies Hybridoma Bank, University of Iowa, 1:50 dilutions (v/v) in PBS) was incubated with the cells overnight at 2-4^{o}C and then removed with three further washes in PBS. Visualisation was carried out using an Alexa Fluor® 488 conjugated goat anti-mouse IgG secondary antibody (Invitrogen, 1:500 dilution (v/v) in PBS) for 1 hour and removed with three washes in PBS. The nuclei were counter stained with SYTO 59 nucleic acid stain (Invitrogen, 1:1000 dilutions (v/v) in PBS) and then visualised immediately. Random field of view (50x magnification) images were captured with the epi-fluorescence microscope using excitation 470-495 nm, emission 510-550 nm filter for the Alexa Fluor® 488 dye and excitation 510-550 nm, emission 590 nm for the SYTO 59 (Best scientific, UK). Images were analysed using Image J image analysis software by counting pixels of β-Tubulin staining compared to the number of cells (SYTO 59 staining) and cell counts of β-Tubulin positive cells was performed to determine the ratio of β-Tubulin positive and negative cells between samples.

2.6.3 Cell viability analysis

The differentiated cells from the different environments and varying supplements were analysed to determine the ratio of cell viability to define the best environment for improved cell growth. SYTO 9 was used to stain all cells and propidium iodide (PI) to stain any cells with a compromised membrane.

The medium was removed from the cells and the cells were washed in three PBS washes. The cells were then fixed in 4% PFA for 10 min, washed in PBS and stained with a mixture of 40 µM PI and 7 µM SYTO 9 (Invitrogen, UK) diluted in PBS, for 30 min at room temperature. The stains were washed off with PBS and then immediately

visualised with EF microscopy using the excitation 470-495 nm, emission 510-550 nm filter for the SYTO 9 and excitation 510-550 nm, emission 590 nm for the PI. Images (10x magnification) of both stains were taken together within the same field of view to allow overlaying of live and dead cell signal within the same image. The ratio of live: dead cells were determined using Image J software and used to compare the cell viability in the different culture conditions.

2.7 Statistical analysis

Statistical analysis in the neuroblastoma prion infection experiments was used to compare the mean pixel counts of ThT positive staining between the uninfected controls and the days or passage post infection. A one way ANOVA was used for comparisons between the means in each data set and then a Tukey HSD post hoc test was used for data with equal variance or a welch test followed by a Games-Howell post hoc test for data with unequal variance was used to determine the statistical difference between the controls and the infected cells at the different times points, p values of ≤ 0.05 were classified as significant. In the NSC experiments statistical analysis was used to compare the differences in the percentage of each cell type and the cell viability between the various different culture conditions. As before a one way ANOVA was used for comparisons between the means in each data set and then a Tukey HSD post hoc test was used for data with equal variance or a welch test followed by a Games-Howell post hoc test for data with unequal variance to determine the statistical difference between the various culture conditions, again p values of ≤ 0.05 were classified as significant.

Chapter 3

N2a time-course prion infectivity assays and SB/ThT detection

3.1 Introduction and aims

The development of cell-based assays to detect prion infectivity has been an important area of prion research as they have the potential to become a standard method to analyse prion infectivity from many biological samples pre and post decontamination. A sensitive cell-based assay could be used as an alternative to current animal infectivity bioassays as they would be cheaper to run, produce a quicker result and possess fewer ethical considerations than animal assays. Moreover, different cell lines have the potential to detect infectivity of a wider range of prion strains.

Cell-based infectivity assays have been researched by a number of groups within the prion field with variations in both cell lines and prion detection methods used (Reviewed in Solassol et al. 2003, Vilette 2008). The three main aspects to take into account when developing a cell based assay for prion infectivity is the cell line used and its susceptibility to propagate different prion strains and the detection method utilised to detect prion propagation and subsequently infectivity. It is important to understand the cell lines used as different cell lines are only susceptible to infection from certain prion strains due to the effect of the "species barrier" and strain conformation (Nuvolone et al. 2009). Detection methods utilised to quantify the prion propagation within the cells currently rely on biochemical techniques, such as Western blot or ELISA to detect accumulation of PrP^{res} (Edgeworth et al. 2009, Klohn et al. 2003, Nishida et al. 2000). These methods focus on the *ex situ* detection of PrP^{res} post PK digestion; however, more recently evidence has arose demonstrating that not all disease-associated PrP^{Sc} is resistant to PK digestion and that a considerable amount of disease related material is potentially lost during these methods (D'Castro et al. 2010, Kuczius and Groschup 1999, Thackray et al. 2007). Furthermore, it has been demonstrated that the PK sensitive PrP^{Sc} still has the ability to induce PrP^{c} conversion (Pastrana et al. 2006). This suggests that these assays could potentially produce false negatives if the infectivity is associated with $sPrP^{Sc}$. As such, the question can be asked as to whether these assays alone are capable of providing a realistic picture of prion propagation.

This chapter will focus on the development of a sensitive method for the detection of prion infectivity to be utilised within cell-based assays. N2a #58 cells were the chosen cell line as they have previously demonstrated susceptibility to infection from several murine prion strains. In addition, they are easy to culture and so represent an excellent model to develop and optimise an infectivity detection method. ThT detection of amyloid associated with prion disease has been utilised in a number of detection methods including RT-QUIC, ASA and the SR/ThT dual stain (Atarashi et al. 2011a, Colby et al. 2007, Herve et al. 2009). Therefore a sensitive ThT-based detection method with *in situ* microscopic analysis was developed to detect prion infectivity in N2a cells over 14 days propagation. This assay was then compared to Western Blot detection of PrP^{Sc} to directly compare sensitivity of the two methods within the same quantity of cells.

3.2 Material and methods

Details of the materials and methods for this section can all be found within Chapter 2 of this report. Briefly, N2a #58 cells (2.1.1) were cultured as described in section 2.2.1 and then subjected to 22L (2.1.3 and 2.3.1) infection following the neuroblastoma time course described in section 2.3.2. Detection of prion infectivity was obtained by utilising both ThT staining alone and a combination of SB (2.4.1) and ThT as described in section 2.4.2. ThT signal was analysed by epi-fluorescent microscopy and quantified using Image J software described in section 2.4.5. Furthermore, cell lysates were analysed for PrP^{res} content using the Western blot protocol described in section 2.4.6. All statistical analysis was carried out as highlighted in section 2.7.

3.3 Results

3.3.1 Colour conversion

Raw images of the blue fluorescent ThT signal were captured; due to printing and visualisation purposes all images have been converted to green to improve the visual image quality post printing within this report (Figure 13). All image quantification and statistical analysis was carried out on the data produced from the original, raw images prior to any image manipulation.

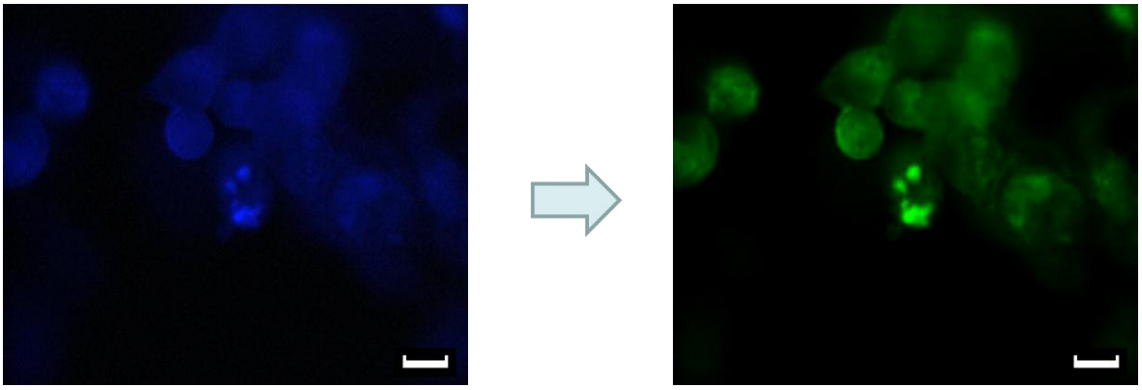

Figure 13 – Micrographs of colour conversion

Example micrographs demonstrating the colour conversion from the raw ThT image (blue) to the visually improved image (green). Scale bars = 10 µm.

3.3.2 Sudan Black

The addition of Sudan black in the ThT staining protocol was used to lower the background autofluorescence which is emitted in the same spectral range as ThT. The autofluorescence was hypothesised to be lipid based and to confirm this 1 µg spots of ME7 murine scrapie-infected brain homogenate were dried onto stainless steel tokens.

The autofluorescence was then visualised under the ThT filter of the EF microscope. The spot was then stained with Nile red to determine the lipid content, thus demonstrating that the lipid positive staining correlated with the autofluorescence. Sudan black was chosen as a quenching agent as it is a histological dye that binds to and stains lipids a deep brown/black without itself fluorescing, therefore quenching the autofluorescence. This was demonstrated by staining one of the ME7 spots with SB and comparing this to the autofluorescence observed prior to staining (Figure 14).

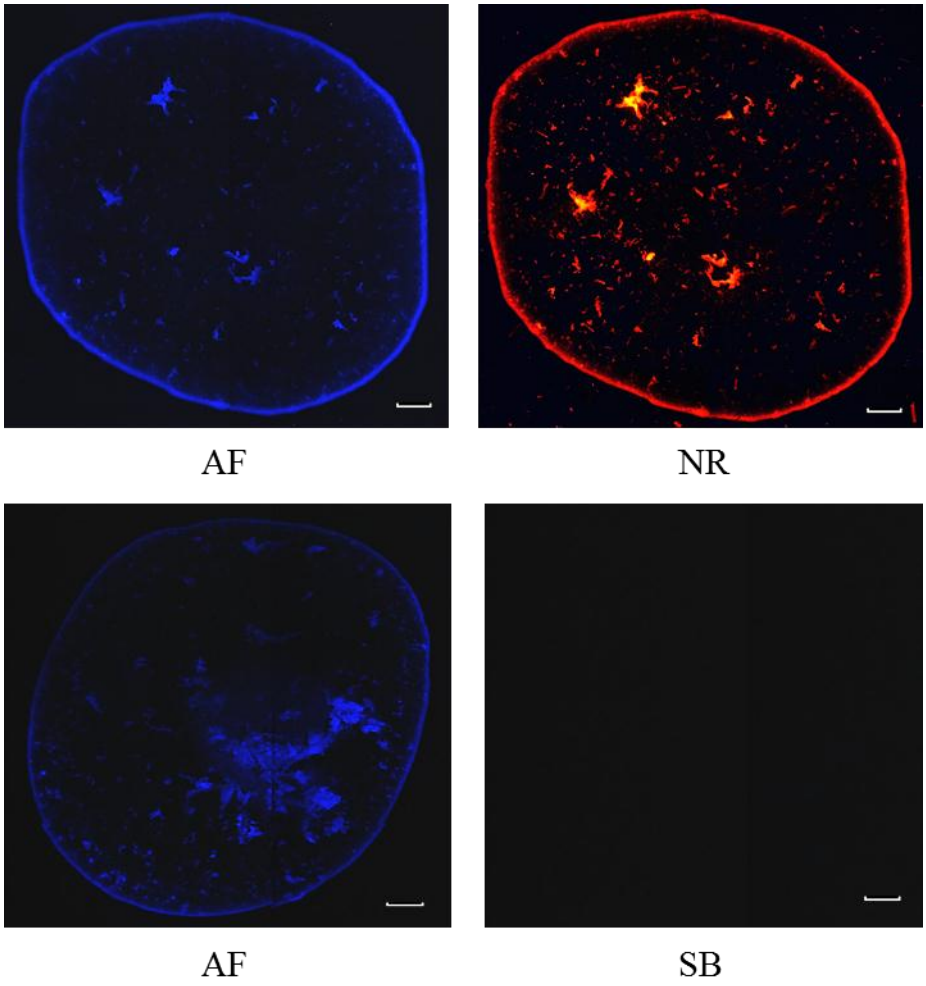

Figure 14 – Example micrographs demonstrating autofluorescence issues

Example micrographs of ME7 infected homogenate spots on stainless steel tokens stained with Nile red (NR) and Sudan black (SB) compared to the autofluorescence (AF) associated with the excitation and emission spectra of the ThT filter block. Scale bars = 100 µm.

3.3.3 Prion time course infections

The 14 day time course infections were used to produce and optimise the best staining method to detect the amyloid plaque build-up in the 22L-infected N2a cultures. Firstly, the ThT staining alone was compared to the ThT staining with the addition of SB to quench the autofluorescence, as demonstrated previously. Secondly the dynamic range of the 14 day time course assay was tested to determine the sensitivity of the ThT assay, SB/ThT assay and the Western Blot detection of PrP^{Sc}. The infections were started with a final 10^{-4} dilution of 22L-infected brain homogenate because novel cell based assays require a detection sensitivity of lower than a final 10^{-6} dilution of infectious material to compete with the sensitivity of current used animal bioassays. As a result, these assays were primarily assessed with higher doses to optimise the detection protocols.

3.3.3.1 ThT alone and SB/ThT staining to determine prion propagation

N2a cells were infected with a final 10^{-4} dilution of 22L infectious material and were stained using either the ThT alone or SB/ThT staining protocol every two days post introduction of the 22L material to determine the increase of prion-associated amyloid and therefore prion infection. Representative micrographs in Figure 15 taken on days 4, 8 and 12 post infection demonstrate an increase in ThT-positive signal compared to the uninfected controls over the time course using both the ThT alone and SB/ThT staining protocols. However, it can be observed from the micrographs that the bright spots of ThT-positive staining within the cells stained with the SB/ThT protocol tend to be more distinct and clearer to visualise especially when localised with the remaining background and autofluorescence of the cell bodies (Figure 15). Background autofluorescence associated with the cells is also observed in the control samples from both sets of experiments.

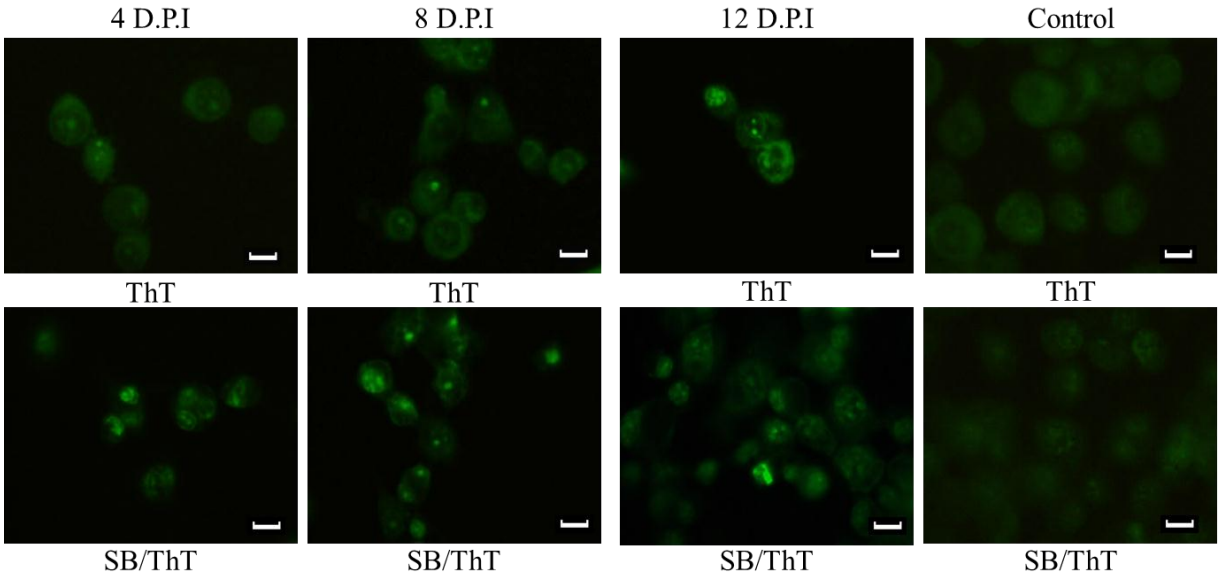

Figure 15 – Example micrographs from the 10^{-4} 22L-infected N2a time-course

Representative micrographs from the 10^{-4} 22L infected N2a cells stained with ThT alone (top) or SB/ThT (bottom) 4, 8 and 12 days post initial infection (D.P.I) and the uninfected controls (left to right respectively). Scale bars = 10 µm.

Image analysis software was used to quantify the number of ThT-positive pixels above an intensity threshold which was set to disregard any pixels associated with the uninfected controls for each sample set. The quantification of the ThT staining alone showed an initial increase in ThT signal at 2 days post infection which decreased until a significant increase was observed at 12 days post infection where the peak of positive signal was demonstrated (Figure 16, Graph A). The intensity of the staining signal within the samples with the lower propagation between days 4 and 8 was difficult to observe because of issues distinguishing between positive staining and autofluorescence with the ThT staining alone.

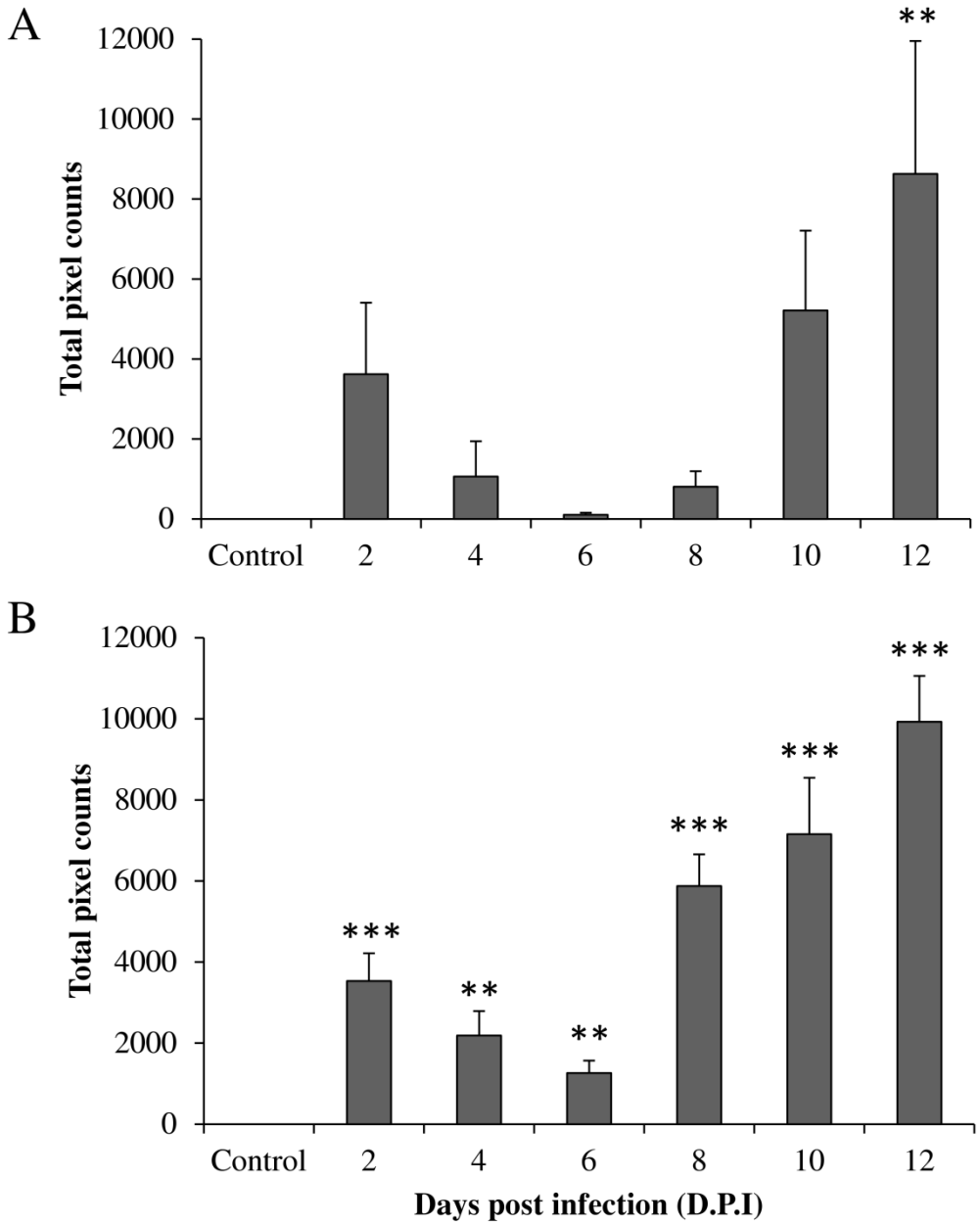

Figure 16 – Image analysis data from the 10^{-4} 22L N2a time-course infection

The pixel counts of ThT-positive staining, taking into account the background autofluorescence of the uninfected controls over 12 days post 10^{-4} 22L infection in N2a cells. A), shows the pixel counts of the ThT staining alone and B), the pixel counts of SB/ThT-positive staining. The Y-axis scale has been normalised to the 10^{-4} 22L infected N2a SB/ThT scale to compare dose response. Error bars shown are SEM (n = 20-40 images over 2-4 experiments), ** = $p \leq 0.01$; *** = $p \leq 0.001$ when compared to the uninfected controls.

The image analysis of the SB/ThT stained samples from the 10^{-4} 22L infected N2a cells showed the same trend as the ThT stained samples, with a slight increase in ThT signal at 2 days and then a decrease over the next 8 days with the peak expression shown at 12 days post infection (Figure 16, Graph B). However, the ThT signal was easier to observe and quantify after the SB staining and the variation between images was also lower than the ThT staining alone, demonstrated by the reduced error post SB. The addition of SB in the staining protocol demonstrated improved visualisation and contrast of the lower intensity ThT-positive staining which allowed the trend and detection of the smaller plaques with reduced ThT staining to be quantified more easily than ThT staining alone.

The sensitivity of the two different staining methods were further tested by comparing which method was able to detect prion propagation in the N2a cells after an initial 10^{-6} 22L infection. The representative micrographs in Figure 17 demonstrate that the brightest spots of ThT-positive signal in ThT alone stained samples were extremely difficult to distinguish from the background autofluorescence. After 12 days several small indistinct areas of positive staining in some fields of view were observed but not enough to demonstrate a trend in propagation compared to the uninfected controls. However, the SB/ThT staining detected amyloid plaque accumulation over the time course with a significant increase in ThT-positive signal observed between 6 and 12 days post infection (Figure 17). No initial increase in ThT signal was observed on day 2 post initial infection as was the case with the 10^{-4} 22L infected samples (Figure 16).

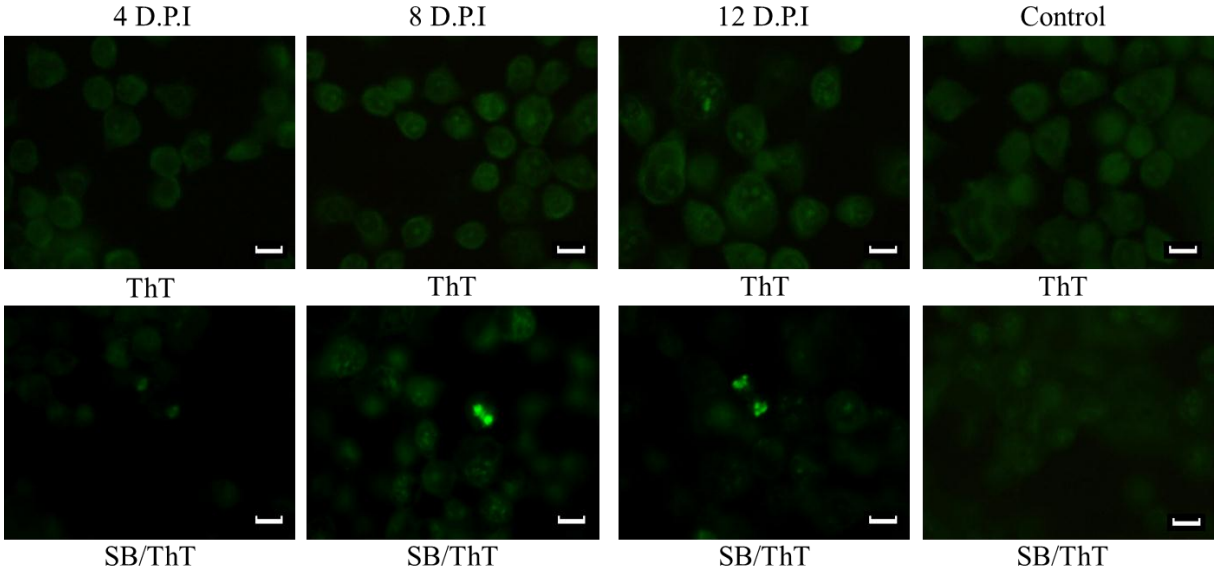

Figure 17 – Example micrographs from the 10^{-6} 22L-infected N2a time-course

Representative micrographs from the 10^{-6} 22L infected N2a cells stained with ThT alone (top) and SB/ThT (bottom) 4, 8 and 12 days post initial infection and the uninfected controls (left to right respectively). Scale bars = 10 µm.

The image analysis of the 10^{-6} 22L infected N2a cells confirmed that there was only a statistically significant increase in ThT signal when using ThT staining alone after 12 days post infection. Conversely, when using the SB/THT staining method, a clear increase in ThT-positive staining was observed when compared to the uninfected controls, with a statistically significant increase in ThT signal observed between 6 and 12 days post infection (Figure 18). The quantified positive ThT signal observed in the SB/ThT stained samples was higher than that observed in the samples stained with ThT only.

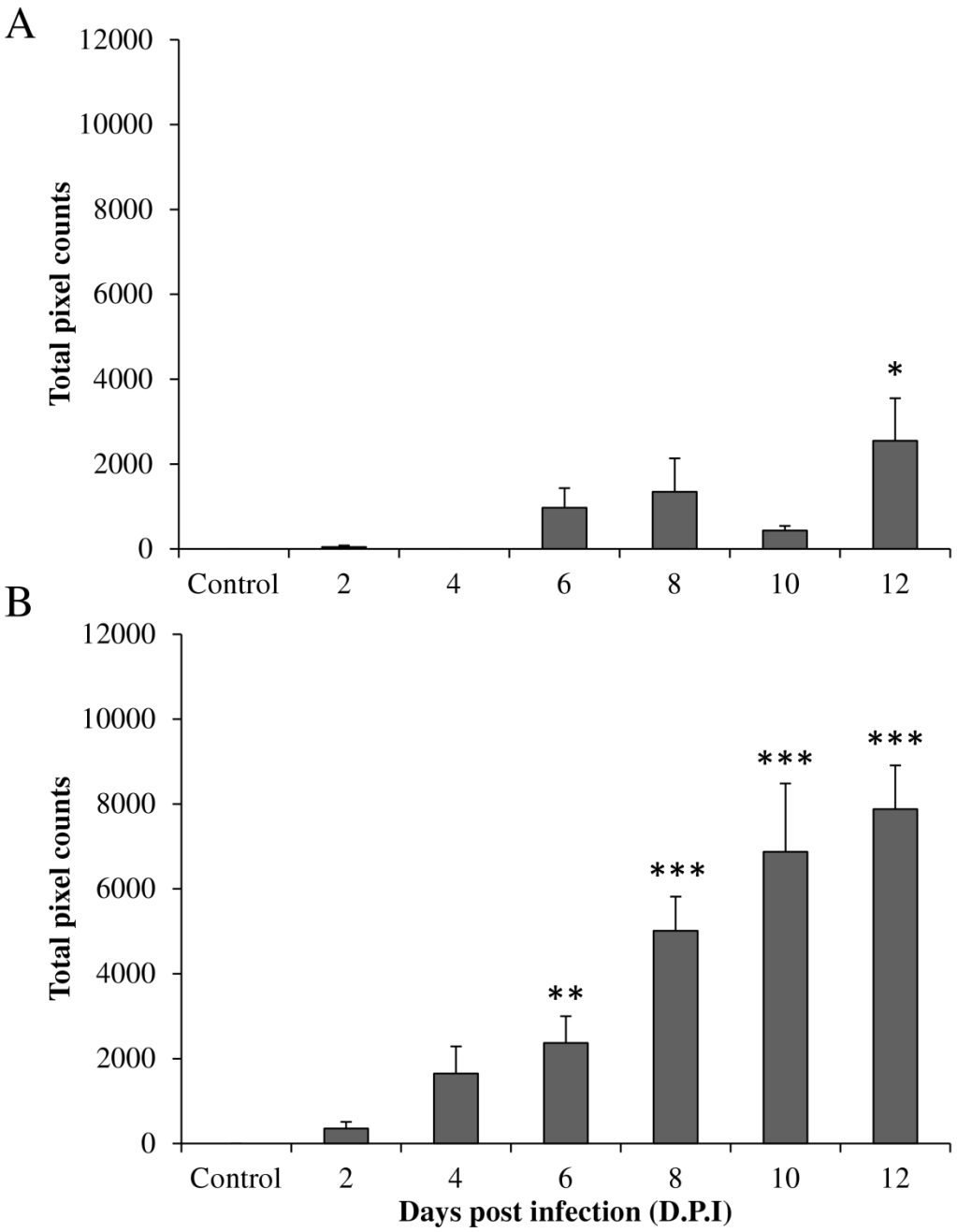

Figure 18 – Image analysis data from the 10^{-6} 22L-infected N2a time-course

The pixel counts of ThT-positive staining, taking into account the background autofluorescence of the uninfected controls over 14 days post 10^{-6} 22L infection in N2a cells. A), shows the pixel counts of the ThT staining alone and B), the pixel counts of SB/ThT-positive staining. The Y-axis scale has been normalised to the 10^{-4} 22L infected N2a SB/ThT scale to compare dose response. Error bars shown are SEM (n = 20-30 images over 2-3 experiments), * = $p \leq 0.05$; ** = $p \leq 0.01$ and *** = $p \leq 0.001$ when compared to the uninfected controls.

As the level of sensitivity for the ThT staining alone had been greatly reduced for the 10^{-6} 22L infected samples, only the SB/ThT staining was further analysed for the sensitivity of amyloid detection within the N2a cells by further reducing the initial 22L dose.

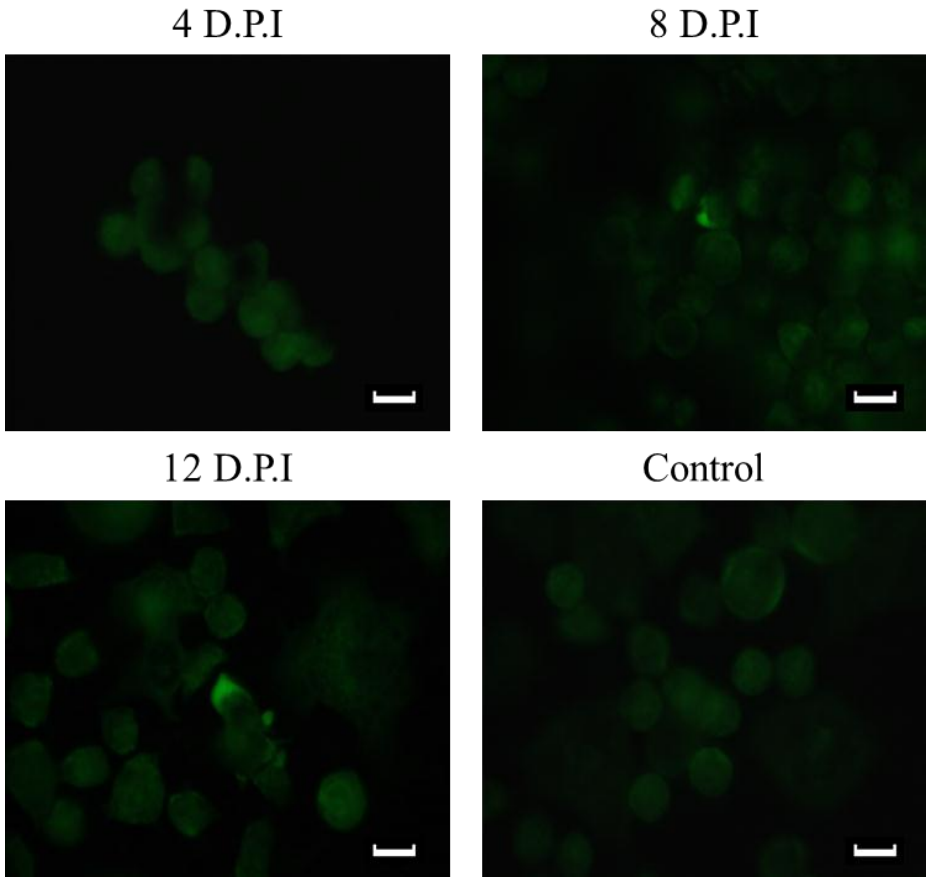

Figure 19 – Example micrographs from the 10^{-8} 22L-infected N2a time-course

Representative micrographs from the 10^{-8} 22L infected N2a cells stained with SB/ThT 4, 8 and 12 days post initial infection and the uninfected controls. Scale bars = 10 μm.

Representative micrographs in Figure 19 demonstrate the accumulation of ThT-positive staining after 8 - 12 days post initial 10^{-8} 22L infection, compared to the uninfected controls in the N2a cells. When compared to the previous higher titre infections, the amyloid plaque accumulation appeared to demonstrate smaller and fewer plaques in this lower 22L dose (Figure 19). The image analysis of the ThT-positive staining in the SB/ThT stained 10^{-8} 22L infected N2a cells confirmed that there was an increase in ThT positive signal after 6 days post infection, with a peak signal observed after 8 - 12 days which seems to plateau over these time points (Figure 20). The peak pixel counts in the 10^{-8} 22L infection were considerably lower than that of the higher dose infections.

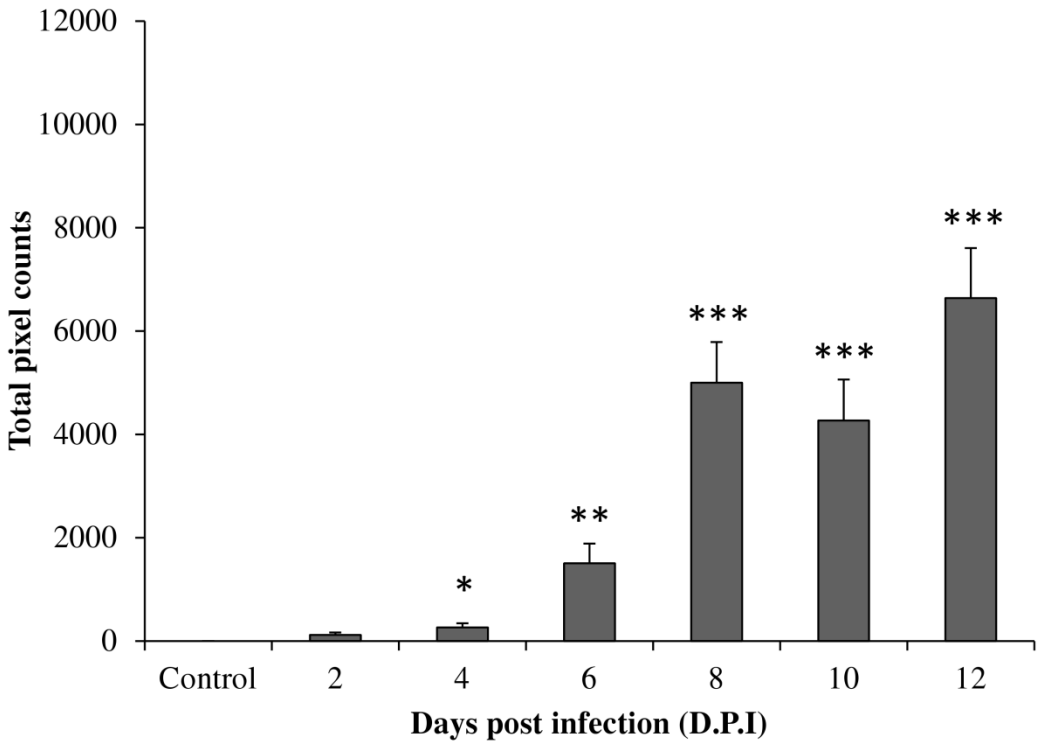

Figure 20 – Image analysis data from the 10^{-8} 22L-infected N2a time-course

The pixel counts of SB/ThT-positive staining, taking into account the background autofluorescence in the uninfected controls over 14 days post 10^{-8} 22L infection in N2a cells. Error bars shown are SEM (n = 30 images from 3 separate experiments), * = $p \leq 0.05$, ** = $p \leq 0.01$ and *** = $p \leq 0.001$ when compared to the uninfected controls.

Finally, N2a cells were infected with a 10^{-9} dilution of 22L infectious material and the prion propagation over 12 days was observed by the accumulation of amyloid specific SB/ThT staining. The representative micrographs in Figure 21 demonstrate no significant increase in ThT positive staining up until 8-12 days post infection. However after 12 days post infection, a number of smaller ThT positive amyloid plaques were observed accumulating around the cells (Figure 21). The plaques observed were visually smaller than the plaques observed in any of the previous higher dose experiments.

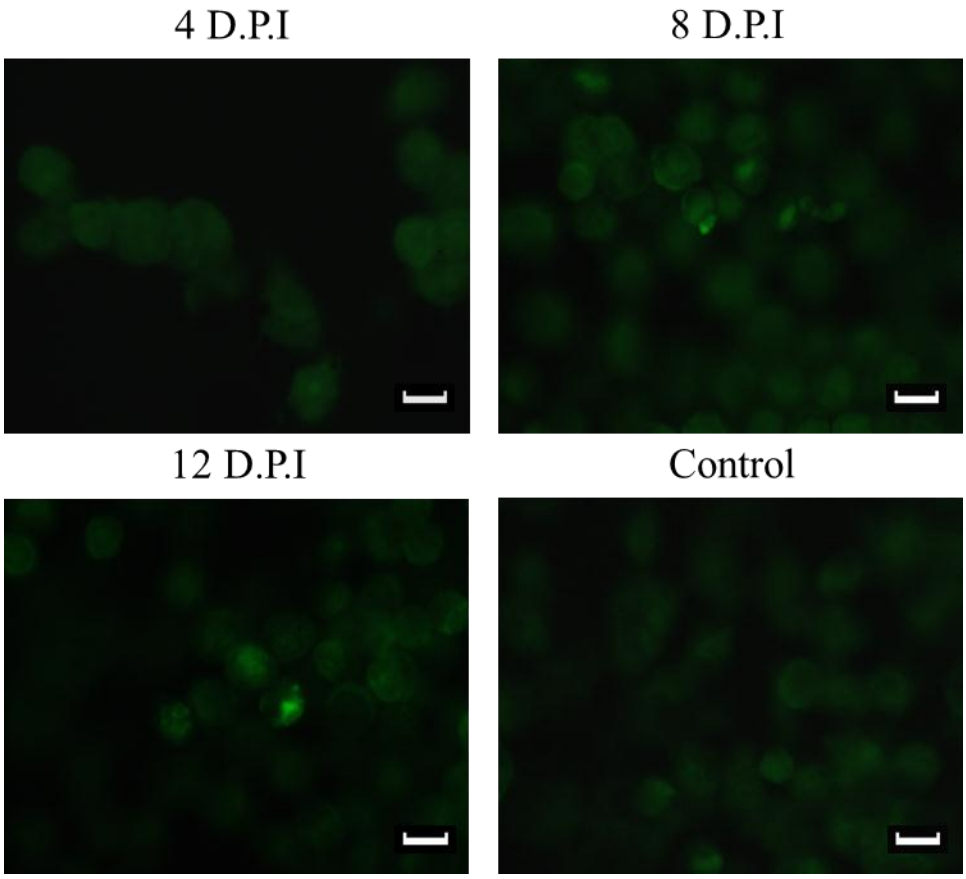

Figure 21 – Example micrographs from the 10^{-9} 22L-infected N2a time-course

Representative micrographs from the 10^{-9} 22L infected N2a cells stained with SB/ThT 4, 8 and 12 days post initial infection and the uninfected controls. Scale bars = 10 μm.

The increase in ThT signal was confirmed by image analysis with a significant peak in ThT signal intensity shown after 8 - 12 days post initial infection (Figure 22). The levels of ThT signal within this lower dose infection where considerably reduced in comparison to the higher dose infections when propagated over 12 days.

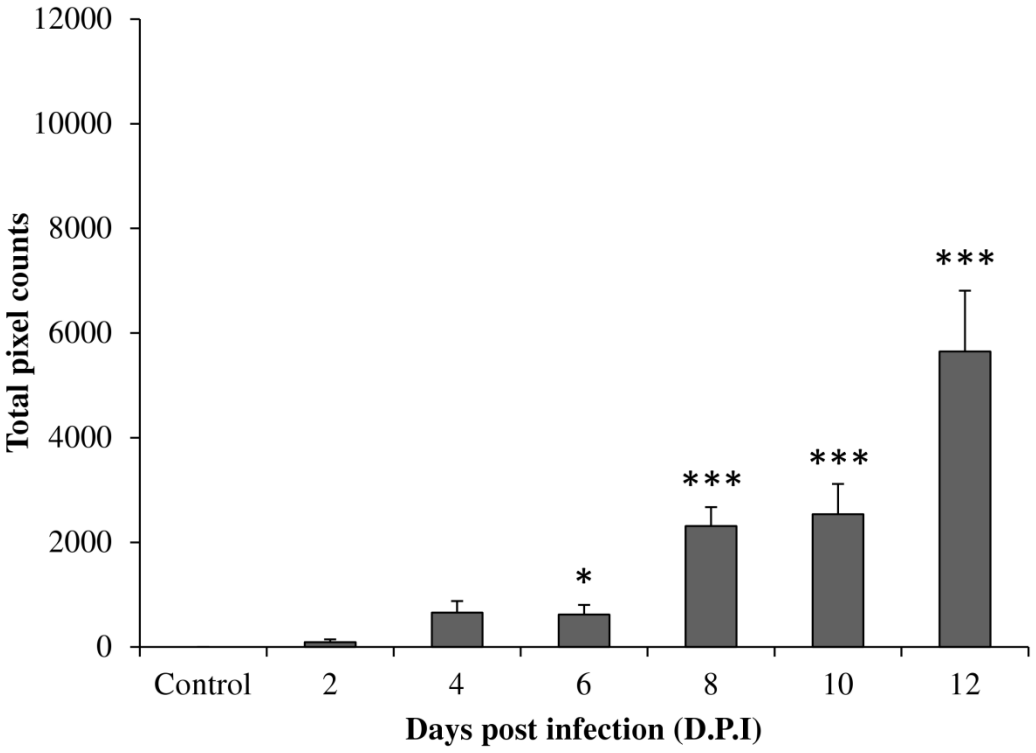

Figure 22 – Image analysis data from the 10^{-9} 22L-infected N2a time-course

The pixel counts of SB/ThT-positive staining, taking into account the background autofluorescence in the uninfected controls over 14 days post 10^{-9} 22L infection in N2a cells. Error bars shown are SEM (n = 30 images from 3 separate experiments), * = $p \leq 0.05$ and *** = $p \leq 0.001$ when compared to the uninfected controls.

3.3.3.2 Western blot analysis

Firstly, a current Western blot protocol used for the detection of PrP^{Sc} in ME7-infected brain homogenate (Herve et al. 2009), was adapted and optimised for the detection of PrP^{Sc} in 22L-infected samples. Initially, two commercially available prion specific antibodies (SAF 60 and 6H4) were tested using different dilutions of PK to determine the level of PK required digesting PrP^{c} and still detecting PrP^{Sc} or PrP^{res} in the 22L-infected brain homogenate.

Initial evaluation of the protocol used for the detection of PrP^{Sc}/PrP^{res} in ME7 infected brain homogenates in previous experiments was tested using SAF 60 (binding to region 142 – 160 of PrP) at a dilution of 1/5000 (v/v) (Figure 23).

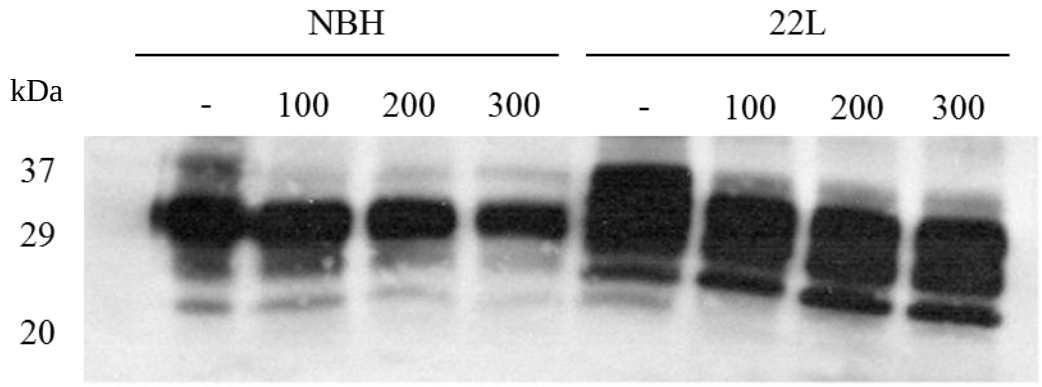

Figure 23 – Western blot optimisation with SAF 60 monoclonal antibody 1

Western blot analysis of prion protein content in normal brain homogenate (NBH) and 22L-infected brain homogenate (22L) after digestion in varying dilutions of proteinase K (PK) (none (-), 100, 200 and 300 ng PK). The primary antibody used was SAF 60 at a dilution of 1/5000 (v/v) and the equivalent of 30 µg of brain homogenate protein was loaded in each lane.

Figure 23 indicates that, even using a PK concentration of 300 ng, PrP^c was not fully degraded. In addition, despite only a 5 sec exposure to the X-ray film, the signal was too high, suggesting that either the primary or secondary antibody concentrations were not optimum. To correct this, the following blot was developed using SAF 60 at a 1/10000 (v/v) dilution to see if an improvement in the quality of the previous blot could be attained (Figure 24).

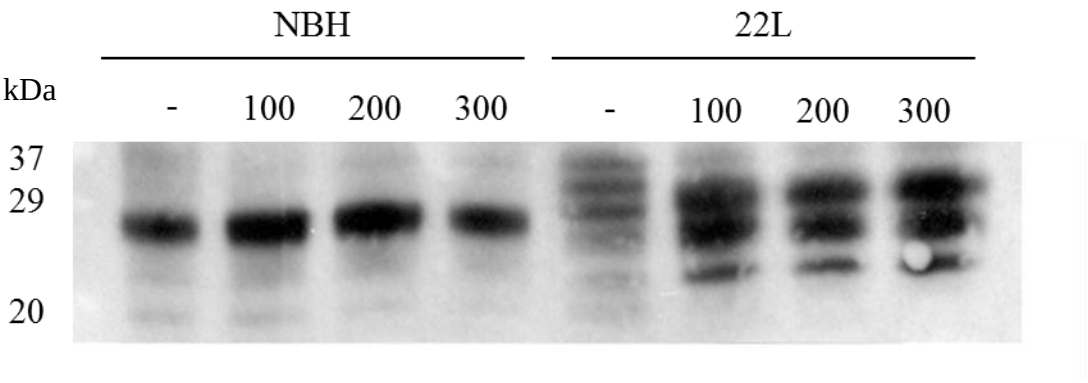

Figure 24 – Western blot optimisation with SAF 60 monoclonal antibody 2

Western blot analysis of prion protein content in normal brain homogenate (NBH) and 22L-infected brain homogenate (22L) after digestion in varying dilutions of proteinase K (PK) (none (-), 100, 200 and 300 ng PK). The primary antibody used was SAF 60 at a dilution of 1/10000 (v/v) and the equivalent of 30 µg of brain homogenate protein was loaded in each lane.

The chemiluminescent signal observed while using the lower concentration of SAF 60 was improved compared to the higher concentration in Figure 24. However, there was still positive signal in the NBH suggesting either the levels of PK are not high enough to digest the PrP^c or that there is some unspecific binding associated with the binding region of this antibody associated with the 22L-infected brain homogenate.

Finally, the primary antibody 6H4 (Prionics, binding to region 144 -152 of the prion protein) was used to replace SAF60 to determine if the bands remaining after PK

digestion were caused by unspecific binding of the SAF 60 antibody. The blot demonstrated a clear reduction in PrP^{c} expression in the NBH controls through increased concentrations of PK (Figure 25). Moreover, $PrP^{27\text{-}30}$, characterised by the three bands (Di, mono and un-glycosylated) associated with PrP^{Sc} digestion by PK, are clearly present in the lanes containing 22L infected homogenate (Figure 25). This blot confirmed that using 6H4 (1/5000 v/v) as the primary antibody and a PK concentration of 10 ng PK per µg of sample protein (300 ng PK digested 30 µg of cellular protein in the optimisation blots) was the chosen parameters for 22L PrP^{Sc} detection using this Western blot protocol.

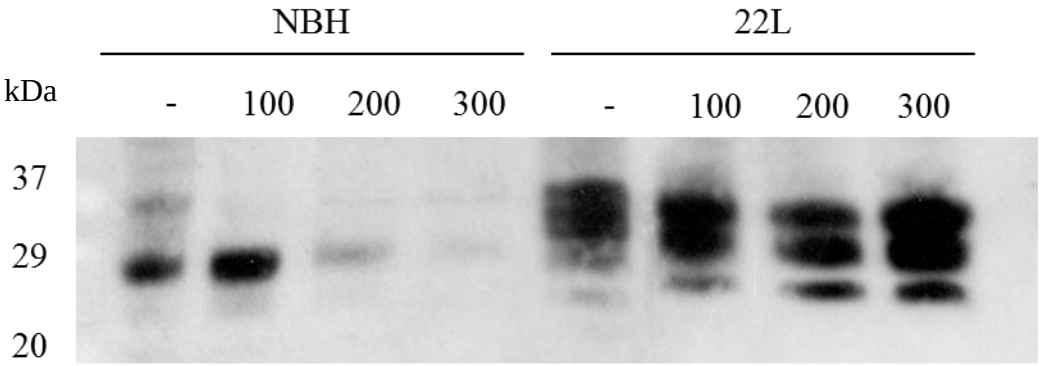

Figure 25 – Western blot optimisation with 6H4 monoclonal antibody

Western blot analysis of prion protein content in normal brain homogenate (NBH) and 22L-infected brain homogenate (22L) after digestion in varying dilutions of proteinase K (PK) (none (-), 100, 200 and 300 ng PK). The primary antibody used was 6H4 at a dilution of 1/5000 (v/v) and the equivalent of 30 µg of brain homogenate protein was loaded in each lane.

The sensitivity of the detection of PrP^{Sc} accumulation in 22L-infected N2a cell lysates from the time course experiments using the Western blot analysis was tested using the described, optimised protocol. Initial blots demonstrated no PrP^{Sc}-associated bands after PK digestion in the uninfected control cell lysates. However, a small accumulation of the di-glycosylated band of PrP^{Sc} over the 12 day time course with an

initial 10^{-2} 22L infection was observed in the infected N2a cell lysates (Figure 26, A and B). Clear triplicate bands associated with PrP^{Sc} in the 22L control lanes post PK digestion were observed (Figure 26, A and B).

A similar result was shown in the 10^{-4} 22L infected samples with a very small amount of the Di-glycosylated PrP^{Sc} isoform present in the infected samples with a slight increase in expression over 10 days post initial infection. The final blot is from the samples taken from the 10^{-6} 22L infected N2a time course and demonstrates no PrP^{Sc} positive bands across the 14 day time course; suggesting that the limit of the WB detection of PrP^{Sc} from 22L propagation in the N2a time course infections is below a 10^{-4} dilution of initial 22L infectious material when analysing the cell lysate material from 35 mm cell culture dishes.

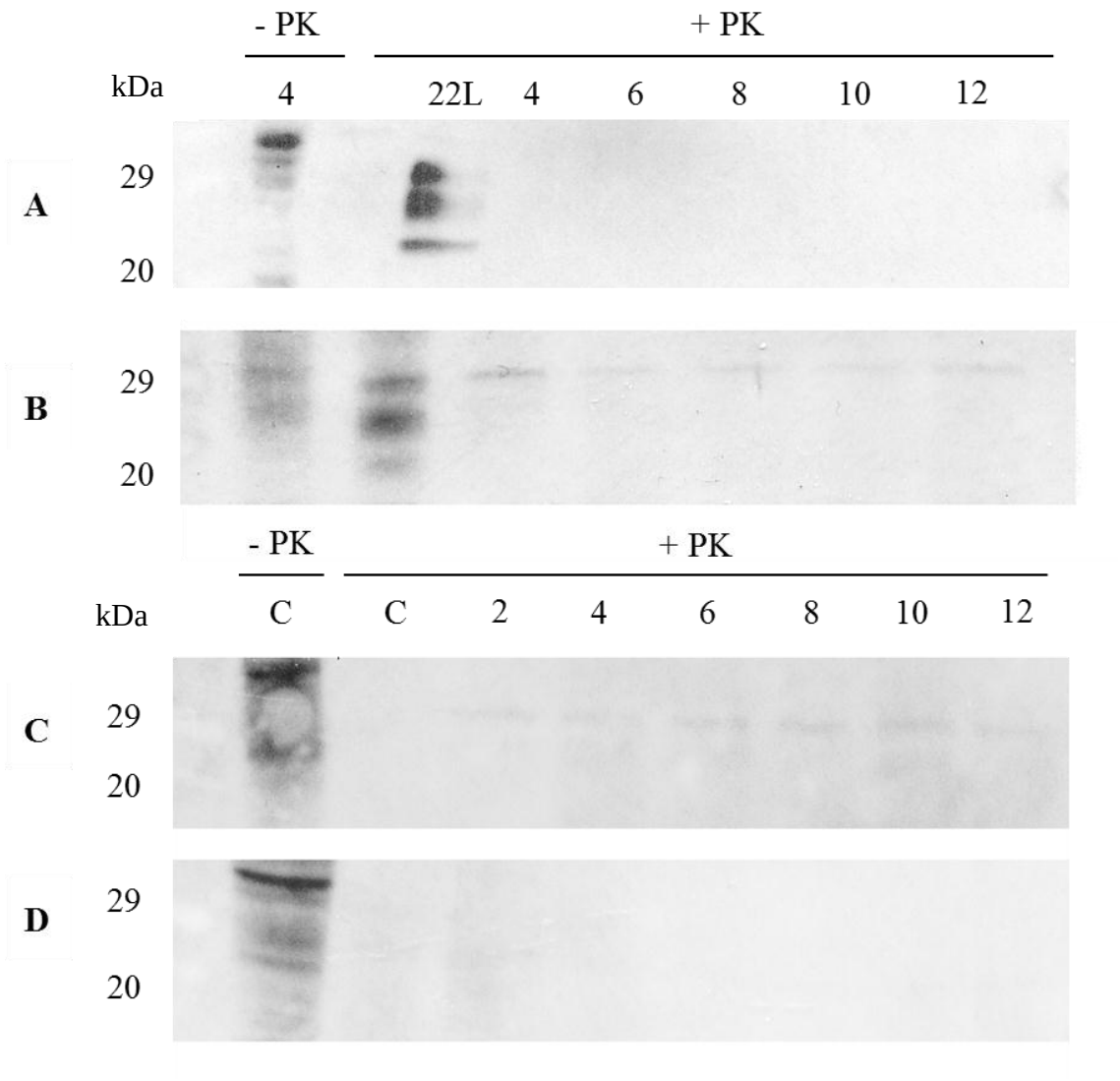

Figure 26 – Western blot of N2a lysates from the 22L infection time-courses

Western blot analysis of the N2a cell lysates, taken from the time course infections, after varying initial doses of 22L-infected brain homogenate. Blot A shows the uninfected controls from the 12-day series. Blot B shows the 10^{-2} infected N2a lysate samples, the lane numbers represent days post infection with or without PK digestion and the "22L" lane represents the 22L-positive control. Blots C and D show the samples from the 10^{-4} 22L-infected N2a time-course (C) and the 10^{-6} 22L-infected N2a time-course (D), lanes represent the days post infection and controls (c) with or without PK digestion. The equivalent of 20 µg of lysate protein was loaded in each lane.

3.4 Discussion

The iatrogenic transmission of infectious prions has been demonstrated in a number of studies confirming the ability of PrP^{Sc} to be transmitted from infected instruments (Duffy et al. 1974, Gibbs et al. 1994, Weissmann et al. 2002), tissue transplants and blood transfusions (Aguzzi et al. 2008, Furtner et al. 2008, Lemmer et al. 2008, Will 2003, Zanusso et al. 2005). Furthermore, the presence of PrP^{Sc} has been observed in a number of other biological samples including urine and stools (Gonzalez-Romero et al. 2008, Maluquer de Motes et al. 2008). The increase in reported anatomical regions associated with PrP^{Sc} accumulation amplifies the risk of iatrogenic CJD; especially from transplants, transfusions and surgical procedures; thus heightening a concern for public health. The poor efficacy of current decontamination protocols regarding prion decontamination used in SSD's also increases the potential risk of iatrogenic CJD transmission.

Although new decontamination techniques are currently being researched (Fichet et al. 2004, Fichet et al. 2007a, Paspaltsis et al. 2009) most methods of prion detection used in these studies rely on Western blot and immunoassays. These methods have previously been reported to have limitations in sensitivity, in addition to only detecting the presence of residual PrP^{Sc} and not the remaining infectivity. Currently, infectivity of remaining prion contamination following decontamination is performed by animal infectivity bioassays (Fichet et al. 2007b, Lawson 2008) which also have limitations as previously reported. As well as being very time consuming, expensive and pose significant ethical issues; they are limited to detecting the infectivity of animal and animal adapted prion strains due to the "species barrier". A recent study by Giles et al. 2008 has alerted the English Department of Health to the validity of animal and animal adapted prions as models for CJD due to the variations in different strains resistance to inactivation (Giles et al. 2008).

These issues in current detection methods have opened the way for the production of sensitive cell-based bioassays to detect prion infectivity from potentially a

number of different prion strains. A study by Edgeworth et al. 2009 produced an N2aPK1-based assay that has the ability to detect prion infectivity from infected wires with a sensitivity of detecting down to a 10^{-10} dilution of RML infected brain homogenate using an immunoblot based assay (Edgeworth et al. 2009). However, as discussed previously, these assays rely of immuno detection of PrP^{Sc} within the cells. More recently it has been questioned that the majority of disease-associated PrP^{Sc} is actually sensitive to PK digestion; therefore, the assays that rely on PK digestion may not be detecting all disease-associated material (D'Castro et al. 2010, Kuczius and Groschup 1999, Thackray et al. 2007). Therefore, this chapter introduced the production of a sensitive N2a based cell assay using *in situ* prion amyloid staining to detect infectivity which can be adapted to different cell lines for the potential detection of CJD infectivity.

N2a#58 cells were used in these studies as opposed to other N2a sub-clones because they have been transfected with wild type mouse Prnp-α cDNA, in order to amplify the production of PrP^{c} therefore increasing the susceptibility of prion infection within these cells (Mange et al. 2002, Nishida et al. 2000). Their susceptibility to infection from several murine prion strains has also been demonstrated (Mange et al. 2002, Nishida et al. 2000). DMEM media without HEPES buffer was used as it has been previously demonstrated in N2a cells and NSC's that HEPES buffer inhibits prion propagation (Delmouly et al. 2011).

Firstly, the sensitivity of two new ThT-based stains, for the detection of prion amyloid as a pathological marker of the propagation of prion infection in N2a cells over 14 days post initial infection was analysed. The N2a cells were initially infected with either a final dilution of 10^{-4} or 10^{-6} 22L and stained with ThT alone. A serial dilution titre of ThT concentration was first analysed to find a compromise between specific signal of ThT bound to prion-associated amyloid and the background autofluorescence observed in previous studies using ThT staining (Herve et al. 2009, Lipscomb et al. 2007a). The optimal dilution of 0.02% (w/v) ThT in 0.01 M HCl was used to stain the infected N2a cells every two days post initial infection over a 14 day time course. In the 10^{-4} 22L-infected N2a cell experiment, ThT staining alone showed an increase in prion amyloid signal from 8 days post initial infection up until a peak level of prion amyloid

observed after 12 days. However, when ThT alone was used for the detection of prion amyloid in the cells initially infected with a final 10^{-6} dilution of 22L-infected brain homogenate there was very limited ThT signal observed until 10 and 12 days post infection where very small amounts of ThT staining was observed. The image analysis was not able to detect a significant increase in ThT-positive signal and demonstrated no correlation in the ThT signal and the expected propagation of 22L prion within the cells.

Initial problems using ThT staining alone were associated with a significant level of autofluorescence, which was confirmed to be caused by lipids in the cells and tissues observed in previous experiments relying on ThT staining. Sudan black is a histochemical stain that binds to, and stains lipids black/deep red and does not itself fluoresce, therefore quenching autofluorescence caused by lipids. As a consequence, the addition of SB staining prior to ThT was evaluated. This SB/ThT staining used in the 10^{-4} 22L infection experiment showed an initial ThT signal in the 2 days post initial infection sample, caused by the initial dose of prion infected material remaining after media change in the cells. This signal increased slowly from 6 – 8 days post infection and then greatly increased up to 12 days post infection. The SB/ThT staining also improved the signal of ThT visible in the 10^{-6} 22L infected N2a cells experiment where an increase in prion amyloid staining up until 12 days post infection was observed. This confirmed that the addition of the SB before the ThT staining improved the sensitivity of this protocol.

The sensitivity of the SB/ThT assay was further demonstrated by initially infecting the N2a cells with a final 10^{-8} or 10^{-9} dilution of 22L-infected homogenate and then observing the propagation over 14 days as before. In both cases a significant propagation of amyloid was observed, however the levels of ThT-positive signal were lower than those in the higher dose infections. In all the time-course infections the levels of prion-associated amyloid peaked at 10 - 12 days post infection. Although all of the time-course experiments were run for 14 days, only data up until day 12 has been shown in this Chapter. Increased and inconsistent loss of viable cells was observed after 12 days culture post initial infection as the levels of confluency in the 35 mm dishes reached around 100 % between 10 and 12 days. After 12 days the cells had become stressed and were lost during media change and staining which deemed the 14 day time

point as un-analysable as the data would be inconsistent between repeat experiments. This observation highlighted the need for cell passages to improve the long term culture of the infected cells.

Western blot (WB) detection is widely used to analyse the levels of PrP^{Sc} in prion infected samples, thus WB was used to analyse the levels of PrP^{Sc} in lysates taken at every time point in the time-course infections so that the sensitivity of WB could be directly compared to the SB/ThT assay. Initial experiments aimed to optimise the WB protocol for the detection of PrP^{Sc} in 22L-infected brain homogenates used to infect the cells. A protocol used for the detection of PrP^{Sc} in ME7-infected brain homogenates was first tested using the monoclonal prion specific antibody SAF60; however, at both 1/10000 and 1/5000 dilutions bands still showed up in the PK digested NBH controls. Therefore, another widely used prion specific monoclonal antibody 6H4 was tested at a dilution of 1/5000. This antibody produced clear three bands associated with PrP^{Sc} in the 22L-infected homogenate and low to no signal was observed in the PK digested NBH control. Consequently, the optimised protocol using the primary antibody 6H4 at a 1/5000 concentration and a PK concentration of 10 ng PK/µg protein alongside the very sensitive Amersham ECL plus chemiluminescent detection were used to analyse the infected lysates.

The band relating to the di-glycosylated isoform of PrP^{Sc} was observed in the 10^{-2} infected N2a lysates showing prion accumulation within the cells over the time course propagation. A similar result was observed in the 10^{-4} 22L-infected N2a lysates with a slight increase in density of the di-glycosylated isoform of the infectious prion observed over 12 days of infection. This correlated with the bands shown in a 10^{-4} 22L-infected NSC's in a previous study (Figure 27) (Milhavet et al. 2006). The increased density of the three PrP^{res} bands demonstrated in the 10^{-2} 22L infection could be due to the higher levels of propagation observed in the NSC's potentially from the increased endogenous PrP^{c} when compared to N2a cells (Milhavet et al. 2006). Furthermore, the increased PrP^{Sc} associated bands found in published WB analysis of cell culture infectivity is caused by the increased protein loaded into each well (~100 – 200 µg) (Delmouly et al. 2011, Mange et al. 2002, Milhavet et al. 2006). Whereas, we are only analysing one 35 mm dish of cells per well (~20 µg of protein) so that the analysis is

directly comparable to the cell population that are analysed with the SB/ThT analysis. No PrP^{Sc} positive bands were observed in the 10^{-6} 22L infected N2a lysates, suggesting this is the level of WB sensitivity for these assays.

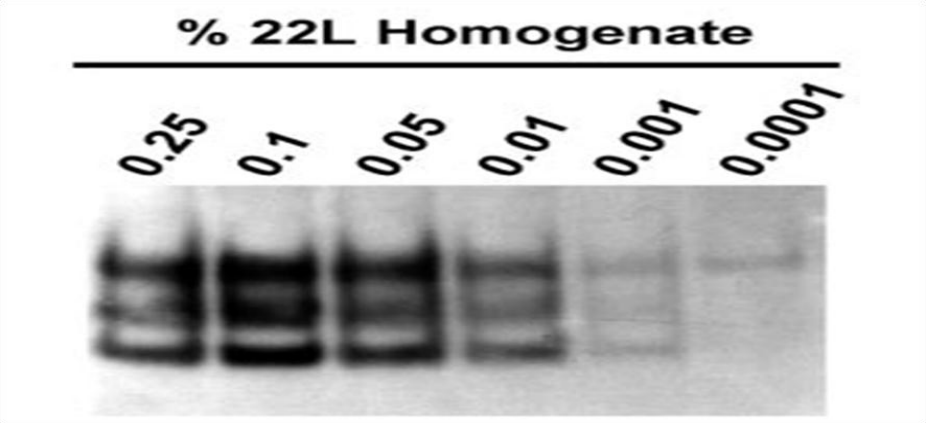

Figure 27 – Example Western blot of 22L titre infection in NSC's

Western blot analysis of 22L titre infections in NSC's taken from Milhavet et al. 2007, used to show the single di-glycosylated band shown in the 10^{-4} 22L infection (0.0001%) (Milhavet et al. 2006).

These preliminary results confirm that the SB/ThT assay has a much higher sensitivity when directly compared to WB analysis and this sensitivity could be further improved in the passage infection assays described later. Amyloid specific ThT is not only specific to amyloids formed from aggregated prion protein but it also binds to amyloids formed in other amyloidosis, including Alzheimer's disease (Herve et al. 2009, Lipscomb et al. 2007a, Maezawa et al. 2008). However, ThT binding to amyloid is still a relevant pathological marker to detect prion infectivity in cell based assays. The sensitivity of this assay is almost equal to that of the Collinge group N2a PK1 scrapie cell assay but the SB/ThT assay has the added benefit of being able to detect the accumulation of prion infectivity *in situ* without having to elute or PK digest the infected cell material (Edgeworth et al. 2009). Consequently, this new assay procedure was utilised for subsequent experiments.

Chapter 4

Neuroblastoma passage infections

4.1 Introduction and aims

The previous chapter introduced the development of a SB/ThT staining protocol for the detection of amyloid accumulation within N2a #58 cells as a marker of prion infectivity. Although the detection of an initial dose of a final 10^{-9} dilution of 22L-infected brain homogenate using SB/ThT staining far surpassed the sensitivity of WB analysis ($10^{-4} – 10^{-6}$ 22L); there were some observed limitations within the initial format of this assay. Primarily, 12 - 14 days growth of the N2a cells without passaging caused significant cell stress within days 10 – 14 and ultimately the level of cell loss with media change and staining at the 14^{th} day led to unreliable and poor quality results. The variations in propagation over the different separate experiments led to larger error within the quantitative results, especially when detecting lower prion doses. Whether this is caused by further issues with background fluorescence or variations in propagation over these short time courses is currently unknown. It could also be postulated that slower cell proliferation at the point that the cells become fully confluent between days 8 – 10 and the poor attachment of newly split cells could lead to a lower turnover of PrP^c and therefore reduced prion conversion within the culture environment.

The majority of the most sensitive assays used to detect both prion presence and prion infectivity rely on several cycles or cell splits/passages to increase incubation time. Furthermore, the introductions of fresh substrates are used to aid the conversion or propagation of the infectious material. PMCA amplification relies on several rounds of sonication and incubation with or without the introduction of new seeds or prion capture beads to aid and increase amplification (Gonzalez-Montalban et al. 2011, Saborio et al. 2001, Weber et al. 2007). RT-QUIC relies on multiple rounds of shaking to induce PrP^c conversion with or without the addition of an immuno-precipitation step (Atarashi et al. 2008, Atarashi et al. 2011a, Orrú et al. 2011). Animal bioassays require >100 days *in vivo* propagation of the prion protein to induce disease and ultimately an end point of death (Fichet et al. 2007b, Lawson 2008). The majority of current cell based assays rely on several cell passages post initial inoculation in the diluted infectious material to improve the sensitivity and reliability of the assays (Edgeworth et al. 2009, Klohn et al. 2003, You et al. 2010).

Therefore, this chapter concentrates on incorporating several cell passages into the N2a #58 cell propagation discussed in Chapter 3. Firstly the, optimal day for cell passage was determined. This was followed by the analysis of the sensitivity of the SB/ThT staining in relation to the increased propagation time introduced with the cell passages. The SB/ThT detection sensitivity was again directly compared to WB analysis as described in the previous chapter.

4.2 Materials and methods

Details of the materials and methods for this chapter can all be found within Chapter 2 of this report. Briefly, N2a #58 cells (2.1.1) were cultured as described in section 2.2.1 and then subjected to 22L (2.1.3 and 2.3.1) infection following the neuroblastoma passage infections described in section 2.3.3. Detection of prion infectivity was obtained by utilising the SB/ThT staining as described in section 2.4.2. ThT signal was analysed by epi-fluorescent microscopy and quantified using image J software described in section 2.4.5. Furthermore, cell lysates were analysed for PrP^{res} content using the Western blot protocol described in section 2.4.6. All statistical analysis was carried out as highlighted in section 2.7.

4.3 Results

4.3.1 Optimising passage day

To improve the sensitivity of the neuroblastoma time-course assays described in Chapter 3 and to minimize the loss of cells associated with increased confluency observed in these assays, the amyloid accumulation associated with prion propagation was analysed over several passages post initial infection to determine if increased propagation time could be used to increase the sensitivity of the assay or subsequently if infection susceptibility was compromised by the splitting of the cells.

Firstly, the optimal day to passage the cells in order to achieve a balance between cell confluency and optimal propagation was tested by comparing passages every 8, 10 and 12 day post initial 10^{-4} 22L inoculation. At each passage point the amyloid accumulation was assessed by SB/ThT staining described previously. Passaging every 8 days post initial infection demonstrated a slow accumulation of amyloid with the peak levels reached after 4 passages or 34 days post infection. Representative micrographs shown in Figure 28 demonstrate very small ThT-positive aggregates after the first and third passages and then the accumulation of larger plaques were observed at each subsequent passage thereafter (Figure 28). The image analysis data showed an initial increase in ThT-positive signal at the point of the first passage (8 days), this signal then dropped after the next passage (16 days) and then significantly increased over the passages 4 – 6 (days 32-48) where a plateau of ThT-positive signal was observed (Figure 28).

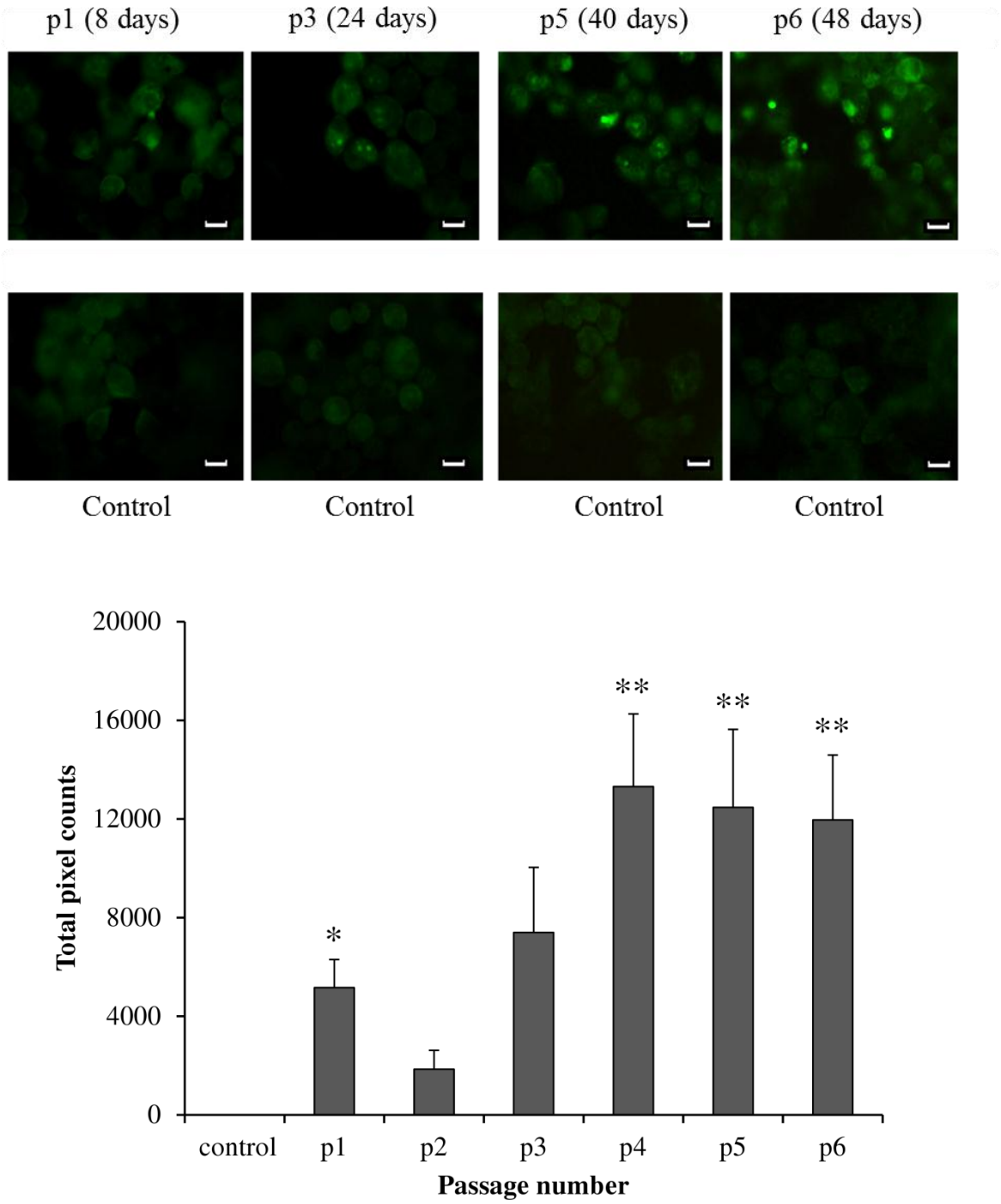

Figure 28 – Example micrographs and SB/ThT image analysis from the 10^{-4} 22L-infected N2a 8 day passage study

Representative micrographs from the 10^{-4} 22L-infected N2a cells stained with SB/ThT after passages every 8 days post initial infection (left to right respectively) and the uninfected controls (below). Scale bars = 10 µm. The image analysis data demonstrates the pixel counts of SB/ThT-positive staining taking into account the background autofluorescence in the uninfected controls. Error bars shown are SEM (n=10), * = $p \leq 0.05$, ** = $p \leq 0.01$ when compared to the uninfected controls.

Passaging the N2a cells every 10 days post initial 10^{-4} 22L infection demonstrated a similar slow initial increase in ThT signal over the first 3 passages, as demonstrated in Figure 28 with the 8 day passages. However no initial drop in signal and amyloid accumulation was observed as was the case in the 8 day passage samples. The representative micrographs highlighted very little amyloid accumulation after the first passage (10 days) with a few infrequent, larger plaques after passages 2 and 3 (days 20 - 30) and larger, more widely occurring plaques were revealed after passage 4 (40 days) (Figure 29). This was further highlighted by the image analysis data which demonstrated a significant increase in ThT-positive signal over the first and third passages (days 10 – 30) even though an increase in plaque size was observed. A further and larger significant increase in ThT-positive signal was demonstrated after four passages (40 days) post initial infection (Figure 29).

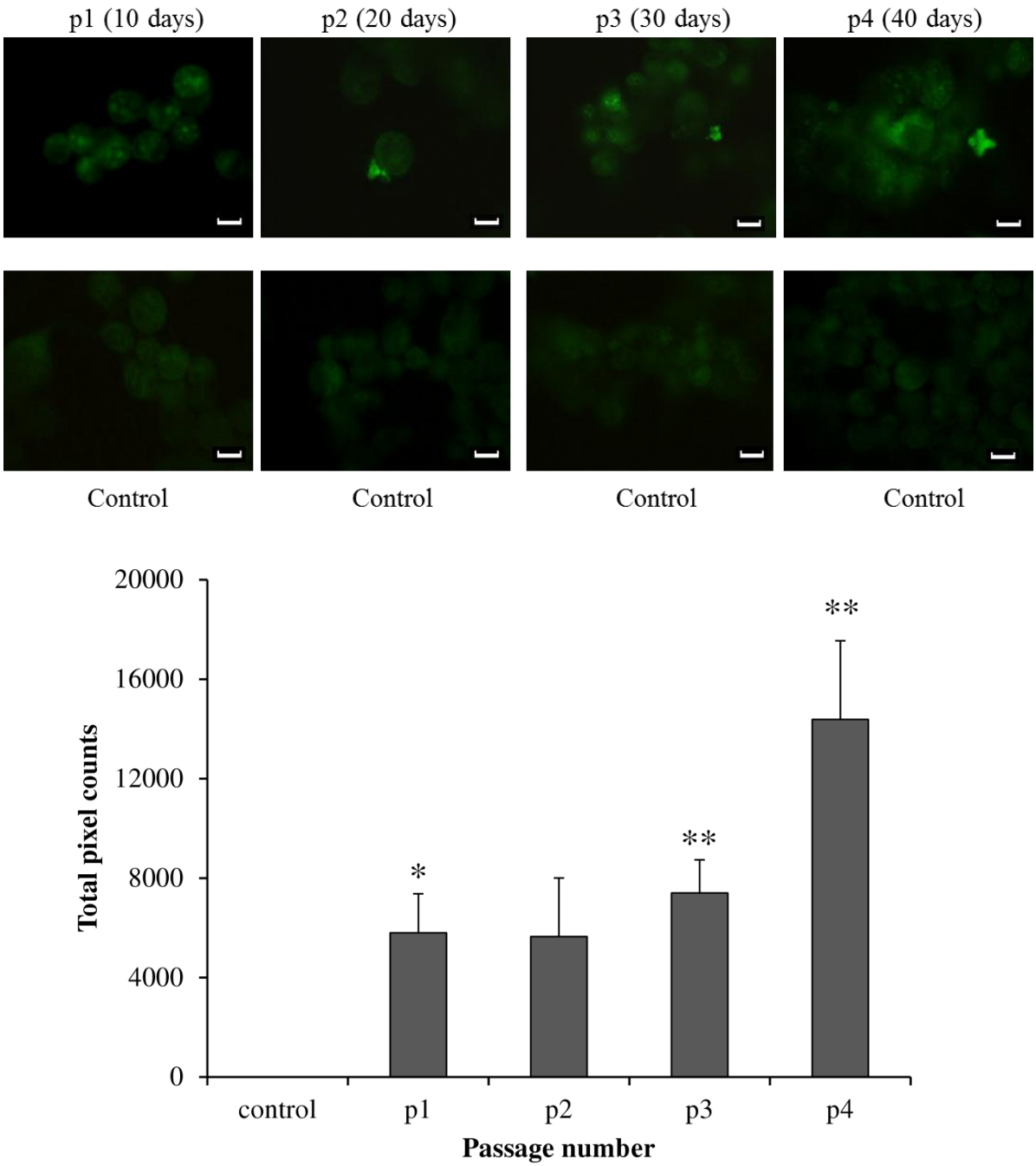

Figure 29 – Example micrographs and SB/ThT image analysis from the 10^{-4} 22L-infected N2a 10 day passage study

Representative micrographs from the 10^{-4} 22L-infected N2a cells (top) stained with SB/ThT after passages every 10 days post initial infection (left to right respectively) and the uninfected controls (below). Scale bars = 10 µm. The image analysis data demonstrates pixel counts of SB/ThT-positive staining from the 10 day passage study samples taking into account the level of background autofluorescence found in the uninfected controls from each passage. Error bars shown are SEM (n=10), * = $p \leq 0.05$, ** = $p \leq 0.01$ when compared to the uninfected controls.

Passaging the N2a cells every 12 days post initial 10^{-4} 22L infection showed a more rapid amyloid accumulation than the 8 and 10 day passages. The representative micrographs highlighted very small ThT positive amyloid plaques formed over the first passage (12 days, Figure 30). Visually the plaque size and frequency significantly increased over the next three passages (days 12 - 48), where the highest level of ThT-positive signal and plaque size was observed at the point of the fourth passage (48 days) (Figure 30). However without extensive 3-dimensional analysis of the plaque size it is difficult to confirm the changes in plaque size apart from what is visually observed in the micrographs. The image analysis data confirmed a clear increase in ThT-positive signal over each of the passages following an almost linear trend. A significant increase in ThT signal was observed at passage 2, 3 and 4 when compared to the signal in the uninfected controls (Figure 30). However a loss of cells during media change between 11 - 12 days was observed questioning the reliability of passaging the infected cells every 12 days.

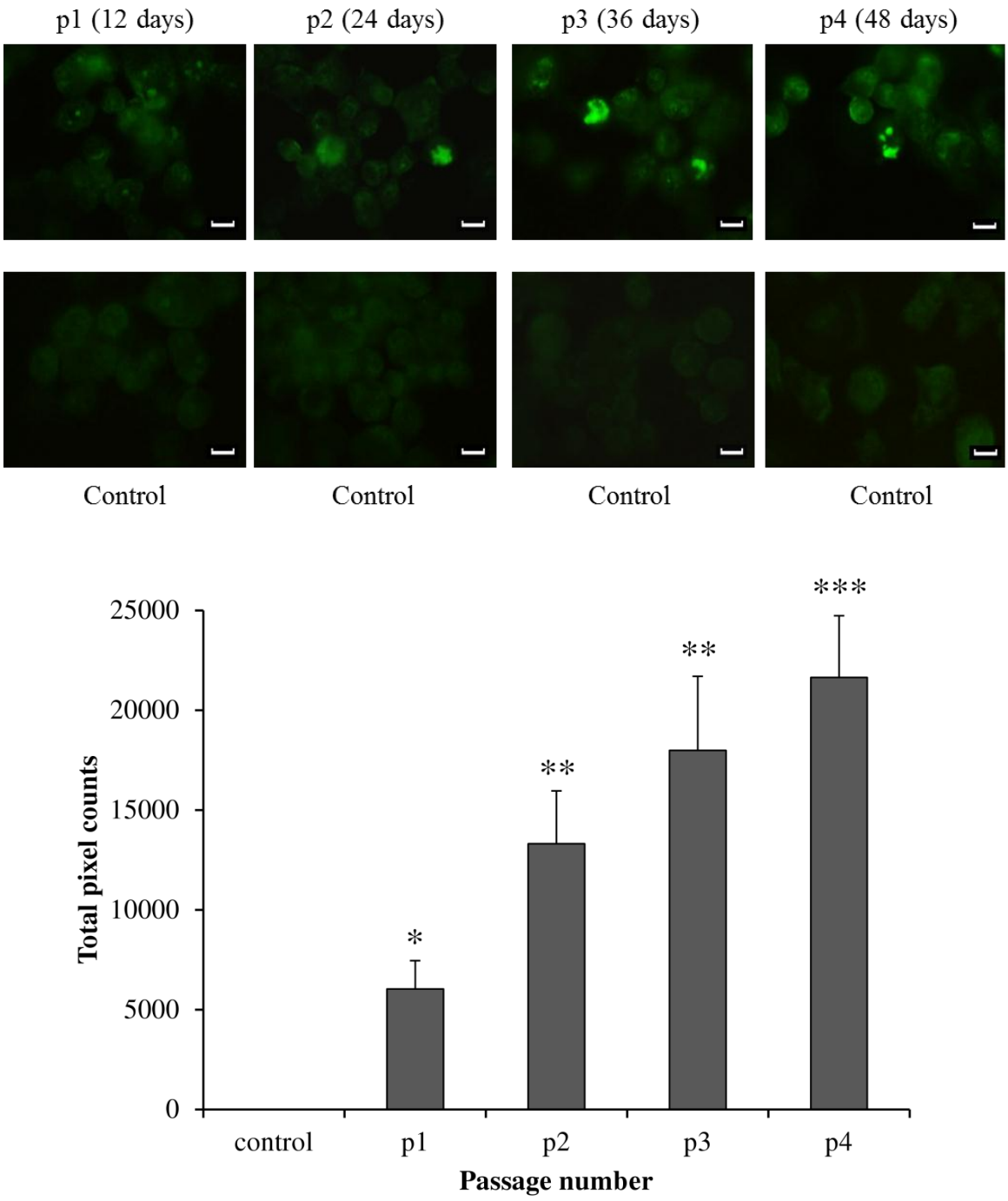

Figure 30 – Example micrographs and SB/ThT image analysis from the 10^{-4} 22L-infected N2a 12 day passage study

Representative micrographs from the 10^{-4} 22L-infected N2a cells stained with SB/ThT after passages every 12 days post initial infection (left to right respectively) and the uninfected controls (below). Scale bars = 10 µm. The image analysis data demonstrates the pixel counts of SB/ThT-positive staining taking into account the levels of background autofluorescence in the uninfected controls at each passage. Error bars shown are SEM (n=10), * = $p \leq 0.05$, ** = $p \leq 0.01$, *** = $p \leq 0.001$ when compared to the uninfected controls.

4.3.1.1 Western blot analysis (optimal passage day)

The accumulation of PrP^{Sc} following several passages was analysed using the optimised Western blot protocol utilising the 6H4 monoclonal antibody (Prionics) described previously in Chapter 3. The cell lysate samples from the 12 day passage study were analysed to determine if the sensitivity of the Western blot protocol is improved by allowing the prion aggregation to propagate over several passages as opposed to just 14 days post initial infection as discussed in the previous chapter. There were no infectious prions bands present in the control samples taken at each passage when compared to the 22L brain homogenate positive control (Figure 31). However, in the 10^{-4} 22L-infected cell lysates there was a 6H4-positive band highlighting the accumulation of the di-glycosylated isoform of PrP^{Sc} that increased in density over the 5 passages (Figure 31).

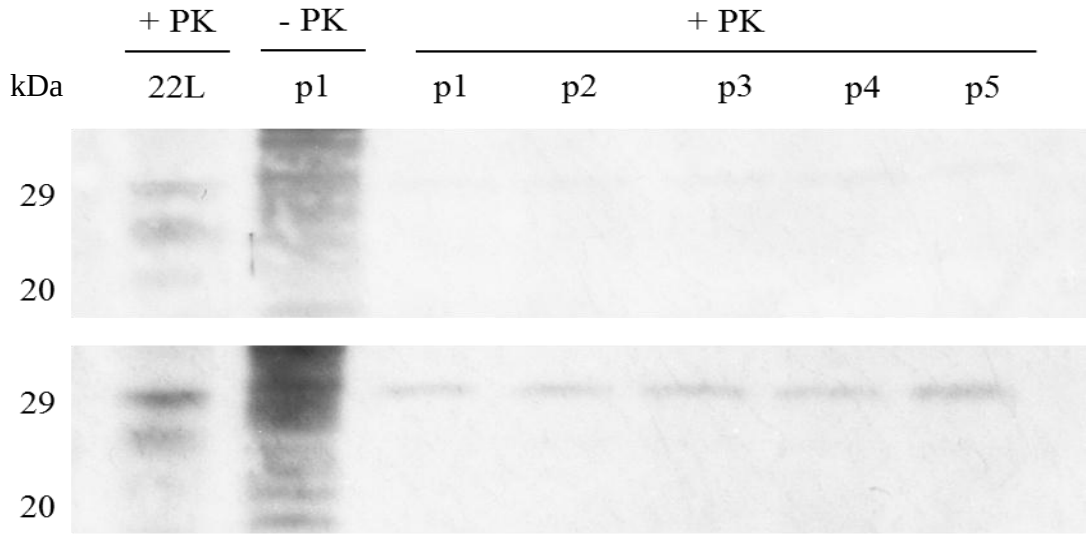

Figure 31 – Western blot analysis of the N2a lysates from the 10^{-4} 22L-infected N2a 12 day passage study

Western blot analysis of the PrP^{Sc} accumulation in the Neuroblastoma cells passaged every 12 days after an initial 10^{-4} 22L infectious dose (bottom) and the uninfected controls samples taken at every passage (top). The lane numbers represent the passage number post infection with or without PK digestion and the "22L" lane represents the 22L positive control. The equivalent of 15 μg of lysate protein was loaded in each lane.

Analysis of the density of the 6H4 immunoreactive bands representing the di-glycosylated isoform of PrP^{Sc} were analysed using the density analysis macro built into the Image J software. The image analysis confirmed an increase in band density over the 5 passages every 12 days post initial infection. This suggests that the di-glycosylated glycoforms of PrP^{Sc} increased during the 5 passages every 12 days post initial infection with a 10^{-4} dilution of 22L-infected brain homogenate (Figure 32).

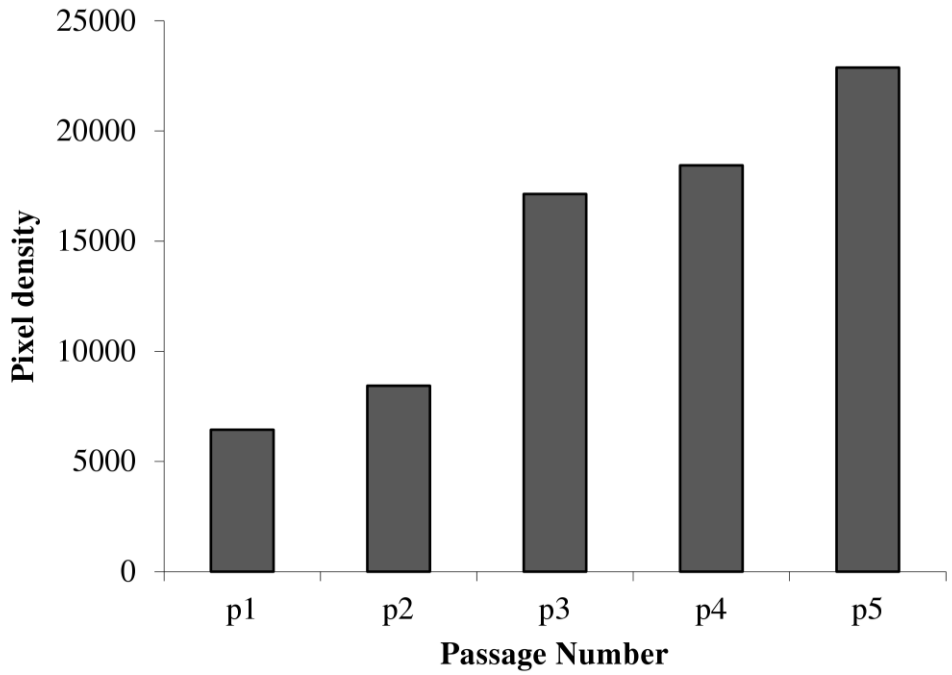

Figure 32 – Image analysis of Western blot band density

Image analysis of the pixel counts of the density of the 6H4 immunoreactive bands present after the WB analysis of the N2a lysate samples, taken at each passage point, every 12 days post initial 10^{-4} 22L infection.

4.3.2 Titre passage infection in N2a cells

The optimal passage day post infection to allow a consistent propagation of the infectious prion in the neuroblastoma cells was every 12 days. However, more crucially, passaging every 12 days was unreliable from experiment to experiment and passage to passage as the cells at this point were fully confluent and contact inhibition caused loss of cells during media changes and staining and subsequently could jeopardise the clarity of the assay. Thus, to compromise between cell viability and consistency of prion propagation, 10 days passaging post infection was determined to be optimal for the subsequent set of experiments used to determine the sensitivity of the N2a passage assays with SB/ThT detection. It was also observed that increased levels of background staining occurred in the confluent cells, which was also further hindered by the spheroid production associated with the cancerous nature of the N2a cells. Therefore a more dilute concentration of ThT [0.004% (v/v)] was used as a compromise between background and positive staining.

A titre infection of the N2a cells over several passages using dilutions of 22L-infected brain homogenate ranging from 10^{-4} to 10^{-10} was analysed. Lowering the initial 22L infectious dose showed a clear reduction in the level of ThT-positive signal. Also, as the dose was lowered, an increased number of passages were required to demonstrate a significant increase in ThT signal. However, a propagation of amyloid was observed over several passages after each of the initial 22L dilutions (Figure 33). Furthermore, the observed size of the plaques decreased whilst, conversely, the numbers of them increased as the infectious dose was lowered (Figure 34). All of the assays reached the highest levels of ThT positive signal after passage 8 (80 days) at which point the assays were terminated as a clear propagation was observed.

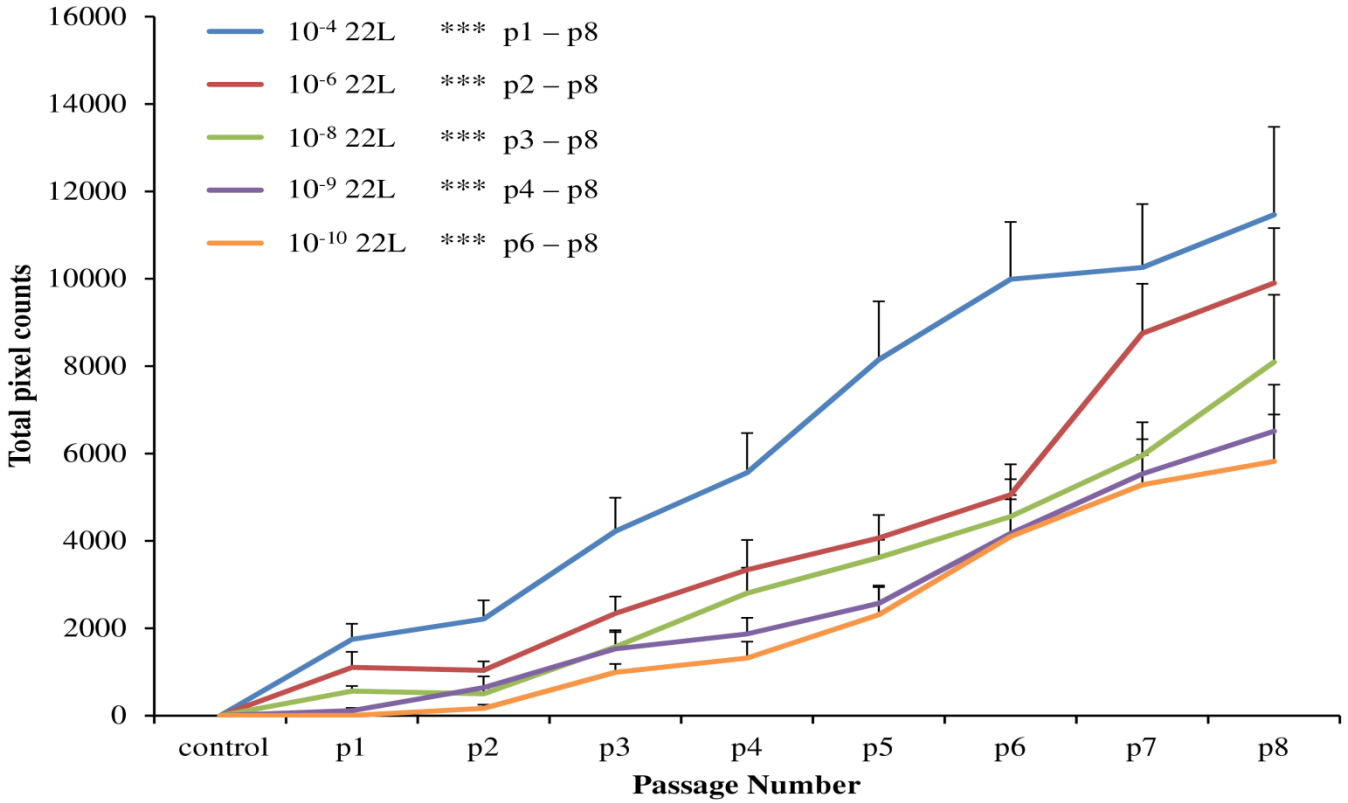

Figure 33 – The image analysis of ThT signal from the 22L titre dose response study

The image analysis of ThT-positive amyloid accumulation in the N2a cells over several passages every 10 days post initial 22L titre dilutions ranging from 10^{-4} – 10^{-10} of 22L-infected brain homogenate. Error bars represent SEM (n = 30) *** = $p \leq 0.001$ when compared to the uninfected controls.

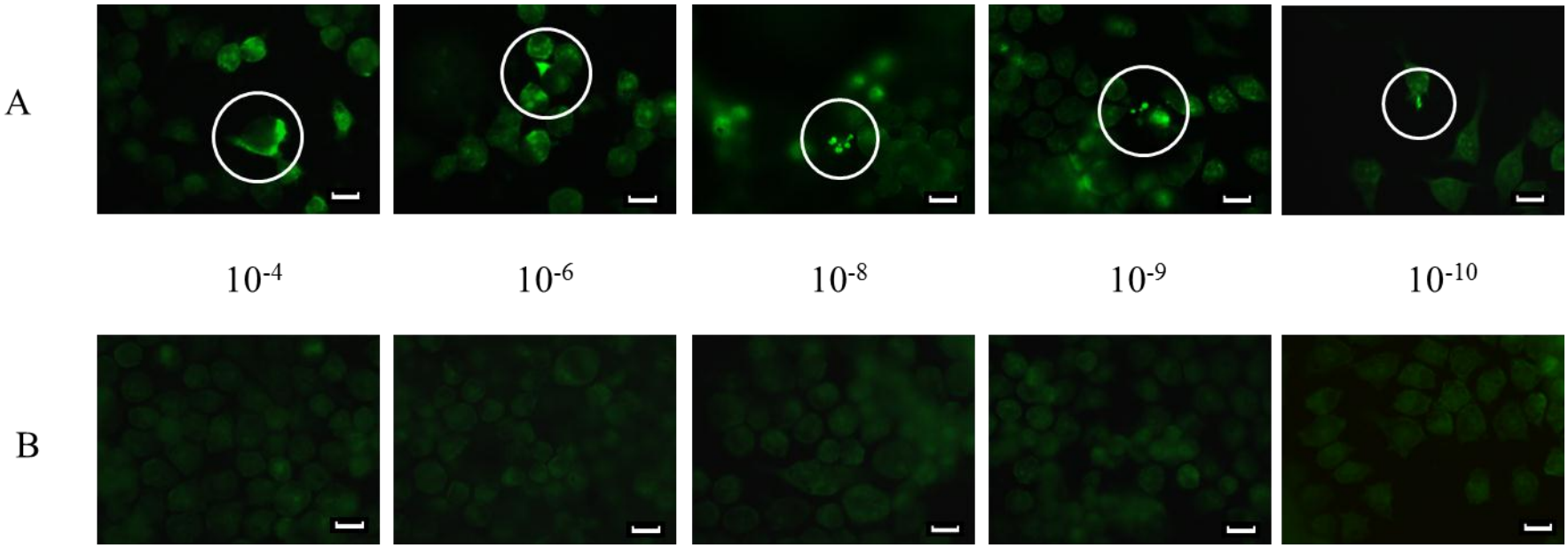

Figure 34 – Example micrographs of 22L dose response propagated in N2a cells

Micrographs of ThT staining taken from infected (A) and uninfected (B) N2a #58 cells at passage 8 (80 days) post initial 22L inoculation. The images represent a dose response from 10^{-4} 22L – 10^{-10} 22L (left to right respectively). The white rings highlight ThT-positive amyloid staining and demonstrate the changes in plaque size associated with the initial 22L dose concentration. Scale bars = 10 µm.

4.4 Discussion

In vivo animal-based bioassays demonstrate increased propagation of PrP^{Sc} over time. This is due to the fact that the natural cell turnover of PrP^{c} within the brain aids the prion conversion process from an infected inoculum or wire, amplifying PrP^{sc} and furthering disease progression. Therefore, current cell based assays used to analyse prion infectivity utilise several cell splits post initial inoculation with the infectious prion material to closer mimic the *in vivo* cell PrP^{c} turnover and therefore improve the sensitivity of the assays. The end point dilution TCIA (tissue culture infectivity assay) demonstrated that weekly passages post inoculation increased the sensitivity of the assay from detecting 10^{-4} dilution of 127S (sheep scrapie strain) infected brain homogenate after 5 passages to detecting $10^{-6.8}$ after 10 passages (You et al. 2010). The SCEPA assay utilises several passages every 3 days using different cell split ratios (1:3 and 1:8) to improve the sensitivity of detection to detect infectivity after an initial 10^{-10} dilution of RML-infected brain homogenate (Edgeworth et al. 2009).

Therefore, to improve the sensitivity, reliability and to prevent the loss of cells observed in the SB/ThT N2a time-course assays, the 22L prion infections were propagated over several passages of the N2a cells. The number of incubation days between passages was thought to be the crucial step to reach an optimal propagation within the cell assay and therefore aid the sensitivity of the SB/ThT detection protocol. Firstly, the optimal day for passaging the infected cells was determined. Passaging every 12 days gave the highest propagation over the shortest time. However the cell confluency after the 12 days was not always consistent and variations in cell loss was observed during media change and staining, thus questioning the clarity of the assay passaging at this time point. Therefore, a day 10 passage was chosen as optimal in order to compromise between the level of prion propagation and cell loss. Ten day passaging, demonstrated a significant increase in ThT over several passages, but an improved consistency in cell number adhered to the tissue culture plates at the point of analysis. After 10 days the N2a cells were ~90% confluent, thus a more reliable and consistent assay than over confluent and potentially stressed cells. The WB analysis of the PrP^{Sc} content in the cell lysates taken from the 12 day passage study demonstrated an increase

in just the di-glycosylated band of the prion protein (as observed in Chapter 3) correlating with the bands shown in the Milhavet NSC blot shown previously (Figure 27). However the discrepancies in band intensities can be explained by the increased protein loads used in the Milhavet work (Milhavet et al. 2006). The increase in the accumulation of the di-glycosylated PrP^{res} was confirmed by analysing the density of the bands over the 5 passages post initial infection.

Once the optimal passage day was confirmed the sensitivity of this assay was tested by inoculating the cells with a titre of final 22L dilutions ranging from 10^{-4} to 10^{-10}. An increase in ThT signal was observed after several passages in all of the cells apart from the uninfected controls. The SB/ThT staining highlighted an increase in amyloid accumulation demonstrating a dose dependent response after 7 – 8 passages. The different dilutions of 22L homogenate reached a statistically significant ($p = \leq 0.001$) increase in ThT signal compared to the uninfected controls at different passage points, with the lower initial 22L dose requiring more passages. This demonstrated that lower initial doses required more passages to reach a detectable level of infectivity; however even the most dilute (10^{-10}) still contained infectious material that was detectable once amplified. Also the size and distribution of the plaques varied depending on the initial 22L dose. Larger and less diffuse amyloid plaques were observed in the higher dose infections, whereas the lower doses resulted in smaller plaques at the same passage point. However, when smaller plaques were observed their frequency seemed to be increased when compared to the larger plaques. This could potentially suggest that the smaller plaques combine together over time to produce the larger plaques observed in the later passages with the higher doses. The passage infectivity studies determined that the SB/ThT detection of prion infectivity was 1 log more sensitive after several passages when compared to the time course assays. The SB/ThT detection also demonstrated >5 log improved sensitivity when directly compared to WB detection of prion propagation in cell lysates from the 35 mm tissue culture dishes.

These results confirm that the SB/ThT assay for the detection of prion-associated amyloid accumulation has a much improved sensitivity when compared to WB analysis of PrP^{Sc} accumulation in the cell lysates. The sensitivity of the SB/ThT assay matches that of the Collinge group scrapie cell assay but the SB/ThT assay has the

added ability of being able to detect the accumulation of prion infectivity *in situ* without having to membrane capture the cells for detection of PrP^{res} material (Edgeworth et al. 2009). Furthermore, the SB/ThT assay does not require PK digestion of the cells prior to detection. Therefore this assay would work well alongside assays using PK digestion and immuno detection as the combined results would portray a more realistic picture of the remaining infectivity within biological samples. This work demonstrates the potential of the SB/ThT assays after the propagation of infectivity over several passages post initial infection to be a novel, sensitive cell based infectivity assay. However, further adaptation of the assay is required for the detection of infectivity remaining on surfaces post decontamination.

Chapter 5

Neuroblastoma wire infectivity assays and the determination of decontamination efficacy

5.1 Introduction and aims

The previous chapter demonstrated the sensitivity of the SB/ThT assay for the determination of prion infectivity in N2a cells when infectious material was incubated in the cells over several passages every 10 days. The assay demonstrated a dose response to different dilutions of 22L homogenate detecting infectivity in samples as dilute as a 10^{-10} dilution of 22L-infected brain homogenate. However, these passage studies were detecting infectivity from the direct introduction of infected brain homogenate to the cells, which is not ideal to test decontamination protocols.

Techniques that analyse the presence of general protein, PrP^{Sc} and amyloid, such as PMCA, RT-QUIC, ASA, SR/THT dual staining and Western blot, are all useful tools in prion research (Atarashi et al. 2011b, Colby et al. 2007, Herve et al. 2010, Saborio et al. 2001). However, it is not always guaranteed that the presence of protein contamination or any other prion related markers post decontamination actually correlate with residual infectivity. Therefore, the questions remains as to whether these techniques can really assess decontamination protocols in relation to residual infectivity post treatment.

Animal bioassays assess decontamination protocols by utilising small lengths of surgical stainless steel (SS) wires to act as model surfaces (Fichet et al. 2004, Fichet et al. 2007b, Flechsig et al. 2001, Lawson 2008, Yan et al. 2004, Zobeley et al. 1999). The wires are inoculated with the prion strain under investigation and then decontaminated using various protocols. Then wires are inserted into the brain of the rodent and disease progression is assessed via behavioural studies, disease incubation time or lack thereof and the analysis of disease markers in the brain post death, depending on the efficacy of decontamination. More recently the standard steel-binding assay (SSBA), an adaptation of the SCEPA cell assay introduced earlier, utilises small 5 mm lengths of surgical grade SS wires to assess decontamination protocols in a cell-based infectivity assay through the analysis of PrP^{Sc} accumulation in N2a-PK1 cells (Edgeworth et al. 2009, Edgeworth et al. 2011b).

This chapter concentrates on the adaptation of the N2a #58 passage-based 22L infectivity assay with SB/ThT detection discussed in the previous chapter, for the analysis of infectivity remaining post decontamination. This will entail the optimisation and incorporation of inoculated surgical SS wires to introduce infectivity to the cells as is used in the SSBA assay. The infectivity will then be compared to the protein, lipid and amyloid contamination present on SS wires pre and post decontamination. This will confirm if residual contamination is related to infectivity. The infectivity results of the SB/ThT analysis of the 22L-infected N2a cells post decontamination will then be compared to animal infectivity assays assessing the same decontamination chemistries.

5.2 Materials and methods

Details of the materials and methods for this chapter can all be found within Chapter 2 of this report. Briefly, N2a #58 cells (2.1.1) were cultured as described in section 2.2.1 and then subjected to 22L (2.1.3 and 2.3.1) infection following the wire infectivity assay protocol described in section 2.3.4 for the optimisation of the number of wires required per dish and to determine the sensitivity of the wire assays. The decontamination efficacy of three commercially available cleaning chemistries; Hamo 100, Klenzyme and Enzol were then analysed in relation to infectivity in N2a cells (2.3.5) and remaining protein, lipid and prion-associated amyloid post decontamination using SR/ThT and NR/ThT staining (2.4.3 and 2.4.4). Detection of prion infectivity post decontamination (2.3.5) in the N2a cells was obtained by utilising the SB/ThT staining protocol as described in section 2.4.2. Fluorescent signal from all of the experiments was analysed by epi-fluorescence microscopy and quantified using Image J software described in section 2.4.5. All statistical analysis was carried out as highlighted in section 2.7.

5.3 Results

5.3.1 Wire number optimisation

Rodent based prion infectivity assays require the implantation of, 5 mm lengths of 0.15 mm diameter surgical grade SS wires inoculated in prion-infected brain homogenate to the brain of each test animal to assess the infectivity pre and post decontamination (Flechsig et al. 2001). Similarly, the SSBA uses 20, 5 mm lengths of RML-inoculated surgical SS wires per 35 mm well of a 6-well plate to induce infectivity within the N2a-PK1 cells (Edgeworth et al. 2009, Edgeworth et al. 2011b). Therefore, the number of 22L inoculated wires required to induce a consistent, SB/ThT detectable infection in the N2a #58 cells was tested. N2a cells were introduced to wells containing 5, 10 or 20, 10^{-4} 22L-inoculated wires or 10 or 20, 10^{-6} 22L-inoculated wires. Cells were grown to confluency at which point the cell coated wires were transferred to new dishes and the cells were cultured to confluency from the wires. Once confluent, the cells were split and treated as a passage study with SB/ThT analysis every 7 days (as it took 7 days to reach confluency from the wires so this was kept standard throughout the assays).

The image analysis of SB/ThT staining clearly demonstrated that the number of wires required per 35 mm dish is crucial to obtain reliable and consistent prion propagation in the N2a cells. The cells that had been in contact with 20, 10^{-4} and 20, 10^{-6} 22L-inoculated wires demonstrated a clear dose dependant prion-associated amyloid accumulation over the 7 passages post wire removal (Figure 35). The cells that had been in contact with 10, 10^{-4} 22L-inoculated wires demonstrated an increase in amyloid accumulation, however, the significance was lost over the last two passages due to increased variance between samples (Figure 35). The cells that had been in contact with 5, 10^{-4} 22L-inoculated wires showed an initial increase in amyloid accumulation that levelled over the 7 passages (Figure 35). The cells that had been in contact with 10, 10^{-6} 22L-inoculated wires demonstrated a minimal increase in amyloid accumulation with high variance between the samples and only passage 4 demonstrated a significant increase when compared to the un-infected controls (Figure 35).

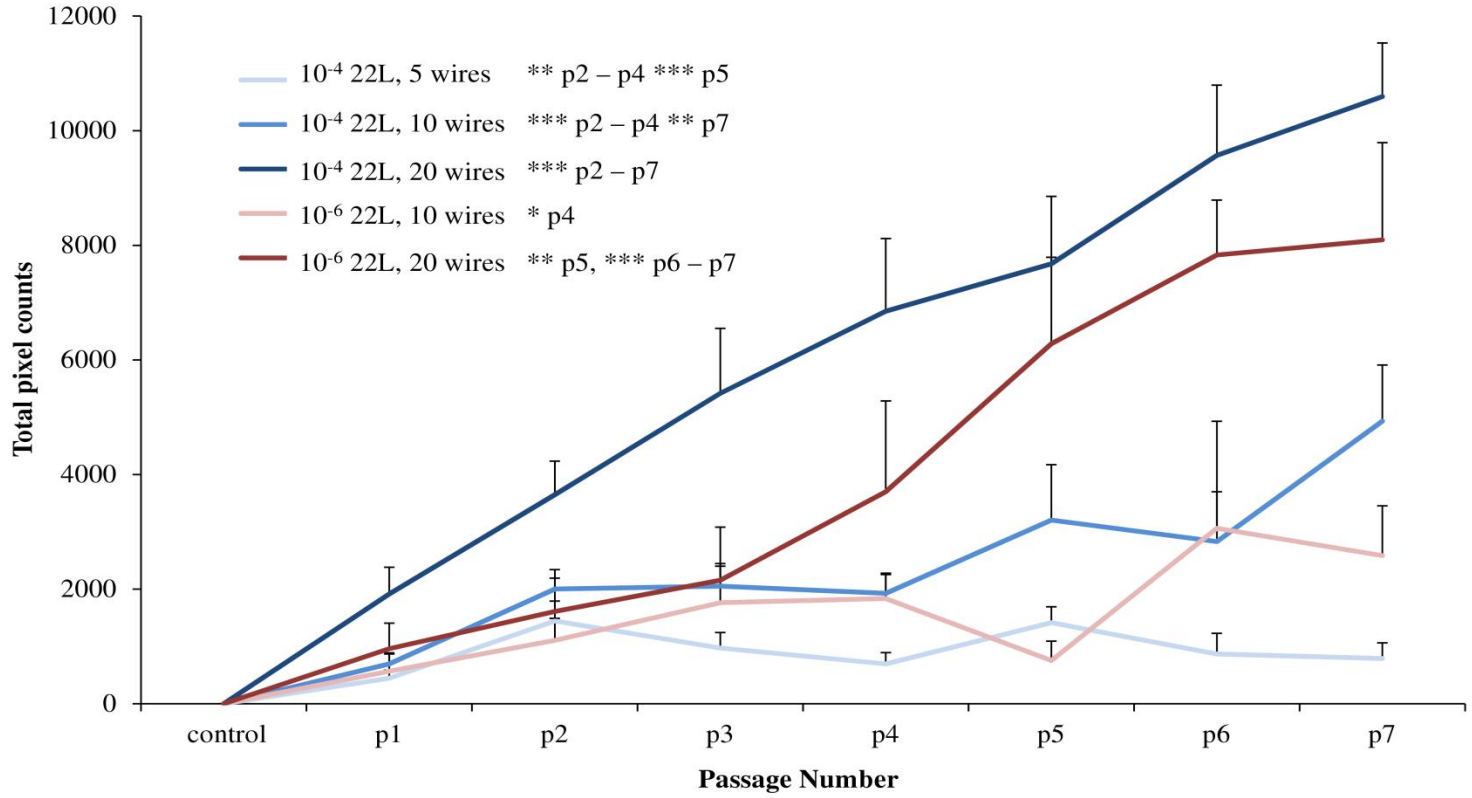

Figure 35 – Determination of the number of wires required for optimal prion propagation per 35 mm dish

Image analysis of SB/ThT-positive staining above the background observed within the controls, to determine the number of wires required, per 35 mm dish, to induce an optimal amyloid accumulation within the N2a cells. Error bars represent SEM (n=10–20). * = $p \leq 0.05$, ** = $p \leq 0.01$ and *** = $p \leq 0.001$ when compared to the uninfected controls.

5.3.2 Wire titre infections

The previous work demonstrated that the number of inoculated wires in contact with the N2a cells in the 35 mm dishes is crucial to induce sufficient prion infection. It was confirmed that 20 wires per 35mm dish of cells was the optimal number of wires required, as observed in previous studies. Therefore, the next step was to determine the sensitivity of the wire infectivity assay in the N2a cells with SB/ThT analysis. Batches of 20, 5 mm surgical stainless steel wires were inoculated in dilutions of 22L-infected brain homogenate ranging from 10^{-4} – 10^{-10}. The cells were then subjected to the wires following the wire infectivity assay protocol described previously, with passaging and SB/ThT analysis every 7 days post wire removal. Furthermore, the cells remaining in the first 35 mm dishes after the cell covered wires were removed were analysed for amyloid accumulation using the SB/ThT staining to determine the levels of infectivity initially transferred from the wires.

Firstly, the image analysis of the SB/ThT-positive signal demonstrated that there was already prion-associated amyloid accumulation in the N2a cells that had been in contact with the inoculated wires prior to wire removal for the first step of the wire infectivity protocol. There was a dose response trend of amyloid accumulation with the cells in contact with wires inoculated with 10^{-4} dilution of 22L-infected brain homogenate demonstrating the highest levels of amyloid and the cells in contact with 10^{-10} 22L-inoculated wires showing the least (Figure 36). A significant increase of ThT positive amyloid accumulation was observed in cells that had been in contact with wires inoculated with 10^{-4}, 10^{-6} and 10^{-8} dilutions of 22L-infected brain homogenate (Figure 36). Cells that had been in contact with wires inoculated with 10^{-9} and 10^{-10} dilutions of 22L-infected brain homogenate showed a small but statistically insignificant increase in ThT signal when compared to the un-infected controls (Figure 36).

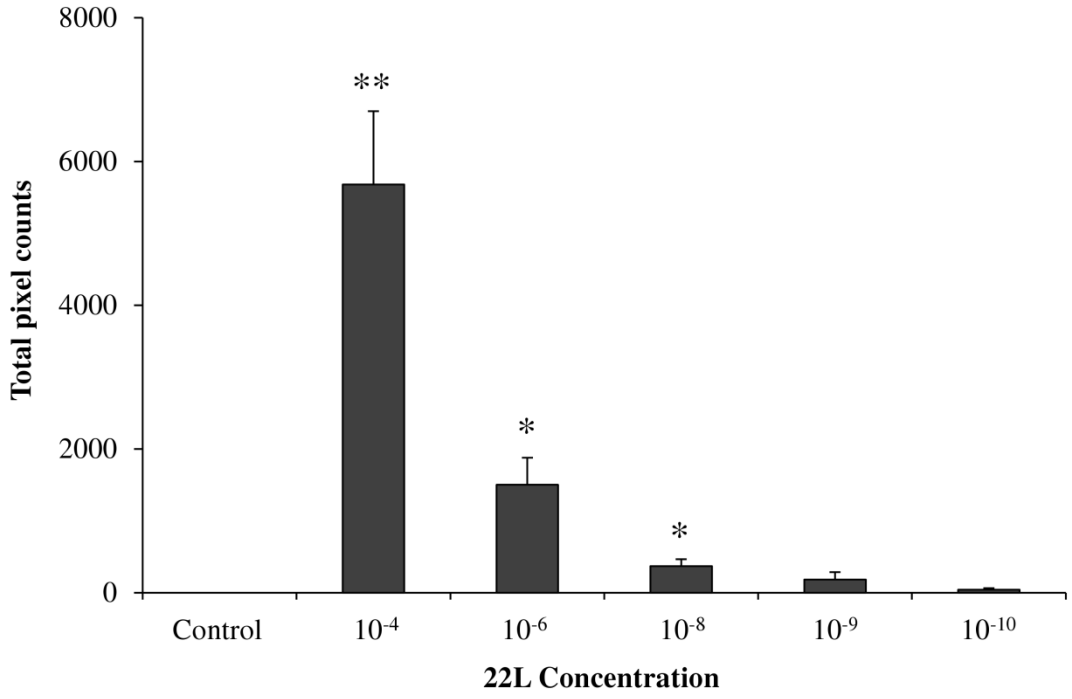

Figure 36 – Analysis of amyloid content in the remaining cells after wire removal

Image analysis of SB/ThT-positive staining to determine the amyloid content within the remaining N2a cells after wire removal at the first passage point. Error bars represent SEM (n=10). * = $p \leq 0.05$ and ** = $p \leq 0.01$ when compared to the uninfected controls.

Secondly, the sensitivity of the SB/ThT detection of amyloid accumulation in N2a #58 cells post contact with 22L-inoculated wires was tested. A dose dependent increase in SB/ThT signal was observed in the N2a cells after 8 cell passages post removal of the wires which were inoculated with varying dilutions of 22L-infected brain homogenate. This was confirmed with the image analysis which demonstrated significant increases in SB/ThT-positive signal in all of the infected N2a samples when compared to the uninfected control cells (Figure 37). A correlation was observed between the different 22L dilutions and the number of passages taken to demonstrate an increase in ThT-positive signal with a significance of $p \leq 0.001$ when compared to the uninfected controls (Figure 37). The cells that had been in contact with the 10^{-4} 22L-inoculated wires demonstrated a more rapid increase in amyloid accumulation when compared to the lower dose infections, especially in the 10^{-10} 22L-infected cells where a significant ($p \leq 0.001$) increase in ThT signal was only observed at passage 7 – 8 post wire removal (Figure 37).

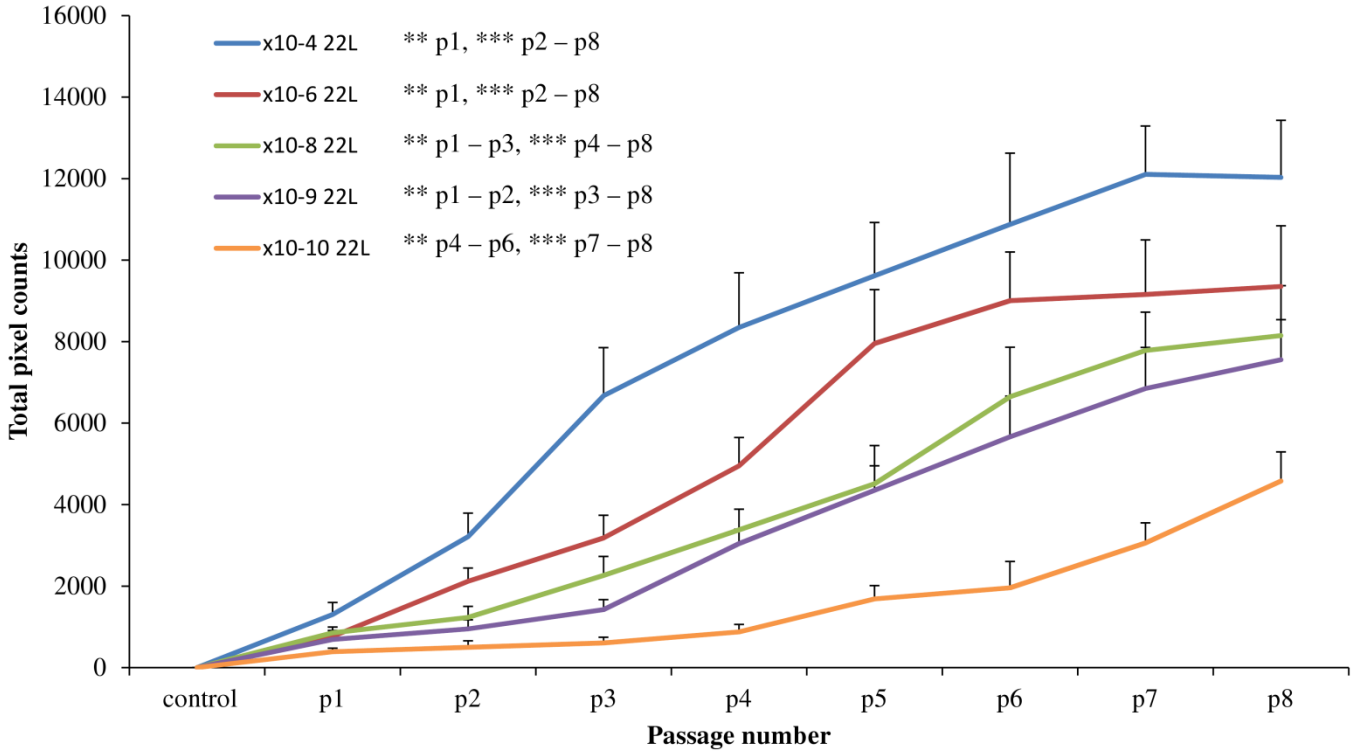

Figure 37 – Amyloid content in the N2a cells demonstrating a titre dilution of 22L infectivity from inoculated wires

Image analysis of SB/ThT-positive staining above the background observed within the controls, from the N2a cells infected from stainless steel wires inoculated with a titre dilution of 22L-infected brain homogenate ranging from 10^{-4} – 10^{-10}. Error bars represent SEM (n = 20). ** = $p \leq 0.01$ and *** = $p \leq 0.001$ when compared to the uninfected controls.

5.3.3 SR/ThT and NR/ThT analysis of decontamination efficacy

Prior to testing residual infectivity post-decontamination of the 22L-inoculated SS wires using the optimised N2a #58 wire infectivity assay; residual protein, lipid and prion-associated amyloid contamination on the wires post decontamination treatment was analysed. As the N2a #58 infectivity assay is only optimised to detect infectivity from 22L-infected samples, the residual contamination from 22L-inoculated wires was also compared to 263K-inoculated wires to compare the resistance of contamination removal of prion strains from two different species. Both 22L and 263K-infected brain homogenates were normalised to 1 mg/ml prior to wire inoculation. Direct SR/ThT and NR/ThT staining was utilised to highlight protein (SR), lipid (NR) and prion-associated amyloid (ThT) biofouling present on the wires.

Firstly, the contamination pre and post decontamination treatment on the 263K-inoculated wires was analysed. Representative micrographs of scans of the whole wires show that the control wires (no decontamination) clearly contained the highest levels of protein, lipid and prion-associated amyloid contamination when compared to the three cleaning chemistries (Figure 38 and Figure 39). The wires decontaminated with Hamo 100 demonstrated the highest levels of protein and prion-associated amyloid contamination post treatment, when compared to the other two cleaners (Figure 38). The micrographs show that Hamo 100 was poorly effective at removing the larger protein deposits (Figure 38). The wires decontaminated with Klenzyme and Enzol demonstrated very similar levels of protein and prion-associated amyloid contamination post treatment (Figure 38). The wires decontaminated with Hamo 100 and Klenzyme demonstrated similar volumes of lipid deposits remaining post treatment (Figure 39). In contrast, treatment with Enzol demonstrated fewer larger lipid deposits but what looked like areas of smaller lipid deposits compared to the other two cleaning chemistries was observed (Figure 39).

The image analysis of the SR, NR and ThT signal quantitated the 263K contamination on the surgical stainless steel wires pre and post decontamination. A significant decrease in protein, lipid and prion-associated amyloid contamination on the

263K inoculated wires was observed after treatment with the three cleaning chemistries when compared to the positive controls (Figure 42). The image analysis confirmed that the largest levels of protein remaining post decontamination treatment was found on the wires treated with Hamo 100 and less was observed on the wires treated with Klenzyme and Enzol (92%, 99% and 98% reduction when compared to the controls, respectively) (Figure 42). Similar amounts of prion-associated amyloid were observed on the wires treated with Hamo 100 and Klenzyme with a lower level of contamination observed on the wires treated with Enzol (71%, 81% and 88% reduction when compared to the controls, respectively) (Figure 42). The levels of residual lipid contamination were similar after treatment with all three cleaning chemistries, with slightly less observed after Enzol treatment (82%, 85% and 89% reduction when compared to the controls, respectively) (Figure 42).

Secondly, the contamination pre and post decontamination treatment on 22L-inoculated wires was analysed. The clearest observation when comparing the micrographs of the 263K and the 22L-inoculated wires is that the wires contaminated with 22L-infected brain homogenate harboured considerable higher levels of contamination, both pre and post decontamination, highlighted by increased staining intensities of the three fluorophores. Representative micrographs of scans of the whole wires show that the control wires (no decontamination) clearly contained the highest levels of protein, lipid and prion-associated amyloid contamination when compared to the three cleaning chemistries (Figure 40 and Figure 41). The wires decontaminated with Hamo 100 demonstrated the highest levels of protein and prion-associated amyloid contamination post treatment when compared to the other two cleaners; however, increased residual contamination was observed compared to the 263K-inoculated wires (Figure 40). The micrographs again show that Hamo 100 was poorly effective at removing the larger protein deposits (Figure 40). The wires decontaminated with Klenzyme and Enzol demonstrated very similar levels of prion-associated amyloid contamination post treatment; however, the wires decontaminated with Enzol demonstrated lower levels of protein compared to Klenzyme treated wires (Figure 40). Decontamination with Hamo 100 and Klenzyme again demonstrated similar volumes and staining of lipid deposits remaining post treatment (Figure 41). However, the wires decontaminated with Enzol showed residual contamination completely the opposite of

the 263K-contaminated wires with larger lipid deposits remaining post treatment compared to the other two cleaning chemistries (Figure 41).

The most obvious observation when comparing the 263K and 22L contamination of the surgical stainless steel wires is that the 22L-infected homogenate attached more readily to the wires surface than the 263K-infected homogenate. Almost a 4-fold increase in contamination was observed on the 22L-positive controls compared to the 263K-positive controls, this clearly lead to increased residual contamination post decontamination treatment. However, the same significant trend of remaining contamination compared between the three cleaning chemistries was observed. Again, wires treated with Hamo 100 demonstrated the highest levels of residual protein with slightly lower levels observed on the Klenzyme and Enzol treated wires (86%, 96% and 98% reduction when compared to the controls, respectively) (Figure 43). A slight decrease in prion-associated amyloid contamination was observed across the three different treatments (89%, 91% and 96% reduction when compared to the controls, respectively) (Figure 43). The levels of residual lipid contamination was the opposite of that observed with the 263K contaminated wires with the lowest levels of lipid found on the wires after Hamo 100 treatment with the highest levels observed after Enzol treatment (91%, 86% and 85% reduction when compared to the controls, respectively) (Figure 43).

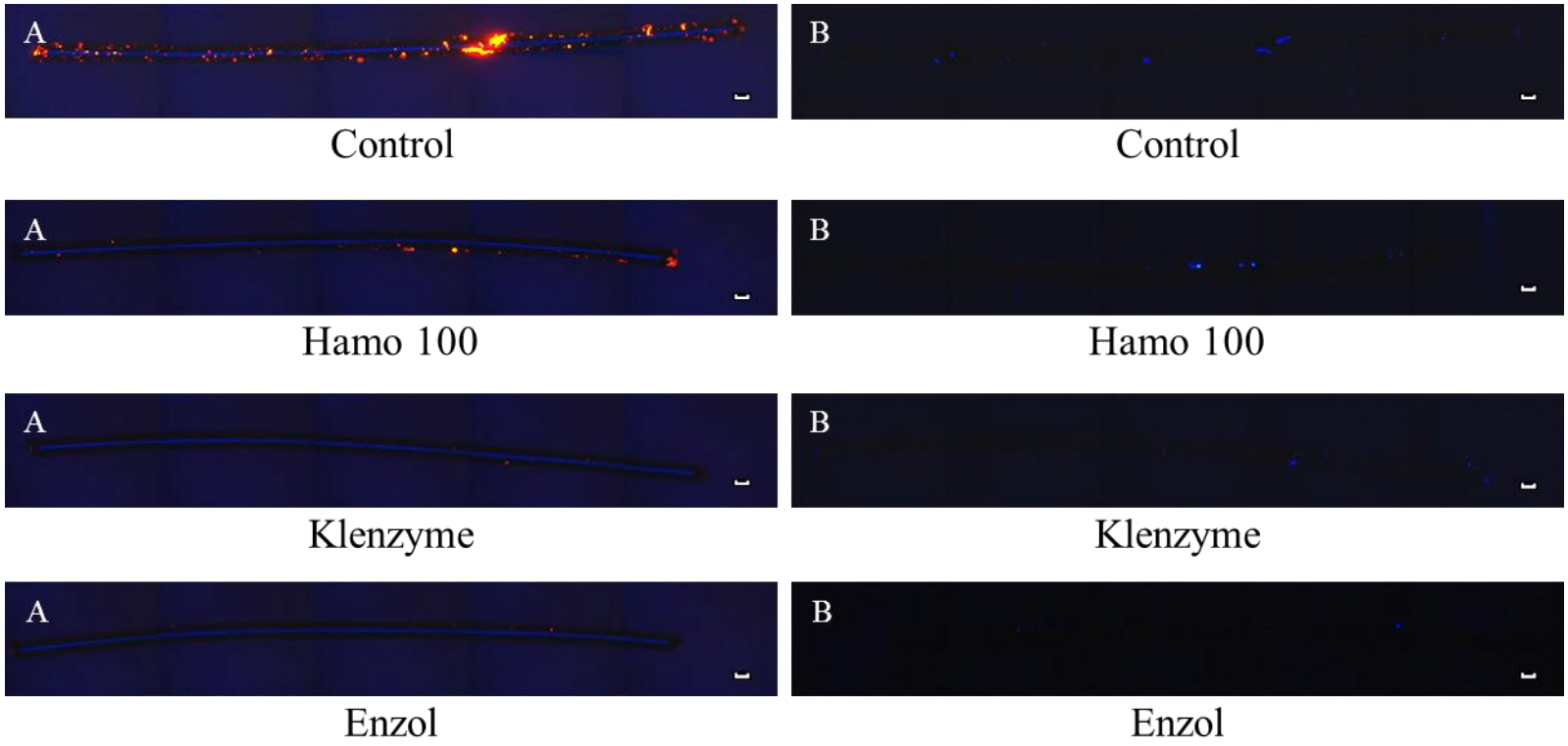

Figure 38 – Micrographs of protein and amyloid contamination on stainless steel wires post 263K contamination

Representative micrographs of protein (SR (A)) and prion-associated amyloid (ThT (B)) contamination on surgical stainless steel wires inoculated with 263K-infected brain homogenate. The micrographs highlight contamination both pre (control) and post (Hamo 100, Klenzyme, Enzol) decontamination treatment. Scale bar = 100 µm.

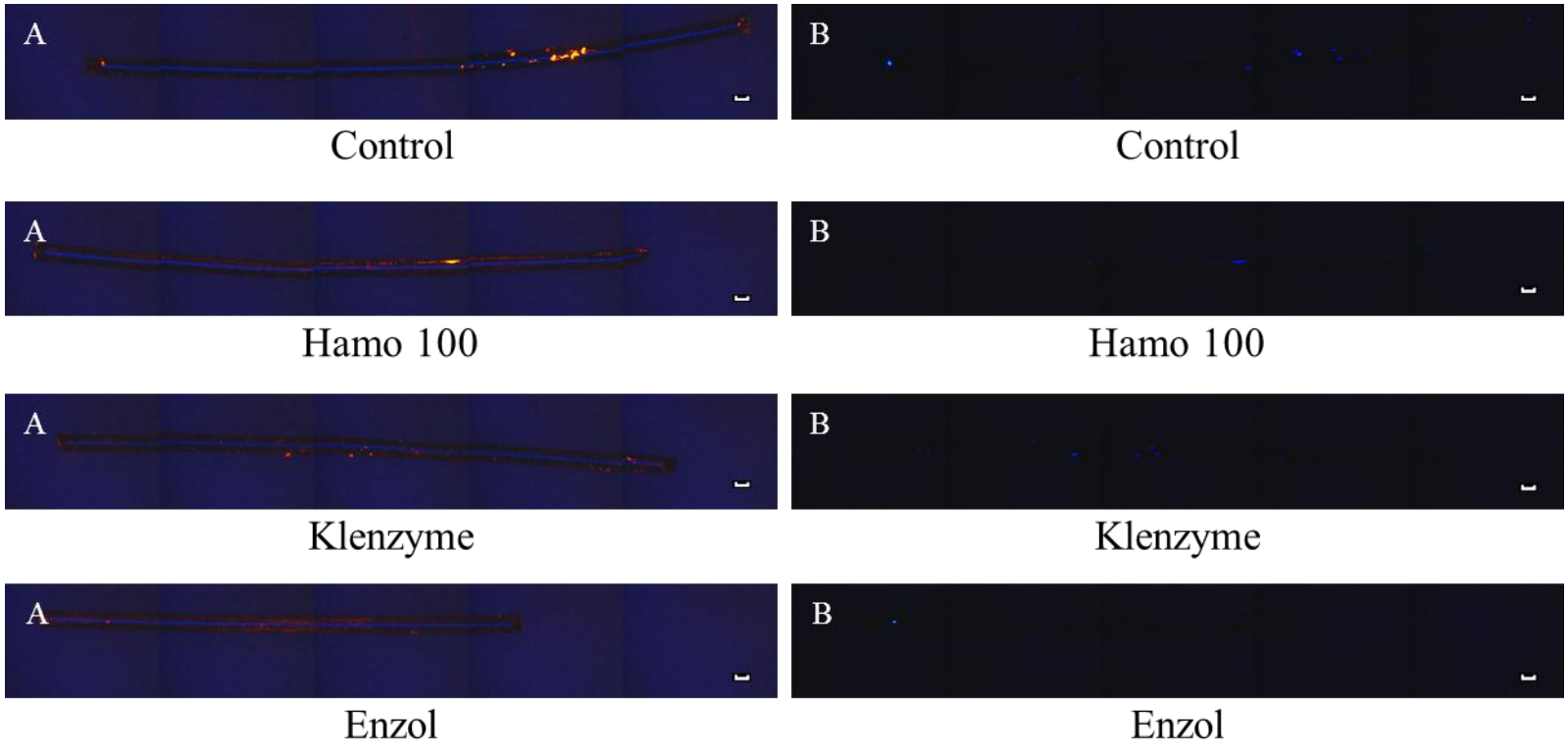

Figure 39 – Micrographs of lipid and amyloid contamination on stainless steel wires post 263K contamination

Representative micrographs of lipid (NR (A)) and prion-associated amyloid (ThT (B)) contamination on surgical stainless steel wires inoculated with 263K-infected brain homogenate. The micrographs highlight contamination both pre (control) and post (Hamo 100, Klenzyme, Enzol) decontamination treatment. Scale bar = 100 µm.

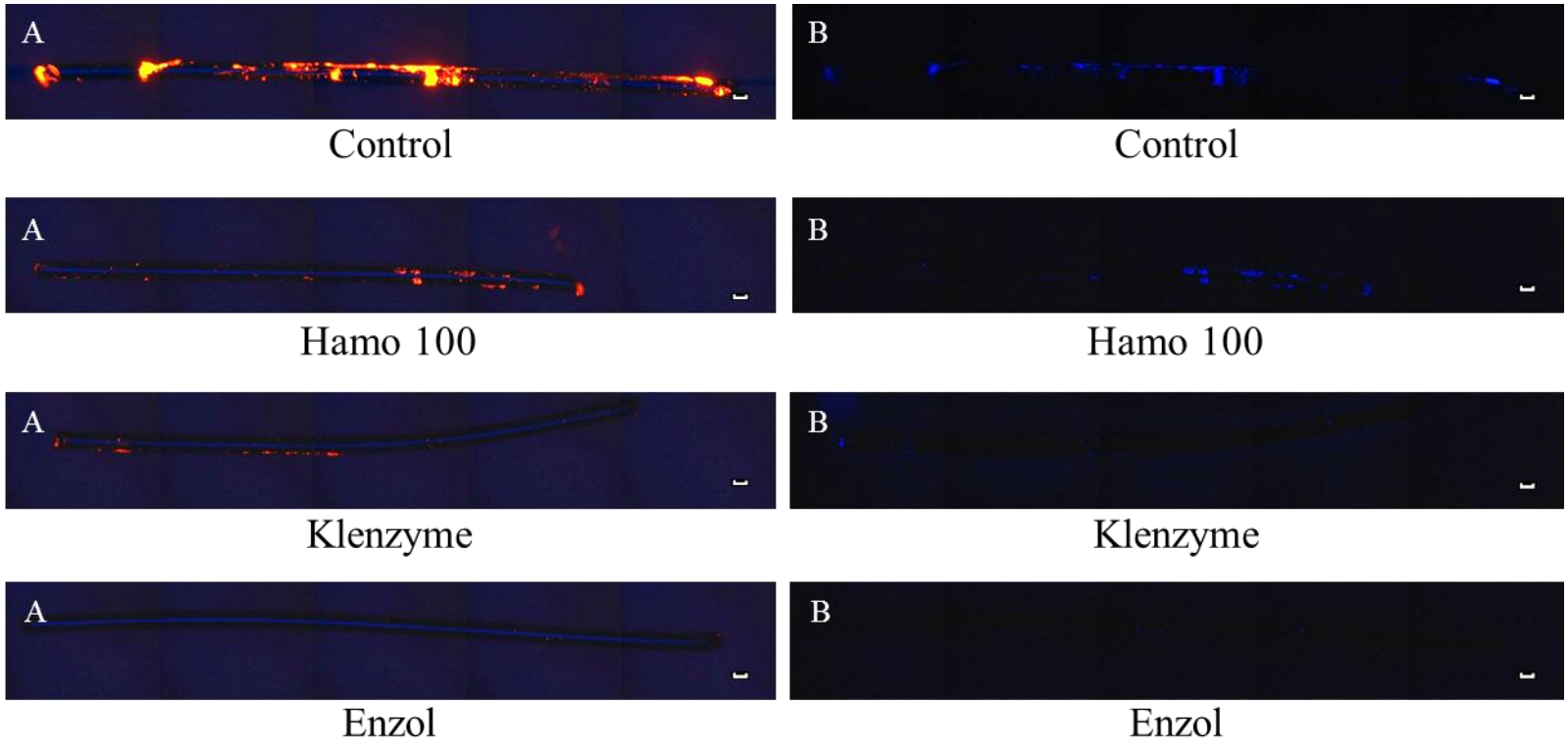

Figure 40 – Micrographs of protein and amyloid contamination on stainless steel wires post 22L contamination

Representative micrographs of lipid (SR (A)) and prion-associated amyloid (ThT (B)) contamination on surgical stainless steel wires inoculated with 22L-infected brain homogenate. The micrographs highlight contamination both pre (control) and post (Hamo 100, Klenzyme, Enzol) decontamination treatment. Scale bar = 100 µm.

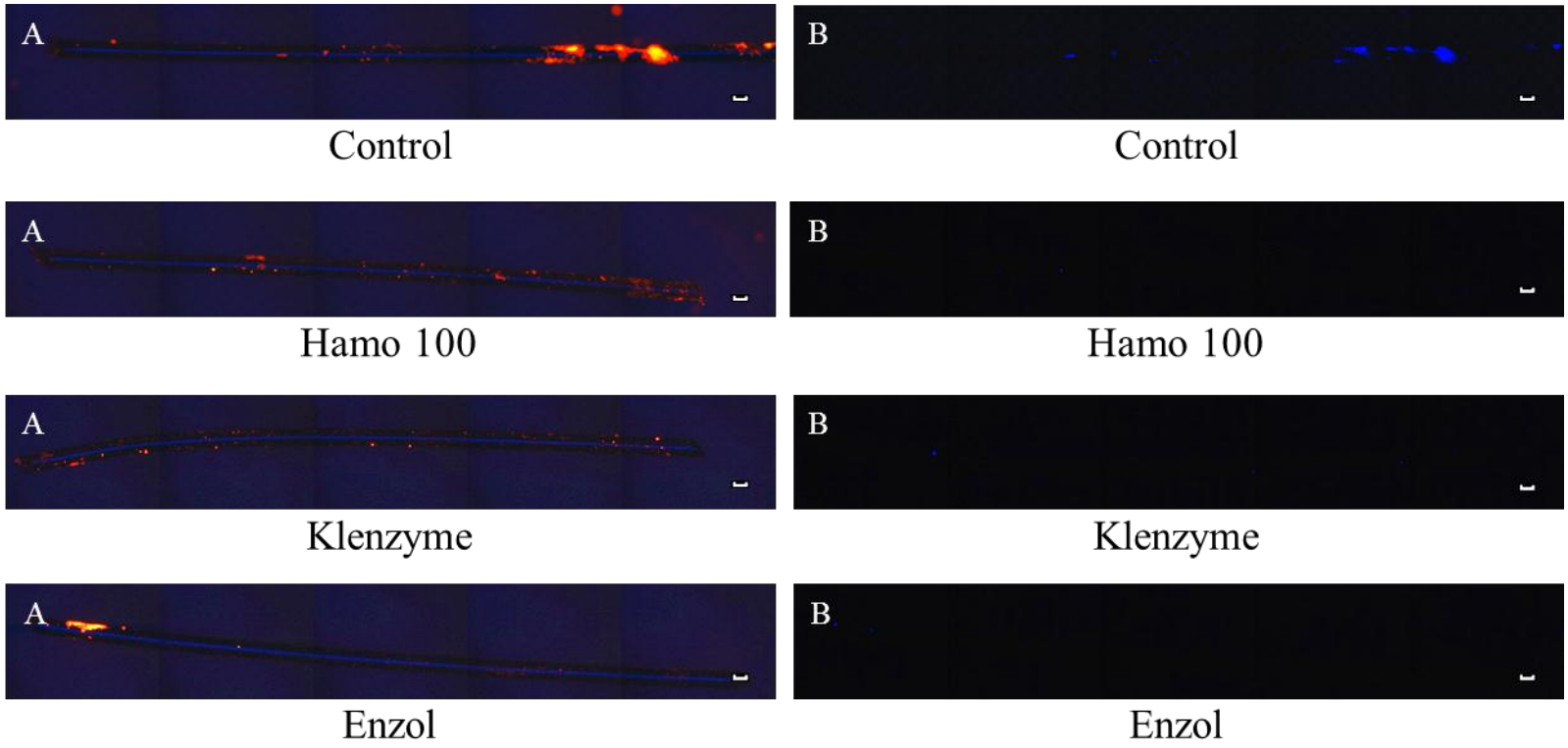

Figure 41 – Micrographs of lipid and amyloid contamination on stainless steel wires post 22L contamination

Representative micrographs of lipid (NR (A)) and prion-associated amyloid (ThT (B)) contamination on surgical stainless steel wires inoculated with 22L-infected brain homogenate. The micrographs highlight contamination both pre (control) and post (Hamo 100, Klenzyme, Enzol) decontamination treatment. Scale bar = 100 µm.

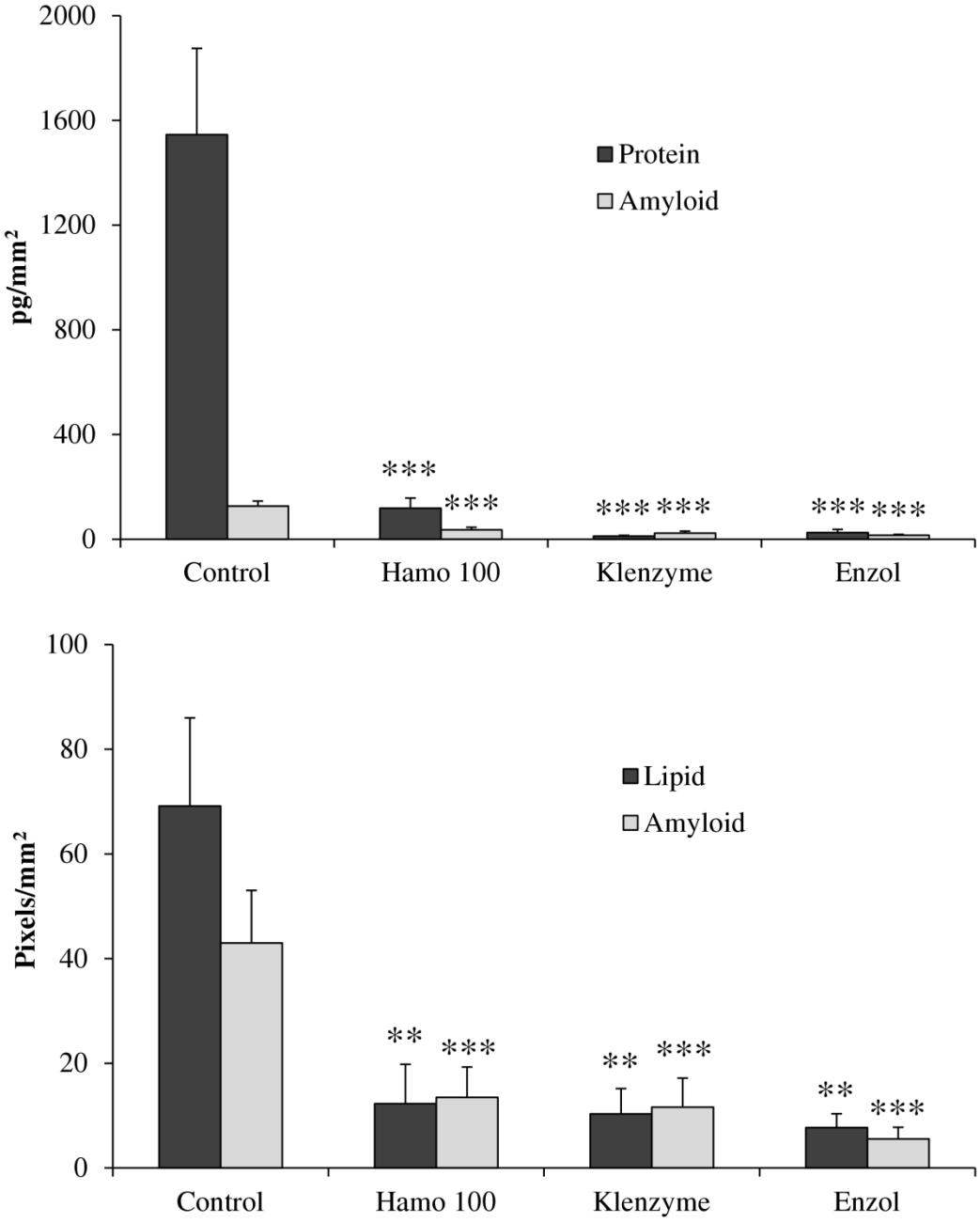

Figure 42 – Image analysis of protein, lipid and amyloid contamination on stainless steel wires post 263k contamination

Image analysis of protein (SR, top), lipid (NR, bottom) and prion-associated amyloid (ThT, top and bottom) residual contamination, both pre and post decontamination with Hamo 100, Klenzyme or Enzol, on surgical stainless steel wires inoculated with 263K-infected brain homogenate. Error bars represent SEM (n = 6-20 wires) ** = $p \leq 0.01$ and *** = $p \leq 0.001$ when compared to the positive controls.

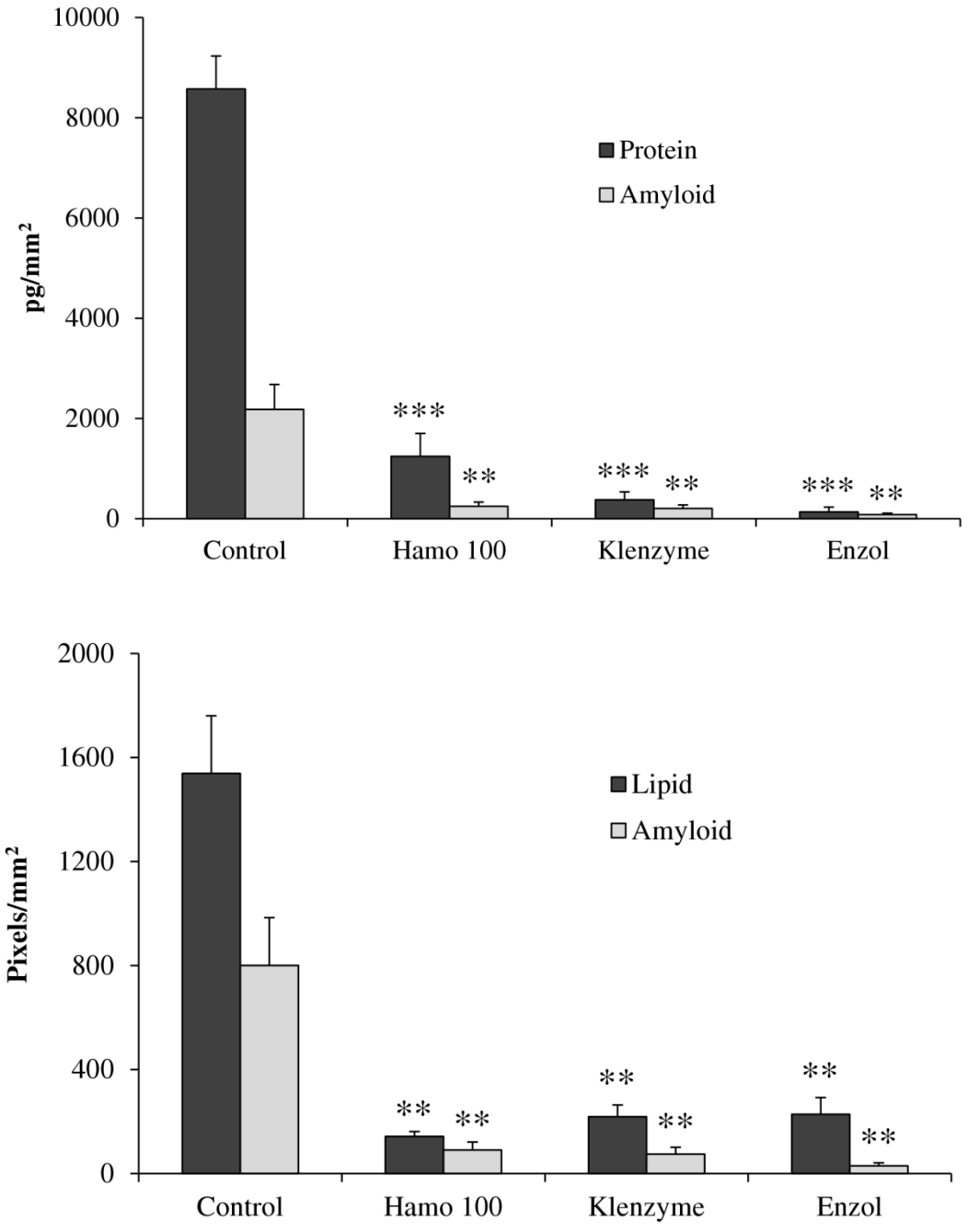

Figure 43 – Image analysis of protein, lipid and amyloid contamination on stainless steel wires post 22L contamination

Image analysis of protein (SR, top), lipid (NR, bottom) and prion-associated amyloid (ThT, top and bottom) residual contamination, both pre and post decontamination with Hamo 100, Klenzyme or Enzol, on surgical stainless steel wires inoculated with 22L-infected brain homogenate. Error bars represent SEM (n = 6-15 wires) ** = $p \leq 0.01$ and *** = $p \leq 0.001$ when compared to the positive controls.

5.3.4 N2a infectivity and SB/ThT analysis of decontamination efficacy

Previously, the sensitivity of the N2a wire passage infectivity assay with SB/ThT analysis for the detection of wire-bound infectivity was determined. The N2a wire infectivity assay was then utilised to determine residual infectivity on 22L-inoculated surgical SS wires post decontamination treatment with Hamo 100, Klenzyme and Enzol for the comparison with the presence of protein, lipid and prion-associated amyloid, discussed in section 5.3.3, and with published infectivity data from animal bioassays assessing the same cleaning chemistries with 263K-infected brain homogenate.

All of the wires pre (positive controls) and post decontamination were originally inoculated in 10% 22L-infected brain homogenate or 10%-NBH for the un-infected controls. The levels of amyloid accumulation was visualised using SB/ThT staining at each passage as described previously. A cut-off threshold of detection of 1000 pixels was chosen to take account for some areas of background fluorescence associated with the spheroid clumping of the N2a cells that were being picked up by the image analysis even after setting the pixel intensity threshold using the control images. The image analysis results of SB/ThT signal clearly demonstrated a significant increase over the 8 weekly passages post wire removal that followed a similar trend as wires inoculated with 10^{-4} diluted 22L-infected brain homogenate (Figure 45). The example micrographs show that there is an accumulation of large ThT-positive plaques at the 7^{th} passage point (49 days) post wire removal in the positive controls (Figure 44). The N2a #58 cell samples that had been in contact with 22L-inoculated wires decontaminated with Klenzyme and Enzol both showed similar amyloid accumulation kinetics over the 8 weekly passages post wire removal. A lag phase of low levels of amyloid accumulation was observed over the first three passages (21 days) post wire removal, followed by a significant increase in ThT-positive amyloid accumulation from passages 3 – 8 (21 – 56 days) post wire removal (Figure 45). Representative micrographs demonstrate smaller ThT-positive plaques, compared to the plaques observed in the positive controls, found in the N2a cells that had been in contact with 22L-inoculated wires treated with Klenzyme (Figure 44). The same smaller plaques were also observed in N2a cells that had been in contact with Enzol treated wires. Very low levels of ThT staining was

observed in the N2a cells that had been in contact with wires treated with Hamo 100; although a significant ($p \leq 0.001$) increase in ThT signal was observed at p5 this dropped from passage 6 – 8 post wire removal (significance of $p \leq 0.01$) and was deemed below the threshold level of detection set at 1000 pixels (Figure 45). The representative micrographs in Figure 44 demonstrate the diffuse background staining of the cells that had been in contact with 22L-inoculated wires treated with Hamo 100; the same diffuse staining was observed in the un-infected controls. All samples demonstrated a slight drop in ThT signal between passage 1 and 2 as this was the first time cells were split post-wire removal (Figure 45).

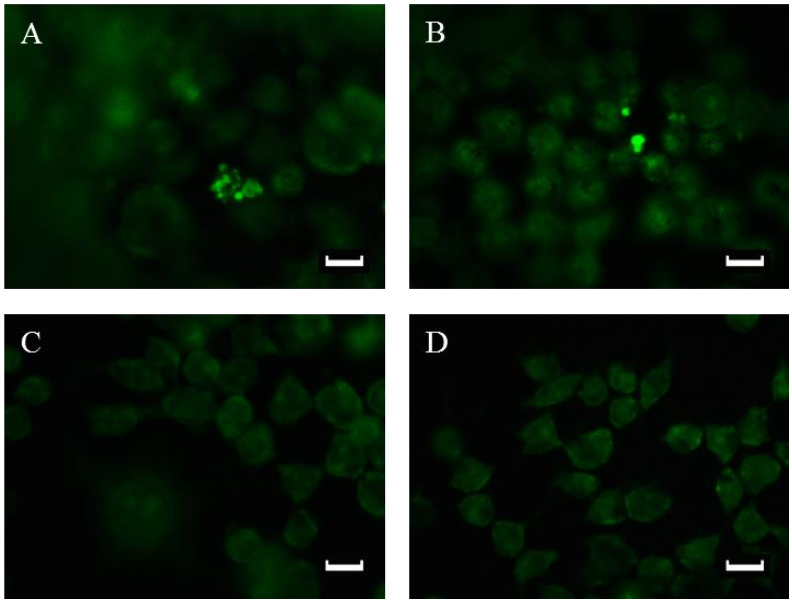

Figure 44 – Example micrographs from the wire decontamination infectivity study

Representative micrographs of SB/ThT stained prion-associated amyloid accumulation in N2a cells after 7 passages following introduction of 22L-inoculated surgical stainless steel wires both pre (A) and post decontamination with Klenzyme (B), Hamo 100 (C) and un-infected NBH controls (D). Scale bars = 10µm

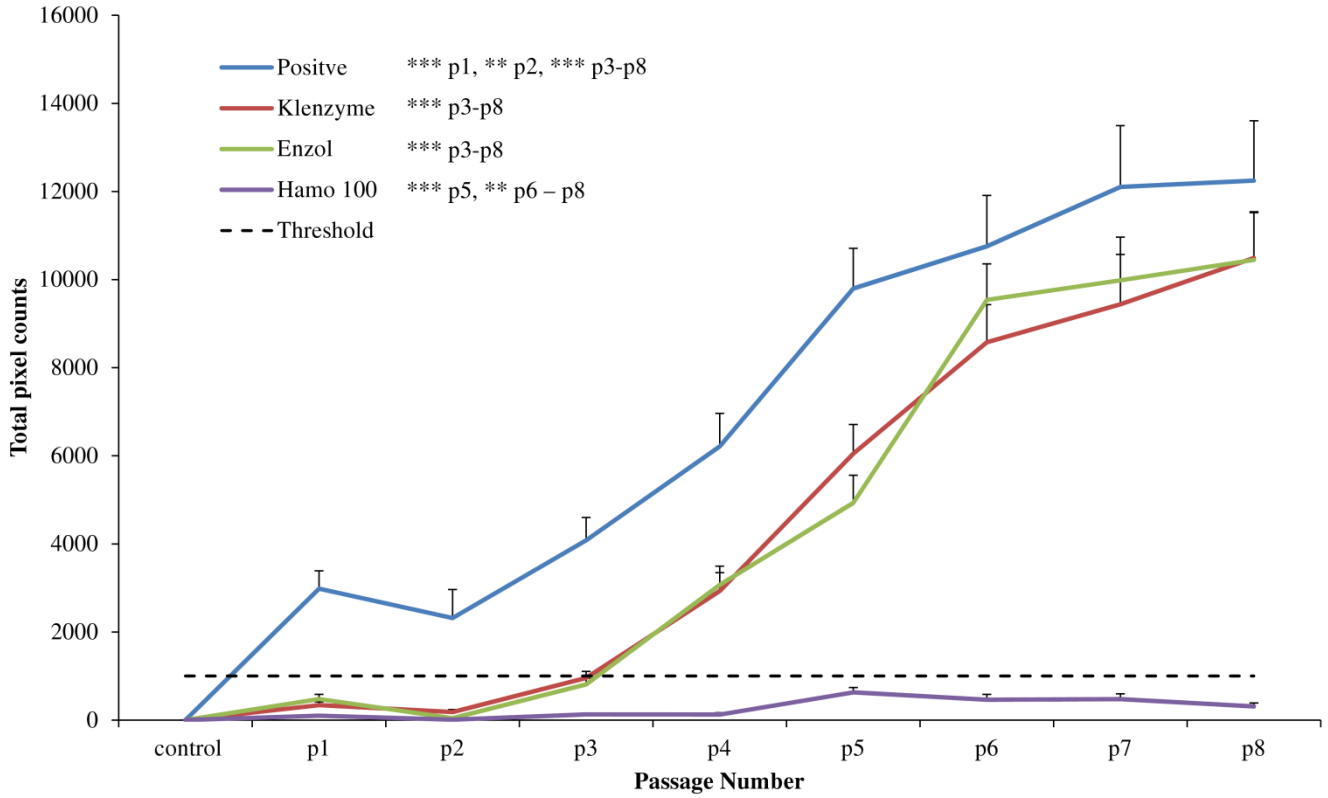

Figure 45 – Amyloid content in N2a cells after inoculation with 22L contaminated wires pre and post decontamination.

Image analysis of SB/ThT-positive staining of prion-associated amyloid accumulation in N2a cells post inoculation with surgical stainless steel wires contaminated with 22L-infected brain homogenate both pre and post decontamination with Hamo 100, Klenzyme and Enzol. Error bars represent SEM (n = 50). ** = $p \leq 0.01$ and *** = $p \leq 0.001$ when compared to the uninfected controls.

The wire infectivity titre study described in section 5.3.2 of this chapter was used to determine the log reductions in infectivity observed from the wires that had been treated with one of the three cleaning chemistries and analysed using the N2a/22L SB/ThT wire infectivity assay. Briefly, the ThT pixel counts from passages 4 – 8 for each initial dilution of 22L in the wire titre study (Section 5.3.2) were used as standard values at those given time points. A standard curve for each passage point was produced using the ThT pixel standards taken from passage 4 – 8. The ThT pixel counts from each cleaner at each passage point were then plotted against the linear regressions of the standards at the corresponding time point. The values determined corresponded to the predicted initial dilutions of 22L on the inoculated wires post decontamination in relation to the amyloid accumulation in the N2a cells at that given time point. The initial 22L dilution value from each passage point was then pooled for each cleaner and the mean was determined. These initial 22L dilution values were then compared to the positive control values to determine the log reduction in infectivity produced by each cleaner. This procedure was used so that the changes in lag phase observed in the amyloid accumulation between the cells that had been in contact with wires treated using different treatments were taken into account and not the just the final ThT signal observed at the 8^{th} passage.

The log reduction in infectivity in the N2a/22L SB/ThT experiments was then compared to infectivity data from 263K hamster bioassay data summarised in Table 5. The log reductions in infectivity for Hamo 100 and Klenzyme using the animal infectivity bioassays were 5.6 and 3.5, respectively (Table 5). However, the log reduction for Enzol was not given but with the very low incubation period is thought to be similar or less than that observed with Klenzyme (Yan et al. 2004). No transmission to the hamsters was observed after Hamo 100 treatment, however, complete transmission was observed after Klenzyme and Enzol treatment (Table 5). The log reductions determined in the N2a/22L SB/ThT assay were 7.9, 2.5 and 2.5 after Hamo 100, Klenzyme and Enzol treatment, respectively (Table 5). The working pH of each cleaner was also included as one argument in prion research is that the pH of the cleaner is crucial for optimal prion degradation and therefore reduction in infectivity.

	Hamo 100	Klenzyme	Enzol
AB log reduction	5.6[1]	3.5[1]	-
AB Incubation (days)	>365[1]	143 (±12)[1]	95 (±0.4)[2]
AB Transmission (%)	0[1]	100[1]	100[2]
SB/ThT log reduction	7.9	2.5	2.5
Cleaner pH	12.9	7.6	9

Table 5 – Comparison of infectivity data and cleaner pH

A comparison of the log reduction in prion infectivity after decontamination in Hamo 100, Klenzyme or Enzol, detected using animal bioassay (AB) or the SB/ThT detection after N2a infectivity assay. The incubation time between animal inoculation and death and the transmission rate is included. The cleaning chemistries' working pH is summarised for comparison to infectivity. [1](Fichet et al. 2004, Fichet et al. 2007b), [2] (Yan et al. 2004).

5.4 Discussion

Prion infectivity assays used to analyse prion decontamination protocols require the detection of prion infectivity remaining on surfaces post decontamination. Therefore, the majority of infectivity assays, both animal and cell-based, use surgical grade stainless steel wires as models of surgical instrument surfaces (Edgeworth et al. 2009, Edgeworth et al. 2011b, Fichet et al. 2004, Fichet et al. 2007b, Flechsig et al. 2001, Yan et al. 2004, Zobeley et al. 1999). The wires are inoculated with the prion strain in question and then either incorporated into the animal brain in animal bioassays or into the cells in cell-based assays to induce prion propagation and fundamentally detection of infectivity.

The previous two chapters of this report demonstrated the optimisation of a sensitive SB/ThT *in situ* detection method for the analysis of amyloid accumulation in N2a #58 cells as a marker of prion infectivity. However, the assay described in these chapters assessed infectivity from the direct inoculation of 22L-infected brain homogenate into the cells which poses difficulties when analysing the efficacy of decontamination protocols, especially in relation to surgical surfaces. Therefore, this chapter focused on the adaptation of the N2a/22L SB/ThT assay for the detection of surface-bound infectivity by introducing the infectious material to the cells on inoculated wires as is demonstrated in the aforementioned published infectivity assays. Firstly, 5 mm lengths of surgical SS wires are used for implantation in the animal brain during animal infectivity assays or incorporated into cells in cell-based assays; therefore, this was kept consistent within this assay (Edgeworth et al. 2011b, Flechsig et al. 2001). However, the number of inoculated wires required for optimal and consistent amyloid propagation needed to be determined. A large number of wires (20 per sample) are required in current cell based infectivity assays (Edgeworth et al. 2009, Edgeworth et al. 2011b) which was again clearly demonstrated in the N2a cells where 20 wires per 35 mm dish of cells were required for an optimal and consistent amyloid accumulation. Amyloid accumulation was observed in the cells that had been in contact with the lower wire numbers; however, the accumulation was very inconsistent between different fields of view suggesting that fewer infected cells from the fewer wires led to an inconsistent spread of amyloid across the tissue culture dish. Furthermore, loss of accumulation was

observed over the 7 passages when the initial prion dose was lowered by 2-log and only 10 wires were used; again suggesting that fewer wires lead to fewer infected cells which would be further diluted with the cell splits at each passage point.

Following the determination of the number of 22L-inoculated wires required to induce prion infection in the N2a cells; the sensitivity of the SB/ThT assay was again assessed for the detection of prion infectivity from wire-bound prions. As was observed with the brain homogenate infectivity studies from the previous chapter, the sensitivity of the wire infectivity assay demonstrated amyloid accumulation in the N2a cells from wires that had been inoculated with a 10^{-10} dilution of 22L-infected brain homogenate. This again matched the sensitivity of the SSBA, SCEPA assay described previously (Edgeworth et al. 2009, Edgeworth et al. 2011b). However, the SB/ThT assay allows the *in situ* detection of amyloid accumulation which can help to visualise the changes in plaque size and distribution observed between the different samples and infectious material titres. Generally it was observed that the lower the initial 22L infectious dose that was introduced to the N2a cells, the smaller and more distributed the plaques were over the latter passages. In the higher dose samples the plaques had polymerised to form larger plaques that were easier to detect. Furthermore, assessing amyloid accumulation at every passage point allows a picture to be produced of the kinetics of amyloid accumulation over time, which can be compared between different samples. It was observed that the lower the initial prion dose was, the longer the lag phase would be until the detection of a significant increase in ThT-positive amyloid signal. This lag phase is also observed when using the ASA protocol, that again utilises ThT signal as a marker of prion propagation (Colby et al. 2007). Furthermore, the SB/ThT assay does not require PK digestion which imitations have been described previously in this report.

Prior to analysing the efficacy of three commercially available cleaning chemistries in regards to remaining infectivity using the N2a/22L SB/ThT assay, the residual contamination on surgical grade SS wires was assessed. The SR/ThT assay was the chosen method as it allows the sensitive detection of residual contamination without the need to remove the residual biofouling from the surface under examination prior to analysis (Herve et al. 2009, Herve et al. 2010, Howlin et al. 2010). Furthermore, the SR/ThT dual stain assay was adapted to incorporate NR staining to allow the sensitive

detection of residual lipid contamination. Due to the association that lipid rafts potentially aid the infectivity of the prion protein we wanted to determine if there was a correlation of residual lipid contamination with remaining infectivity (Reviewed in Taylor et al. 2006, Wadia et al. 2008). The analysis of residual contamination of both 263K and 22L-infected brain homogenate was compared on stainless steel wires as a comparison of prions strains from two different species as 263K is used in the animal bioassays and 22L was used in the N2a/22L SB/ThT assays.

Both of the infected brain homogenates were normalised to 1 mg/ml prior to wire inoculation to allow for the comparison of the attachment of biofouling to the wires surfaces. The biggest difference that was observed when comparing the attachment of protein, lipid and prion-associated amyloid between the two different homogenates is that around 4-fold higher levels of attachment were observed with the 22L-infected homogenates. Although higher levels of contamination were observed in the 22L controls, higher percentage reductions after the three cleaning treatments were also observed compared to the 263K-inoculated wires. However, the remaining contamination was still greater with the 22L-inoculated wires, which is a factor to take into consideration regarding variations in the infectivity of different prion strains.

The three cleaning chemistries all demonstrated significant decreases in protein, lipid and prion-associated amyloid contamination with both of the homogenates tested. The wires treated with Hamo 100 demonstrated slightly, but not significantly higher levels of protein when compared to the other two cleaners, with Enzol demonstrating the lowest levels of residual protein. Enzol treatment also demonstrated the greatest reduction of prion-associated amyloid remaining when compared to the other two cleaners that demonstrated similar levels with both homogenates. Analysis of residual lipid contamination demonstrated different trends with the two different homogenates. Hamo 100 treatment demonstrated the lowest levels of residual lipid from the 22L-infected homogenate and Enzol the highest, whereas the opposite was found with the 263K-infected homogenate. These results were similar to the efficacy of these cleaning chemistries with regards to residual ME7 infected homogenate protein and prion-associated amyloid on SS wires (Howlin et al. 2010) and tokens (Herve et al. 2010). However, the opposite was found when a technique utilising thermostable adenylate

kinase (tAK) activity mixed in browns soil (Steris©) which demonstrated a higher reduction in tAK activity post alkaline treatment (Hamo 100) than compared to enzymatic treatment (Klenzyme, Enzol) (Ungurs et al. 2010). Of course, reduced activity could have been due to tAK enzyme inactivation rather than actual removal of the enzyme protein *per se*. Browns soil is only associated with protein contamination and does not contain any prion related material so it is unknown and hazardous to suggest how residual protein contamination correlates with prion attachment or decontamination efficacy. Furthermore, WB analysis of residual PrP^{res} post PK digestion demonstrated that alkaline treatment removed all PrP^{res} from test surfaces, however no or low levels of PrP^{res} removal has been previously observed with enzymatic treatments (Fichet et al. 2004, Fichet et al. 2007b, Howlin et al. 2010).

One of the most important questions in prion decontamination research is how does residual contamination correlate with infectivity and how does different prion strain infectivity vary? Therefore, the N2a/22L SB/ThT assay was used to compare the infectivity remaining on 22L-inoculated wires post decontamination with the three cleaning chemistries tested previously. It was clearly demonstrated that no infectivity was present on the wires treated with Hamo 100 with a log reduction in infectivity of ~7.9. This correlates with the 263K hamster bioassays which also demonstrate no transmission to the animals post Hamo 100 treatment and a log reduction in infectivity of ~ 5.6 (Fichet et al. 2004, Fichet et al. 2007b). The higher log reduction in infectivity observed in the N2a/22L SB/THT assay is most likely due to the higher sensitivity of this assay compared to the 10^{-7} limit of detection of the animal bioassays. However, these results contradicted the results obtained using the SSBA SCEPA assay which demonstrated remaining tissue culture infectivity units (TCIU) in the N2a PK1 cells after Hamo 100 treatment, whereas, no TCIU were found after enzymatic treatment with Prionzyme (Edgeworth et al. 2011b). The contradictions between these two assays could be caused by the different prion strains tested (22L or RML) or by the different methods used for detection (detection of amyloid or PrP^{res}). This highlights the importance of understanding both the prion strain analysed and the detection methods used. Rather than relying on one infectivity assay, the amalgamation of two cell-based infectivity assays with different methods of detection could be more beneficial in understanding the remaining prion infectivity post decontamination.

The infectivity remaining on the SS wires post decontamination with Klenzyme and Enzol demonstrated the same trend, with a lag in amyloid accumulation onset compared to the controls using the N2a/22L SB/ThT assay. A log reduction in infectivity of ~2.5 was observed with both cleaners which were again comparable to the ~3.5 demonstrated for Klenzyme treatment in the hamster 263K model and the low incubation time observed for Enzol treatment (Fichet et al. 2004, Yan et al. 2004). The lower reduction in infectivity observed in the N2a/22L SB/ThT assay can be explained by the higher attachment of residual 22L contamination observed post decontamination in the SR/ThT and NR/ThT assay when compared to the 263K-infected homogenate.

No correlation was observed when comparing residual protein, lipid and prion-associated amyloid contamination with infectivity. In fact, the highest protein contamination was observed after Hamo 100 treatment; however Hamo 100 was the only cleaner that demonstrated a total loss of infectivity. It could be argued that slightly lower levels of lipid contamination were observed after Hamo 100 treatment of the 22L homogenate, however, this was not the case for the 263K homogenate and the same results were obtained using the 263K hamster infectivity bioassays. A correlation can be observed when comparing PrP^{res} deposition with WB detection post decontamination. Both the enzymatic cleaners demonstrated high levels of PrP^{res} post treatment whereas the alkaline cleaner demonstrated no PrP^{res} (Fichet et al. 2004, Fichet et al. 2007b, Howlin et al. 2010). However, as mentioned before the SSBA SCEPA assay demonstrated remaining PrP^{res} based infectivity post decontamination with the alkaline cleaner which again does not correlate with these results. The only correlation between cleaner properties and reduction in infectivity that was observed within our N2a/22L SB/ThT assay and the 263K hamster models is that higher pH of the cleaner leads to reduced/no infectivity. Although this is difficult to confirm with the small number of cleaners tested. However, this has also been observed post treatment with other cleaning protocols that utilise high pH; for example, NaOH (~ pH 13) (Fichet et al. 2004, Fichet et al. 2007b, Flechsig et al. 2001, Yan et al. 2004) and more recently gaseous hydrogen peroxide treatment (~ pH 11.5) (Fichet et al. 2007a). Further research is required to determine whether this affect is caused by the actual pH of the cleaner or the available alkalinity of the various cleaning chemistries.

This chapter has demonstrated the sensitivity of the wire based N2a/22L SB/ThT infectivity assay. This assay has also been utilised to analyse the remaining infectivity post decontamination using three commercially available cleaning chemistries. Furthermore, this assay correlated with currently used animal infectivity bioassays. It has been previously demonstrated that wires are easier to decontaminate than larger tokens; thus, questioning whether wires are a good model of surgical instruments (Lipscomb et al. 2006a). The N2a/22L SB/THT assay has the potential to be adapted to analyse infectivity from a number of different surface types which is not possible in animal bioassays. The N2a/22L SB/ThT assay for wire-bound infectivity could also be utilised to test further decontamination protocols described previously such as gaseous hydrogen peroxide and DLC coated surfaces (Fichet et al. 2007a, Secker et al. 2012b). Furthermore, post contamination conditions such as drying times could also be analysed with regards to residual infectivity (Secker et al. 2011). This chapter also demonstrates that relying on the analysis of residual contamination post decontamination does not always correlate with remaining infectivity. Furthermore, the prion strain tested does not always correlate in regards to remaining contamination or infectivity. Therefore the incorporation of the SB/ThT detection methods with the propagation of different prion strains in different cells lines could further increase the potential of this assay especially in relation to the analysis of CJD infectivity which would not be possible in human subjects.

Chapter 6

Improvements in NSC culture

6.1 Introduction

This report has demonstrated the sensitivity and specificity of the N2a #58 cells and SB/ThT staining for the detection of prion infectivity pre and post decontamination. However, limitations in the detectability of infectivity of different prion strains are observed when utilising many of the animal cell lines for prion propagation. The major limitation of murine neuroblastoma cells in relation to prion infectivity is that they are only susceptible to infection from a minimal number of murine prion strains; for example, 22L, Fukuoka-1, 139A and Chandler for the N2a #58 cells, as summarised in Chapter 1 of this report (Nishida et al. 2000, Nuvolone et al. 2009). Furthermore, N2a cells primarily require genetic manipulation to express increased levels of PrP^c to increase their susceptibility to prion infection. Thus, questioning the relevance of these cell models in relation to disease propagation using natural PrP^c levels associated with animal or human brains. Neural stem cells (NSC) have the potential to be more constructive as a realistic model of prion infectivity as their multi-potent nature allows them to differentiate into neuronal cells that naturally express higher levels of PrP^c. Therefore they offer the potential for sensitive prion propagation without artificial genetic manipulation. The detection of a 10^{-4} 22L infection has already been determined in these cells using WB analysis (Milhavet et al. 2006). However, the SB/ThT detection protocol has already demonstrated a much greater sensitivity in the N2a #58 cells that could be utilised with the NSC's. Furthermore, the number of prion strains that NSC's will be susceptible to is currently unknown and could potentially be more than the N2a cells, offering excellent scope for further development (Milhavet et al. 2006, Nuvolone et al. 2009).

Therefore, the SB/ThT detection method, described previously, was utilised for the detection of amyloid accumulation from a 10^{-4} 22L infection within a neuron rich culture of differentiated NSC's. However, it was quickly observed that a number of cells that die during the differentiation process accumulate around the live cells and readily autofluoresce hindering the SB/ThT staining process. The cell loss observed could also affect the validity of the NSC assay as a loss of cells could potentially cause decreased prion propagation in comparison to *in vivo* propagation.

Some natural cell loss is observed in NSC proliferation as there is a mixture of cells types produced within the progeny; not all daughter cells become stem cells, some of the cells become transient and some will spontaneously differentiate and not survive the prolonged culture conditions in the proliferation media (Reviewed in Galli et al. 2003). Furthermore, the differentiated cells will die at the point where the proliferating neurospheres are passaged for expansion due to the lack of culture nutrients required for the maturation of the differentiated cells (Reviewed in Galli et al. 2003). Two main reasons hypothesised for the increased loss of cells at the point of induced differentiation in *in vitro* NSC cultures are the lack of nutrients or trophic support upon the removal of the mitotic factors (bFGF/EGF) or that culture conditions do not mimic pathological conditions (Niidome et al. 2006). DMEM/F12 media supplemented with N2 supplement is replaced at the point of differentiation with Neurobasal media for the improved culture of neuronal cells. However, the DMEM/F12 media contains more nutrients than the Neurobasal media and the N2 supplement contains insulin, apo-transferrin, sodium selenite, progesterone and putrescine that are all removed at the point of differentiation. Furthermore, almost all cell culture is carried out at normal oxygen levels or normoxia (~21% O_2); however, not all regions of the body that cells are derived from contain these levels of oxygen. In the brain the levels of O_2 range from 0.5 – 7%, therefore the normoxia conditions used are in fact hyperoxic for these cells and mild hypoxic conditions are "*in situ* normoxia" for brain derived cells (Reviewed in Ivanovic 2009, López-Barneo et al. 2001).

Improvements in the *in vitro* culture of NSC needed to be addressed prior to utilising the cells for prion propagation assays. Therefore, this chapter studied the improvements in NSC culture conditions in relation to media supplementation and atmospheric conditions. Furthermore, the percentage of neuronal and glial cells post differentiation in the different conditions was assessed so that the improved conditions did not alter the percentage of these cells types as a neuron rich culture is more ideal for optimal prion propagation.

6.2 Material and methods

Details of the materials and methods for this section can all be found within Chapter 2 of this report. Briefly, NSC's (2.1.2) were cultured according to the protocol described in section 2.2.2. The NSC's were then subjected to a 22L (2.1.3 and 2.3.1) infection at the point of induced differentiation following the N2a time course assay described in section 2.3.2. The prion propagation was analysed with SB/ThT staining and EF microscopy described in sections 2.4.2 and 2.4.5, respectively. The NSC culture conditions were then addressed as described in section 2.5 comparing normoxia and hypoxia (2.5.1) environments and improved supplementation (2.5.2). Cell type analysis and live dead staining was carried out as described in section 2.6. All EF images were captured and analysed as described in sections 2.4.5. Statistical analysis was carried out as described in section 2.7.

6.3 Results

6.3.1 Dead cells hinder SB/ThT analysis

Firstly, during the analysis of the 10^{-4} 22L propagation in the NSC's using the SB/ThT analysis, a large number of bright spots were observed in both the control and infected cell samples (Figure 46). The problem associated with the SB/ThT staining on the infected NSC's was hypothesised to be caused from the autofluorescence or accumulation of ThT fluorescence in the chromatin of dying/dead cells observed 1 – 2 days post differentiation of the NSC's. The dead cells show up clearly as they shrink and glow readily under the ThT filter block parameters. The presence of the bright spots observed in both the uninfected controls and the 10^{-4} 22L-infected NSC's made it impossible to determine the ThT-positive amyloid staining and therefore analyse the 22L infectivity (Figure 46).

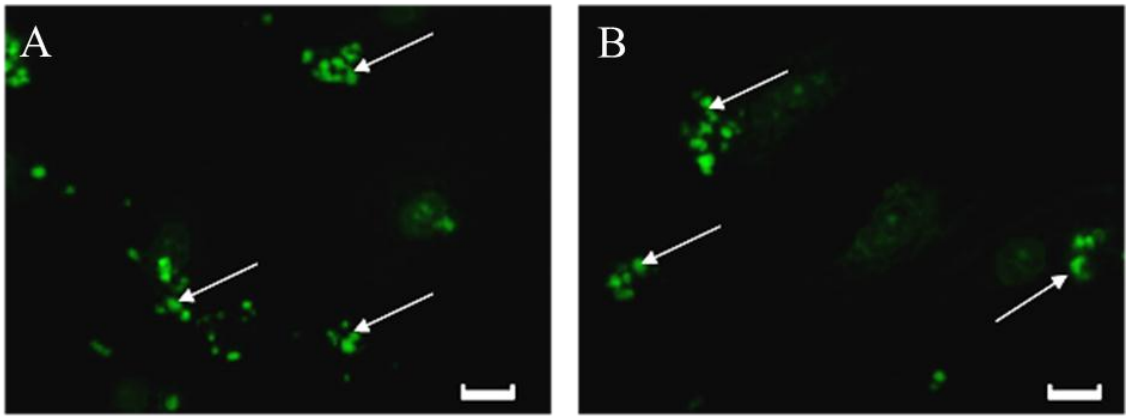

Figure 46 – NSC micrographs demonstrating dead cell fluorescence issue

Example micrographs of the SB/ThT staining on A) the 10^{-4} 22L-infected NSC's and B) the uninfected NSC controls demonstrating the hindrance of the bright auto/background fluorescence associated with the shrunken dead cells (highlighted by the arrows) observed in both samples. Scale bars = 10 μm.

The bright spots of ThT fluorescence was confirmed to be caused by dead cells by comparing the morphology and location of dead cells stained with propidium iodide (PI) in comparison to live cells stained with SYTO 9 (S9, Figure 47, A and B). The PI stained dead cells showed the same morphology as the shrunken dead cells fluorescing within the ThT detection parameters. Furthermore, the location of the PI stained dead cells surrounding the cell bodies of the S9 stained live cells correlated with the location observed with the bright spots of ThT-associated fluorescence (Figure 47, C). Therefore, improvements in the culture conditions were required to be able to utilise the NSC's and SB/ThT detection for the analysis of prion infectivity.

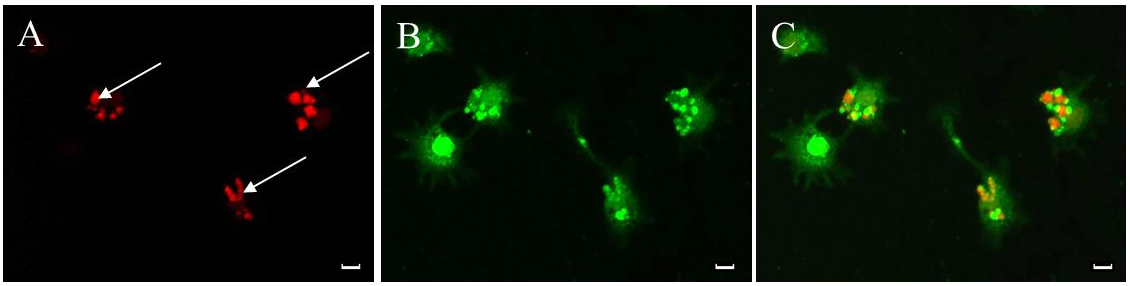

Figure 47 – Micrographs of SYTO 9/PI staining to confirm presence of dead cells

Example micrographs of live/dead staining to demonstrate and confirm the location of the dead NSC's observed with the SB/ThT staining. A) Propidium iodide (PI) staining of the dead cells highlighted by the arrows. B) SYTO 9 staining of all cells, both live and dead. C) Image A and B merged to show the location of the dead cells accumulating around the live cells as observed in the SB/ThT stained samples. Scale bars = 10 µm.

6.3.2 Differentiation confluency

Firstly, before addressing the culture conditions the confluency at which the NSC's were differentiated was analysed to determine if the NSC's were differentiated at too higher confluency and therefore cell loss was increased by the excess cells. The NSC's were grown to different visual confluences ranging from 40 - 90%, by estimating the percentage coverage of cells in the tissue culture dishes, at which point the mitotic factors were removed, media changed to the NB differentiation media and the cells were

left to differentiate for 7 days. Over the 7 days differentiation the cells were checked on a daily basis with phase contrast microscopy to visualise the quality of the cells in culture and subsequently the amount of floating dead cells. No visual difference in the quantity of cell death was observed when the confluency prior to differentiation was altered; suggesting that the confluency levels between 40 – 90% had no relation to the increased number of dead cells observed in the original NSC cultures.

6.3.3 Hypoxia environment for NSC culture

Following the discovery that the confluency range analysed had no effect on the level of cell death, the adaptation of the culture conditions was potentially the way to improve the culture quality. Firstly, changing the levels of oxygen that the cells were incubated in to try and closer mimic the physiological conditions from the cells origin was analysed. Originally the cells were cultured at normoxia (~21% O_2) which could have caused stress within the cells as this is not physiological conditions However, in this study the NSC's were seeded into increasing oxygen concentrations starting at 1% O_2 until a concentration was reached in which the cells were growing comfortably and consistently. The cells were observed using phase contrast microscopy daily and observations were recorded. The cells died within the first 24 hours post seeding when grown in the lower oxygen concentration (1 – 4% O_2). Between 4 and 6% O_2 the cells would stay alive for up to 2 weeks but the proliferation would be extremely slow and the cells would aggregate in one group, then within 2 – 3 days cell apoptosis was observed, suggesting this level of O_2 was too low for cell survival. The optimal concentration where the cells would proliferate to 100% confluency within 7 days consistently was at 8% O_2. Therefore, for the rest of the hypoxia experiments this was the oxygen concentration used. The numbers of cells after 7 days culture in normoxia and hypoxia was tested to determine the efficiency of proliferation within these environments (Figure 48). A significant increase in the number of cells after 7 days proliferation was observed in the cells grown in hypoxia (43 ± 6) compared to the cells grown in normoxia (24 ± 3) (Figure 48). This suggests that the cells proliferate more rapidly when grown in the lower oxygen environment.

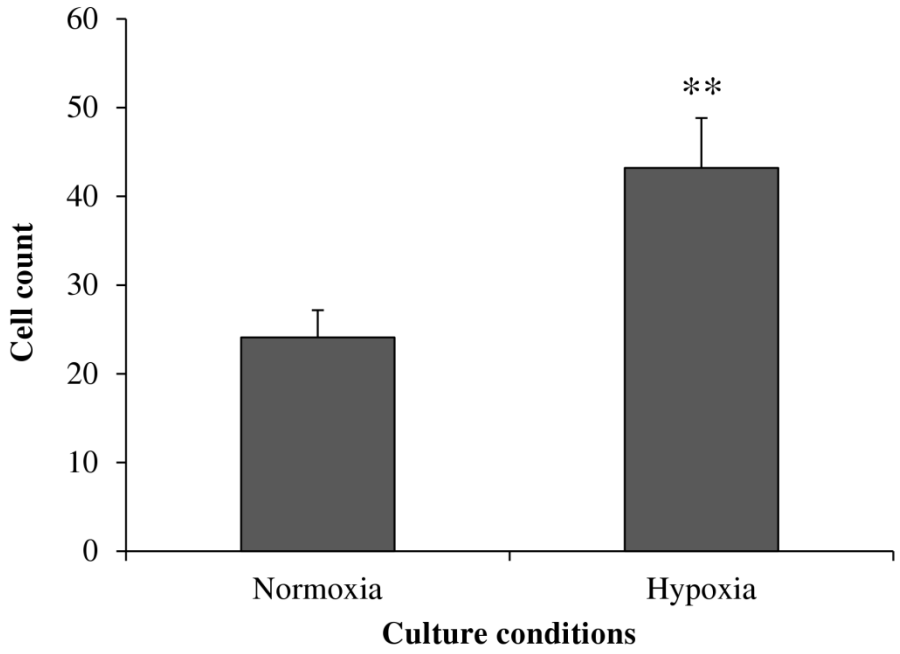

Figure 48 – Cell counts of NSC's cultured in a normoxia or hypoxia environment

Cell counts of the NSC's using SYTO 59 to label all cell nuclei from cells grown in either normoxia (~21% O_2) or hypoxia (8% O_2) for seven days post seeding. Error bars represent the SEM (n = 10), ** = $p \leq 0.01$ when compared to normoxia.

Nestin immuno labelling of the undifferentiated dividing cells was used to visualise the percentage of neuronal progenitor cells and subsequently highlight which environment is associated with more spontaneous differentiation within the proliferating cells. Image analysis was used to quantify the percentage of nestin-positive cells in all of the samples as a comparison (Figure 49). The percentage of nestin-expressing cells was increased, but not significantly, in the cells grown in 8% O_2 (88% ± 6.9) compared to the cells grown in normoxia (80% ± 5.9). The representative micrographs in Figure 49 also demonstrate the similar levels of nestin positive cells, but also the increased cell numbers observed when cultured in the 8% O_2 environment compared to the normoxia cultured cells.

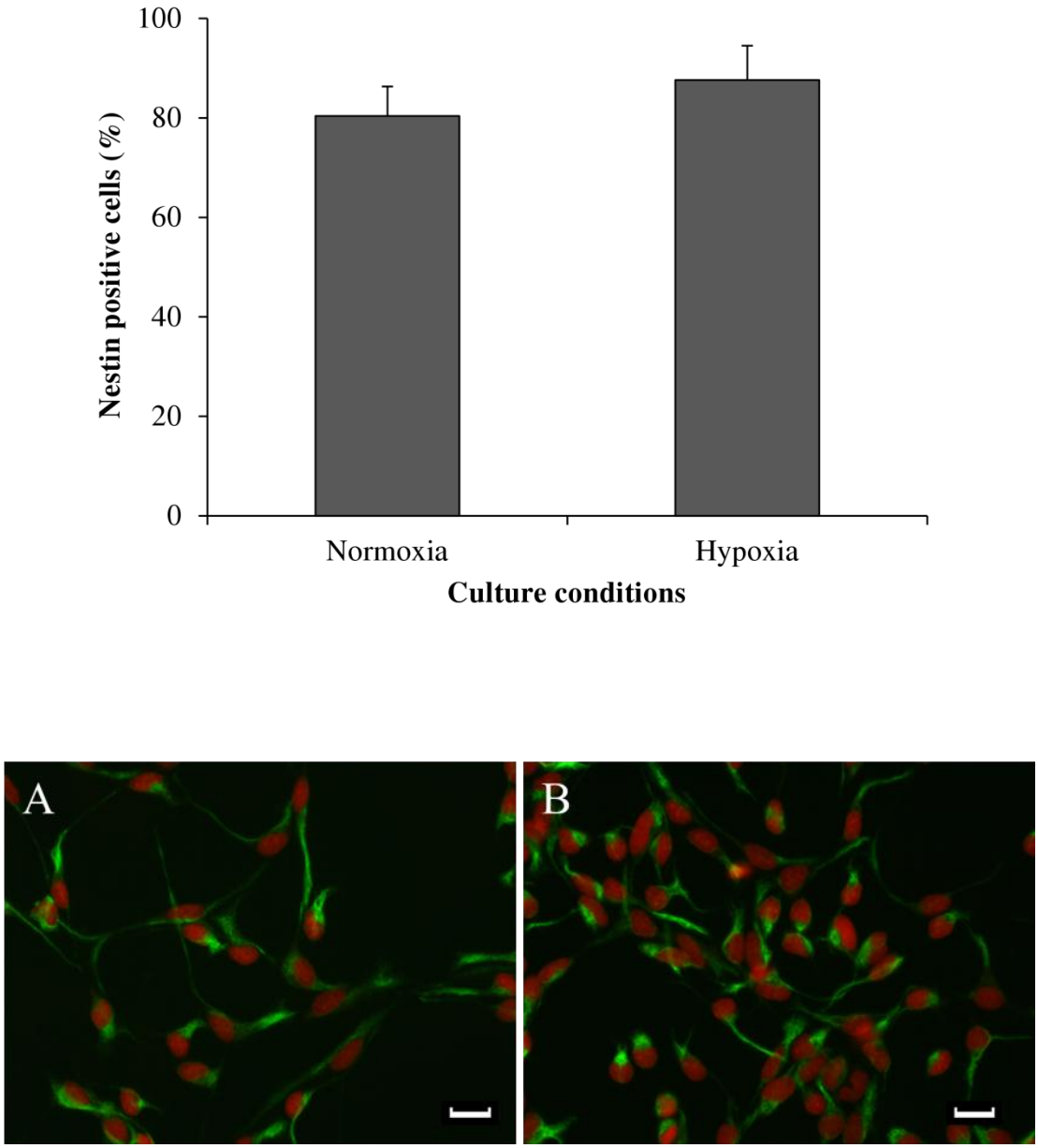

Figure 49 – Comparison of the percentage of nestin-positive cells grown in the different atmospheric conditions

The percentage of nestin-positive cells present after 7 days culture in different atmospheric conditions. The representative micrographs demonstrate example images of nestin (green) immuno labelled cells and SYTO 59 (red) nuclei staining of NSC's cultured in A) normoxia and B) 8% O_2 for 7 days post seeding. Error bars represent SEM (n = 10). Scale bars = 10 µm.

6.3.4 Varying culture supplements post differentiation in the different atmospheric conditions

Another hypothesis for the occurring cell loss was the media change and removal of the mitotic factors at the point of differentiation, thus removing a lot of the nutrients that the cells were receiving during the proliferation stages. This would cause the cells to become shocked and ultimately die. Therefore, alongside comparing the normoxia and hypoxia culture environments, one of two supplements (0.1% bFGF and 0.1% FBS) was introduced to the cells for two days post differentiation to wean the cells of the original nutrients. The cells were incubated for 7 days before cell type analysis was performed. During this period phase contrast images were taken every 2 days to compare the differences in cell morphology. The micrographs at 5 days demonstrated clear differences in the cell morphology between the three different environments (Figure 50). The bFGF supplemented cells demonstrating the most differences showing a higher number of cells and vacuoles associated with cell death; however it is impossible to comment on the levels of differentiation without cell type immuno-labelling (Figure 50). There did not appear to be any difference in appearance of the cells when comparing the unsupplemented media with FBS.

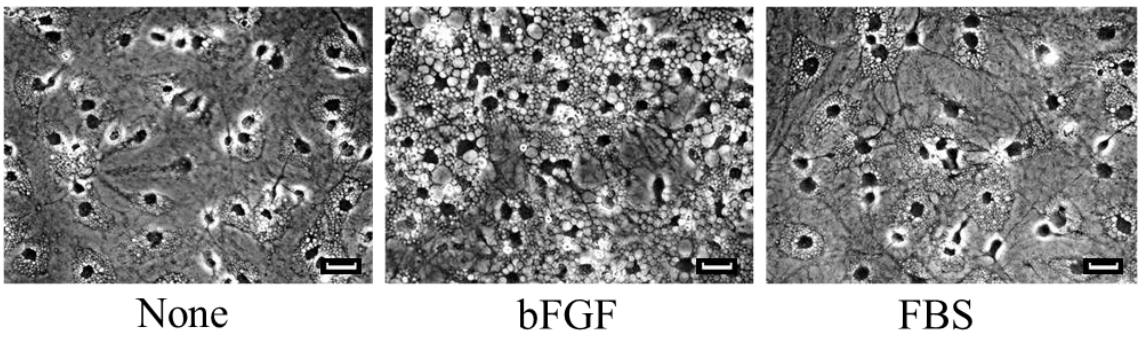

Figure 50 – Phase contrast images of differentiated NSC's culture in different conditions

Example inverted phase contrast micrographs of live NSC's five days post differentiation with no supplement (None) or supplemented with 0.1% basic fibroblast growth factor (bFGF) or 0.1% fetal bovine serum (FBS) for 2 days post differentiation. Scale bars = 10 μm.

6.3.4.1 Cell type analysis post differentiation in the different culture conditions

Phase contrast microscopy of the live cells during differentiation demonstrated variations in the cell morphology between the different culture conditions. Therefore, immuno labelling was utilised to determine the percentage of progenitor cells (Nestin-positive), astrocytes (GFAP-positive) and neurones (β-III-Tubulin-positive) present in the different supplemented culture conditions and environments.

After altering the culture condition, the levels of undifferentiated progenitor cells remaining post differentiation was analysed. This can be used to determine the number of dividing cells remaining post induced differentiation; thus, demonstrating the differences in the levels of differentiation between the different culture conditions. No significant increase in the percentage of nestin-positive cells post differentiation was observed between the cells cultured within the different culture conditions, all ranging between 20 – 30% (Figure 51). However, a slight increase, but not significant, in nestin-positive cells was observed in the cells grown in the normoxia (24 – 30%) atmosphere when compared to the hypoxia (20 – 22%) (Figure 51). The representative micrographs demonstrate the similar faint nestin-positive staining observed in the conditions containing the highest and lowest percentage of nestin-positive cells (Figure 51).

GFAP immuno-labelling was used to analyse and compare the levels of astrocytic cells post differentiation in the different supplemented culture conditions and atmospheric environments. A significant increase in the percentage of GFAP-expressing cells was observed in the cells grown with FBS supplementation in normoxia and hypoxia (44% ± 5 and 44% ± 3, respectively), no supplementation in hypoxia (54% ± 4) and bFGF supplementation in hypoxia (67% ± 7) when compared to the cells grown in normoxia with bFGF supplementation (Figure 52). The highest percentage of GFAP-expressing cells was observed in the cultures grown in hypoxia with the addition of bFGF post differentiation. This was significantly higher than the cells grown with no supplementation in the normoxia environment and the cells supplemented with FBS in the normoxia and hypoxia environments. The lowest percentage of GFAP-expressing

cells was observed in the cells grown in the normoxia environment with again the addition of bFGF (21% ± 5) (Figure 52). The representative micrographs in Figure 52 demonstrate the clear difference of GFAP-positive cells in the conditions containing the lowest and highest percentage of astrocytic cells.

Class III β-Tubulin immuno-labelling was utilised to analyse and compare the levels of neuronal cells cultured within the different oxygen conditions and the different supplements post differentiation. Similar percentages of neurons were observed in the cultures grown in the hypoxic environment with no supplements (74% ± 4), supplemented with bFGF (68% ± 5) or supplemented with FBS (82% ± 3) (Figure 53). A significant decrease in the percentage of β-III-Tubulin-expressing cells was observed in the cultures grown in normoxia with no supplements post differentiation (60% ± 4) or supplemented with bFGF (45% ± 6) (Figure 53). The lowest percentage of β-III-Tubulin-expressing cells was observed in the normoxia environment supplemented with bFGF post differentiation. The highest percentage of β-III-Tubulin-expressing cells was observed in the cultures grown in hypoxia and normoxia supplemented with FBS (79% ± 5 and 82% ± 3, respectively) (Figure 53). Generally the level of β-III-Tubulin staining was lower in the cells grown in normoxia apart from the cells supplemented with FBS which had close to the same expression as the hypoxia cultured cells (Figure 53). The representative micrographs demonstrate the different percentages of neuronal cells present in the conditions that cultured the lowest and highest percentages of neuronal cells.

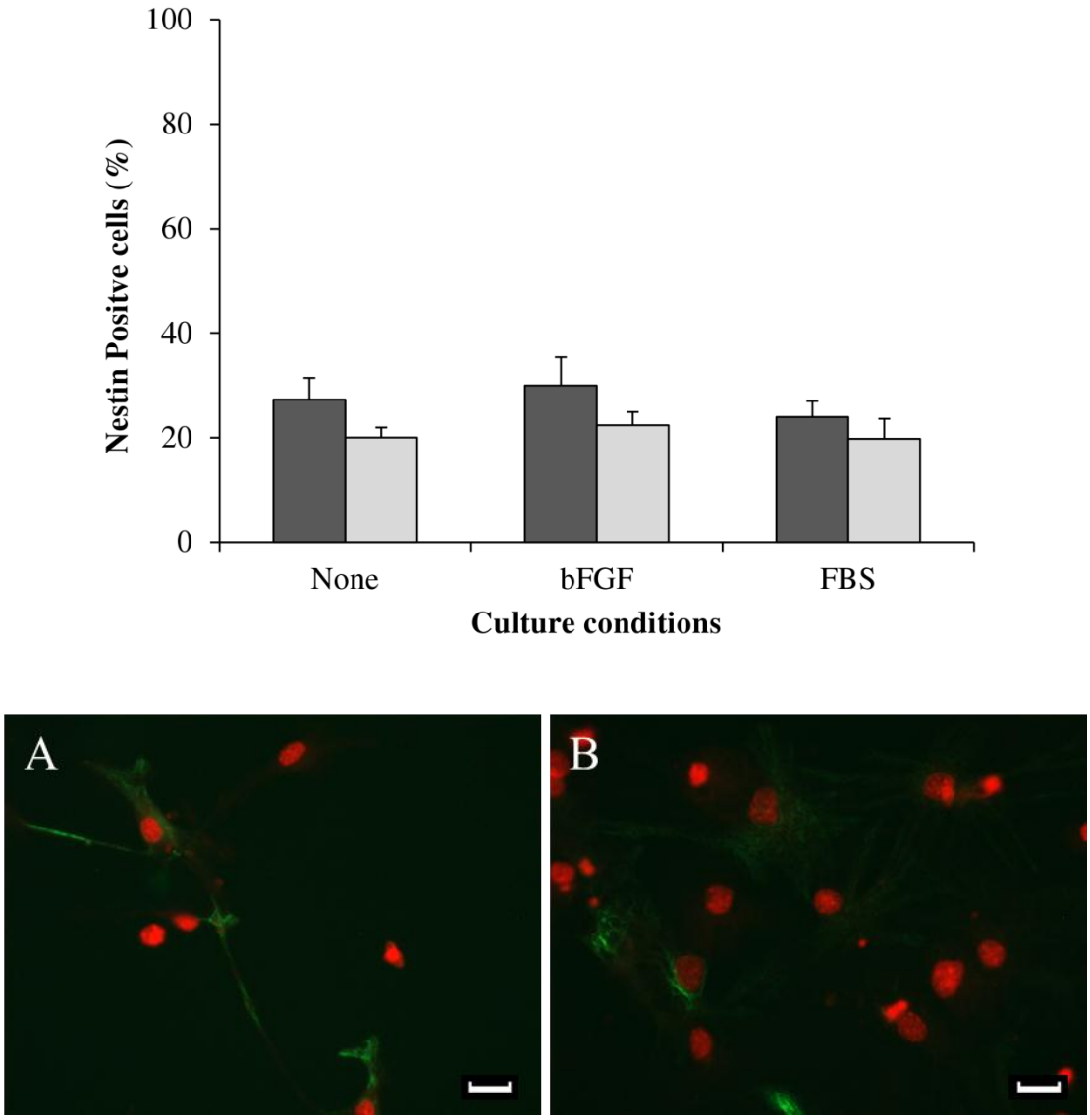

Figure 51 – Comparison of the percentage of nestin-positive cells cultured in the different culture conditions

The percentage of nestin-positive cells after 7 days differentiation with different supplements and cultured within different atmospheric conditions (Normoxia (Dark grey bars) and Hypoxia (Light grey bars)). The representative micrographs demonstrate example images of nestin (green) immuno-labelled cells and SYTO 59 (red) nuclei staining of NSC's supplemented with; A) 0.1% fetal bovine serum (FBS) and cultured in a hypoxia normoxia and B) 0.1% basic fibroblast growth factor (bFGF) and cultured in normoxia post differentiation. Error bars represent SEM (n = 10). Scale bars = 10 µm.

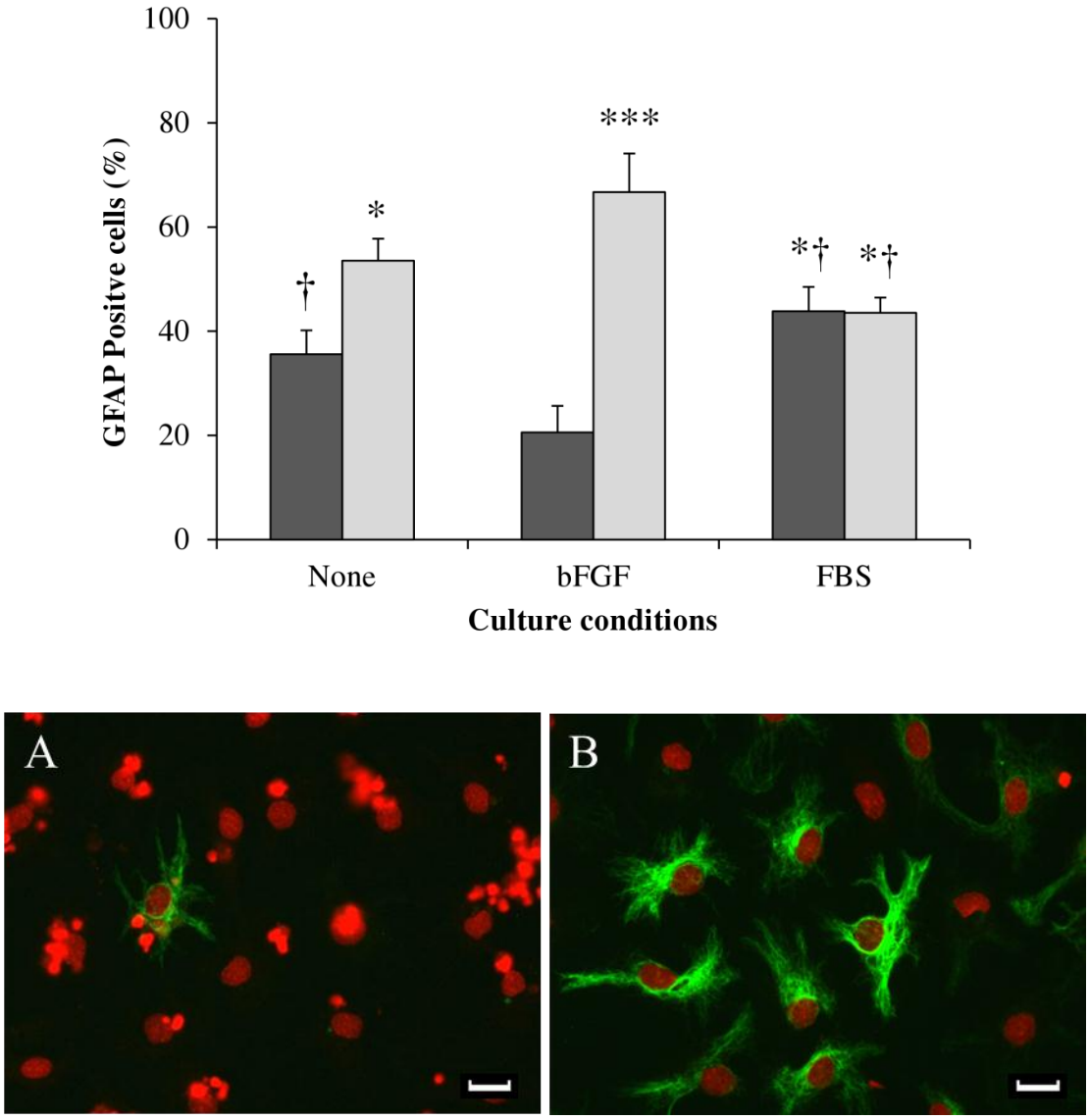

Figure 52 - Comparison of the percentage of GFAP-positive cells cultured in the different culture conditions

The percentage of GFAP-positive cells after 7 days differentiation with different supplements and cultured within different atmospheric conditions (Normoxia (Dark grey bars) and Hypoxia (Light grey bars)). The representative micrographs demonstrate example images of GFAP (green) immuno-labelled cells and SYTO 59 (red) nuclei staining of NSC's supplemented with; A) 0.1% basic fibroblast growth factor (bFGF) and cultured in normoxia and B) 0.1% basic fibroblast growth factor (bFGF) and cultured in hypoxia post differentiation. Error bars represent SEM (n = 10). * = $p \leq 0.05$, *** = $p \leq 0.001$ when compared to Normoxia/bFGF and † = $p \leq 0.05$ when compared to Hypoxia/bFGF. Scale bars = 10 µm.

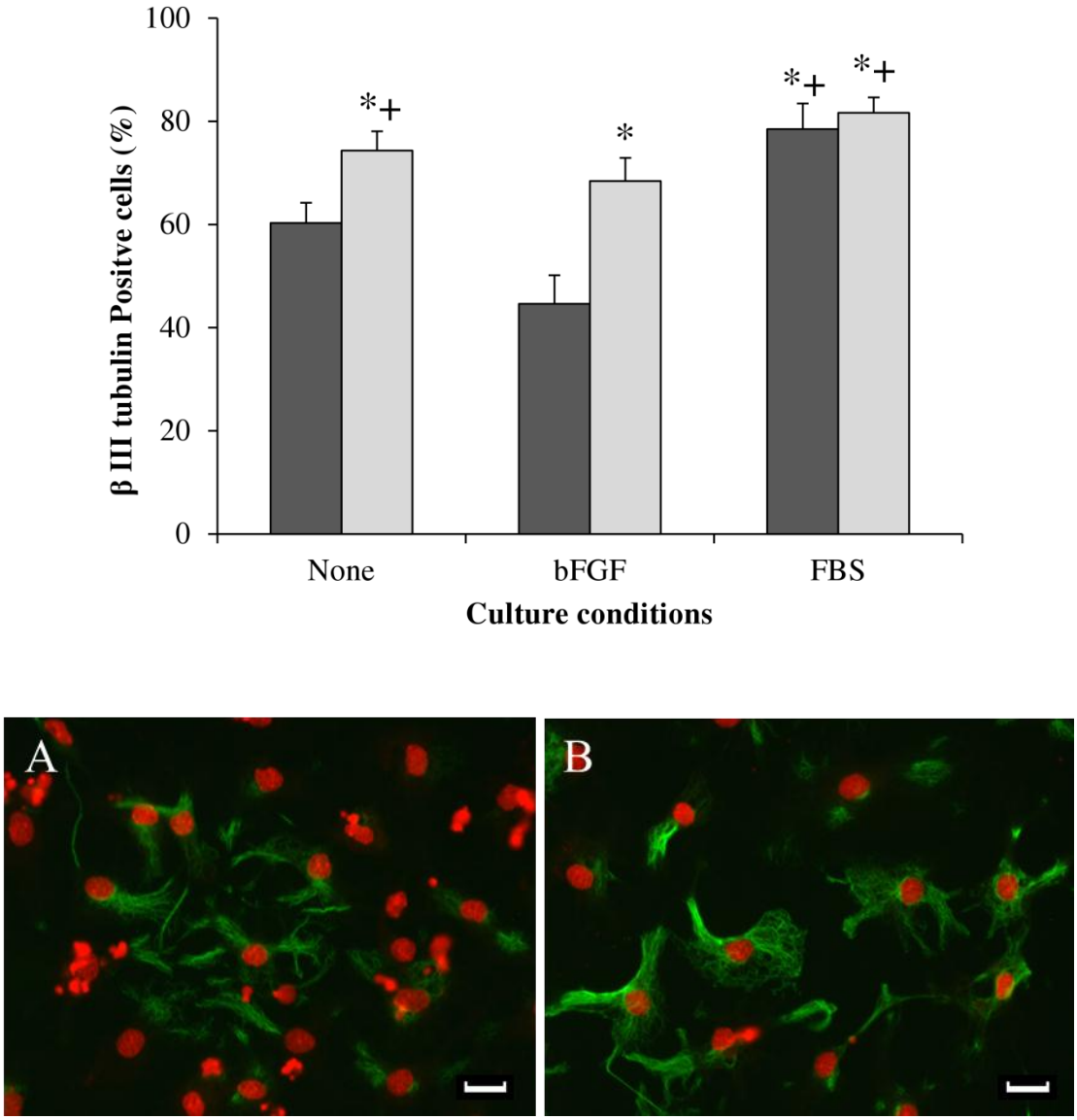

Figure 53 – Comparison of the percentage of β-(III) Tubulin-positive cells cultured in the different culture conditions

The percentage of β-(III) Tubulin-positive cells after 7 days differentiation with different supplements and cultured within different atmospheric conditions (Normoxia (Dark grey bars) and Hypoxia (Light grey bars)). The representative micrographs demonstrate example images of β-(III) Tubulin (green) immuno-labelled cells and SYTO 59 (red) nuclei staining of NSC's supplemented with; A) 0.1% basic fibroblast growth factor (bFGF) and cultured in normoxia and B) 0.1% fetal bovine serum (FBS) and cultured in hypoxia post differentiation. Error bars represent SEM (n = 10). * = $p \leq 0.05$ when compared to Normoxia/bFGF and $^{+}$ = $p \leq 0.05$ when compared to Normoxia/None. Scale bars = 10 µm.

6.3.4.2 Comparison of the ratio of live: dead cells between the different culture conditions

Finally, the cell loss observed in the cultures kept under all of the conditions was quantified by labelling all cells with SYTO 9 and cells with compromised membranes (i.e. dead cells) with propidium iodide. The ratio of live to dead cells was then compared between cells grown within the different conditions and supplementation. A significant increase in the ratio of live to dead cells was observed in the cells cultured in hypoxia with no supplementation (3.5 ± 0.4) and the cells cultured in normoxia and hypoxia with the FBS supplementation (3.9 ± 0.5 and 4.1 ± 0.4, respectively) when compared to the cells cultured in the other three conditions (Figure 54). The lowest ratios of live to dead cells was observed in the cells cultured at normoxia with no supplementation and the cells cultured in normoxia and hypoxia supplemented with bFGF (1.8 ± 0.2, 1.4 ± 0.1 and 1.7 ± 0.1, respectively) (Figure 54). The highest ratio of live to dead cells was observed in the cells cultured in normoxia or hypoxia supplemented with FBS post differentiation. Twice as many live cells to dead cells were observed in the FBS supplemented cells when compared to the original culture conditions of normoxia cultured cells with no supplementation post differentiation. The representative micrographs demonstrate the live/dead staining in the hypoxia cultured cells and the three supplemented conditions. From these it is clear to see that the number of red (dead) cells is greatly increased in the bFGF supplemented cells. The other clear observation from these micrographs is the increase in the number of live (green) cells present in the FBS supplemented cells, so not only is there a higher ratio of live to dead cells there are also a larger number of live cells present post differentiation compared to the other conditions (Figure 54).

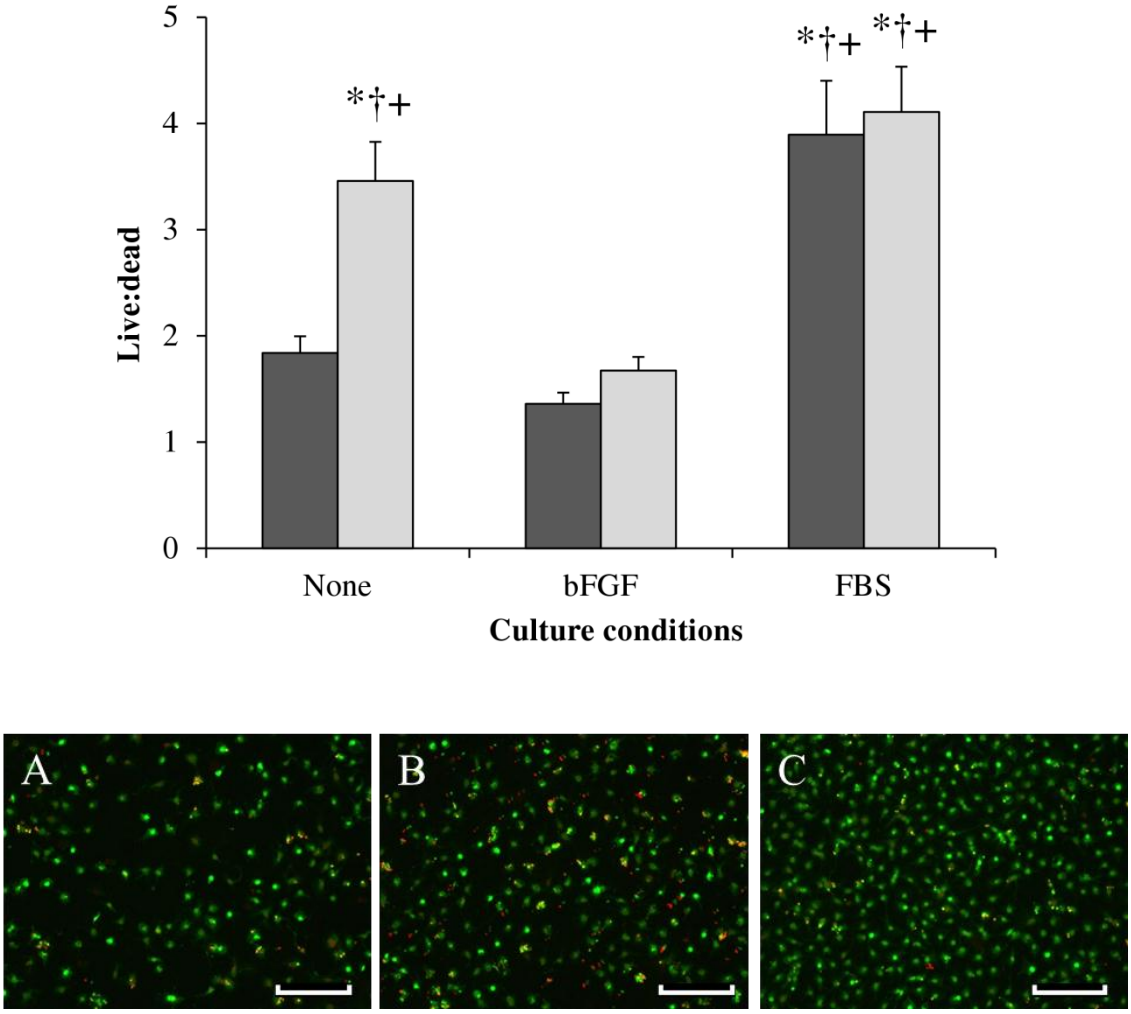

Figure 54 – Comparison of the ratio of live: dead cells when cultured in the different culture conditions

The percentage ratio of live: dead NSC's after 7 days differentiation with different supplements and cultured within different atmospheric conditions (Normoxia (Dark grey bars) and Hypoxia (Light grey bars)). The representative micrographs demonstrate images of SYTO 9 (green) labelling all cells and PI (red) nuclei staining of dead NSC's supplemented with; A) no supplements, B) 0.1% basic fibroblast growth factor (bFGF) and C) 0.1% fetal bovine serum (FBS) and cultured in hypoxia post differentiation. Error bars represent SEM (n = 10). * = $p \leq 0.05$ when compared to Normoxia/bFGF, $^{+}$ = $p \leq 0.05$ when compared to Normoxia/None and † = $p \leq 0.05$ when compared to Hypoxia/bFGF. Scale bars = 50 μm.

6.4 Discussion

The importance of cell-based assays for the detection of prion infectivity has been widely discussed within this report. The main advantage of neural stem cells, against other discussed cells, for the propagation of PrP^{Sc} is their multi-potent ability. This allows them to differentiate, with the addition of different supplements *in vitro,* into three important cell types of the CNS; neurons, astrocytes and oligodendrocytes (Morrison 2001). Neuronal cells are the most susceptible cells in the body to infection from PrP^{Sc} because they naturally contain higher levels of PrP^{c}. Therefore they would be an ideal model for prion infectivity as they require no genetic manipulation to increase PrP^{c} expression and are therefore, a closer model of prion infections *in vivo* than the modified neuroblastoma assays presented in the previous chapters. The other potential advantage of the NSC assays is that the different prion strains that the cells are susceptible to infection from are unknown and could potentially be more or different to the strains observed in the mouse N2a assays.

The use of NSC's for the propagation of the infectious prion alongside the sensitive SB/ThT detection method demonstrated in the N2a cells could produce a highly sensitive and diverse prion infectivity assay. This was first tested with a 10^{-4} 22l infection in the NSC's. However, an issue arose when the NSC's were differentiated in that a considerable amount of cell death was observed. Furthermore, the dead cells readily autofluoresce under the same spectral range as ThT, thus hindering the detection of the amyloid accumulation. This was clearly confirmed with live/dead staining, highlighting the accumulation of the dead cells around the live cell bodies. Therefore, it was determined that the NSC culture conditions needed to be carefully revised and improved, so firstly, the SB/ThT staining would not be hindered and secondly, the level of cell death did not invalidate the assay.

The confluency that the cells were differentiated at was first believed to be the problem so the level of cell confluency was altered to see if this altered the amount of cell death previously observed. However, changing the confluency showed no visual change in the quality of the cultured cells. The next hypothesis was that the atmospheric

conditions that the NSC's were cultured in were not optimal for cell growth. Standard cell culture conditions use 37^{o}C, 5% CO_2 and 20% O_2. Whilst this temperature mimics the body temperature and the CO_2 is the same as arteriole CO_2, the levels of O_2 in different regions of the body are not always at atmospheric levels (~21%) (Studer et al. 2000). It has been documented that the partial pressures of O_2 in the brain range for 10 – 40 mm Hg PO_2 which translates to between 3 – 7% O_2 (Masamoto et al. 2009, Wion et al. 2009). Levels of O_2 in the cerebral cortex of rat brain of around 27.6 mm Hg or 2.5 – 5.3% O_2 have also been documented (Masamoto and Tanishita 2009, Studer et al. 2000). This information suggests that cortical NSC culture should be carried out at lower oxygen levels than the standard cell culture conditions to closer mimic the physiological conditions that the cells were derived from (Reviewed in Ivanovic 2009). Therefore, the NSC's were cultured in increasing oxygen levels from 1-8% to determine the lowest oxygen concentration that gave optimal cell proliferation. The optimal cell growth was observed at 8% O_2 which is higher than previously documented studies that use 5% but is closer to physiological conditions than atmospheric oxygen (Clarke et al. 2009, Studer et al. 2000). The efficiency of cell proliferation over 7 days increased by almost double in the cells cultured in the hypoxia environment when compared to the cells cultured at normoxia, which correlated with previous studies (Clarke and van der Kooy 2009, Studer et al. 2000). The percentage of nestin-positive cells was very similar in both hypoxia and normoxia prior to differentiation suggesting no obvious difference in the percentage of progenitor cells and therefore the level of spontaneous differentiation observed between the two culture conditions. These results confirmed that the hypoxia environment improved the NSC culture prior to differentiation.

Following these observations the two atmospheric conditions were compared for the quality of NSC differentiation with the added addition of one of two supplements (bFGF or FBS) for two days post differentiation. Firstly the percentage of nestin-positive cells remaining post differentiation was analysed to determine the number of progenitor cells remaining. A similar percentage of undifferentiated cells were observed within all of the culture conditions with slightly lower percentages observe in the hypoxia cultured cells when compared to the normoxia grown cells. This suggested that the hypoxia environment also supported slightly higher levels of differentiation within the cultured cells. The percentage of GFAP-expressing cells was used to determine the number of astrocytes in all of the conditions seven days post differentiation. The highest

percentage of astrocytic cells was observed in the cells cultured in the hypoxic environment with no or bFGF supplementation. This suggests that the hypoxia environment improved the levels of differentiation towards the lineage of astrocytic cells compared to the original culture conditions. The higher percentage of astrocytic cells could also be a marker of stress, which may be observed in the hypoxia cultured bFGF supplemented cells as this condition gave rise to an excess of cells post differentiation. Lastly the percentage of β-III-Tubulin-expressing cells was used as a marker for the percentage of neuronal cells in all of the conditions. The percentage of neurons in all of the culture conditions was observed to be higher than the percentage of astrocytes. This was hypothesised as the supplementation of the NB media with B27 factor is a common method utilised to fabricate culture conditions that favour the differentiation of the NSC progenitor cells into neuronal cells (Milhavet et al. 2006). Furthermore, B27 supplements also contains molecules which reduce oxidative stress and therefore help to promote cell survival (Hall et al. 2008). An increased percentage of neuronal cells were observed in the hypoxia cultured cells which is most likely to be caused by the lower levels of reactive oxygen species observed in the mild hypoxic environments (Fan et al. 2008, Ivanovic 2009, Niidome et al. 2006). In addition, the FBS supplementation increased the percentage of neurons observed in the normoxia environment. This could be caused by numerous growth factors that are observed in FBS (Even et al. 2006), but without Mass spectrometry analysis of the composition of the FBS used in our experiment it would be difficult to comment directly. Potentially, there could be a key role for the presence of insulin-like growth factor-1 (IGF-1) found in FBS as it has a similar structure to insulin which is commonly used to improve cell viability within culture (Singh et al. 1997). Furthermore, the highest percentage of neuronal cells was observed in the cultures that contained over 40% astrocytic cells. Astrocytic cells have demonstrated a neuroprotective role and will protect neurons especially *in vitro* culture which is most likely the reason for this observed correlation (Brown 1999, Chen et al. 2001, Liu et al. 2012).

More importantly was the comparison of the ratios of live to dead cells between the different culture conditions as it was the dead cells that were hindering the SB/ThT staining. The highest ratio of live to dead cells was observed in the hypoxia conditions with no supplement and FBS supplementation and the normoxia environment with FBS supplementation. This suggests again that the lower levels of reactive oxygen species

(ROS) observed in mild hypoxia environments helps to decrease cell death and that the increased growth factors introduced from the FBS is also improving the viability of the cells. The lowest ratios of live to dead cells was observed in the cells supplemented with bFGF and cultured in both normoxia and hypoxia environments. This is likely to be caused by the introduction of bFGF post differentiation initially inhibiting differentiation and increasing cell confluency. When the supplement was removed, increased cell death and less differentiation was observed suggesting this supplement does not enhance the culture conditions post differentiation. The lack of trophic support or nutrients in *in vitro* culture of neuronal progenitor cells was also observed with a mouse multi-potent cell line MEB5 which are similar to mouse NSC's (Niidome et al. 2006). Furthermore, in this study they also demonstrated that molecules that block the levels of ROS present in the cell culture environment protected the cells and subsequently lowered the levels of cell death (Niidome et al. 2006). This is also true for the hypoxia environments used within our culture systems. The lower levels of cell death associated with the cells grown in the lower oxygen environment in our work could be associated with the documented lower levels of ROS present in mild hypoxic environments, thus correlating with the results obtained using molecules that block ROS production (Fan et al. 2008, Ivanovic 2009, Niidome et al. 2006). Therefore a mixture of the wrong O_2 concentrations and the lack of nutrients for differentiated cell survival were the contributing factors to the cell death primarily observed.

This study highlights the importance of understanding the physiological conditions of different cell types so that the optimal culture conditions can be used. Growing the cells in hypoxia has improved the efficiency of NSC proliferation and cell viability and improved the number of neurons post differentiation, thus potentially improving the infectivity potential of the NSC cultures. The supplementation of the cells with FBS improved the culture conditions with regards to all of the cell markers analysed and the ratio of live to dead cells in both normoxia environments. However, a mixture of hypoxic conditions to improve proliferation of the undifferentiated NSC's and FBS supplementation post differentiation to improve differentiation and cell viability is the optimal conditions for the NSC culture. These conditions can then be used in future work to analyse SB/ThT analysis of prion propagation without the hindrance of the original, sub-optimal culture conditions.

Chapter 7

Final discussion and future work

7.1 Discussion and future work

The aim of this project was to design and develop a cell-based infectivity assay system that incorporated sensitive *in situ* staining for the microscopic detection of prion infectivity that has the potential to be adapted to analyse a wide range of prion stains. Furthermore, this assay was designed to focus on the assessment of surgical instrument decontamination procedures in relation to remaining prion infectivity. This *in situ* staining procedure aimed to be transferable between cell lines that are susceptible to prion infection from prion strains of different species and ultimately be able to detect infectivity from CJD contaminated instruments and biological samples.

The first important question to address when developing a novel cell based infectivity assay is the cell line used. Cell lines vary in their susceptibility to infection from different prion strains due to the effect of the "species barrier" and their ability to establish a consistent infection that is not lost during cell division and passage steps. The variations in cell line susceptibility to different prion strains has been discussed previously in this report (Summarised in Nuvolone et al. 2009). Furthermore, it is important to establish a balance between a steady consistent propagation and uncompromised cell viability. This is because an accumulation of PrP^{Sc} that is too rapid will cause cell death and therefore loss of infected cells and subsequently loss of detectable material. Consequently, it is important to use a cell line that will amplify PrP^{Sc} to a level in which the prion propagation is at a steady state but not engulfing the cells (Ghaemmaghami et al. 2007, Mahal et al. 2007).

Neuroblastoma cell subclone N2a #58 has already been established as a cell line that is susceptible to prion infection from three murine scrapie prion strains; 22L, Fukuoka-1 and 139A (also known as chandler of RML) (Mange et al. 2002, Nishida et al. 2000). Therefore, N2a #58 cells were initially utilised to develop and determine the sensitivity of this novel staining procedure in relation to prion decontamination. Mouse adapted scrapie prion isolate 22L was the prion strain used to infect the cells as it has been established to reliably infect the N2a #58 cells at higher doses (Mange et al. 2002, Nishida et al. 2000). Thioflavin T was chosen as the fluorophore to identify prion-

associated amyloid as a marker of prion propagation and subsequently infectivity within the N2a cells. Thioflavin T has been established in a number of techniques to detect prion associated-amyloid upon SS surfaces and surgical instruments and has previously shown 2-log greater sensitivity when compared to WB detection of PK resistant PrP^{Sc} (Herve et al. 2009, Herve et al. 2010, Howlin et al. 2010, Lipscomb et al. 2007a). Furthermore, ThT is also utilised in the amyloid seeding assay (ASA) to detect the amplification of PrP^{Sc} in solution via increased ThT fluorescence using a fluorescent plate reader (Colby et al. 2007). Furthermore, the ASA was incorporated into the RT-QUIC assays to combine the improved quaking conversion of PrP^{Sc} with the sensitive amyloid based detection of prion amplification (Atarashi et al. 2008, Atarashi et al. 2011a, Atarashi et al. 2011b). The majority of current cell-based prion infectivity assays rely on the immuno-detection of PK digested PrP^{Sc} known as PrP^{res}; however, more recently it has been established that a high percentage (~80% of disease associated prion material) is sensitive to PK digestion, denoted $sPrP^{Sc}$ (D'Castro et al. 2010, Gambetti et al. 2008, Kuczius and Groschup 1999, Pastrana et al. 2006, Thackray et al. 2007). Therefore, there is considerable doubt as to whether these assays are able to detect the true remaining infectivity of this infectious agent or whether the disease associated material is lost during digestion. As a result, ThT was chosen in this novel *in situ* staining procedure to avoid the loss of disease-associated material associated with PK digestion and provide an alternative method of detection.

Chapter 3 of this report introduced the *in situ* ThT detection of amyloid accumulation in the N2a cells from initial 22L doses ranging from a 10^{-4} – 10^{-9} dilution of 10% 22L-infected brain homogenates propagated over 14 days post inoculation with no cell passaging. Initial experiments observed high autofluorescence and non-specific binding associated with ThT in the assay. One step to partially address this was a final acetic acid wash within the protocol as it has been previously discussed that increased pH reduces non-specific binding of ThT to nucleic acids (Khurana et al. 2005). Furthermore, initial assays also noted a significant amount of autofluorescence associated with tissue lipids. Work aimed to address this issue and, subsequently, Sudan black was used to quench lipid-associated autofluorescence. The incorporation of Sudan black to the ThT staining protocol increased the sensitivity of amyloid accumulation detection from a 10^{-6} 22L infection with the ThT alone, to a 10^{-9} 22L infection with the SB/ThT staining. This also demonstrated a >3 log increase in sensitivity when directly

compared to the WB detection of PrP^{Sc} content of the 22L-infected N2a lysates form the 35 mm cell culture dishes. However, variability in the propagation and amyloid accumulation was observed between different experiments especially within the lower dose samples. This was thought to be associated with the 100% confluency of the N2a cells observed between 8-10 days post infection. Therefore, PrP^{Sc} propagation between 8-14 days was inconsistent and subsequently the cell loss due to contact inhibition observed at 14 days post infection made the results un-comparable.

The majority of cell assays for the detection of prion infectivity incorporate cell splits or passages to improve the sensitivity of the assay by essentially allowing the cells increased time in contact with the infectious material. This subsequently increases the chance for prolonged PrP conversion and ultimately increased infection (Archer et al. 2004, Edgeworth et al. 2009, Edgeworth et al. 2011b, Klohn et al. 2003, You et al. 2010). Furthermore, the increased turnover of cells producing PrP^{c} that will potentially come into contact with infectious material will closer mimic the natural turnover of PrP^{c} within an *in vivo* environment associated with animal infectivity assays. Cell passages are required for cell lines, such as the N2a cells, that do not survive well at high confluency. However, RK13 epithelial cells (genetically modified to encode prion proteins from different species) have demonstrated the sensitive detection of a number of prion strains from different hosts within two experimental cycles (Arellano-Anaya et al. 2011). The RK13 cells survive well at high confluency for >3 weeks with weekly media changes, allowing an increased time for prion propagation without the need for cell splits (Arellano-Anaya et al. 2011). However, these cells also need to be genetically modified to improve prion susceptibility and rely on WB detection of PrP^{res}.

When introducing cell passages into prion infectivity assays it is important to split the cells at the optimal point to allow consistent propagation without the loss of cell susceptibility over time and ultimately a decrease in PrP^{Sc} (Ghaemmaghami et al. 2007, Mahal et al. 2007). Therefore, in Chapter 4, the time-course infections in the N2a cells were adapted to incorporate cell passages to improve sensitivity and decrease the variability observed in the time-course experiments. Firstly, the optimal day for cell passage to compromise between adequate prion propagation for a steady accumulation and cell culture consistency was found to be every ten days post initial infection. The

sensitivity of the passage-based N2a/22L infectivity assays with SB/ThT assessment was demonstrated to detect a final 10^{-10} dilution of original 10% 22L-infected brain homogenate. Furthermore, the reliability of this assay was improved as the variability associated with the time-course experiments was decreased. However, some variability observed in the samples is important as it highlights the variations in the uniformity of amyloid distribution between the different samples, taken into account by the capture of random fields of view. The sensitivity of this assay was greater than the sensitivity of a number of the cell-based assays relying on WB based detection, ranging from $10^{-4} – 10^{-7}$ dilutions of the original infected brain homogenates (Archer et al. 2004, Arellano-Anaya et al. 2011, You et al. 2010). This assay also demonstrated ~3 log increase in sensitivity when compared to the animal infectivity bioassays (Fichet et al. 2004, Fichet et al. 2007b, Yan et al. 2004). Moreover, the passage assays matched the sensitivity of the SCEPA SSBA used for the detection of prion infectivity from prion-inoculated wires (Edgeworth et al. 2009, Edgeworth et al. 2011b).

The first two research chapters of this report introduced the sensitive SB/ThT staining of amyloid accumulation within N2a #58 cells inoculated with 22L=infected brain homogenate. An adaptation in the way infectious material is introduced to the cells has to be made, as it is difficult to assess decontamination protocols directly on infectious brain homogenate. Furthermore, reduction of prion infectivity has to be assessed in relation to the decontamination of surgical instruments via the analysis of prion attachment to model surgical surfaces. Therefore both animal bioassays and cell based infectivity assays which are used for the assessment of decontamination protocols introduce the infectious material from inoculated surgical grade SS wires both pre and post decontamination (Edgeworth et al. 2009, Edgeworth et al. 2011b, Fichet et al. 2007a, Fichet et al. 2007b, Flechsig et al. 2001, Lawson 2008, Yan et al. 2004). Therefore, Chapter 5 concentrated on the adaptation of the N2a/22L SB/ThT assay by using inoculated wires to assess decontamination protocols.

Importantly, and crucially for inter-assay comparisons, the length and diameter of the wires (5mm length, 0.16mm diameter) used was comparable to the size of wire used within the majority of cell and animal-based assays (Edgeworth et al. 2009, Edgeworth et al. 2011b, Fichet et al. 2004, Fichet et al. 2007b, Flechsig et al. 2001).

The numbers of inoculated wires introduced to each 35 mm dish was assessed to give a consistent and optimal propagation detected with the SB/ThT staining and was determined to be 20 wires per 35mm dish. Importantly, this is also the number of wires used in other assays (Edgeworth et al. 2009, Edgeworth et al. 2011b, Flechsig et al. 2001). The sensitivity of the assay for the detection of wire-bound 22L infectivity matched the sensitivity of the passage assays, detecting as low as a 10^{-10} dilution of 22L-infected homogenate. Consequently, this data indicates again that this assay is more sensitive than animal bioassays and is comparable in sensitivity with the SSBA and SCEPA detection methods (Edgeworth et al. 2009, Edgeworth et al. 2011b, Fichet et al. 2004, Yan et al. 2004).

The N2a/22L SB/ThT assay was then utilised to assess the decontamination efficacy of three commercially available cleaning chemistries in relation to their reduction of infectivity. Amyloid accumulation was observed in the cells that had been in contact with 22L-inoculated wires that had been decontaminated with Klenzyme and Enzol; however, there was a delay in infection onset of three weekly passages post-wire introduction. The cells that had been in contact with 22L-inoculated wires that had been treated with Hamo 100 demonstrated no amyloid accumulation and suggested infectivity levels below the detection range of this assay. The log reductions in infectivity were determined for these three cleaning chemistries and interestingly correlated well with those observed in the animal bioassays (Fichet et al. 2004, Fichet et al. 2007b, Yan et al. 2004). The increased log reduction observed for Hamo 100 could be explained by the increased sensitivity of the SB/ThT assay. However, the complete loss of infectivity observed post-Hamo 100 treatment was not observed in the SSBA with SCEPA (Edgeworth et al. 2011b). This observation could be explained by variations in the prion strain used or the differences in markers used in the detection protocols (Edgeworth et al. 2011b). This highlights the importance of understanding the scientific credentials of the prion strain analysed and the limitations of the detection method used.

To partially address this issue the SR/ThT assay for the sensitive detection of protein and prion-associated amyloid pre- and post-decontamination was utilised to compare the attachment of 22L and 263K (used in the animal bioassays) infected brain

homogenates to the surgical SS wires. Furthermore, the SR/ThT staining was adapted to produce the NR/ThT staining for the detection of residual lipid contamination as an association between prion infectivity and lipid content has been previously hypothesised (Reviewed in Gale 2007). The most important observation from these experiments was the >4-fold increase in protein, prion-associated amyloid and lipid attachment to the stainless steel wires inoculated with the 22L-infected brain homogenate when compared to the 263K-inoculated wires. The brain homogenates were normalised prior to inoculating the wires so that both strain inoculants were at the same concentration. This observation was either a result of the different prion strains or could be caused by the different nature of the proteins present in hamster brain (263K) and mouse brain (22L).

Although a greater percentage of removal using all of the cleaning chemistries was associated with the 22L-inoculated wires, the increased initial bio-burden meant a higher concentration of residual contamination still remained on the 22L-inoculated wires compared to the 263K-innoculated wires. This could explain the slightly lower log reductions in infectivity demonstrated by Klenzyme and Enzol treatment when analysed using the N2a/22L SB/ThT analysis compared to the 263K hamster bioassays. The lowest concentrations of protein and prion-associated amyloid contamination observed on both the 263K and 22L-inoculated wires was observed post-Enzol treatment, followed closely by the Klenzyme treatment and the highest remaining contamination was observed after the Hamo 100 treatment. This was the same trend observed with the residual lipid contamination on the 263K-inoculated wires; however, the opposite was observed for the residual lipid contamination on the 22L-inoculated wires. No correlation was observed with the remaining contamination on the wires and the log reduction in infectivity associated with the animal bioassays or the N2a/22L SB/ThT assay. This could be explained by the nature of the cleaners. The most efficient cleaners (Klenzyme and Enzol) are enzymatic chemistries and could be removing and breaking up the large plaques to form smaller aggregates but are ineffective at breaking up the aggregates to smaller single prion molecules. In agreement with this is that several studies have already documented that the intermediate small aggregates of about 14 – 28 prion molecules are the most infectious units (Gale 2007, Silveira et al. 2005). Conversely, Hamo 100 alkaline treatment may not be as efficient at removing the gross contamination but due to its alkaline nature may be more likely to break up the aggregates to small monomers or trimers, which have demonstrated “virtually absent”

infectivity (Gale 2007, Silveira et al. 2005). Alternatively, the alkaline cleaner could be denaturing the prion proteins but not removing them. The only correlation that was observed with the cleaning chemistries was that cleaners with the highest pH; like Hamo 100 and NaOH demonstrate the greatest reductions in infectivity. Again no correlation was observed for the lipid staining and infectivity. The pixels of the lipid stain may not really give us an idea of the mass of remaining lipid as the process of producing a stained lipid standard to compare the pixel numbers to mass was not achieved within this study. Furthermore, the types of lipid that Nile red binds to is fairly unknown. However, it has been documented that Nile red binds to intercellular lipid droplets, whereas the lipids associated with PrP are more likely to be membrane phospholipids or sphingolipids (Gale 2007, Greenspan et al. 1985).

This chapter demonstrated the sensitivity of the N2a/22L SB/ThT assay for the *in situ* detection of prion infectivity post decontamination. This assay could now be utilised to analyse various other cleaning chemistries and novel decontamination protocols. Furthermore, the decontamination parameters discussed in the wet vs. dry study (Secker et al. 2011, Appendix A) and the novel DLC surfaces (Secker et al. 2012b) could be assessed for remaining infectivity as the original work was carried out with SR/ThT which within this report has demonstrated no correlation with remaining infectivity. It has previously been reported that wires are not ideal models of surgical instruments as they do not portray a worst case scenario; furthermore, it has been demonstrated that larger tokens are more difficult to clean (Lipscomb et al. 2006a). The N2a/22L SB/ThT assay could be adapted to determine residual infectivity on different, more complex surfaces that would not be possible to test in small rodent brains in the animal infectivity bioassays. Cell culture assays could potentially assess the remaining infectivity on a whole instrument if grown to a lawn of cells within a large culture tray. Furthermore, the N2a/22L SB/ThT assay could be adapted to assess prion infectivity within blood products by incorporating previously reported magnetic beads for prion capture that could then be introduced to the cells and subsequently initiate prion propagation (Miller and Supattapone 2011). The most important adaptation of this assay would be replacing the N2a cells with different cells that are susceptible to different prion strains without the need of transfection and ultimately cell lines for the amplification and detection of CJD infectivity.

Consequently, the final research chapter of this report began to adapt the N2a/22L SB/ThT assay for the use of NSC's as opposed to the N2a cells. This is because, once differentiated, the high levels of PrP^c expressed on neurons negate the need for transfection to artificially increase PrP^c levels. This makes the NSC's a more representative and relevant model to wild-type prion infections as the amplification is induced by the endogenous PrP^c. However, it was observed that an increase in cells undergoing apoptosis at the point of differentiation hindered the SB/ThT staining and thus reduced the potential of these cells, in the first instance, to be used in an infectivity assay without addressing the culture conditions.

It was observed during this work that two main conditions were affecting the quality of the NSC's within culture. Firstly, sub-optimal oxygen concentrations were being used and secondly, it was noted that there was a lack of trophic support at the point of differentiation. The culture of NSC's at 8% O_2 doubled the rate of proliferation of the undifferentiated NSC progenitor cells without changing the levels of spontaneous differentiation when compared to the cells grown at normoxia. Furthermore, the cells cultured in 8% O_2 differentiated into a higher percentage of neurons than astrocytes when compared to the cells cultured at normoxia. This is likely to further increase the cells susceptibility to prion infection because neuronal cells naturally express increased levels of PrP^c. The 8% O_2 cultured NSC's supplemented with FBS also demonstrated around half the number of dead cells when compared to the normoxia cultured cells. FBS supplementation also increased the percentage of neurons in culture when compared to the bFGF supplemented cells and those with no supplementation at all. The improvements observed in this chapter can be easily explained as the lower oxygen concentrations used closer mimic the "*in vivo* normoxia" of the lower oxygen levels observed in the cortical region where the NSC's are derived from. The improved culture in this environment is likely caused by a lower level of ROS build up associated with the mild hypoxic conditions, therefore decreasing the cell death usually associated with increased ROS levels (Galli et al. 2003, Ivanovic 2009, Niidome et al. 2006). The FBS supplementation most likely improves the cultures by replacing the lost nutrients from the point of differentiation and therefore lowering the levels of trophic support deprivation (Niidome et al. 2006). However, it is difficult to pinpoint what in the FBS is aiding the cell culture as there is an amalgamation of growth factors present in FBS that varies from batch to batch (Even et al. 2006). This chapter highlighted the importance of

optimising cell culture conditions and not always relying on standard procedures. This also demonstrated that an understanding of the *in vivo* physiological conditions that cell types are derived from is crucial and should be translated into the *in vitro* culture conditions. Not only will this affect the quality of culture it will also affect many of the *in vivo* processes and actions of these cells; for example, the levels of ROS or complement molecules that would affect the comparability of *in vitro* models in relation to *in vivo* results.

Future work with the NSC's in the new culture conditions will now look to develop them for the analysis of prion infectivity using the SB/ThT analysis system with 22L infection without the hindrances associated with the original culture conditions. Once established, the infectivity of various prion strains will then be tested within the NSC's to determine which prion strains the NSC's are susceptible to. Furthermore, the SB/ThT analysis will be incorporated into different cell lines that have or could demonstrate susceptibility to CJD infection; such as SH-SY5Y human neuroblastoma or GT-1 hypothalamic cells (Ladogana et al. 1995, Oesch et al. 1985). This would allow the production of a sensitive, *in situ* method for the detection of CJD infectivity before and after decontamination treatment.

Although the current levels of iCJD and vCJD are in decline there is still a potential threat of a further outbreak of vCJD leading to an increase in iCJD. The number of asymptomatic carriers is currently unknown. However, it can be estimated by the most recent appendices studies that the number of carriers is around 1/2000. Furthermore, the effect of genetic background on disease progression is still questioned but it has been demonstrated in humanised mice that MV heterozygous and VV homozygous polymorphisms on codon 129 of the PRNP gene lead to far increased incubation periods prior to disease progression. Moreover, the risk of prion transmission to humans from other prion diseases such as CWD has not yet been confirmed. Therefore, with the potential of the increased numbers of asymptomatic carriers with potentially prolonged disease progression and the increased risk of iCJD from surgical procedures and blood transfusions; the importance of addressing decontamination protocols with these improved infectivity assays is crucial to negate the potential future risks. Furthermore, due to the generic amyloid staining of ThT which is not solely

specific to prion diseases, the SB/ThT could also be utilised to detect amyloid accumulation within Alzheimer's disease if the suggested transmissibility of AD is confirmed (Kane et al. 2000, Morales et al. 2011, Rosen et al. 2012). The potential impact of transmissible AD on public health would be huge so any assay with the potential to detect AD transmission and analyse decontamination protocols would be of great benefit.

In final summary, this report has introduced the N2a/22L SB/ThT as a sensitive *in situ* infectivity assay for the assessment of the prion infectivity remaining on surgical surfaces post decontamination. Rather than having a single cell based infectivity assay for the detection of prion infectivity, an amalgamation of the SCEPA assay and the SB/ThT assay would be most beneficial for a greater understanding of prion infectivity. The SCEPA assay would analyse the end-point infectivity in relation to PrP^{res} accumulation, whereas the SB/ThT would analyse the kinetics of amyloid build up over several passages to demonstrate the delay in amyloid accumulation and furthermore, the variations in plaque size observed between different time points and different samples. Ultimately the limitations of these two assays would be addressed when both assays are utilised in unison. Furthermore the introduction of the SB/ThT to different cell lines could produce a sensitive assay for the detection of CJD infectivity from instruments or blood samples which would aid in the detection of potential iCJD sources and improve decontamination protocols to negate the potential risk of a future iCJD or vCJD outbreak.

References

Aguzzi A, Sigurdson C, Heikenwaelder M. 2008. Molecular mechanisms of prion pathogenesis. AnnuRevPathol 3:11-40.

Aguzzi A, Larry RS. 2009. Prion Diseases. In: Encyclopedia of Neuroscience. Oxford: Academic Press. p. 1065-1069.

Alper T, Cramp WA, Haig DA, Clarke MC. 1967. Does the Agent of Scrapie Replicate without Nucleic Acid ? Nature 214:764-766.

Anderson RM, Donnelly CA, Ferguson NM, Woolhouse MEJ, Watt CJ, Udy HJ, MaWhinney S, Dunstan SP, Southwood TRE, Wilesmith JW, Ryan JBM, Hoinville LJ, Hillerton JE, Austin AR, Wells GAH. 1996. Transmission dynamics and epidemiology of BSE in British cattle. Nature 382:779-788.

Andrievskaia O, Algire J, Balachandran A, Nielsen K. 2008. Prion protein in sheep urine. Journal of Veterinary Diagnostic Investigation 20:141-146.

Archer F, Bachelin C, Andreoletti O, Besnard N, Perrot G, Langevin C, Le Dur A, Vilette D, Baron-Van Evercooren A, Vilotte J-L, Laude H. 2004. Cultured Peripheral Neuroglial Cells Are Highly Permissive to Sheep Prion Infection. Journal of Virology 78:482-490.

Arellano-Anaya ZE, Savistchenko J, Mathey J, Huor A, Lacroux C, Andréoletti O, Vilette D. 2011. A Simple, Versatile and Sensitive Cell-Based Assay for Prions from Various Species. Plos One 6:e20563.

Asante EA, Linehan JM, Gowland I, Joiner S, Fox K, Cooper S, Osiguwa O, Gorry M, Welch J, Houghton R, Desbruslais M, Brandner S, Wadsworth JDF, Collinge J. 2006. Dissociation of pathological and molecular phenotype of variant Creutzfeldt Jakob disease in transgenic human prion protein 129 heterozygous mice. Proceedings of the National Academy of Sciences 103:10759-10764.

Atarashi R, Wilham JM, Christensen L, Hughson AG, Moore RA, Johnson LM, Onwubiko HA, Priola SA, Caughey B. 2008. Simplified ultrasensitive prion detection by recombinant PrP conversion with shaking. Nat Meth 5:211-212.

Atarashi R, Sano K, Satoh K, Nishida N. 2011a. Real-time quaking-induced conversion: A highly sensitive assay for prion detection. Prion 5:150-153.

Atarashi R, Satoh K, Sano K, Fuse T, Yamaguchi N, Ishibashi D, Matsubara T, Nakagaki T, Yamanaka H, Shirabe S, Yamada M, Mizusawa H, Kitamoto T, Klug G, McGlade A, Collins SJ, Nishida N. 2011b. Ultrasensitive human prion detection in cerebrospinal fluid by real-time quaking-induced conversion. Nat Med 17:175-178.

Baker HF, Poulter M, Crow TJ, Frith CD, Lofthouse R, Ridley RM, Collinge J. 1991. Aminoacid polymorphism in human prion protein and age at death in inherited prion disease. The Lancet 337:1286.

Barria MA, Mukherjee A, Gonzalez-Romero D, Morales R, Soto C. 2009. *De Novo* Generation of Infectious Prions *In Vitro* Produces a New Disease Phenotype. PLoS Pathog 5:e1000421.

Belay ED. 1999. Transmissible spongiform encephalopathies in humans. Annual review of microbiology 53:283-314.

Benetti F, Legname G. 2009. De novo mammalian prion synthesis. Prion 3:213-219.

Béringue V, Herzog L, Reine F, Le Dur A, Casalone C, Vilotte JL, Laude H. 2008a. Transmission of atypical bovine prions to mice transgenic for human prion protein. Emerging Infectious Diseases 14:1898-1901.

Béringue V, Vilotte JL, Laude H. 2008b. Prion agent diversity and species barrier. Vet Res 39:3.

Bessen RA, Marsh RF. 1992a. Identification of two biologically distinct strains of transmissible mink encephalopathy in hamsters. J Gen Virol 73:329-334.

Bessen RA, Marsh RF. 1992b. Biochemical and physical properties of the prion protein from two strains of the transmissible mink encephalopathy agent. Journal of Virology 66:2096-2101.

Biacabe A-G, Laplanche J-L, Ryder S, Baron T. 2004. Distinct molecular phenotypes in bovine prion diseases. EMBO Rep 5:110-115.

Biasini E, Seegulam ME, Patti BN, Solforosi L, Medrano AZ, Christensen HM, Senatore A, Chiesa R, Williamson RA, Harris DA. 2008. Non-infectious aggregates of the prion protein react with several PrPSc-directed antibodies. Journal of Neurochemistry 105:2190-2204.

Bishop MT, Hart P, Aitchison L, Baybutt HN, Plinston C, Thomson V, Tuzi NL, Head MW, Ironside JW, Will RG, Manson JC. 2006. Predicting susceptibility and incubation time of human-to-human transmission of vCJD. The Lancet Neurology 5:393-398.

Borisenko KB, Reavy HJ, Zhao Q, Abel EW. 2008. Adhesion of protein residues to substituted (111) diamond surfaces: An insight from density functional theory and classical molecular dynamics simulations. J BiomedMaterResA 86A:1113-1121.

Bosque PJ, Ryou C, Telling G, Peretz D, Legname G, DeArmond SJ, Prusiner SB. 2002. Prions in skeletal muscle. ProcNatlAcadSciUSA 99:3812-3817.

Bradley R, Brown P. 2012. The epidemic of Bovine Spongiform Encephalopathy (BSE) in the United Kingdom (UK). In: Decontamination of Prions. Dusseldorf: Dusseldorf University Press. p. 53-80.

Brown DR, Qin K, Herms JW, Madlung A, Manson J, Strome R, Fraser PE, Kruck T, von Bohlen A, Schulz-Schaeffer W, Giese A, Westaway D, Kretzschmar H. 1997. The cellular prion protein binds copper in vivo. Nature 390:684-687.

Brown DR, Schmidt B, Kretzschmar HA. 1998. Effects of Copper on Survival of Prion Protein Knockout Neurons and Glia. Journal of Neurochemistry 70:1686-1693.

Brown DR. 1999. Neurons Depend on Astrocytes in a Coculture System for Protection from Glutamate Toxicity. Molecular and Cellular Neuroscience 13:379-389.

Brown DR, Wong BS, Hafiz F, Clive C, Haswell SJ, Jones IM. 1999. Normal prion protein has an activity like that of superoxide dismutase. Biochem J 344:1-5.

Brown SA, Merritt K, Woods TO, Busick DN. 2005. Effects on instruments of the World Health Organization–recommended protocols for decontamination after possible exposure to transmissible spongiform encephalopathy–contaminated tissue. Journal of Biomedical Materials Research Part B: Applied Biomaterials 72B:186-190.

Bruce ME, McBride PA, Farquhar CF. 1989. Precise targeting of the pathology of the sialoglycoprotein, PrP, and vacuolar degeneration in mouse scrapie. Neuroscience Letters 102:1-6.

Bruce ME. 1993. Scrapie strain variation and mutation. British Medical Bulletin 49:822-838.

Bruce ME, McConnell I, Will RG, Ironside JW. 2001. Detection of variant Creutzfeldt-Jakob disease infectivity in extraneural tissues. The Lancet 358:208-209.

Bucciantini M, Giannoni E, Chiti F, Baroni F, Formigli L, Zurdo J, Taddei N, Ramponi G, Dobson CM, Stefani M. 2002. Inherent toxicity of aggregates implies a common mechanism for protein misfolding diseases. Nature 416:507-511.

Bueler H, Fischer M, Lang Y, Bluethmann H, Lipp HP, Dearmond SJ, Prusiner SB, Aguet M, Weissmann C. 1992. Normal development and behaviour of mice lacking the neuronal cell-surface PrP protein. Nature 356:577-582.

Büeler H, Aguzzi A, Sailer A, Greiner RA, Autenried P, Aguet M, Weissmann C. 1993. Mice devoid of PrP are resistant to scrapie. Cell 73:1339-1347.

Butler DA, Scott MR, Bockman JM, Borchelt DR, Taraboulos A, Hsiao KK, Kingsbury DT, Prusiner SB. 1988. Scrapie-infected murine neuroblastoma cells produce protease-resistant prion proteins. J Virol 62:1558-1564.

Carlson GA, Westaway D, DeArmond SJ, Peterson-Torchia M, Prusiner SB. 1989. Primary structure of prion protein may modify scrapie isolate properties. Proceedings of the National Academy of Sciences 86:7475-7479.

Casalone C, Zanusso G, Acutis P, Ferrari S, Capucci L, Tagliavini F, Monaco S, Caramelli M. 2004. Identification of a second bovine amyloidotic spongiform encephalopathy: Molecular similarities with sporadic Creutzfeldt-Jakob disease. Proceedings of the National Academy of Sciences of the United States of America 101:3065-3070.

Castilla J, Morales R, Saa P, Barria M, Gambetti P, Soto C. 2008. Cell-free propagation of prion strains. Embo Journal 27:2557-2566.

Caughey B. 2003. Prion protein conversions: insight into mechanisms, TSE transmission barriers and strains. British Medical Bulletin 66:109-120.

Caughey B, Lansbury PT. 2003. Protofibrils, pores, fibrils, and neurodegeneration: Separating the responsible protein aggregates from the innocent bystanders. Annual Review of Neuroscience 26:267-298.

Caughey B, Baron GS. 2006. Prions and their partners in crime. Nature 443:803-810.

Caughey BW, Dong A, Bhat KS, Ernst D, Hayes SF, Caughey WS. 1991. Secondary structure analysis of the scrapie-associated protein PrP 27-30 in water by infrared spectroscopy. Biochemistry 30:7672-7680.

Charvériat M, Reboul M, Wang Q, Picoli C, Lenuzza N, Montagnac A, Nhiri N, Jacquet E, Guéritte F, Lallemand J-Y, Deslys J-P, Mouthon F. 2009. New inhibitors of prion replication that target the amyloid precursor. Journal of General Virology 90:1294-1301.

Chen Y, Vartiainen NE, Ying W, Chan PH, Koistinaho J, Swanson RA. 2001. Astrocytes protect neurons from nitric oxide toxicity by a glutathione-dependent mechanism. Journal of Neurochemistry 77:1601-1610.

Clarke L, van der Kooy D. 2009. Low Oxygen Enhances Primitive and Definitive Neural Stem Cell Colony Formation by Inhibiting Distinct Cell Death Pathways. STEM CELLS 27:1879-1886.

Colby DW, Zhang Q, Wang S, Groth D, Legname G, Riesner D, Prusiner SB. 2007. Prion detection by an amyloid seeding assay. Proceedings of the National Academy of Sciences of the United States of America 104:20914-20919.

Collinge J, Palmer MS, Dryden AJ. 1991. Genetic predisposition to iatrogenic Creutzfeldt-Jakob disease. The Lancet 337:1441-1442.

Collinge J, Whittington MA, Sidle KCL, Smith CJ, Palmer MS, Clarke AR, Jefferys JGR. 1994. Prion protein is necessary for normal synaptic function. Nature 370:295-297.

Collinge J, Sidle KCL, Meads J, Ironside J, Hill AF. 1996. Molecular analysis of prion strain variation and the aetiology of 'new variant' CJD. Nature 383:685-690.

Collinge J. 1997. Human Prion Diseases and Bovine Spongiform Encephalopathy (BSE). Human Molecular Genetics 6:1699-1705.

Collinge J. 2001. PRION DISEASES OF HUMANS AND ANIMALS: Their Causes and Molecular Basis. Annual Review of Neuroscience 24:519-550.

Collinge J, Whitfield J, McKintosh E, Beck J, Mead S, Thomas DJ, Alpers MP. 2006. Kuru in the 21st century—an acquired human prion disease with very long incubation periods. The Lancet 367:2068-2074.

Collinge J, Clarke AR. 2007. A General Model of Prion Strains and Their Pathogenicity. Science 318:930-936.

D'Castro L, Wenborn A, Gros N, Joiner S, Cronier S, Collinge J, Wadsworth JDF. 2010. Isolation of Proteinase K-Sensitive Prions Using Pronase E and Phosphotungstic Acid. Plos One 5:e15679.

Deleault NR, Harris BT, Rees JR, Supattapone S. 2007. Formation of native prions from minimal components in vitro. Proceedings of the National Academy of Sciences 104:9741-9746.

Deleault NR, Walsh DJ, Piro JR, Wang F, Wang X, Ma J, Rees JR, Supattapone S. 2012. Cofactor molecules maintain infectious conformation and restrict strain properties in purified prions. Proceedings of the National Academy of Sciences 109:E1938–E1946.

Delmouly K, Belondrade M, Casanova D, Milhavet O, Lehmann S. 2011. HEPES inhibits the conversion of prion protein in cell culture. Journal of General Virology 92:1244-1250.

Deslys J-P, Marcé D, Dormont D. 1994. Similar genetic susceptibility in iatrogenic and sporadic Creutzfeldt-Jakob disease. Journal of General Virology 75:23-27.

Dickinson AG, Meikle VMH, Fraser H. 1968. Identification of a gene which controls the incubation period of some strains of scrapie agent in mice. Journal of Comparative Pathology 78:293-299.

Dickinson J, Murdoch H, Dennis MJ, Hall GA, Bott R, Crabb WD, Penet C, Sutton JM, Raven NDH. 2009. Decontamination of prion protein (BSE301V) using a genetically engineered protease. Journal of Hospital Infection In Press, Corrected Proof.

Doi S, Ito M, Shinagawa M, Sato G, Isomura H, Goto H. 1988. Western Blot Detection of Scrapie-associated Fibril Protein in Tissues outside the Central Nervous System from Preclinical Scrapie-infected Mice. Journal of General Virology 69:955-960.

Duffy P, Wolf J, Collins G, DeVoe AG, Streeten B, Cowen D. 1974. Letter: Possible person-to-person transmission of Creutzfeldt-Jakob disease. N Engl J Med 290:692-693.

Edgeworth JA, Jackson GS, Clarke AR, Weissmann C, Collinge J. 2009. Highly sensitive, quantitative cell-based assay for prions adsorbed to solid surfaces. Proceedings of the National Academy of Sciences 106:3479-3483.

Edgeworth JA, Gros N, Alden J, Joiner S, Wadsworth JDF, Linehan J, Brandner S, Jackson GS, Weissmann C, Collinge J. 2010. Spontaneous generation of mammalian prions. Proceedings of the National Academy of Sciences.

Edgeworth JA, Farmer M, Sicilia A, Tavares P, Beck J, Campbell T, Lowe J, Mead S, Rudge P, Collinge J, Jackson GS. 2011a. Detection of prion infection in variant Creutzfeldt-Jakob disease: a blood-based assay. The Lancet 377:487-493.

Edgeworth JA, Sicilia A, Linehan J, Brandner S, Jackson GS, Collinge J. 2011b. A standardized comparison of commercially available prion decontamination reagents using the Standard Steel-Binding Assay. Journal of General Virology 92:718-726.

Enari M, Flechsig E, Weissmann C. 2001. Scrapie prion protein accumulation by scrapie-infected neuroblastoma cells abrogated by exposure to a prion protein antibody. ProcNatlAcadSciUSA 98:9295-9299.

Even MS, Sandusky CB, Barnard ND. 2006. Serum-free hybridoma culture: ethical, scientific and safety considerations. Trends in Biotechnology 24:105-108.

Fan J, Cai H, Yang S, Yan L, Tan W. 2008. Comparison between the effects of normoxia and hypoxia on antioxidant enzymes and glutathione redox state in ex vivo culture of CD34+ cells. Comparative Biochemistry and Physiology Part B: Biochemistry and Molecular Biology 151:153-158.

Fichet G, Comoy E, Duval C, Antloga K, Dehen C, Charbonnier A, McDonnell G, Brown P, Lasmezas CI, Deslys JP. 2004. Novel methods for disinfection of prion-contaminated medical devices. Lancet 364:521-526.

Fichet G, Antloga K, Comoy E, Deslys JP, McDonnell G. 2007a. Prion inactivation using a new gaseous hydrogen peroxide sterilisation process. Journal of Hospital Infection 67:278-286.

Fichet G, Comoy E, Dehen C, Challier L, Antloga K, Deslys JP, McDonnell G. 2007b. Investigations of a prion infectivity assay to evaluate methods of decontamination. J Microbiol Methods 70:511-518.

Flechsig E, Hegyi I, Enari M, Schwarz P, Collinge J, Weissmann C. 2001. Transmission of scrapie by steel-surface-bound prions. Molecular Medicine 7:679-684.

Fraser H, Dickinson AG. 1968. The sequential development of the brain lesions of scrapie in three strains of mice. Journal of Comparative Pathology 78:301-311.

Furtner M, Gelpi E, Kiechl S, Knoflach M, Zangerl A, Gotwald T, Willeit J, Maier H, Strobel T, Unterberger U, Budka H. 2008. Iatrogenic Creutzfeldt-Jakob disease 22 years after human growth hormone therapy: clinical and radiological features. J Neurol Neurosurg Psychiatry. 2008 Feb;79(2):229-31.

Gajdusek DC, Zigas V. 1957. Degenerative Disease of the Central Nervous System in New Guinea. New England Journal of Medicine 257:974-978.

Gajdusek DC, Gibbs CJ, Alpers M. 1966. Experimental Transmission of a Kuru-like Syndrome to Chimpanzees. Nature 209:794-796.

Gale P. 2007. The prion/lipid hypothesis – further evidence to support the molecular basis for transmissible spongiform encephalopathy risk assessment. Journal of Applied Microbiology 103:2033-2045.

Galli R, Gritti A, Bonfanti L, Vescovi AL. 2003. Neural Stem Cells. Circulation Research 92:598-608.

Gambetti P, Dong Z, Yuan J, Xiao X, Zheng M, Alshekhlee A, Castellani R, Cohen M, Barria MA, Gonzalez-Romero D, Belay ED, Schonberger LB, Marder K, Harris C, Burke JR, Montine T, Wisniewski T, Dickson DW, Soto C, Hulette CM, Mastrianni JA, Kong QZ, Zou WQ. 2008. A novel human disease with abnormal prion protein sensitive to protease. Annals of Neurology 63:697-708.

Ghaemmaghami S, Phuan PW, Perkins B, Ullman J, May BC, Cohen FE, Prusiner SB. 2007. Cell division modulates prion accumulation in cultured cells. ProcNatlAcadSciUSA 104:17971-17976.

Gibbs CJ, Gajdusek DC, Asher DM, Alpers MP, Beck E, Daniel PM, Matthews WB. 1968. Creutzfeldt-Jakob Disease (Spongiform Encephalopathy): Transmission to the Chimpanzee. Science 161:388-389.

Gibbs CJ, Jr., Asher DM, Kobrine A, Amyx HL, Sulima MP, Gajdusek DC. 1994. Transmission of Creutzfeldt-Jakob disease to a chimpanzee by electrodes contaminated during neurosurgery. J Neurol Neurosurg Psychiatry 57:757-758.

Giles K, Glidden DV, Beckwith R, Seoanes R, Peretz D, DeArmond SJ, Prusiner SB. 2008. Resistance of Bovine Spongiform Encephalopathy (BSE) Prions to Inactivation. Plos Pathogens 4:-.

Giri RK, Young R, Pitstick R, DeArmond SJ, Prusiner SB, Carlson GA. 2006. Prion infection of mouse neurospheres. Proceedings of the National Academy of Sciences of the United States of America 103:3875-3880.

Gonzalez-Montalban N, Makarava N, Ostapchenko VG, Savtchenk R, Alexeeva I, Rohwer RG, Baskakov IV. 2011. Highly Efficient Protein Misfolding Cyclic Amplification. PLoS Pathog 7:e1001277.

Gonzalez-Romero D, Barria MA, Leon P, Morales R, Soto C. 2008. Detection of infectious prions in urine. FEBS Lett 582:3161-3166.

Graner E, Mercadante AF, Zanata SM, Forlenza OV, Cabral ALB, Veiga SS, Juliano MA, Roesler R, Walz R, Minetti A, Izquierdo I, Martins VR, Brentani RR. 2000. Cellular prion protein binds laminin and mediates neuritogenesis. Molecular Brain Research 76:85-92.

Grassi J, Maillet S, Simon S, Morel N. 2008. Progress and limits of TSE diagnostic tools. Vet Res 39:15.

Greenspan P, Mayer EP, Fowler SD. 1985. Nile red: a selective fluorescent stain for intracellular lipid droplets. The Journal of Cell Biology 100:965-973.

Griffith JS. 1967. Self-replication and scrapie. Nature 215:1043-1044.

Hall P, Lathia J, Caldwell M, ffrench-Constant C. 2008. Laminin enhances the growth of human neural stem cells in defined culture media. BMC Neuroscience 9:71.

Harrison PM, Bamborough P, Daggett V, Prusiner SB, Cohen FE. 1997. The prion folding problem. Curr Opin Struct Biol 7:53-59.

Herms J, Tings T, Gall S, Madlung A, Giese A, Siebert H, Schürmann P, Windl O, Brose N, Kretzschmar H. 1999. Evidence of Presynaptic Location and Function of the Prion Protein. The Journal of Neuroscience 19:8866-8875.

Herve R, Collin R, Pinchin HE, Secker T, Keevil CW. 2009. A rapid dual staining procedure for the quantitative discrimination of prion amyloid from tissues reveals how interactions between amyloid and lipids in tissue homogenates may hinder the detection of prions. J Microbiol Methods 77:90-97.

Herve R, Secker TJ, Keevil CW. 2010. Current risk of iatrogenic Creutzfeld-Jakob disease in the UK: efficacy of available cleaning chemistries and reusability of neurosurgical instruments. J Hosp Infect 75:309-313.

Hewitt PE, Llewelyn CA, Mackenzie J, Will RG. 2006. Creutzfeldt–Jakob disease and blood transfusion: results of the UK Transfusion Medicine Epidemiological Review study. Vox Sanguinis 91:221-230.

Hill AF, Desbruslais M, Joiner S, Sidle KCL, Gowland I, Collinge J, Doey LJ, Lantos P. 1997. The same prion strain causes vCJD and BSE. Nature 389:448-450.

Hilton DA, Ghani AC, Conyers L, Edwards P, McCardle L, Ritchie D, Penney M, Hegazy D, Ironside JW. 2004. Prevalence of lymphoreticular prion protein accumulation in UK tissue samples. The Journal of Pathology 203:733-739.

Howlin R, Harrison J, Secker T, Keevil C. 2009. Acquisition of proteinaceous contamination through the handling of surgical instruments by hospital staff in sterile service departments. Journal of Infection Prevention 10:106-111.

Howlin RP, Khammo N, Secker T, McDonnell G, Keevil CW. 2010. Application of a fluorescent dual stain to assess decontamination of tissue protein and prion amyloid from surgical stainless steel during simulated washer-disinfector cycles. Journal of Hospital Infection 75:66-71.

HPA. 9 September 2011. Health Protection Agency, News Archives. Health Protection Report, Volume 5

Hsiao K, Dlouhy SR, Farlow MR, Cass C, Da Costa M, Michael Conneally P, Hodes ME, Ghetti B, Prusiner SB. 1992. Mutant prion proteins in Gerstmann-Straussler-Scheinker disease with neurofibrillary tangles. Nat Genet 1:68-71.

Hutter G, Heppner FL, Aguzzi A. 2003. No superoxide dismutase activity of cellular prion protein in vivo. Biological chemistry 384:1279-1285.

Ironside JW, Bishop MT, Connolly K, Hegazy D, Lowrie S, Grice ML, Ritchie DL, McCardle LM, Hilton DA. 2006. Variant Creutzfeldt-Jakob disease: prion protein genotype analysis of positive appendix tissue samples from a retrospective prevalence study. BMJ 332:1186-1188.

Isaacs JD, Jackson GS, Altmann DM. 2006. The role of the cellular prion protein in the immune system. Clin Exp Immunol 146:1-8.

Ivanovic Z. 2009. Hypoxia or in situ normoxia: The stem cell paradigm. Journal of Cellular Physiology 219:271-275.

Jackson GS, McKintosh E, Flechsig E, Prodromidou K, Hirsch P, Linehan J, Brandner S, Clarke AR, Weissmann C, Collinge J. 2005. An enzyme-detergent method for effective prion decontamination of surgical steel. Journal of General Virology 86:869-878.

Kane MD, Lipinski WJ, Callahan MJ, Bian F, Durham RA, Schwarz RD, Roher AE, Walker LC. 2000. Evidence for Seeding of β-Amyloid by Intracerebral Infusion of Alzheimer Brain Extracts in β-Amyloid Precursor Protein-Transgenic Mice. The Journal of Neuroscience 20:3606-3611.

Keevil CW. 2003. Rapid detection of biofilms and adherent pathogens using scanning confocal laser microscopy and episcopic differential interference contrast microscopy. Water SciTechnol 47:105-116.

Kellermann O, Lafay-Chebassier C, Ermonval M, Lehmann S, Mouillet-Richard S. 2002. From stem cells to prion signalling. C R Biol 325:9-15.

Khurana R, Coleman C, Ionescu-Zanetti C, Carter SA, Krishna V, Grover RK, Roy R, Singh S. 2005. Mechanism of thioflavin T binding to amyloid fibrils. Journal of Structural Biology 151:229-238.

Kim JG, Lee KR, Yang SJ. 2008. Wear-corrosion performance of Si-DLC coatings on Ti-6Al-4V substrate. J BiomedMaterResA 86:41-47.

Klohn PC, Stoltze L, Flechsig E, Enari M, Weissmann C. 2003. A quantitative, highly sensitive cell-based infectivity assay for mouse scrapie prions. ProcNatlAcadSciUSA 100:11666-11671.

Kong Q, Zheng M, Casalone C, Qing L, Huang S, Chakraborty B, Wang P, Chen F, Cali I, Corona C, Martucci F, Iulini B, Acutis P, Wang L, Liang J, Wang M, Li X, Monaco S, Zanusso G, Zou W-Q, Caramelli M, Gambetti P. 2008. Evaluation of the Human Transmission Risk of an Atypical Bovine Spongiform Encephalopathy Prion Strain. Journal of Virology 82:3697-3701.

Korth C, Stierli B, Streit P, Moser M, Schaller O, Fischer R, Schulz-Schaeffer W, Kretzschmar H, Raeber A, Braun U, Ehrensperger F, Hornemann S, Glockshuber R, Riek R, Billeter M, Wuthrich K, Oesch B. 1997. Prion (PrPSc)-specific epitope defined by a monoclonal antibody. Nature 390:74-77.

Kroes-Nijboer A, Lubbersen YS, Venema P, van der Linden E. 2009. Thioflavin T fluorescence assay for [beta]-lactoglobulin fibrils hindered by DAPH. Journal of Structural Biology 165:140-145.

Kuczius T, Groschup MH. 1999. Differences in proteinase K resistance and neuronal deposition of abnormal prion proteins characterize bovine spongiform encephalopathy (BSE) and scrapie strains. Mol Med 5:406-418.

Ladogana A, Liu Q, Geng Xi Y, Pocchiari M. 1995. Proteinase-resistant protein in human neuroblastoma cells infected with brain material from Creutzfeldt-Jakob patient. The Lancet 345:594-595.

Laurent M. 1996. Prion diseases and the 'protein only' hypothesis: a theoretical dynamic study. Biochem J 318:35-39.

Lawson VA. 2008. Quantitative bioassay of surface-bound prion infectivity. Methods Mol Biol 459:265-273.

Legname G, Baskakov IV, Nguyen H-OB, Riesner D, Cohen FE, DeArmond SJ, Prusiner SB. 2004. Synthetic Mammalian Prions. Science 305:673-676.

Lemmer K, Mielke M, Pauli G, Beekes M. 2004. Decontamination of surgical instruments from prion proteins: in vitro studies on the detachment, destabilization and degradation of PrPSc bound to steel surfaces. J Gen Virol 85:3805-3816.

Lemmer K, Mielke M, Kratzel C, Joncic M, Oezel M, Pauli G, Beekes M. 2008. Decontamination of surgical instruments from prions. II. In vivo findings with a model system for testing the removal of scrapie infectivity from steel surfaces. Journal of General Virology 89:348-358.

Lipscomb IP, Pinchin HE, Collin R, Harris K, Keevil CW. 2006a. Are surgical stainless steel wires used for intracranial implantation of PrPsc a good model of iatrogenic transmission from contaminated surgical stainless steel instruments after cleaning? J HospInfect 64:339-343.

Lipscomb IP, Pinchin HE, Collin R, Harris K, Keevil CW. 2006b. The sensitivity of approved Ninhydrin and Biuret tests in the assessment of protein contamination on surgical steel as an aid to prevent iatrogenic prion transmission. J HospInfect 64:288-292.

Lipscomb IP, Sihota AK, Botham M, Harris KL, Keevil CW. 2006c. Rapid method for the sensitive detection of protein contamination on surgical instruments. J HospInfect 62:141-148.

Lipscomb IP, Sihota AK, Keevil CW. 2006d. Comparative study of surgical instruments from sterile-service departments for presence of residual gram-negative endotoxin and proteinaceous deposits. J ClinMicrobiol 44:3728-3733.

Lipscomb IP, Sihota AK, Keevil CW. 2006e. Diathermy forceps and pencils: reservoirs for protein and prion contamination? J HospInfect 64:193-194.

Lipscomb IP, Herve R, Harris K, Pinchin H, Collin R, Keevil CW. 2007a. Amyloid-specific fluorophores for the rapid, sensitive in situ detection of prion contamination on surgical instruments. Journal of General Virology 88:2619-2626.

Lipscomb IP, Pinchin H, Collin R, Keevil CW. 2007b. Effect of drying time, ambient temperature and pre-soaks on prion-infected tissue contamination levels on surgical stainless steel: concerns over prolonged transportation of instruments from theatre to central sterile service departments. Journal of Hospital Infection 65:72-77.

Liu C, Zhao Q, Liu Y, Wang S, Abel EW. 2008. Reduction of bacterial adhesion on modified DLC coatings. Colloids SurfB Biointerfaces 61:182-187.

Liu Y, Wang L, Long Z, Zeng L, Wu Y. 2012. Protoplasmic Astrocytes Enhance the Ability of Neural Stem Cells to Differentiate into Neurons <italic>In Vitro</italic>. Plos One 7:e38243.

Llewelyn CA, Hewitt PE, Knight RSG, Amar K, Cousens S, Mackenzie J, Will RG. 2004. Possible transmission of variant Creutzfeldt-Jakob disease by blood transfusion. The Lancet 363:417-421.

López-Barneo J, Pardal R, Ortega-Sáenz P. 2001. Cellular mechanisms of oxygen sensing. Annual Review of Physiology 63:259-287.

Lumley JSP. 2008. The impact of CreutzfeldtJakob disease on surgical practice. Annals of The Royal College of Surgeons of England 90:91-94.

Maezawa I, Hong HS, Liu R, Wu CY, Cheng RH, Kung MP, Kung HF, Lam KS, Oddo S, Laferla FM, Jin LW. 2008. Congo red and thioflavin-T analogs detect Abeta oligomers. J Neurochem 104:457-468.

Mahal SP, Baker CA, Demczyk CA, Smith EW, Julius C, Weissmann C. 2007. Prion strain discrimination in cell culture: The cell panel assay. Proceedings of the National Academy of Sciences 104:20908-20913.

Malchiodi-Albedi F, Paradisi S, Matteucci A, Frank C, Diociaiuti M. 2011. Amyloid Oligomer Neurotoxicity, Calcium Dysregulation, and Lipid Rafts. International Journal of Alzheimer's Disease 2011.

Maluquer de Motes C, Grassi J, Simon S, Herva ME, Torres JM, Pumarola M, Girones R. 2008. Excretion of BSE and scrapie prions in stools from murine models. Vet Microbiol 131:205-211.

Mange A, Milhavet O, Umlauf D, Harris D, Lehmann S. 2002. PrP-dependent cell adhesion in N2a neuroblastoma cells. FEBS Lett 514:159-162.

Masamoto K, Tanishita K. 2009. Oxygen transport in brain tissue. J Biomech Eng 131:074002.

Masters CL, Gajdusek DC, Gibbs CJ, Jr. 1981. Creutzfeldt-Jakob disease virus isolations from the Gerstmann-Straussler syndrome with an analysis of the various forms of amyloid plaque deposition in the virus-induced spongiform encephalopathies. Brain 104:559-588.

McDonnell G, Burke P. 2003. The Challenge of Prion Decontamination. Clinical Infectious Diseases 36:1152-1154.

McGuire LI, Peden AH, Orrú CD, Wilham JM, Appleford NE, Mallinson G, Andrews M, Head MW, Caughey B, Will RG, Knight RSG, Green AJE. 2012. Real time quaking-induced conversion analysis of cerebrospinal fluid in sporadic Creutzfeldt–Jakob disease. Annals of Neurology 72:278-285.

Meyer-Luehmann M, Coomaraswamy J, Bolmont T, Kaeser S, Schaefer C, Kilger E, Neuenschwander A, Abramowski D, Frey P, Jaton AL, Vigouret J-M, Paganetti

P, Walsh DM, Mathews PM, Ghiso J, Staufenbiel M, Walker LC, Jucker M. 2006. Exogenous Induction of Cerebral ß-Amyloidogenesis Is Governed by Agent and Host. Science 313:1781-1784.

Milhavet O, Casanova D, Chevallier N, McKay RD, Lehmann S. 2006. Neural stem cell model for prion propagation. STEM CELLS 24:2284-2291.

Miller MB, Supattapone S. 2011. Superparamagnetic Nanoparticle Capture of Prions for Amplification. Journal of Virology 85:2813-2817.

Millhauser GL. 2007. Copper and the Prion Protein: Methods, Structures, Function, and Disease. Annual Review of Physical Chemistry 58:299-320.

Moore RA, Taubner LM, Priola SA. 2009. Prion protein misfolding and disease. Current Opinion in Structural Biology 19:14-22.

Morales R, Duran-Aniotz C, Castilla J, Estrada LD, Soto C. 2011. De novo induction of amyloid-[beta] deposition in vivo. Mol Psychiatry.

Morrison SJ. 2001. Neuronal potential and lineage determination by neural stem cells. Current Opinion in Cell Biology 13:666-672.

Murayama Y, Yoshioka M, Horii H, Takata M, Yokoyama T, Sudo T, Sato K, Shinagawa M, Mohri S. 2006. Protein misfolding cyclic amplification as a rapid test for assessment of prion inactivation. Biochem Biophys Res Commun 348:758-762.

Murdoch H, Taylor D, Dickinson J, Walker JT, Perrett D, Raven NDH, Sutton JM. 2006. Surface decontamination of surgical instruments: an ongoing dilemma. Journal of Hospital Infection 63:432-438.

Neary K, Caughey B, Ernst D, Race RE, Chesebro B. 1991. Protease sensitivity and nuclease resistance of the scrapie agent propagated in vitro in neuroblastoma cells. J Virol 65:1031-1034.

Nicholson EM, Kunkle RA, Hamir AN, Lebepe-Mazur S, Orcutt D. 2007. Detection of the disease-associated isoform of the prion protein in formalin-fixed tissues by Western blot. Journal of Veterinary Diagnostic Investigation 19:548-552.

Niidome T, Morimoto N, Iijima S, Akaike A, Kihara T, Sugimoto H. 2006. Mechanisms of cell death of neural progenitor cells caused by trophic support deprivation. European Journal of Pharmacology 548:1-8.

Nishida N, Harris DA, Vilette D, Laude H, Frobert Y, Grassi J, Casanova D, Milhavet O, Lehmann S. 2000. Successful transmission of three mouse-adapted

scrapie strains to murine neuroblastoma cell lines overexpressing wild-type mouse prion protein. J Virol 74:320-325.

Novitskaya V, Makarava N, Sylvester I, Bronstein IB, Baskakov IV. 2007. Amyloid fibrils of mammalian prion protein induce axonal degeneration in NTERA2-derived terminally differentiated neurons. Journal of Neurochemistry 102:398-407.

Nuvolone M, Aguzzi A, Heikenwalder M. 2009. Cells and prions: a license to replicate. FEBS Lett 583:2674-2684.

Oesch B, Westaway D, Wälchli M, McKinley MP, Kent SBH, Aebersold R, Barry RA, Tempst P, Teplow DB, Hood LE, Prusiner SB, Weissmann C. 1985. A cellular gene encodes scrapie PrP 27-30 protein. Cell 40:735-746.

Orrú CD, Wilham JM, Raymond LD, Kuhn F, Schroeder B, Raeber AJ, Caughey B. 2011. Prion Disease Blood Test Using Immunoprecipitation and Improved Quaking-Induced Conversion. mBio 2.

Owen F, Poulter M, Collinge J, Crow TJ. 1990. Codon 129 changes in the prion protein gene in Caucasians. American journal of human genentics 46:1215-1216.

Palmer MS, Dryden AJ, Hughes JT, Collinge J. 1991. Homozygous prion protein genotype predisposes to sporadic Creutzfeldt-Jakob disease. Nature 352:340-342.

Pan KM, Baldwin M, Nguyen J, Gasset M, Serban A, Groth D, Mehlhorn I, Huang Z, Fletterick RJ, Cohen FE. 1993. Conversion of alpha-helices into beta-sheets features in the formation of the scrapie prion proteins. Proceedings of the National Academy of Sciences 90:10962-10966.

Pankiewicz J, Prelli F, Sy MS, Kascsak RJ, Kascsak RB, Spinner DS, Carp RI, Meeker HC, Sadowski M, Wisniewski T. 2006. Clearance and prevention of prion infection in cell culture by anti-PrP antibodies. EurJ Neurosci 23:2635-2647.

Paspaltsis I, Berberidou C, Poulios I, Sklaviadis T. 2009. Photocatalytic degradation of prions using the photo-Fenton reagent. Journal of Hospital Infection 71:149-156.

Pastrana MA, Sajnani G, Onisko B, Castilla J, Morales R, Soto C, Requena JR. 2006. Isolation and Characterization of a Proteinase K-Sensitive PrPSc Fraction. Biochemistry 45:15710-15717.

Pattison IH, Millson GC. 1961. Scrapie produced experimentally in goats with special reference to the clinical syndrome. J Comp Pathol 71:101-109.

Peretz D, Scott MR, Groth D, Williamson RA, Burton DR, Cohen FE, Prusiner SB. 2001. Strain-specified relative conformational stability of the scrapie prion protein. Protein Sci 10:854-863.

Peretz D, Supattapone S, Giles K, Vergara J, Freyman Y, Lessard P, Safar JG, Glidden DV, McCulloch C, Nguyen H-OB, Scott M, DeArmond SJ, Prusiner SB. 2006. Inactivation of Prions by Acidic Sodium Dodecyl Sulfate. Journal of Virology 80:322-331.

Prior M, Lehmann S, Sy MS, Molloy B, McMahon HE. 2007. Cyclodextrins inhibit replication of scrapie prion protein in cell culture. J Virol 81:11195-11207.

Prusiner SB, McKinley MP, Groth DF, Bowman KA, Mock NI, Cochran SP, Masiarz FR. 1981. Scrapie agent contains a hydrophobic protein. Proc Natl Acad Sci U S A 78:6675-6679.

Prusiner SB. 1997. Prion diseases and the BSE crisis. Science 278:245-251.

Prusiner SB. 1998. Prions. Proceedings of the National Academy of Sciences 95:13363-13383.

Redecke L, Binder S, Elmallah MIY, Broadbent R, Tilkorn C, Schulz B, May P, Goos A, Eich A, Rübhausen M, Betzel C. 2009. UV light induced conversion and aggregation of prion proteins. Free Radical Biology and Medicine In Press, Accepted Manuscript.

Riek R, Hornemann S, Wider G, Glockshuber R, Wüthrich K. 1997. NMR characterization of the full-length recombinant murine prion protein, mPrP(23–231). FEBS Letters 413:282-288.

Riesner D. 2003. Biochemistry and structure of PrPC and PrPSc. British Medical Bulletin 66:21-33.

Robakis NK, Devine-Gage EA, Jenkins EC, Kascsak RJ, Brown WT, Krawczun MS, Silverman WP. 1986. Localization of a human gene homologous to the PrP gene on the p ARM of chromosome 20 and detection of PrP-related antigens in normal human brain. Biochemical and Biophysical Research Communications 140:758-765.

Roesler R, Walz R, Quevedo J, de-Paris F, Zanata SlM, Graner E, Izquierdo I, Martins VR, Brentani RR. 1999. Normal inhibitory avoidance learning and anxiety, but increased locomotor activity in mice devoid of PrPC. Molecular Brain Research 71:349-353.

Rosen RF, Fritz JJ, Dooyema J, Cintron AF, Hamaguchi T, Lah JJ, LeVine H, Jucker M, Walker LC. 2012. Exogenous seeding of cerebral β-amyloid deposition in βAPP-transgenic rats. Journal of Neurochemistry 120:660-666.

Roy RK, Lee KR. 2007. Biomedical applications of diamond-like carbon coatings: a review. J BiomedMaterResB ApplBiomater 83:72-84.

Saborio GP, Permanne B, Soto C. 2001. Sensitive detection of pathological prion protein by cyclic amplification of protein misfolding. Nature 411:810-813.

Safar J, Wille H, Itri V, Groth D, Serban H, Torchia M, Cohen FE, Prusiner SB. 1998. Eight prion strains have PrPSc molecules with different conformations. Nat Med 4:1157-1165.

Sakudo A, Nakamura I, Ikuta K, Onodera T. 2007. Recent Developments in Prion Disease Research: Diagnostic Tools and In Vitro Cell Culture Models. The Journal of Veterinary Medical Science 69:329-337.

Schwartz K, Boles BR. 2013. Microbial amyloids – functions and interactions within the host. Current Opinion in Microbiology.

Secker TJ, Hervé R, Keevil CW. 2011. Adsorption of prion and tissue proteins to surgical stainless steel surfaces and the efficacy of decontamination following dry and wet storage conditions. Journal of Hospital Infection 78:251-255.

Secker TJ, Hervé R, Keevil CW. 2012a. Response to the letter from M. Feckie. Journal of Hospital Infection 80:181-182.

Secker TJ, Hervé R, Zhao Q, Borisenko KB, Abel EW, Keevil CW. 2012b. Doped diamond-like carbon coatings for surgical instruments reduce protein and prion-amyloid biofouling and improve subsequent cleaning. Biofouling 28:563-569.

Shewmaker F, McGlinchey RP, Wickner RB. 2011. Structural Insights into Functional and Pathological Amyloid. Journal of Biological Chemistry.

Sigurdson C, J. 2008. A prion disease of cervids: Chronic wasting disease. Vet Res 39:41.

Silva CJ, Onisko BC, Dynin I, Erickson ML, Requena JsR, Carter JM. 2011. Utility of Mass Spectrometry in the Diagnosis of Prion Diseases. Analytical Chemistry 83:1609-1615.

Silveira JR, Raymond GJ, Hughson AG, Race RE, Sim VL, Hayes SF, Caughey B. 2005. The most infectious prion protein particles. Nature 437:257-261.

Simoneau S, Rezaei H, Sales N, Kaiser-Schulz G, Lefebvre-Roque M, Vidal C, Fournier JG, Comte J, Wopfner F, Grosclaude J, Schatzl H, Lasmezas CI. 2007. In vitro and in vivo neurotoxicity of prion protein oligomers. PLoSPathog 3:e125.

Singh B, Armstrong DT. 1997. Insulin-like growth factor-1, a component of serum that enables porcine cumulus cells to expand in response to follicle-stimulating hormone in vitro. Biol Reprod 56:1370-1375.

Šišková Z, Reynolds RA, O'Connor V, Perry VH. 2013. Brain Region Specific Pre-Synaptic and Post-Synaptic Degeneration Are Early Components of Neuropathology in Prion Disease. Plos One 8:e55004.

Solassol J, Crozet C, Lehmann S. 2003. Prion propagation in cultured cells. British Medical Bulletin 66:87-97.

Soto C, Saborío GP. 2001. Prions: disease propagation and disease therapy by conformational transmission. Trends in Molecular Medicine 7:109-114.

Soto C, Castilla J. 2004. The controversial protein-only hypothesis of prion propagation. Nat Med 10:S63-67.

Soto C, Anderes L, Suardi S, Cardone F, Castilla J, Frossard MJ, Peano S, Saa P, Limido L, Carbonatto M, Ironside J, Torres JM, Pocchiari M, Tagliavini F. 2005. Pre-symptomatic detection of prions by cyclic amplification of protein misfolding. FEBS Lett 579:638-642.

Stephenson J. 2007. Halting the spread of human prion disease--exceptional measures for an exceptional problem. J Hosp Infect 2:14-18.

Stohr J, Weinmann N, Wille H, Kaimann T, Nagel-Steger L, Birkmann E, Panza G, Prusiner SB, Eigen M, Riesner D. 2008. Mechanisms of prion protein assembly into amyloid. Proceedings of the National Academy of Sciences of the United States of America 105:2409-2414.

Studer L, Csete M, Lee S-H, Kabbani N, Walikonis J, Wold B, McKay R. 2000. Enhanced Proliferation, Survival, and Dopaminergic Differentiation of CNS Precursors in Lowered Oxygen. The Journal of Neuroscience 20:7377-7383.

Tattum MH, Jones S, Pal S, Khalili-Shirazi A, Collinge J, Jackson GS. 2010. A highly sensitive immunoassay for the detection of prion-infected material in whole human blood without the use of proteinase K. Transfusion 50:2619-2627.

Taylor DR, Hooper NM. 2006. The prion protein and lipid rafts (Review). Molecular Membrane Biology 23:89-99.

Telling GC, Parchi P, DeArmond SJ, Cortelli P, Montagna P, Gabizon R, Mastrianni J, Lugaresi E, Gambetti P, Prusiner SB. 1996. Evidence for the Conformation of the Pathologic Isoform of the Prion Protein Enciphering and Propagating Prion Diversity. Science 274:2079-2082.

Thackray AM, Hopkins L, Bujdoso R. 2007. Proteinase K-sensitive disease-associated ovine prion protein revealed by conformation-dependent immunoassay. Biochem J 401:475-483.

Tobler I, Gaus SE, Deboer T, Achermann P, Fischer M, Rulicke T, Moser M, Oesch B, McBride PA, Manson JC. 1996. Altered circadian activity rhythms and sleep in mice devoid of prion protein. Nature 380:639-642.

Ungurs M, Hesp JR, Poolman T, McLuckie G, O'Brien S, Murdoch H, Wells P, Raven NDH, Walker JT, Sutton JM. 2010. Quantitative measurement of the efficacy of protein removal by cleaning formulations; comparative evaluation of prion-directed cleaning chemistries. Journal of Hospital Infection 74:144-151.

Van Dorsselaer A, Carapito C, Delalande F, Schaeffer-Reiss C, Thierse D, Diemer H, McNair DS, Krewski D, Cashman NR. 2011. Detection of Prion Protein in Urine-Derived Injectable Fertility Products by a Targeted Proteomic Approach. Plos One 6:e17815.

Vassallo N, Herms J. 2003. Cellular prion protein function in copper homeostasis and redox signalling at the synapse. Journal of Neurochemistry 86:538-544.

Veith NM, Plattner H, Stuermer CAO, Schulz-Schaeffer WJ, Bürkle A. 2009. Immunolocalisation of PrPSc in scrapie-infected N2a mouse neuroblastoma cells by light and electron microscopy. European Journal of Cell Biology 88:45-63.

Vilette D. 2008. Cell models of prion infection. Vet Res 39:10.

Wadia JS, Schaller M, Williamson RA, Dowdy SF. 2008. Pathologic Prion Protein Infects Cells by Lipid-Raft Dependent Macropinocytosis. Plos One 3:e3314.

Wadsworth JDF, Collinge J. 2007. Update on human prion disease. Biochimica et Biophysica Acta (BBA) - Molecular Basis of Disease 1772:598-609.

Warner JC, Rothwell SD, Keevil CW. 2008. Use of episcopic differential interference contrast microscopy to identify bacterial biofilms on salad leaves and track colonization by Salmonella Thompson. Environmental Microbiology 10:918-925.

Weber P, Giese A, Piening N, Mitteregger G, Thomzig A, Beekes M, Kretzschmar HA. 2007. Generation of genuine prion infectivity by serial PMCA. Veterinary Microbiology 123:346-357.

Weissmann C, Enari M, Klohn PC, Rossi D, Flechsig E. 2002. Transmission of prions. ProcNatlAcadSciUSA 99 Suppl 4:16378-16383.

Wilesmith J, Ryan J, Atkinson M. 1991. Bovine spongiform encephalopathy: epidemiological studies on the origin. Veterinary Record 128:199-203.

Wilesmith J, Ryan J, Hueston W, Hoinville L. 1992. Bovine spongiform encephalopathy: epidemiological features 1985 to 1990. Veterinary Record 130:90-94.

Wilham JM, Orrú CD, Bessen RA, Atarashi R, Sano K, Race B, Meade-White KD, Taubner LM, Timmes A, Caughey B. 2010. Rapid End-Point Quantitation of Prion Seeding Activity with Sensitivity Comparable to Bioassays. PLoS Pathog 6:e1001217.

Will RG, Ironside JW, Zeidler M, Cousens SN, Estibeiro K, Alperovitch A, Poser S, Pocchiari M, Hofman A, Smith PG. 1996. A new variant of Creutzfeldt-Jakob disease in the UK. Lancet 347:921-925.

Will RG. 2003. Acquired prion disease: iatrogenic CJD, variant CJD, kuru. Br Med Bull 66:255-265.

Wion D, Christen T, Barbier EL, Coles JA. 2009. PO2 Matters in Stem Cell Culture. Cell stem cell 5:242-243.

Wroe SJ, Pal S, Siddique D, Hyare H, Macfarlane R, Joiner S, Linehan JM, Brandner S, Wadsworth JDF, Hewitt P, Collinge J. 2006. Clinical presentation and pre-mortem diagnosis of variant Creutzfeldt-Jakob disease associated with blood transfusion: a case report. The Lancet 368:2061-2067.

Yan ZX, Stitz L, Heeg P, Pfaff E, Roth K. 2004. Infectivity of prion protein bound to stainless steel wires: a model for testing decontamination procedures for transmissible spongiform encephalopathies. Infection control and hospital epidemiology : the official journal of the Society of Hospital Epidemiologists of America 25:280-283.

You B, Aubin J-T, Le-Hir G, Arzel A, Laude H, Flan B. 2010. In vitro infectivity assay for prion titration for application to the evaluation of the prion removal capacity of biological products manufacturing processes. Journal of Virological Methods 164:1-6.

Zanusso G, Monaco S. 2005. Molecular mechanisms of human prion diseases. Drug Discovery Today: Disease Mechanisms 2:511-518.

Zernike F. 1942. Phase contrast, a new method for the microscopic observation of transparent objects. Physica 9:686-698.

Zhang Y, Spiess E, Groschup MH, Burkle A. 2003. Up-regulation of cathepsin B and cathepsin L activities in scrapie-infected mouse Neuro2a cells. J Gen Virol 84:2279-2283.

Zobeley E, Flechsig E, Cozzio A, Enari M, Weissmann C. 1999. Infectivity of scrapie prions bound to a stainless steel surface. Mol Med 5:240-243.

Appendices

Appendix A

Previous publications

A list of my previous publications that are relevant to this work, but are not a direct result of the research carried out during within this thesis.

Secker, T.J., Hervé, R., Zhao, Q., Borisenko, K.B., Abel, E.W. and Keevil, C.W. (2012) Doped diamond-like carbon coatings for surgical instruments reduce protein and prion-amyloid biofouling and improve subsequent cleaning. Biofouling, 28, (6), 563-569. (doi:10.1080/08927014.2012.698387).

Secker, T.J., Hervé, R. and Keevil, C.W. (2012) Response to the letter from M. Feckie. Journal of Hospital Infection, 80, (2), 181-182. (doi:10.1016/j.jhin.2011.11.006)

Secker, T.J., Hervé, R. and Keevil, C.W. (2011) Adsorption of prion and tissue proteins to surgical stainless steel surfaces and the efficacy of decontamination following dry and wet storage conditions. Journal of Hospital Infection, 78, (4), 251-255. (doi:10.1016/j.jhin.2011.03.021)

Hervé, R., **Secker, T.J**. and Keevil, C.W. (2010) Current risk of iatrogenic Creutzfeldt–Jakob disease in the UK: efficacy of available cleaning chemistries and reusability of neurosurgical instruments. Journal of Hospital Infection, 75, (4), 309-313. (doi:10.1016/j.jhin.2010.01.024)

Howlin, R.P., Khammo, N., **Secker, T.**, McDonnell, G. and Keevil, C.W. (2010) Application of a fluorescent dual stain to assess decontamination of tissue protein and

prion amyloid from surgical stainless steel during simulated washer-disinfector cycles. Journal of Hospital Infection, 75, (1), 66-71. (doi:10.1016/j.jhin.2009.12.023)

Hervé, R., Collin, R., Pinchin, H.E., **Secker, Thomas** and Keevil, C.William (2009) A rapid dual staining procedure for the quantitative discrimination of prion amyloid from tissues reveals how interactions between amyloid and lipids in tissue homogenates may hinder the detection of prions. Journal of Microbiological Methods, 77, (1), 90-97. (doi:10.1016/j.mimet.2009.01.017)

Howlin, R., Harrison, J., **Secker, T**. and Keevil, C.W. (2009) Acquisition of proteinaceous contamination through the handling of surgical instruments by hospital staff in sterile service departments. Journal of Infection Prevention, 10, (3), 106-111. (doi:10.1177/1757177409105073)